Synthesis and catalytic applications of metal nanoparticles

CUMULATIVE DISSERTATION

submitted to the faculty of

Heinrich-Heine-Universität Düsseldorf
Institut für Anorganische Chemie I: Bioanorganische Chemie und Katalyse

in partial fulfillment of the requirements for the degree of

Dr. rer. nat.

submitted by

Christian Peter Vollmer

Düsseldorf, May 2012

Printed with permission of the

Mathematisch-Naturwissenschaftliche Fakultät
Heinrich-Heine-Universität Düsseldorf

Graduate referee: Prof. Dr. Christoph Janiak

Co-referee: Prof. Dr. Christian Ganter

Date of graduate thesis defense: 15.05.2012

Herewith, I affirm that this dissertation was written by myself without using any unauthorized materials regarding “Grundsätze zur Sicherung guter wissenschaftlicher Praxis an der Heinrich-Heine-Universität Düsseldorf”. Neither this dissertation nor any similar documents have been submitted to any other faculty. No unsuccessful dissertation attempts have been undertaken.

ACKNOWLEDGMENT

First and foremost I would like to thank Prof. Dr. Christoph Janiak for giving me the opportunity to work in his group and for the guidance to my doctoral research. I really appreciate all his contributions of time, ideas and helpful and valuable advice. For the prolific discussions I would like to express my sincere gratitude. He gave me freedom in my field of research and realized the cooperation with the group of Prof. Dr. Chris Hardacre at Queen's University in Belfast, Northern Ireland.

I would like to give my thanks to my co-referee Prof. Dr. Christian Ganter.

I would like to express my sincere thanks to Dr. Ralf Thomann und Dr. Yi Thomann for their countless TEM und SEM measurements and analysis, Angela Thiemann and Anette Ricken for the AAS analysis and Dietmar Frunzke for the IR spectroscopy.

I would like to say thank you to PD Dr. Peter Kunz for having a sympathetic ear for my chemical and physical challenges.

Many thanks go to all my colleagues in the institutes in Düsseldorf and Freiburg. In this regard I would particularly like to thank Francisca Alberti, Dagmar Biercher, Frederik Blank, Ishtvan Boldog, Victoria Gräfner, Björn Hildebrand, Daniel Himmel, Hajo Meyer, Beate Rau, Mareike Richter, Claudia Schäfer, Kai Schütte, Abdelaziz Makhloufi, Axel Mundt and Corinna Wetzel for their advice and their helping hands.

I would also like to thank Prof. Dr. Chris Hardacre und Dr. Haresh Manyar at Queen's University in Belfast for the collaboration and the fruitful stays at the Centre for the Theory and Application of Catalysis. I also would like to say thanks to my colleagues Richard Morgan, Eoghain O'Hara and Thomas Sheppard.

I owe many thanks to my family and to all of my friends for giving me their encouragement and for their belief in me. They have always supported me in all my pursuits.

to my parents

This cumulative dissertation is based on the following published, accepted or submitted publications (in the reverse chronological order):

4. *"Organic carbonates as stabilizing solvents for transition metal nanoparticles"*
Christian Vollmer, Ralf Thomann, Christoph Janiak, manuscript submitted to Dalton Transactions

3. *"Turning Teflon-coated magnetic stirring bars to catalyst systems with metal nanoparticle trace deposits - A caveat and a chance"*
Christian Vollmer, Marcel Schröder, Yi Thomann, Ralf Thomann, Christoph Janiak, Appl. Cat. A: Gen. 425-426 (2012) 178-183.

2. *"Naked metal nanoparticles from metal carbonyls in ionic liquids: Easy synthesis and stabilization"*
Christian Vollmer, Christoph Janiak, Coord. Chem. Rev. 255 (2011) 2039-2057.

1. *"The use of microwave irradiation for the easy synthesis of graphene-supported transition metal nanoparticles in ionic liquids"*
Dorothea Marquardt, Christian Vollmer, Ralf Thomann, Peter Steurer, Rolf Mülhaupt, Engelbert Redel, Christoph Janiak, Carbon 49 (2011) 1326-1332.

Additionally, the following publications, which are <u>not</u> part of this thesis, appeared while the thesis was in progress:

1a. *"'Ligand-free' Cluster Quantized Charging in an Ionic Liquid"*
Stijn F. L. Mertens, Christian Vollmer, Alexander Held, Myriam H. Aguirre, Michael Walter, Christoph Janiak, Thomas Wandlowski, Angew. Chem. Int. Ed. 50 (2011) 9735-9738.

1b. *„Quantisierte Aufladung von „ligandenfreien" Clustern in einer ionischen Flüssigkeit"*
Stijn F. L. Mertens, Christian Vollmer, Alexander Held, Myriam H. Aguirre, Michael Walter, Christoph Janiak, Thomas Wandlowski Angew. Chem. 123 (2011) 9909-9912.

Additionally, parts of this thesis have been presented in form of poster contributions:

1. *"Naked, ligand-free metal nanoparticles from synthesis to application"*
Dorothea Marquardt, Francisca Alberti, Hajo Meyer, Christian Vollmer, Christina Rutz, Myriam Türkmen, Christoph Janiak, *8. Koordinationschemie-Treffen*, TU Dortmund, 26.2.-28.2.2012. Dortmund, Germany.

1 TABLE OF CONTENTS

I. ZUSAMMENFASSUNG

Metall Nanopartikel sind auf Grund ihrer großen Anwendungsbreite unter anderem in Bereichen der Katalyse, Medizin und Materialwissenschaften von großem wissenschaftlichem Interesse. Synthese und Stabilisierung kleinster Partikel stellen immer noch eine große Herausforderung dar.

Das Ziel dieser Dissertation war es, kleine Metall Nanopartikel mit Partikeldurchmessern kleiner 5 nm ausgehend von ihren binären Carbonylen reproduzierbar herzustellen und ohne Stabilisator-Liganden alleine mit Hilfe eines schwach koordinierenden Lösungsmittels oder durch Immobilisierung auf einer Oberfläche zu stabilisieren. Ausgewählte Metall Nanopartikel sollten auf ihre katalytischen Hydrieraktivitäten untersucht werden. Im Kontext der *Grünen Chemie* sollte die Nanopartikel-Präparation und die anschließende Katalyse unter möglichst milden, energiesparenden Bedingungen durchgeführt werden.

Im Rahmen der vorliegenden Arbeit wurden folgende Ziele erreicht:

1. Sphärische Nanopartikel der Übergangsmetalle Molybdän, Wolfram, Rhenium, Eisen, Ruthenium, Osmium, Cobalt, Rhodium und Iridium konnten ausgehend von ihren Metallcarbonylen in racemischem Propylencarbonat mit Hilfe von kurzzeitiger und geringer Mikrowellenstrahlung (5 min, 50 W) erzeugt werden. Die Hydrierung von Cyclohexen und 1-Hexin mit elementarem Wasserstoff und Rhodium Nanopartikeln in Propylencarbonat gelang mit Aktivitäten von bis zu 1875 mol Produkt × (mol Rh) $^{-1}$ × h^{-1}. Rhodium und Ruthenium Nanopartikeln konnten mit Hilfe von 3-Mercaptopropionsäure oder Trioctylphosphinoxid (TOPO) aus der Propylencarbonatphase extrahiert und für 3 Wochen stabilisiert werden ohne Änderung der Partikeldurchmesser.
2. Rhodium Nanopartikel konnten ausgehend von $Rh_6(CO)_{16}$ in der ionischen Flüssigkeit n-1-Butyl-3-methyl-imidazolium tetrafluoroborat ($BMImBF_4$) mit kurzzeitiger und geringer Mikrowellenstrahlung (6 min, 10 W) erzeugt werden. Nach der Trägerung der Partikel auf einem PTFE ummantelten, handelsüblichen Rührfisch wurde mit dem diesem „Katalysatorsytem“ in mehreren Durchläufen Cyclohexen und Benzol mit elementarem Wasserstoff hydriert. Die Aktivitäten der Hydrierung von Cyclohexen zu Cyclohexan verringerten sich über zehn Durchläufe von 14.9×10^3 auf 6.6×10^3 mol Produkt × $(\text{mol Rh})^{-1}$ × h^{-1}. Die Aktivitäten der Hydrierung von Benzen zu

Cyclohexan verringerten sich über drei Durchläufe von 750 auf 460 mol Produkt × $(\text{mol Rh})^{-1} \times h^{-1}$.

3. Rhodium und Ruthenium Nanopartikel wurden ausgehend von ihren Carbonylen in der ionischen Flüssigkeit $BMImBF_4$ auf chemisch erhaltenem Graphen (CDG) geträgert und die M-NP/CDG-Systeme in mehreren Durchläufen für die Hydrierung von Cyclohexen und Benzol mit elementarem Wasserstoff verwendet. Die Aktivitäten blieben über zehn Durchgänge für die Hydrierung von Cyclohexen zu Cyclohexan von 1570 mol Produkt × $(\text{mol Ru})^{-1} \times h^{-1}$ mit Ru-NP/CDG und von 360 mol Produkt × $(\text{mol Rh})^{-1} \times h^{-1}$ mit Rh-NP/CDG konstant. Die Aktivitäten von Rh-NP/CDG wurden bei der Hydrierung von Benzen zu Cyclohexan bei verschiedenen Reaktionstemperaturen (25, 50, 75°C) untersucht. Die höchste Aktivität von 310 mol Produkt × $(\text{mol Rh})^{-1} \times h^{-1}$ wurde bei 50°C ermittelt.

II. ABSTRACT

Metal nanoparticles are of high scientific interest because of their broad range of applications in the fields of catalysis, medicine and material science. Synthesis and stabilization of small particles still pose a big challenge.

The aim of this thesis was to obtain reproducible particles with the size smaller than 5 nm originated from their binary carbonyls and to stabilize the particles only with the help of a weak coordinating solvent or by deposition on a surface. Selected metal nanoparticles should be screened for their catalytic activities in hydrogenation reactions. In the context of *green chemistry* the synthesis of the nanoparticles and the following catalysis should be carried out in mild, energy-saving conditions.

In the context of this thesis following aims were accomplished:

1. Spherical nanoparticles of the transition metals molybdenum, tungsten, rhenium, iron, ruthenium, cobalt, rhodium and iridium from their carbonyl precursors in racemic propylene carbonate could be obtained via low and rapid microwave irradiation (5 min, 50 W). The hydrogenation of cyclohexene and 1-hexyne was successful with elemental hydrogen and rhodium nanoparticle in propylene carbonate with activities up to 1875 mol product × $(\text{mol Rh})^{-1}$ × h^{-1}. Rhodium and Ruthenium nanoparticles could be extracted with 3-mercaptopropionic acid or trioctylphosphine oxide (TOPO) from the propylene carbonate phase and were stabilized without a big change in the particle diameter for 3 weeks.
2. Rhodium nanoparticles could be obtained from $Rh_6(CO)_{16}$ in the ionic liquid n-1-butyl-3-methyl-imidazolium tetrafluoroborate ($BMImBF_4$) via low and rapid microwave irradiation (6 min, 10 W). After the deposition of the particles on a PTFE coated, commercially available stirring bar, this “catalytic system” was used for catalytic hydrogenation runs from cyclohexene or benzene to cyclohexane. The activities of the hydrogenation cyclohexene to cyclohexane decreased in ten runs from 14.9×10^3 to 6.6×10^3 mol product × $(\text{mol Rh})^{-1}$ × h^{-1}. The activities of the hydrogenation from benzene to cylohexane slowly decreased in three runs from von 750 auf 460 mol product × $(\text{mol Rh})^{-1}$ × h^{-1}.
3. Chemical derived graphene was synthesized from natural graphite over graphite oxide (Hummers and Offeman) and a following thermal reduction process. Rhodium and Ruthenium nanoparticles were obtained from their carbonyl precursors in the ionic liquid $BMImBF_4$ and deposited onto chemical derived graphene (CDG) and the M-

NP/CDG-system was used for hydrogenation runs from cyclohexene or benzene to cyclohexane with elemental hydrogen. The activities remained constant in ten runs from cyclohexene to cyclohexane of 1570 mol product × (mol Rh)$^{-1}$ × h^{-1}. The activities of Rh-NP/CDG were examined during the hydrogenation of benzene to cylcohexane at different temperatures (25, 50, 75 °C). The highest activity of 310 mol product × (mol Rh)$^{-1}$ × h^{-1} was measured at 50 °C.

III. ABBREVIATIONS

AAS	atomic absorption spectrometry
acac	acetylacetonate
BIM	n-butylimidazolium
$BMImBF_4$	1-butyl-3-methylimidazolium tetrafluoroborate
CDG	chemical derived graphene
DLS	dynamic light scattering
EDX	energy dispersive X-ray
EXAFS	X-ray absorption spectroscopy
FT-IR	Fourier transformed infrared
IL(s)	ionic liquid(s)
h	hour(s)
M-NP(s)	metal nanoparticle(s)
nm	nanometer(s)
MWI	microwave irradiation
NP(s)	nanoparticle(s)
p	pressure
PC	propylene carbonate
PTFE	polytetrafluoroethylene
rpm	rounds per minute
RT	room temperature
SEM	scanning electron microscopy
STEM	scanning transmission electron diffraction
T	temperature
t	time
TED	transmission electron diffraction

TEM	transmission electron microscopy
THF	tetrahydrofuran
TOF	turnover frequency
TOPO	trioctylphosphine oxide
wt.%	weight-%
XMCD	x-ray magnetic circular dichroism
°C	degree

2 INTRODUCTION

Metal nanoparticles (M-NPs) are of significant interest for technological applications in several areas of science and industry, especially in catalysis due to their high activity. The controlled and reproducible synthesis of defined and stable M-NPs with a small size distribution is very important for a range of applications.[1-6] Note that through the years metal nanoparticles were also referred to as nanophase metal clusters, metal nanocrystals and metal colloids. In the following the term (metal) nanoparticles for simplicity is primarily used. M-NPs are only kinetically stable and will combine to thermodynamically favored larger metal particles via agglomeration. This M-NP tendency for aggregation is due to the high surface energy and the large surface area. To avoid this agglomeration, M-NPs need to be stabilized with strongly coordinating protective ligand layers which provide electrostatic and/ or steric protection like polymers and surfactants.[7-9] The immobilization of M-NP onto a surface is a route of stabilization that goes along without the need of ligand layers.[10] Ionic liquids (ILs) can be an alternative to ligand layers as well (Scheme 1). ILs may be seen to act as a "novel nanosynthetic template"[11] that stabilize M-NPs on the basis of their ionic nature,[12] high polarity, high dielectric constant and supramolecular network without the need of additional protective ligands (cf. Scheme 4a).[13-17]

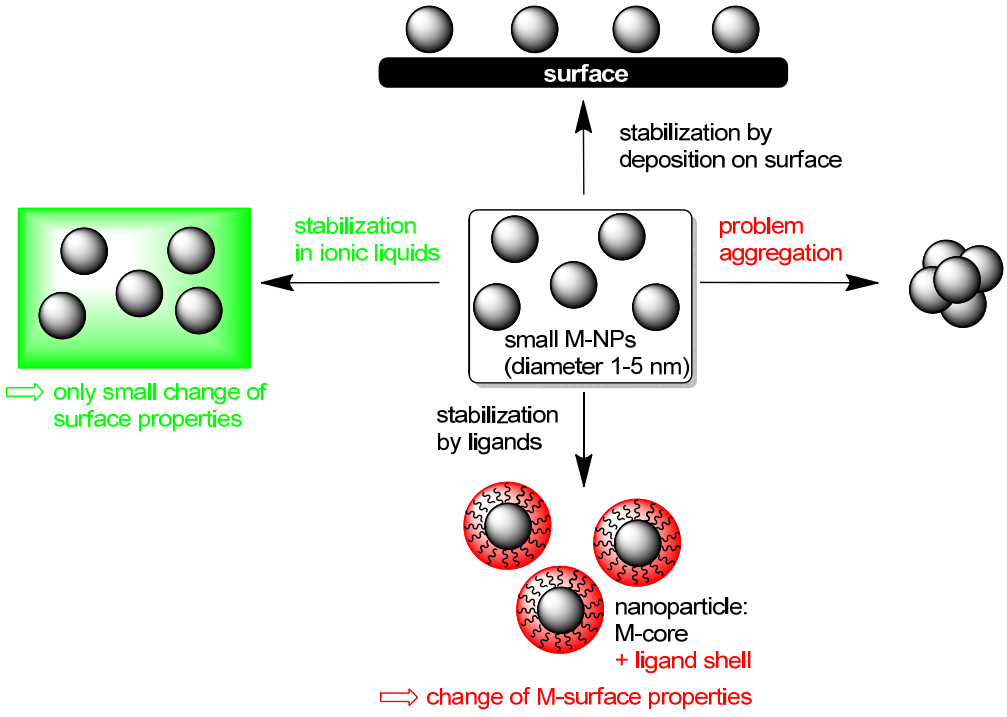

Scheme 1. Stabilization of metal nanoparticles through protective ligand stabilizers or in ionic liquids (IL) or by deposition on a surface.

In the absence of strongly coordinating protective ligand layers, M-NPs in ILs should be effective catalysts. The IL network contains only weakly coordinating cations and anions (Scheme 4) that bind less strongly to the metal surface and, hence, are less deactivating, than the commonly employed capping or protective ligands. The combination of M-NPs and ILs can be considered a *green catalytic system* because it can avoid the use of organic solvents. ILs are interesting in the context of green catalysis[18] which requires that catalysts be designed for easy product separation from the reaction products and multi-time efficient reuse/recycling.[19-21] Firstly, the very low vapor pressure of the IL and designable low miscibility of ILs with organic substrates allows for a facile separation of volatile products by distillation or removal in vacuum. Secondly, the IL is able to retain the M-NPs for catalyst reuse and recycling. For example, Dupont and coworkers have shown that a M-NP/ IL system can be recycled quite easily and can be reused several times without any significant changes in catalytic activity.[13] In recent reports of Rh-NP/IL in hydrogenation reactions, the catalytic activity did not decrease upon repeated reuse.[22,23] A sizable number of catalytic reactions have successfully been carried out in ILs.[24] Generally, the catalytic properties (activity and selectivity) of dispersed M-NPs indicate that they possess pronounced surface-like (multi-site) rather than single-site-like character.[25]

2.1 Green Chemistry

Before the Bhophal desaster in 1984[26] the chemical industry neglected ecological aspects. High yields and the interrelated profits were prioritized over security and ecological effects. In the 1990s scientific, ecological and sustainable chemistry, also known as *green chemistry*, gained in importance. Rethinking took place both in industry and in scientific research. In 1991 Trost was the first to bring in the concept of *atom economy*.[27,28] Around that time Sheldon established the term *E(nvironmental) Factor.*[18] *Green chemistry* became more prominent through the publications of Anastas,[29] Warner[29] and Clarke.[30,31] It can easily be defined as:[32] *Green chemistry efficiently utilises (preferably renewable) raw materials, eliminates waste and avoids the use of toxic and/or hazardous reagents and solvents in the manufacture and application of chemical products*. In the context of *green chemistry* among others catalysis itself, catalysis in non-conventional media, e.g. ionic liquids, and alternative energy input, e.g. microwave, are at the forefront.[18,33] This trend is

being increasingly supported by politicians. Since 1995 the U.S. agency "Environmental Protection Agency" (EPA) has rewarded this ecological tendency with the "Presidential Green Chemistry Challenge Award".

The following twelve principles in Table 1 were established by Anastas and Warner and should be understood as general criteria in chemistry, like yields and selectivity.[29] Anastas consequently expanded this issue into the field of engineering by defining the twelve principles of *green engineering*.[34]

Table 1. The 12 principles of *green chemistry*.

1	It is better to prevent waste than to treat or clean up waste after it has been created.
2	Synthetic methods should be designed to maximize the incorporation of all materials used in the process to create the final product.
3	Wherever practicable, synthetic methods should be designed to use and generate substances that possess little or no toxicity to people or the environment.
4	Chemical products should be designed to effect their desired function while minimizing their toxicity.
5	The use of auxiliary substances (e.g., solvents or separation agents) should be made unnecessary whenever possible and innocuous when used.
6	Energy requirements of chemical processes should be recognized for their environmental and economic impacts and should be minimized. If possible, synthetic methods should be conducted at ambient temperature and pressure.
7	A raw material or feedstock should be renewable rather than depleting whenever technically and economically practicable.
8	Unnecessary derivatization (use of blocking groups, protection/de-protection, and temporary modification of physical/chemical processes) should be minimized or avoided if possible, because such steps require additional reagents and can generate waste.
9	Catalytic reagents (as selective as possible) are superior to stoichiometric reagents.
10	Chemical products should be designed so that at the end of their function they break down into innocuous degradation products and do not persist in the environment.
11	Analytical methodologies need to be further developed to allow for real-time, in-process monitoring and control prior to the formation of hazardous substances.
12	Substances and the form of a substance used in a chemical process should be chosen to minimize the potential for chemical accidents, including releases, explosions, and fires.

These twelve principles have recently been summarized by Poliakoff to a catchy phrase: PRODUCTIVELY:[35]

P	Prevent wastes
R	Renewable materials
O	Omit derivatisation steps
D	Degradable chemical products
U	Use of safe synthetic methods
C	Catalytic reagents
T	Temperature, pressure ambient
I	In-Process monitoring
V	Very few auxiliary subtrates
E	*E Factor*, maximize feed in products
L	Low toxicity of chemical products
Y	Yes, it is safe

Scheme 2 shows a simple example to clarify the term *atom economy* by means of two different routes to proplylene oxide: The upper part describes the classical chlorohydrin route with an *atom economy* of 25% and the lower part is the route with hydroperoxide with an *atom economy* of 75%. *Atom economy* is a theoretical number based on a yield of 100 % and acts on the assumption that reactants are used in stoichiometric amounts.

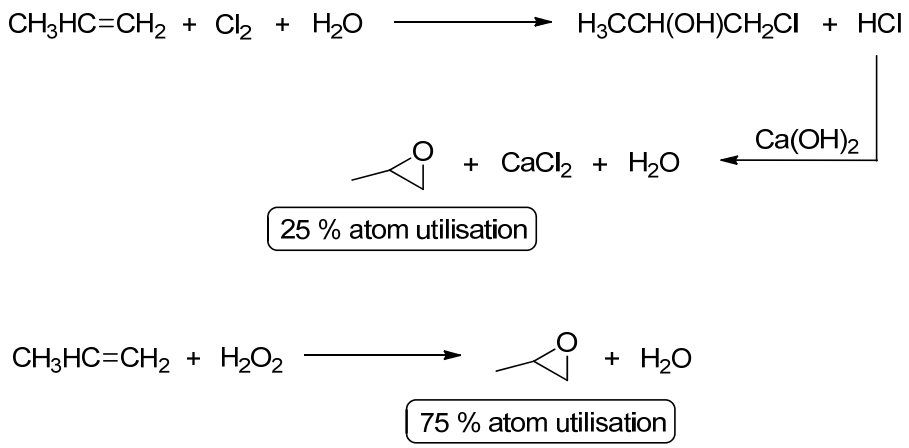

Scheme 2. Chlorohydrin process and atom utilization.[36]

The *E Factor* is the actual amount of waste produced in the process, defined as everything but the desired product. It includes all reagents, solvent losses, all process aids and even the energy required, when carbon dioxide is produced, whereby water is excluded.[36]

The higher the *E Factor* the higher is the negative environmental impact. Table 2 illustrates the level of waste production in different segments of the chemical industry and the interrelated challenge for scientists to provide greener processes.

Table 2. *E factors* in the chemical industry.[18]

Industry Segment	Volume (tons/annum)[a]	E Factor (kg waste/kg product)
Bulk chemicals	10^4-10^6	< 1-5
Fine chemicals	10^2-10^4	5- > 50
Pharmaceutical Industry	10-10^3	25- > 100

[a]Annual production world-wide or at a single site.

2.2 Ionic liquids

Ionic liquids are salts which are composed of charged inorganic and organic ion pairs. By definition their melting point is below 100 °C, more typically ILs are liquid at room temperature.[20,37] Such room temperature ionic liquids are occasionally abbreviated as RTILs.[38] ILs are liquid under standard ambient conditions because the liquid state is thermodynamically favorable, due to the large size and conformational flexibility of the ions involved, which leads to small lattice enthalpies and large entropy changes that favor melting.[39] ILs are characterized and set apart from other solvents by their physical properties like high charge density, high polarity, high dielectric constant and supramolecular network formation (Scheme 4).[16] Typical IL cations include 1-alkyl-3-methylimidazolium, tetraalkylammonium, 1-alkylpyridinium and oxazolium. Typical anions for ILs are halide anions, tetrafluoroborate BF_4^-, hexafluorophosphate PF_6^-, tetrahalogenidoaluminate AlX_4^-, trifluoromethylsulfonate (triflate) $CF_3SO_3^-$ (TfO^-) or bis(trifluoromethylsulfonyl)amide [also named *N*-bis(trifluoromethanesulfonyl)imidate, $(CF_3SO_2)_2N^-$, Tf_2N^-] (Scheme 3).[24,40]

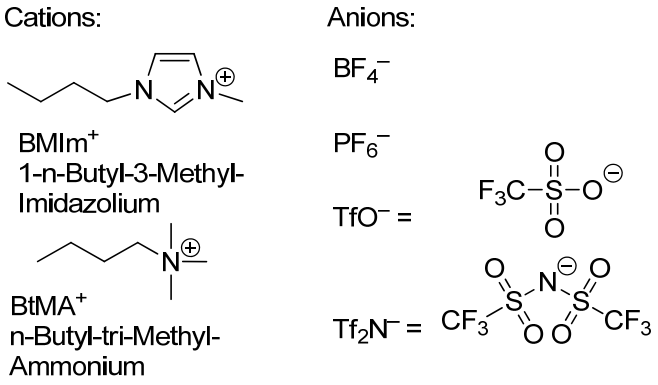

Scheme 3. Typical cations and anions of most common commercially available ILs. $BMIm^+$ is also abbreviated as BMI in the literature.

The desired properties of the IL can be designed through judicious combination of anions and cations which presents an advantage over other solvent systems for the various envisioned IL applications. For instance: ILs containing Tf_2N^- offer low viscosity and high electrochemical and thermal stability.[41] If bis(*trifluoro*methylsulfonyl)amide Tf_2N^- is replaced by bis(methylsulfonyl)amide, viscosity increases and stability decreases.[42] This variety leads to a high interest towards ILs as new *green* reusable reaction media, especially in the field of catalysis.[25]

Scattering experiments on ILs provided important information on the structure of ionic liquids which, thus, are not liquids in the conventional sense, but may rather be considered as mesophases. ILs have an intrinsic "nanostructure" which is caused by electrostatic, hydrogen bonding and van der Waals interactions.[37,43] The mesoscopic structure of imidazolium ionic liquids in particular can be described in part as a supramolecular three-dimensional hydrogen-bonded network (Scheme 3a).[44] Pure 1,3-dialkylimidazolium ILs can be described as a hydrogen-bonded[44] polymeric supramolecular network of the type $\{[(RR'Im)_x(A)_{x-n})]^{n+}[(RR'Im)_{x-n}(A)_x)]^{n-}\}_n$ where RR'Im is the 1,3-dialkylimidazolium cation and A the anion. This structural pattern is not only seen in the solid phase but is also maintained to a great extent in the liquid phase. The introduction of other molecules and macromolecules proceeds with a disruption of the hydrogen bonding network and in some cases can generate nano-structures with polar and non-polar regions where inclusion-type compounds can be formed.[13,14] When mixed with other molecules or M-NPs, ILs become nanostructured materials with polar and nonpolar regions.[45-47]

Ionic liquids are nanostructural liquid media.[48] Nanometer-scale structuring in room-temperature ILs was observed by molecular simulation for ionic liquids belonging to the 1-alkyl-3-methylimidazolium family with hexafluorophosphate or with bis(trifluoro-

methylsulfonyl)amide as the anions. For ionic liquids with alkyl side chains longer than or equal to C_4, aggregation of the alkyl chains in nonpolar domains was observed. These domains permeate a tridimensional network of charged or polar ionic channels formed by anions and by the imidazolium rings of the cations (cf. Scheme 4a). As the length of the alkyl chain increases, the nonpolar domains become larger and more connected and cause swelling of the ionic network, in a manner analogous to systems exhibiting microphase separation.[48] In other words, ILs are nanostructurally organized with nonpolar regions arising from clustering of the alkyl chains and ionic networks arising from charge ordering of the anions and imidazolium rings of the cations.[38] The combination of undirected Coulomb forces and directed hydrogen bonds leads to a high attraction of the IL building units. This is the basis for their (high) viscosity, negligible vapor pressure and three-dimensional constitution. The IL network properties should be well suited for the synthesis of defined nano-scaled metal colloid structures (Scheme 4).[13-15]

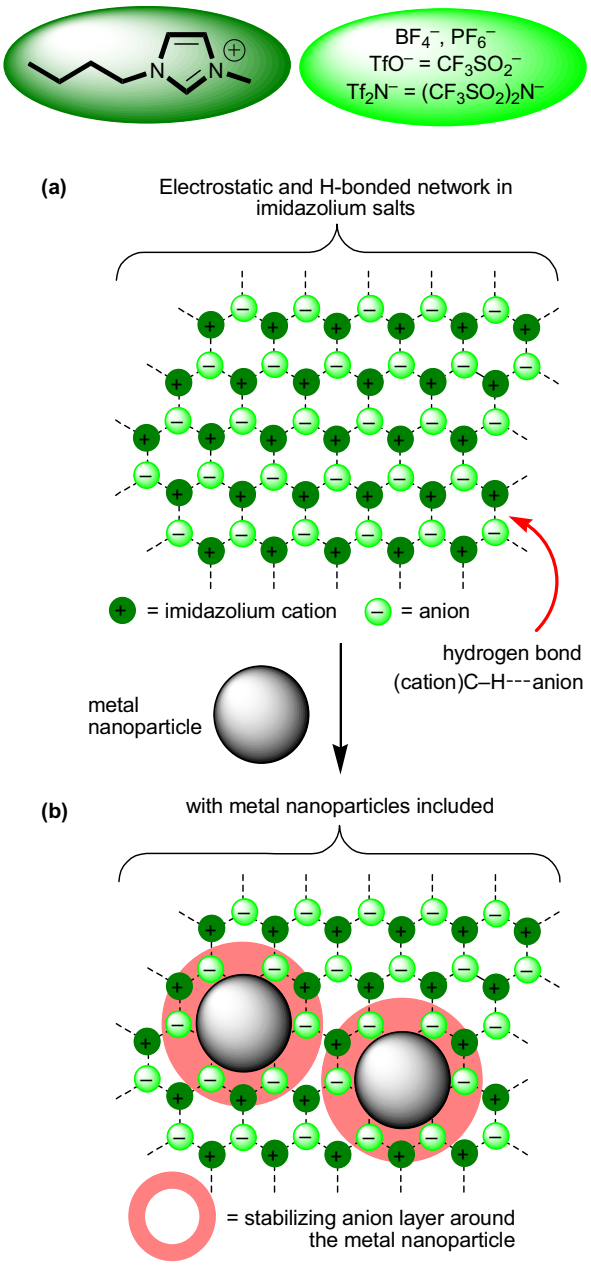

Scheme 4. (a) Schematic network structure in 1,3-dialkylimidazolium-based ionic liquids. (b) The inclusion of metal nanoparticles (M-NPs) in the supramolecular IL network with electrostatic and steric (= *electrosteric*) stabilization is indicated through the formation of the suggested primary anion layer forming around the M-NPs.

2.3 Synthesis of metal nanoparticles from metal carbonyls

The use of binary metal carbonyls for the synthesis of metal nanoparticles is sensible and logical. Metal carbonyls are commercially available (Table 3). $Fe(CO)_5$ and $Ni(CO)_4$ are industrially produced on a multi-ton scale.[49] Compounds $M_x(CO)_y$ are easily purifyable and handable, even if care should be exerted for the possible liberation of poisonous CO. The metal carbonyls contain the metal atoms already in the zero-valent oxidation state needed for M-NPs. No reducing agent is necessary. The side product CO is largely given off to the gas phase and removed from the dispersion. Contamination from by- or decomposition products, which are otherwise generated during the M-NP synthesis (see below), are greatly reduced. Thus, metal carbonyls were used early on for the preparation of M-NPs. It will be evident from the following examples that all these metal nanoparticles which were prepared in the condensed phase needed stabilization through additional ligands, like dispersants, surfactants or through passivation with a metal-oxide shell. Also the majority of the work uses the metal carbonyls $Fe(CO)_5$ and $Co_2(CO)_8$. The following excerpts from the literature are roughly arranged in chronological order according to the year of publication. Much of the work on Fe- or Co-NPs at large is devoted to their magnetism.[50]

Table 3. Binary metal carbonyls.[a]

Group	5	6	7	8	9	10
Metal	V, Nb, Ta	Cr, Mo, W	Mn, Tc, Re	Fe, Ru, Os	Co, Rh, Ir	Ni, Pd, Pt
mononuclear complexes	$V(CO)_6$	**$Cr(CO)_6$** **$Mo(CO)_6$** **$W(CO)_6$**		**$Fe(CO)_5$** $Ru(CO)_5$ $Os(CO)_5$		**$Ni(CO)_4$**
polynuclear complexes			**$Mn_2(CO)_{10}$** $Tc_2(CO)_{10}$ **$Re_2(CO)_{10}$**	**$Fe_2(CO)_9$** **$Fe_3(CO)_{12}$** $Ru_2(CO)_9$ **$Ru_3(CO)_{12}$** $Os_2(CO)_9$ **$Os_3(CO)_{12}$**	**$Co_2(CO)_8$** **$Co_4(CO)_{12}$** **$Rh_4(CO)_{12}$** **$Rh_6(CO)_{16}$** **$Ir_4(CO_{12}$**	

[a] Metal carbonyls given in bold were confirmed to be commercially available, e.g., from Aldrich, ABCR or Acros.

In early reports Hess and Parker (1966)[51] and Thomas (1966)[52] described processes for preparing metallic cobalt particles of uniform size in the 10-1000 Å range (0.1-100 nm). Dicobalt octacarbonyl $Co_2(CO)_8$ was thermally decomposed in typcially toluene solutions of dispersant polymers, such as methyl methacrylate-ethyl acrylate-vinylpyrrolidone terpolymers, high-purity polystyrene, styrene-acrylonitrile polymers, polyacrylonitril, chloropolyethylene sulfonamide, polyester and polyether urethanes to form stable colloids of discrete particles which are separated by polymer coatings. Variation of polymer composition, molecular weight and solvent used results in a variation of particle size and colloid stability. Preparation of single-domain ferromagnetic cobalt particles with good magnetic properties was possible through a balance between dispersant polymer, solvent, and the growing metal particle.[51]

Papirer et al. (1983) prepared a stable suspension of metallic cobalt particles in an organic solvent (ferrofluid) by decomposition of $Co_2(CO)_8$.[53,54] The cobalt particles originate from the thermolysis of the dicobalt octacarbonyl solution in the presence of a chosen surface active agent. The reaction temperature, the nature of the solvent and of the surfactant, the weight ratio of carbonyl and surfactant, and the initial concentration of the cobalt carbonyl solution were varied. Spherical particles, of a narrow size distribution, are obtained when the decomposition of $Co_2(CO)_8$ is carried out in an aromatic solvent above 110 °C and in the presence of a surfactant possessing a long hydrocarbon chain and a strong ionic group (sulfonate). The decomposition in toluene, in which ethyl (2-hexyl) sodium sulfo-succinate is dissolved, leads to particles of about 70 Å in diameter. When a ferrofluid is being formed, an initial and rapid evolution of CO corresponding to the formation of $Co_4(CO)_{12}$ is recorded. Part of this compound is insoluble in the reaction medium and appears to be a regulating intermediate. After this short initial stage the rate of decomposition of $Co_4(CO)_{12}$ slows down and becomes practically constant. Later the CO formation is accelerated again and finally it decreases as the reaction goes to completion. This S-shaped curve which describes the decomposition of $Co_2(CO)_8$ is always observed when a ferrofluid is in progress of formation.[53] The diameters of the particles, and the number of growing particles have been measured using also small-angle X-ray scattering and magnetic methods. The presence of microreactors in the reaction medium and a diffusion controlled growth mechanism are seen as the responsible two factors for the formation of particles of very narrow size distribution.[54]

Suslick et al. (1996) reported the synthesis of "monosized" iron nanoparticles from 3 to 8 nm (amorphous according to electron microdiffraction) through the sonochemical

decomposition of iron pentacarbonyl, $Fe(CO)_5$ in octanol or hexadecane in the presence of polyvinylpyrrolidone (PVP) or oleic acid, respectively, as a stabilizer.[55]

Platonova et al. (1996) obtained Co nanoparticles in polystyrene(PS)-poly-4-vinyl-pyridine (PVP) micelles by thermal decomposition of $Co_2(CO)_8$ in micellar solutions of such block copolymers. Co particles are effectively stabilized by the block copolymer matrix and do not aggregate. Thermal treatment of such dried polymers at 200 °C for 2 h leads to spherical particles of 3-5 nm in size. The polymeric hybrid materials displayed remarkably high values of magnetization at rather low Co contents in the polymer.[56]

Lee et al. (1998) produced nanoparticles of iron, chromium, molybdenum and tungsten by laser decomposition of the corresponding metal carbonyls with a 10.6 μm CO_2 laser in the presence of Ar and SF_6.[57] Argon helped to increase the purity of the metal clusters by suppressing the formation of $(M)_x(CO)_y$ for M = Cr, Mo, W). SF_6 acted as an infrared photosensitizer, which initially absorbed the 10.6 μm IR photons from the CO_2 laser and transferred its energy to a metal carbonyl via collisions. The M-NP size distributions were narrow and the average diameter was 6, 3.5, 2 and ~1 nm for Fe, Cr, Mo and W clusters, respectively, as determined by TEM. The structure was found to be bcc for both Fe and Cr clusters, fcc for Mo clusters, and amorphous for W clusters as determined from the X-ray diffraction patterns (note that all the bulk metals have bcc structure). The cluster size (n) in one cluster of average diameter was estimated by assuming a spherical shape such that n = (cluster volume/atomic volume) × packing fraction = $(r/r_0)^3 f$, with r the cluster radius, r_0 the atomic radius and f the packing fraction (0.68 for bcc and 0.74 for fcc). Considering the cluster sizes (n = 9630, 1870, 230 and ~30 for Fe-, Cr-, Mo- and W-NPs, respectively) estimated from their average diameters, it was found likely that there exists a structural transition from fcc to bulk bcc with increasing cluster size in these metal clusters.[57]

Dinega and Bawendi (1999) used the kinetic control of crystal growth in the presence of a coordinating ligand for the formation of a new structure of elemental cobalt (ε-cobalt), which was discovered upon analyzing the metallic powder produced by the thermal decomposition of $Co_2(CO)_8$ in solution in the presence of trioctylphosphane oxide.[58]

Giersig and Hilgendorff (1999) prepared cobalt nanoparticles by thermolysis of $Co_2(CO)_8$ in Ar-saturated toluene as an organic carrier at 110 °C in the presence of two different surfactants. The surfactants used were sodium bis 2-(ethyl-hexyl)sulfosuccinate and oleoylsarcosine. The magnetic nanoparticles were then ordered into a two-dimensional array using a magnetophoretic technique. The quality of the ordering was observed by electron microscopy and the lattice constants determined by electron diffraction. It could be shown

that the cobalt particles condense into a hexagonal close packed array.[59] These arrays of monodisperse colloidal 11.4-nm Co nanoparticles were investigated by multifrequency ferromagnetic resonance and x-ray magnetic circular dichroism (XMCD) to determine the ratio of orbital-to-spin magnetic moment as μ_L/μ_S^{eff}=0.24±0.06 by XMCD.[60]

Van Wonterghem, Mørup et al. (1985, 1988),[61,62] Pathmamanoharan et al. (2000),[63] Gossens et al. (2002)[64] and Butter, Philipse et al. (2003)[65] formed iron nanoparticles by thermolysis of $Fe(CO)_5$ in decalin with modified polyisobutene and oleic acid as stabilizers. The magnetic Fe-NPs are fairly monodisperse even for particle radii below 10 nm. The particle size can be increased by seeded growth, and the particle shape can be changed by using a mercaptan stabilizer, which leads to rod-like iron colloids. The thermal decomposition of iron pentacarbonyl in a mixture of decalin and sarkosyl-O (*n*-oleyoyl sarcosine) has been studied by Moessbauer spectroscopy. Together the X-ray diffraction it was shown that the sample contained small particles of a metallic glass (amorphous material). Annealing of the particles at 523 K resulted in crystallization of the particles into a mixture of α-Fe and Fe_5C_2.[61] Fe^{2+} was found in all samples. After some time of reaction, a new iron carbonyl complex appeared. During the final stages of the reaction, this intermediate carbonyl complex decomposed, and ultrafine particles of an amorphous $Fe_{100-x}C_x$ alloy were formed.[62] Moessbauer spectroscopy also showed that the Fe-NPs with r = 5.3, 6.9 and 8.2 nm are dominated by the broadened sextuplet with H_{eff} =262 kOe similar to that found in the sarcosyl and oleic acid stabilized colloids. This hyperfine field characterizes $Fe_{1-x}C_x$ species with $x \approx 0.25$ by comparison with sputtered amorphous $Fe_{1-x}C_x$ films.[66] In addition, a small contribution of a sextuplet with H_{eff} = 496 kOe characterising an Fe(III) oxidic contribution is visible in the spectra of the Fe-NPs with r = 5.3 and 6.9 nm. This Fe(III) oxidic contribution is absent for the largest NP with r = 8.2 nm, while the spectrum of the NPs with the smallest radius (r = 2.1 nm) turned out to be completely oxidic.[64]

Huh et al. combined a thermal decomposition of metal carbonyls with a collision induced clustering. Metal carbonyls $Fe(CO)_5$ and $Mo(CO)_6$ were thermally decomposed with a hot filament and resultant bare metal atoms underwent collisions to produce high purity Fe, Mo, and alloy Fe/Mo nanometer size metal particles.[67]

Park, Hyeon et al. (2000) prepared monodisperse 2 nm spherical iron nanoparticles by the thermal decomposition of $Fe(CO)_5$ in the presence of the stabilizing surfactant trioctylphosphine oxide (TOPO). Subsequently, nearly uniform rodshaped iron nanoparticles were then obtained from the controlled growth of these monodisperse spherical nanoparticles.[68]

By thermal decomposition of $Fe(CO)_5$ with simultaneous reduction of platinum acetylacetonate $Pt(acac)_2$ in the presence of oleic acid and oleyl amine Sun, Murray et al. (2000) synthesized monodisperse iron–platinum nanoparticles.[69] Chen and Nikles (2002) used this procedure for the preparation of FePd and FeCoPt alloy nanoparticles with very narrow size distribution, using $Fe(CO)_5$, $Pd(acac)_2$ or $Pt(acac)_2$ and $Co(acac)_2$.[70,71]

From $Co_2(CO)_8$ and $Pt(hfac)_2$ in hot toluene and oleic acid very small and monodisperse $CoPt_3$ alloy nanoparticles with 1.8(1) nm were obtained by Park and Cheon (2001).[72]

Puntes, Krishnan and Alivisatos (2001) reported the synthesis of monodisperse ε-Co nanoparticles with spherical shapes and sizes ranging from 3 to 17 nm by the rapid pyrolysis of a dicobalt octacarbonyl solution in dichlorobenzene in the presence of a surfactant mixture composed of oleic acid, lauric acid and trioctylphosphine. The size distribution and the shape of the nanocrystals were controlled by varying the surfactant (oleic acid, phosphonic oxides and acids, etc.) its concentration, and the reaction temperature.[73]

Hyeon et al. (2001) utilized a high-temperature (300 °C) aging of an iron-oleic acid metal complex, which was in turn prepared by the thermal decomposition of iron pentacarbonyl in the presence of oleic acid at 100 °C to generate monodisperse iron nanoparticles. The Fe-NP particle size ranged from 4 to 20 nm. The resulting iron nanoparticles were then transformed to monodisperse γ-Fe_2O_3 nanocrystallites by controlled oxidation using trimethylamine oxide as a mild oxidant.[74] With a similar procedure Kim, Hyeon et al. (2001) prepared cobalt nanoparticles from $Co_2(CO)_8$, oleic acid, trioctylphosphine and dioctyl ether under reflux. The Co-NPs were applied as recyclable catalysts for Pauson–Khand reactions, which involve the cycloaddition of alkynes, alkenes and carbon monoxide to cyclopentenones.[75]

Burke, Stöver et al. (2002) prepared polymer-coated iron nanoparticles by the thermal decomposition of $Fe(CO)_5$ in the presence of ammonia and polymeric dispersants.[76] The dispersants consist of polyisobutylene (PIB), polyethylene, or polystyrene chains functionalized with tetraethylenepentamine, a short polyethyleneimine chain. Inorganic-organic core-shell nanoparticles were formed with all three types of dispersants. With the PIB dispersants, the particle size is determined, in part, by the iron pentacarbonyl loading, increasing from 8 ± 1 nm for a 1:1 $Fe(CO)_5$/dispersant ratio to 20 ± 4 nm for a 5.5:1 ratio.[76]

Butter et al. (2002) studied the preparation and properties of metallic iron particles, synthesized by thermal decomposition of $Fe(CO)_5$ in the presence of the stabilizer modified polyisobutylene. By varying the iron carbonyl/polymer ratio, the particle size could be varied

from 2 to 10 nm. Particles were characterized by magnetization measurements, transmission electron microscopy (TEM), small angle X-ray scattering and cryo-TEM. Cryo-TEM pictures show linear structures of the larger particles as a consequence of magnetic interaction. From susceptibility measurements, it is seen that particles oxidize fast on exposure to air.[77]

Rutnakornpituk, Riffle et al. (2002) use copolymers as micelles in toluene to serve as nanoreactors for the thermal decomposition of $Co_2(CO)_8$ to superparamagnetic Co-NP dispersions. The steric stabilizers are poly[dimethylsiloxane-*b*-(3-cyanopropyl)methyl-siloxane-*b*-dimethylsiloxane] (PDMS-PCPMS-PDMS) triblock copolymers in poly-(dimethylsiloxane) carrier fluids. The nitrile groups on the PCPMS central blocks are thought to adsorb onto the particle surface. The Co-NP size could be controlled by adjusting the Co-to-copolymer ratio. TEM showed non-aggregated Co-NPs with narrow size distributions and evenly surrounded by the copolymer sheaths.[78]

Diana et al. (2003) synthesized cobalt nanoparticles within inverse micelles of polystyrene-*block*-poly(2-vinylpyridine) copolymer in toluene by the pyrolysis of $Co_2(CO)_8$ at 115 °C.[79] The nanoparticle structure at different reaction times was investigated using transmission electron microscopy and Fourier transform infrared spectroscopy (FT-IR). At early reaction stages, the nanoparticles were found to be noncrystalline from TEM, and FT-IR showed that the precursor was only partially decomposed. After 15 min of reaction, the nanoparticles became crystalline, forming chains due to magnetic interactions. The noncrystalline nanoparticles could be crystallized upon heating to 420 °C on grids in the transmission electron microscope. This produced nearly monodisperse single nanocrystals inside each micelle, with limited aggregation, but such annealing led to the degradation of the polymer.[79]

Bönnemann, Behrens et al. (2003-2007) obtained monodisperse Co, Fe, and FeCo nanoparticles through thermal decomposition of the metal carbonyls $Co_2(CO)_8$, $Fe(CO)_5$ or $Fe(CO)_5/Co_2(CO)_8$ in the presence of aluminium alkyls (AlR_3), as air-stable magnetic metal nanoparticles after surface passivation.[80-83] After decomposition the metal particles were treated with synthetic air through a thin capillary (*smooth oxidation*) (Scheme 5) to yield particles stable in air under ambient conditions for over one year, as confirmed by magnetic measurements.

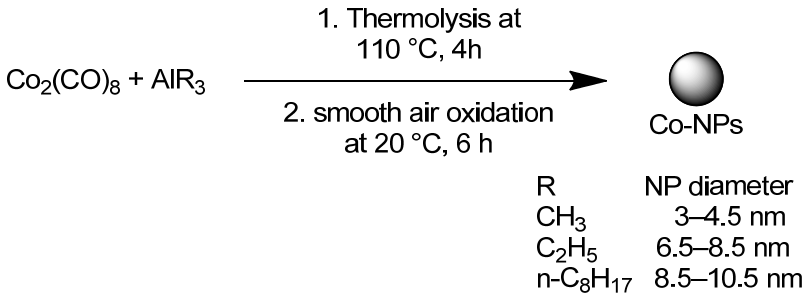

Scheme 5. Thermolysis of $Co_2(CO)_8$ in the presence of aluminium alkyls to Co-NPs and smooth air oxidation for surface passivation.

The aluminium alkyl acts as a catalyst, activating the thermal decomposition of the metal carbonyl as well as the surface passivation during the *smooth oxidation*. The resulting particles strongly depend on the alkyl chain length *R* of the aluminium alkyl and the $Co_2(CO)_8$ to AlR_3 ratio. Monodisperse Co nanoparticles, 3–4.5 nm, 6.5–8.5 nm to 8.5–10.5 nm in diameter, were obtained for $Al(CH_3)_3$, $Al(C_2H_5)_3$, and $Al(C_8H_{17})_3$, respectively.[81] The particles were characterized by electron microscopy (SEM, TEM, ESI), electron spectroscopy (MIES, UPS, and XPS) and X-ray absorption spectroscopy (EXAFS). EXAFS measurements showed that this preparation pathway provides long term stable zerovalent magnetic cobalt particles. The chemical nature of the surfactant used exerts a significant influence on the stability and the local electronic and geometric structure of the analyzed nanoparticles.[80] With the help of surfactants, for instance oleic acid or cashew nut shell liquid, the metal particles can be peptized in organic solvents like toluene or kerosene, resulting in magnetic fluids. The saturation of magnetization, *M*s, of the fluids was determined by specific magnetization. The sizes and structure of the particles were investigated by transmission electron microscopy, and Moessbauer analysis showed that the core of the particles was metallic or alloyed, respectively. The particle surface termination was studied by X-ray photoelectron and Auger electron spectroscopy.[81] The particles were also peptized by surfactants to form stable magnetic fluids in various organic media and water, exhibiting a high volume concentration and a high saturation magnetization. In view of potential biomedical applications of the particles, several procedures for surface modification are possible, including peptization by functional organic molecules, silanization, and *in situ* polymerization.[81] Other procedures for surface modification of these pre-stabilized, metallic Co-NPs include direct anchoring of surface-active functional groups and biocompatible dextran layers as well as silica and polymer coatings. As a result, individually coated nanoparticles as well as microspheres can be obtained.[83]

Yin, Alivisatos et al. (2004) formed a Pt@CoO yolk-shell nanostructure in which a platinum nanocrystal of a few nanometers was encapsulated in a CoO shell.[84] This was achieved by first reducing platinum acetylacetonate with a longchain polyol to form uniform platinum nanoparticles in the presence of surfactants such as oleic acid, oleylamine, and trioctylphosphine. The size of the platinum particles was tuned from 1 to 10 nm, depending on the concentration of surfactants. $Co_2(CO)_8$ was then injected into the hot solution and decomposed to form a conformal coating on the platinum nanocrystals. Oxidation of the Pt@Co nanocrystals was performed a few minutes after introduction of the cobalt carbonyl by blowing a stream of O_2/Ar mixture into the colloidal solution at 455 K.[84]

Zubris, King, Tannenbaum et al. (2005) describe the synthesis of iron and cobalt alloy nanoparticles by the co-decomposition of iron and cobalt carbonyl precursors in the presence of polystyrene as a surface stabilizing agent.[85] The decomposition kinetics of the $Fe(CO)_5$ and $Co_2(CO)_8$ were established and controlled. The results suggest that $Fe(CO)_5$ decomposition is a higher-order process (not first-order as previously assumed), with a complicated intermediate mechanism. Equal initial concentrations of both precursors generated nanoalloys with a crystalline core–shell dense morphology, while precursor concentrations corresponding to initial equal rates of decomposition generated polycrystalline nanoalloys with a diffuse morphology.[85]

Hütten et al. (2005) prepared ferromagnetic FeCo-alloyed nanoparticles from the two precursors $Co_2(CO)_8$ and $Fe(CO)_5$ aiming for a Fe to Co ratio of 50:50.[86] Characterization of the alloyed nanoparticles utilized high-resolution transmission electron microscopy and dispersive X-ray analyses.[87]

Korth, Pyun et al. (2006) synthesized polystyrene (PS)-coated cobalt nanoparticles by the thermolysis of $Co_2(CO)_8$ in the presence of end-functional polymeric surfactants in refluxing 1,2-dichlorobenzene.[88] A mixture of amine and phosphine oxide PS surfactants (4:1 wt ratio) was used in the thermolysis of $Co_2(CO)_8$ to prepare polymer-coated cobalt nanoparticles, where the ligating end group passivated the colloidal surface. The combination of both amine and phosphine oxide ligands on the PS chain was found necessary to yield uniform ferromagnetic nanoparticles. These polymer-coated cobalt nanoparticles (PS-Co) were then characterized using TEM, atomic force microscopy (AFM), and magnetic force microscopy (MFM) to determine particle size and morphology of magnetic colloids and nanoparticle chains.[88]

It is obvious that the use of metal carbonyls for M-NP preparation will also be noted in the patent literature. An example is given by Mercuri (2007), describing "a process for

producing nano-scale metal particles which includes feeding at least one metal carbonyl into a reactor vessel; exposing the metal carbonyl to a source of energy sufficient to decompose the metal carbonyl to produce nano-scale metal particles; and depositing or collecting the metal nanoparticles. Oxygen is fed into the reactor vessel to partially oxidize the nanoscale metal particles produced by decomposition of the decomposable moiety. The nanoscale metal particles are then brought onto an end-use substrate which are intended to be employed, such as the aluminum oxide or other components of an automotive catalytic converter, or the electrode or membrane of a fuel cell or electrolysis cell".[89,90]

Gergely et al. describe "a process for preparing superparamagnetic transition metal nanoparticles by introducing into a gas stream a hydrocarbon and a transition metal carboxyl wherein the transition metal carbonyl is introduced downstream from the hydrocarbon; wherein at the point of introduction of the hydrocarbon the gas stream is as a plasma, and wherein at the point of introduction of the transition metal carbonyl the gas stream is at a temperature of at least 1000 °C, followed by quenching to form C-coated transition metal nanoparticles; and wherein the gas stream consists essentially of at least one inert gas and H".[91]

Gürler, Schmidt et al. (2008) showed that hydroxyfunctional cobalt nanoparticles can be obtained in a single step by thermal decomposition of $Co_2(CO)_8$ in the presence of ricinolic acid as a functional surfactant. The chemisorbed ricinolic acid through the carboxylic acid group served to introduce hydroxyl groups that serve as an initiator for the ring-opening polymerization of 3-caprolactone to give the desired hybrid cobalt/polycaprolactone brush particles.[92]

Doan, Johans et al. (2010) investigated the oxidation of Co nanoparticles stabilized with various ligands in an autoclave.[93] Tridodecylamine stabilized Co nanoparticles with different sizes (8 nm, 22 nm and 36 nm) were prepared by thermal decomposition of $Co_2(CO)_8$ in dodecane. The oxidation of the particles was studied by introducing oxygen into the autoclave and following the oxygen consumption with a pressure meter. Tridodecylamine capped particles were initially oxidized at a high rate, however, the oxidation layer quickly inhibited further oxidation. The thickness of the oxide layer estimated from the oxygen consumption was 0.8 nm for all three particle sizes showing that the oxidation is size independent in the studied particle size range. The tridodecylamine ligand was exchanged for various long chain carboxylic acids followed by subsequent oxidation. With the carboxylic acids the formed oxide layer does not inhibit further oxidation as effectively as in the case of tridodecylamine. TEM studies show that tridodecylamine capping leads to particles with a

metal core surrounded by an oxide layer, while particles capped with long chain carboxylic acids form hollow cobalt oxide shells.[93]

The aforementioned examples together with reviews on the chemical synthesis of metal nanoparticles[50] illustrate the wide applicability of $Fe(CO)_5$ and $Co_2(CO)_8$ for the preparation of iron- and cobalt-containing nanoparticles. Yet, it is also evident that the utilization of metal carbonyls in nanoparticle synthesis is largely limited to these two carbonyl compounds. This may in part be due to the strong interest in magnetic M-NPs. It also becomes clear that the prepared M-NPs need a protecting layer to prevent aggregation to larger particles or oxidation.

2.4 Synthesis of metal nanoparticles in ionic liquids

Metal nanoparticles can be synthesized in ILs[94] through chemical reduction[23,95-99] or decomposition,[100,134,143,147] by means of photochemical reduction[101,102] or electro-reduction[103-105] of metal salts where the metal atom is in a formally positive oxidation state and by decomposition of metal carbonyls with zero-valent metal atoms[11,22,23,106] without the need of extra stabilizing molecules or organic solvents.[7,13,15,107,108]

A myriad of M-NPs have been prepared in ILs from compounds with the metal in a formally positive oxidation state M^{n+}. Such M-NPs then include, for example, the main-group metals and metalloids Al,[109] Te,[110] and the transition metals Ru,[111] Rh,[98] Ir,[112] Pt,[113] Ag,[95,114] Au,[115] (cf. Table 4).

The inclusion of metal nanoparticles in the supramolecular ionic liquid network brings with it the needed electrostatic and steric (= *electrosteric*) stabilization through the formation of an ion layer forming around the M-NPs. The type of this ion layer, hence, the mode of stabilization of metal nanoparticles in ILs is still a matter of some discussion.[15,135] Aside from the special case of thiol-, ether-, carboxylic acid-, amino-, hydroxyl- and other functionalized ILs (see below) one could decide between IL-cation or –anion coordination to the NP surface. Schrekker and co-workers proposed electrostatic stabilization of a negatively charged surface of Au-NPs by parallel coordination mode of the imidazolium cation on the basis of surface-enhanced Raman spectroscopy (SERS) studies.[116] This proposal was supported by Alvarez-Puebla and co-workers who found a negative zeta potential of M-NPs

prepared by chemical reduction processes which indicated a negative charge of such NPs in aqueous solutions.[117]

According to DLVO (Derjaugin-Landau-Verwey-Overbeek) theory (see chapter 1.5),[118] ILs provide an electrostatic protection in the form of a "protective shell" for M-NPs.[107,119-123] DLVO theory predicts that and the first inner shell must be anionic and the anion charges should be the primary source of stabilization for the electrophilic metal nanocluster.[118] DLVO theory treats anions as ideal point charges. Real-life anions with a molecular volume would be better classified as "*electrosteric* stabilizers" meaning to combine both the *electro*static and the *steric* stabilization. However, the term "electrosteric" is contentious and ill-defined.[124] The stabilization of metal nanoclusters in ILs could, thus, be attributed to "extra-DLVO" forces[124] which includes effects from the network properties of ILs such as hydrogen bonding, the hydrophobicity and steric interactions.[2,125]

Density functional theory (DFT) calculations in a gas phase model favor interactions between IL anions, such as BF_4^-, instead of imidazolium cations and Au_n clusters (n = 1, 2, 3, 6, 19, 20). This suggests a Au···F interaction and anionic Au_n stabilization in fluorous ILs. A small and Au-concentration dependent ^{19}F-NMR chemical shift difference (not seen in ^{11}B -or ^{1}H-NMR) for Au-NP/$BMIm^+BF_4^-$ supports the notion of a BF_4^--fluorine···Au-NP contact seen as crucial for the NP stabilization in dynamic ILs.[126] The DFT study used the binding energy (BE) of different IL-ions, free bases and the Cl^- anion to gold clusters of various sizes as a relative measure for the interaction strength The BE is defined as the difference of the relaxed energies of the gas phase anions and the Au_n clusters to the energy of their adduct (Eqn. 1).[126,137]

$$\mathrm{BE} = \mathrm{E(anion)} + \mathrm{E}(Au_n) - \mathrm{E(anion\ adduct\ to}\ Au_n) \quad (1)$$

Fig. 1 shows the Au_n–IL anion binding configurations and the variation of the BE with cluster size *n*. Fig. 2 illustrates Au_n–substrate binding configurations and the variation of the BE with cluster size *n* for BF_4^- in comparison with other common substrate ligands. The BE of $BMIm^+$ is found to be very weak and not shown.[126,137] BE comparison with chloride, citrate, PH_3 and H_2O illustrates the critical influence of the ionic charge and electron delocalization from the ligand to Au_n (Fig. 4). The softer the anion or ligand, that is, the more charge transfer or electron delocalization (according to Pearsons hard-soft concept and the nephelauxetic series)[127] to Au_n is possible, the better the stabilizing effect. H_2O as a hard and neutral ligand offers the least stabilization, hence, reduction of gold salts by $SnCl_2$ in water

led immediately to the red purple solution (known as the Purple of Cassius). Remarkably, the relatively soft chloride anion shows the largest BE in agreement with the strong covalent binding of chloride ions to the Au(111) surface found in recent DFT simulations.[128]

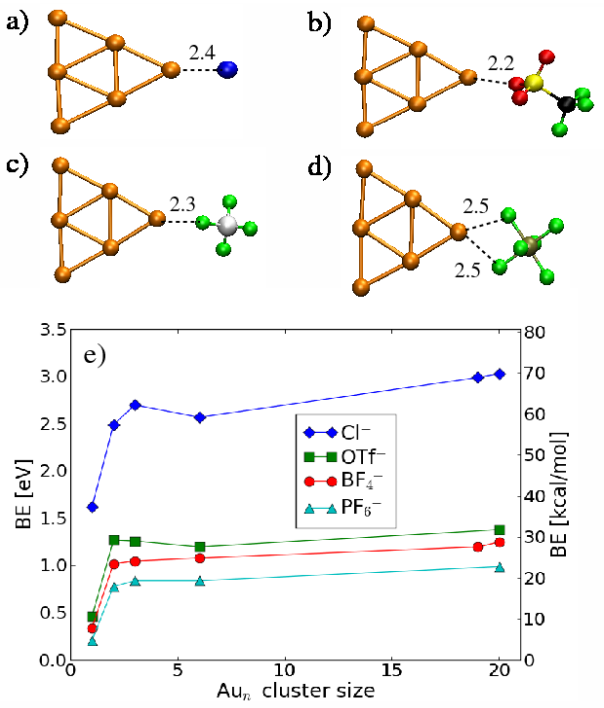

Fig. 1. Relaxed configurations of Au6 bound to a) Cl^-, b) TfO^-, c) BF_4^- and d) PF_6^-. The bond lengths are given in Å. e) Binding energy. All the anions show a similar behavior in their BE: The BE to a single gold atom n = 1 is quite low and more than doubles for Au_2 (n = 2). Increasing the cluster size to n = 20 does not change the BE substantially anymore, i.e., the BE is already saturated for Au_2. the chloride anion shows the largest BE of all anions and can, hence, be expected to be bound to the clusters if it is present in the dispersion.[126]

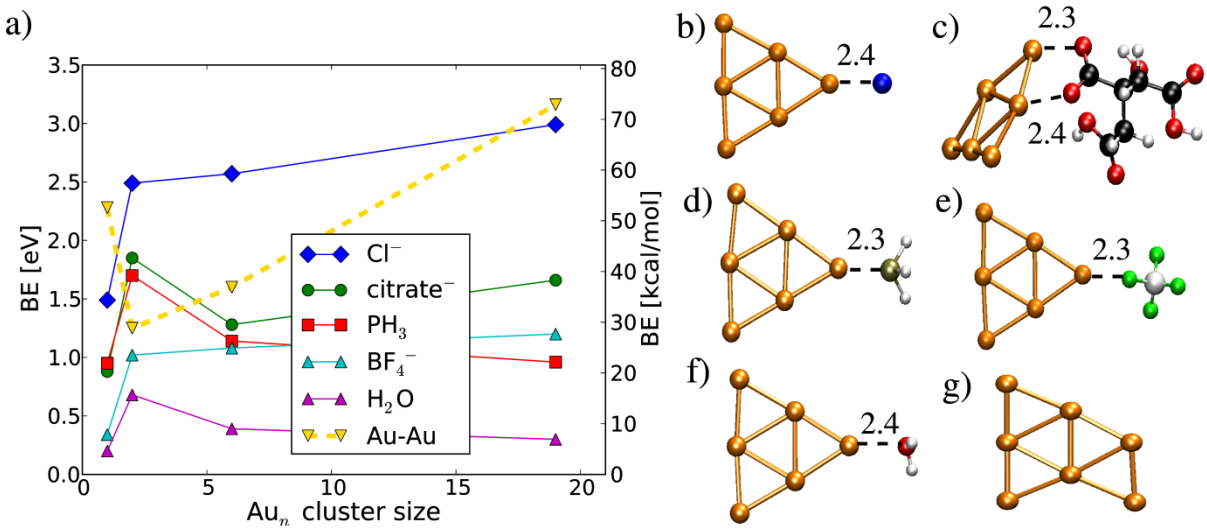

Fig. 2. (a) Binding energies (BE) and Au-atom addition energies depending on the cluster size. (b–f) Relaxed configurations of Au_6 bound to (b) Cl^-, (c) citrate$^-$ ($C_6H_7O_7^-$), (d) PH_3, (e) BF_4^- and (f) H_2O. (g) Relaxed configuration of Au_7. The bond lengths are given in Å.

The DFT calculations also indicate a weak covalent part in this Au···F interaction. Free imidazole bases (e.g. 1-methylimidazole) show similar binding energies. The Cl^- anions are found to have the highest binding energy and can therefore be expected to bind to the NP if present in the solution. At the same time no significant binding of the $BMIm^+$ or MIm^+ imidazolium cations is found. These findings support the model of preferred interaction between anions and Au-NPs, but also confirm the importance to consider a possible presence of Cl^- anions in the ionic liquid solution.[126,137]

Compared with the unfunctionalized imidazolium-ILs (cf. Scheme 3), functionalized imidazolium-ILs stabilize aqueous dispersed metal NPs much more efficiently because of the special functional group. Thiol-,[115,129,130] ether-,[116] carboxylic acid-,[135] amino-,[131,135] and hydroxyl-functionalized[129] imidazolium-ILs (Scheme 6) have been used to synthesize aqueous dispersed noble, primarily gold metal NPs.

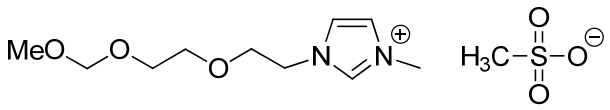

1-triethylene glycol monomethyl ether-3 methyl-imidazolium methylsulfonate

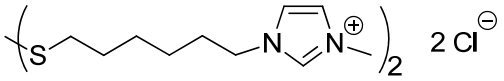

3.3'-[disulfanylbis(hexane-1,6-diyl)]-bis(1-methylimidazolium) dichloride

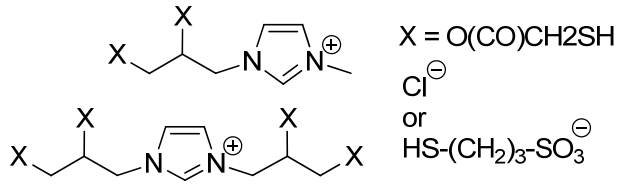

thiol-functionalized imidazolium ILs (HSIm+),
e.g., 1-(2',3'-dimercaptoacetoxypropyl)-3-methylimidazolium

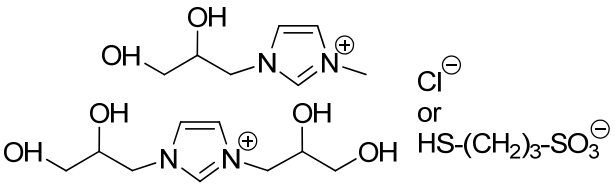

hydroxy-functionalized imidazolium ILs (HOIm+),
e.g., 1-(2',3'-dihydroxypropyl)-3-methylimidazolium

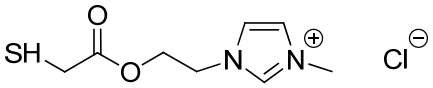

1-methyl-3-(2'-mercaptoacetoxyethyl)imidazolium chloride

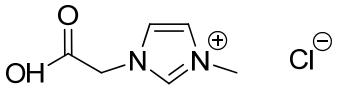

1-carboxymethyl-3-methylimidazolium chloride

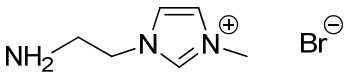

1-aminoethyl-3-methylimidazolium bromide

Scheme 6. Examples of functionalized imidazolium-ILs.[115,116,129-131,135]

2.4.1 Chemical reduction

The reduction of metal salts is the most utilized method to generate NPs in solution and also in ILs in general. Many different types of reducing agents are used, like gases (H_2), organic (citrate, ascorbic acid, imidazolium cation of IL) and inorganic ($NaBH_4$, $SnCl_2$) agents.

Table 4. Examples of M-NPs prepared in ILs by chemical reduction.

Metal	Metal salt precursor	Reducing agent	IL [a]	M-NP size, average ∅ (standard deviations) [nm]	Ref.
Ru	Ru(COD)(COT)	H_2	$BMIm^+Tf_2N^-$	0.9-2.4	96
	Ru(COD)(COT)	H_2	$BMIm^+BF_4^-$, $BMIm^+PF_6^-$, $BMIm^+TfO^-$	2.6(4)	111
Rh	$RhCl_3 \times 3H_2O$	H_2	$BMIm^+PF_6^-$	2.0-2.5	98
	[Rh(COD)-μ-Cl]$_2$	H_2 + laser radiation	$BMIm^+PF_6^-$	7.2(1.3)	132
Ir	[Ir(COD)Cl]$_2$	H_2	$BMIm^+BF_4^-$, $BMIm^+PF_6^-$, $BMIm^+TfO^-$	2-3	133
	[Ir(COD)$_2$]BF_4, [Ir(COD)Cl]$_2$	H_2	1-alkyl-3-methyl-$Im^+BF_4^-$	irregular 1.9(4), 3.6(9)	43
Pd	H_2PdCl_4	$NaBH_4$	$HSCO_2Im^+Cl^-$ [e]	nanowires	130
	$PdCl_2$	H_2 + laser radiation	$BMIm^+PF_6^-$	4.2(8)	132
	Pd(acac)$_2$	H_2	$BMIm^+PF_6^-$	10(2)	134
Pt	$Na_2Pt(OH)_6$	$NaBH_4$	$HSIm^+A^-$ or $HOIm^+A^-$ [d]	3.2(1.1), 2.2(2), 2.0(1)	129
	H_2PtCl_6	$NaBH_4$	$CMMIm^+Cl^-$ [f], $AEMIm^+Br^-$ [g]	2.5	135
	PtO_2	H_2	$BMIm^+BF_4^-$, $BMIm^+PF_6^-$	2-3	136
Ag	$AgBF_4$	H_2	$BMIm^+BF_4^-$	2.8	96
			$BMIm^+PF_6^-$	4.4	96
			$BMIm^+TfO^-$	8.7	96
			$BtMA^+Tf_2N^-$	26.1	96

Au	$KAuCl_4$	$SnCl_2$	$BMIm^+BF_4^-$	2.6-200	137
	$HAuCl_4$	Na_3citrate/ $NaBH_4$	$EMIm^+EtSO_4^-$	9.4	139
		Na_3citrate	$EMIm^+EtSO_4^-$	3.9	139
		ascorbic acid	$EMIm^+EtSO_4^-$	nanorods	139
	$HAuCl_4 \times 3H_2O$	$H_2NNH_2 \times H_2O$ (hydrazine monohydrate)	$TriMIm^+MeSO_3^-$ [a]	~7.5	116
	$HAuCl_4$	$NaBH_4$	$ShexMIm^+Cl^-$ [c]	5.0	115
	$HAuCl_4$	$NaBH_4$	$HSIm^+A^-$ or $HOIm^+A^-$ [d]	3.5(7), 3.1(5), 2.0(1)	129
	$HAuCl_4$	$NaBH_4$	$CMMIm^+Cl^-$ [f], $AEMIm^+Br^-$ [g]	3.5	135
	$HAuCl_4$	Na_3citrate	$CMMIm^+Cl^-$ [f], $AEMIm^+Br^-$ [g]	23-98	135
	$HAuCl_4$	cellulose	$BMIm^+Cl^-$	300-800	99

[a] common ILs: $BMIm^+BF_4^-$, $BMIm^+PF_6^-$, $BMIm^+TfO^-$ = 1-*n*-butyl-3-methylimidazolium tetrafluoroborate, hexafluorophosphate, trifluoromethylsulfonate, $BtMA^+Tf_2N^-$ *n*-butyl-trimethyl-ammonium bis(trifluoromethylsulfonyl)amide (cf. Scheme 2); $EMIm^+EtSO_4^-$ = 1-ethyl-3-methyl-imidazolium ethylsulfate, [b] $TriMIm^+MeSO_3^-$ = 1-triethylene glycol monomethyl ether-3-methyl-imidazolium methylsulfonate (cf. Scheme 6), [c] $ShexMIm^+Cl^-$ = 3.3'-[disulfanylbis(hexane-1,6-diyl)]-bis(1-methylimidazolium) dichloride, [d] $HSIm^+A^-$ = thiol-functionalized imidazolium ILs, e.g., 1-(2',3'-dimercaptoacetoxypropyl)-3-methylimidazolium, $HOIm^+A^-$ = hydroxy-functionalized imidazolium ILs, e.g., 1-(2',3'-dihydroxypropyl)-3-methylimidazolium, $A^- = Cl^-$ or $HS\text{-}(CH_2)_3\text{-}SO_3^-$ (cf. Scheme 5), [e] $HSCO_2Im^+Cl^-$ = 1-methyl-3-(2'-mercaptoacetoxyethyl)imidazolium chloride (cf. Scheme 5), [f] $CMMIm^+Cl^-$ = 1-carboxymethyl-3-methylimidazolium chloride (cf. Scheme 6), [g] $AEMIm^+Br^-$ = 1-aminoethyl-3-methylimidazolium bromide (cf. Scheme 6), [h] COD = 1,5-cyclo-octadiene, COT = 1,3,5-cyclooctatriene.

Molecular hydrogen (H_2) is often taken as clean reductant. Dupont et al. used $RhCl_3 \times 3H_2O$ as a precursor in $BMIm^+PF_6^-$ for the formation of Rh-NPs. For Ir-NPs the precursor $[Ir(COD)Cl]_2$ (COD = 1,5-cyclooctadiene) was reduced with H_2. The formation to M-NPs was carried out at 75 °C and 4 bar hydrogen pressure. Transmission electron microscopy (TEM) analysis showed the particle sizes of 2.0-2.5 nm.[98] Redel, Janiak and coworkers used hydrogen and $AgBF_4$ for the synthesis of Ag-NPs in different ILs. A correlation between the IL-anion molecular volume and the NP size was noted. The larger the volume of the IL-anion the larger is the size of the Ag-NPs. Thereby it was possible to form Ag-NPs in the sizes from 2.8 to 26.1 nm with a narrow size distribution.[95]

Different researchers used hydrogen as a reagent not to reduce the metal but to reduce (hydrogenate) the ligands COD and COT (COT = 1,3,5-cyclooctatriene) of an Ru(0)

organometallic precursor.[96,111] They dissolved Ru(COD)(COT) in imidazolium based ILs and heated the mixture under 4 bar of hydrogen under different conditions. Both organic ligands were reduced to cyclooctane and thereby dissociate from the already zero-valent metal atom. Cyclooctane can then be removed under reduced pressure.

It is also possible to use less-noble metals for the reduction of noble metals. The reduction of $KAuCl_4$ by $SnCl_2$ leads to the formation of Au-NPs.[137] By variation of the molar Au^{III} : Sn^{II} ratio it was possible to synthesize Au-NPs in different sizes in a stop-and-go, stepwise and "ligand-free" nucleation, nanocrystal growth process which can be stopped and resumed at different color steps and Au-NP sizes from 2.6 to 200 nm. This stepwise Au-NP formation was possible because the IL apparently acted as a *kinetically* stabilizing, dynamic molecular network in which the reduced Au^0 atoms and clusters can move by diffusion and cluster together, as verified by TEM analysis.[137]

A well-known method to generate Au-NPs was already established by Turkevich et al. in 1951.[138] The reducing agent was citrate. Bockstaller and coworkers used this method and carried out the reduction in the imidazolim-based IL 1-ethyl-3-methylimidazolium ethyl-sulfate ($EMIm^+EtSO_4^-$). Afterwards it was possible to give these particles different shapes by adding Ag^I.[139]

Taubert et al. reacted $HAuCl_4$ with cellulose.[99] Thereby cellulose has two roles: First, cellulose is the reducing agent for Au(III). Second, cellulose acts as a morphology- and size-directing agent, which drives the crystallization towards polyhedral particles or thick plates. The gold particle morphologies and sizes mainly depend on the reaction temperature. With this route it was possible to synthesize plates with a thickness from 300 nm at 110 °C to 800 nm at 200 °C.

Gold nanoparticles of 1-4 nm size could be prepared by sputter deposition of the metal onto the surface of the ionic liquid $BMIm^+BF_4^-$ to generate nanoparticles in the liquid with no additional stabilizing agents.[140] Likewise, Au-NPs were prepared by sputter deposition of Au metal in $BMIm^+PF_6^-$. The size of Au nanoparticles was increased from 2.6 to 4.8 nm by heat treatment at 373 K.[141] Sputter deposition of indium in the ionic liquids $BMIm^+BF_4^-$, $EMIm^+BF_4^-$, (1-allyl)$MIm^+BF_4^-$ and (1-allyl)(3-ethyl)$Im^+BF_4^-$ could produce stable In metal nanoparticles whose surface was covered by an amorphous In_2O_3 layer to form In/In_2O_3 core/shell particles. The size of the In core was tunable from ca. 8 to 20 nm by selecting the IL.[142]

In the presence of imidazolium-based ILs Pd-NPs from palladium(II) salts could synthesized without the need for an additional reducing agent. It is suggested that formation

of *N*-heterocyclic Pd-carbene complexes takes place as an intermediate preceding the formation of Pd-NPs (Scheme 7) which can then catalyze Suzuki C-C coupling reactions.[143,144] Pd-carbene complexes are able to catalyze the Heck reaction.[145,146]

Deshmukh et al. used $Pd(OAc)_2$ or $PdCl_2$ in the imidazolium-based ILs BBImBr or $BBImBF_4$ to irradiate the mixtures with ultrasound for 1 h. The Pd-NPs were nearly spherical and a size of 20 nm was observed.[143]

Anderson, Marr et al. formed Pd-NPs with a diameter of ~1 nm from $Pd(OAc)_2$ in $BMIm^+Tf_2N^-$ simply by heating to 80 °C in the presence of PPh_3.[147]

Ruta, Kiwi-Minsker et al. synthesized monodispersed Pd nanoparticles of 5 and 10 nm through reduction of $Pd(acac)_2$ dissolved in the hydroxyl-functionalized butyl-3-methylimidazolium bis(trifluoromethylsulfonyl)amide IL $HOBMIm^+Tf_2N^-$ by simple heating in the absence of an additional reducing agent.[134]

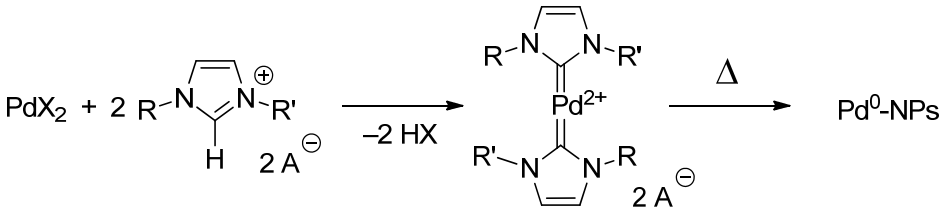

Scheme 7. Reduction of Pd(+II)-species with an imidazolium-based IL through intermediate formation of Pd-carbene complexes. Decomplexation and reduction occurs during heating.

D/H exchange reactions at C2, C4 and C5 of the imidazolium cation in catalytic hydrogenation reactions promoted by classical Ir(I) colloid precursors and Ir-NPs in deuterated imidazolium ILs supported the participation of carbene species in this media.[148]

Also by thermal decomposition, albeit from an Ni(0) source, Ni nanoparticles with 4.9(9) to 5.9(1.4) nm were prepared from the bis(1,5-cyclooctadiene)nickel(0) organometallic precursor dissolved in 1-alkyl-3-methylimidazolium bis(trifluoromethylsulfonyl)amide ionic liquids.[100]

Carboxylic acid- and amino-functionalized ionic liquids $CMMIm^+Cl^-$ = 1-carboxylmethyl-3-methylimidazolium chloride and $AEMIm^+Br^-$ = 1-aminoethyl-3-methylimidazolium bromide (cf. Scheme 6) were used as the stabilizer for the synthesis of gold and platinum metal nanoparticles in aqueous solution. Smaller Au-NPs (3.5 nm) and Pt-NPs (2.5 nm) were prepared with $NaBH_4$ as the reductant. Larger gold nanospheres (23, 42, and 98 nm) were synthesized using different quantities of trisodium citrate reductant. The morphology and the surface state of the metal nanoparticles were characterized by high-resolution transmission electron microscopy, UV-visible spectroscopy, and X-ray photoelectron

spectroscopy. X-ray photoelectron spectroscopy spectra indicated that binding energies of C 1s and N 1s from ionic liquids on the surface of metal nanoparticles shifted negatively compared with that from pure ionic liquids. The mechanism of stabilization is proposed to be due to the interactions between imidazolium ions/functional groups in ionic liquids and metal atoms. The imidazolium ring moiety of ionic liquids might interact with the π-electronic nanotube surface by virtue of cation-π and/or π-π interactions, and the functionalized group moiety of ionic liquids might interact with the metal NPs surface.[135]

2.4.2 Photochemical reduction

Photochemical methods for the synthesis of M-NPs present a rather clean procedure because contaminations by reducing agents are excluded. Zhu, Zhang et al used $HAuCl_4 \times 4 H_2O$ in a mixed solution of $BMIm^+BF_4^-$ and acetone (ratio 10:1) and irradiated the salt for 8 h with a UV light at a wave length of 254 nm. The UV light turns the acetone into a free radical, which then reduces the cationic Au^{III} to Au-NPs. The obtained Au nanosheets were about 4 µm long and 60 nm thick.[101] Firestone, Zaluzec and coworkers used this route to form Au-NPs from $HAuCl_4$ in the IL 1-decyl-3-methyl-imidazolium chloride in water. The irradiation was carried out with 254 nm UV-light for 30 to 70 min. The obtained Au-NPs were analyzed by scanning electron microscopy (SEM). The nanorods had different shapes and morphologies. The sizes varied between 100 and 1000 nm.[102] Harada, Isoda et al. used a high-pressure mercury lamp to irradiate $AgClO_4$ in a mixture of an IL, water and Tween 20 (polyoxyethylene sorbitan monolaurate). Benzoin was used as photoactivator. The average diameters of Ag-NPs prepared in water/$BMIm^+BF_4^-$ and water/$OMIm^+BF_4^-$ (1-octyl-3-methylimidazolium) microemulsions were 8.9 and 4.9 nm, respectively.[149]

2.4.3 Electroreduction

Another clean route to prepare nanoparticles is electroreduction as only electrons are used as the reducing agent. It should be noted, however, that the size of the metal nanoparticles from electroreduction is often above the 100 nm definition limit for nanoparticles.

Imanishi, Kuwabata et al. used a low-energy electron beam irradiation to synthesize Au-NPs from a $NaAuCl_4 \times 2H_2O$ precursor in the IL $BMIm^+Tf_2N^-$. The obtained particles had a large size of 122 nm.[150] It is also possible to deposite particles on supporting material. Roy,

Schmucki et al. prepared Ag-NPs from $AgBF_4$ in $BMIm^+BF_4^-$ on TiO_2. The electroreduction was performed in the high vacuum chamber of a SEM. The resulting Ag-NPs arranged themselves in a dendritic network structure.[151] Fu, Zhou and coworkers reduced graphene oxide (GO) and $HAuCl_4$ simultaneously in $BMIm^+PF_4^-$ at a potential of –2.0 V. The obtained Au-NPs on the electrochemical reduced graphene had a size of 10 nm.[152] El Abedin and Endres used Ag(TfO) as a source of silver. The precursor was electrochemically reduced in 1-ethyl-3-methylimidazolium trifluoromethylsulfonate, $EMIm^+TfO^-$. The prepared Ag nanowires were 3 μm long and 200 nm wide.[153] CuCl as precursor was used by Lu, Chen and coworkers and reduced in a cavity microelectrode in $BMIm^+PF_6^-$. The electrode potential was varied. The smallest particles had a size of 10 nm and were obtained at an electrode potential of –1.8 nm.[154]

2.4.4 Metal carbonyl precursors for metal nanoparticles in ILs

As pointed out in section 2.4.3 metal carbonyls contain the metal atoms already in the zero-valent oxidation state needed for the metal nanoparticles. No reducing agent is necessary. The side product CO is largely given off to the gas phase and removed from the M-NP/IL dispersion. The M-NP synthesis in IL from $M_x(CO)_y$ is generally carried out without any additional stabilizers, surfactants or capping molecules which is different from the use of metal carbonyls for the M-NP syntheses described in section 2.4.3.

Metal carbonyls can be decomposed to metal nanoparticles in ILs by microwave irradiation (MWI), UV-photolysis or conventional thermal heating (Fig. 3).

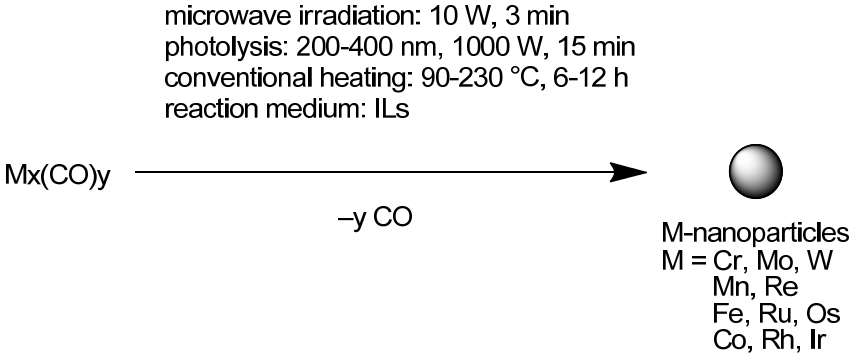

Fig. 3. M-NPs synthesis from $M_x(CO)_y$ by microwave irradiation, photolysis or conventional heating.

ILs are an especially attractive media for microwave reactions and have significant absorption efficiency for microwave energy because of their high ionic charge, high polarity and high dielectric constant.[20] Microwave heating is extremely rapid. Microwaves are a low-

frequency energy source that is remarkably adaptable to many types of chemical reactions.[155] Microwave radiation can interact directly with the reactions components, the reactant mixture absorbs the microwave energy and localized superheating occurs resulting in a fast and efficient heating time.[156,157] Using microwaves is a fast way to heat reactants compared with conventional thermal heating. Any presumptions about abnormal "microwave effects" [158-160] have been proven wrong in the meantime.[161,162] Moreover, microwave reactions are also an "instant on/instant off" energy source, significantly reducing the risk of overheating reactions.[155,156]

Metal nanoparticles were reproducibly obtained by easy, rapid (3 min) and energy-saving 10 Watt microwave irradiation (MWI) under an argon atmosphere from their metal carbonyl precursors $M_x(CO)_y$ in ILs. This MWI synthesis was compared to UV-photolytic (1000 W, 15 min) or conventional thermal decomposition (180-250 °C, 6-12 h) of $M_x(CO)_y$ in ILs. The MWI-obtained nanoparticles have a very small (< 5 nm) and uniform size and are prepared without any additional stabilizers or capping molecules as long-term stable M-NP/IL dispersions [characterization by transmission electron microscopy (TEM), transmission electron diffraction (TED) and dynamic light scattering (DLS)]

Stable chromium, molybdenum and tungsten nanoparticles could be obtained reproducibly by thermal or photolytic decomposition under argon from their mononuclear metal carbonyl precursors $M(CO)_6$ (M = Cr, Mo, W) suspended in the ionic liquids $BMIm^+BF_4^-$, $BMIm^+TfO^-$ and $BtMA^+Tf_2N^-$ (Scheme 8).[106] Later it was also shown that an even more rapid and energy-saving decomposition could be achieved with a 10 W microwave irradiation for 3 min of 0.4 ml (0.48 g) of a $BMIm^+BF_4^-$ sample with a 0.5 wt.% M/IL-dispersion.[23] The resulting Cr-, Mo- and W-NPs were of very small and uniform size of 1 to 1.5 nm in $BMIm^+BF_4^-$ (Table 5) which increases with the molecular volume of the ionic liquid anion to ~100 nm in $BtMA^+Tf_2N^-$ (Fig. 4). Characterization was done by TEM, dynamic light scattering (DLS) and transmission electron diffraction (TED) analysis.[106]

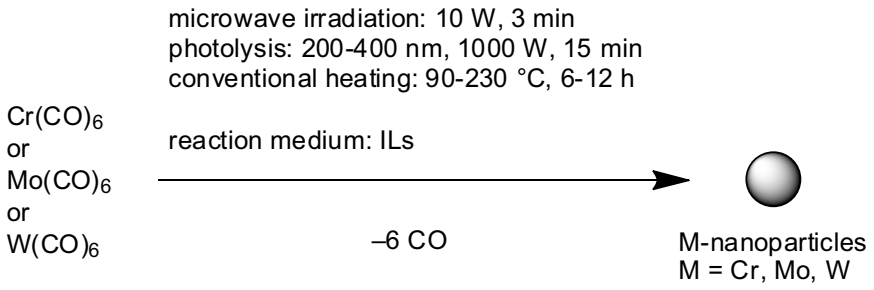

Scheme 8. Formation of Cr, Mo and W nanoparticles by microwave, photolytic or thermal, decomposition of metal carbonyls $M(CO)_6$ under argon in ionic liquids.[23,106]

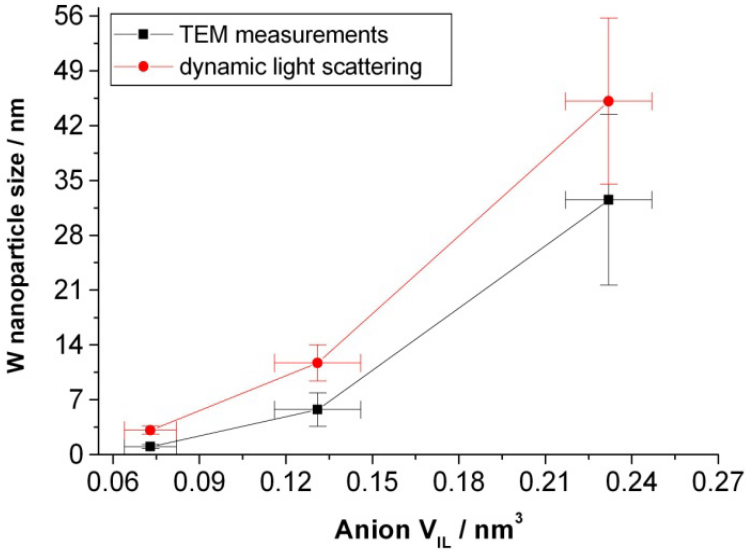

Fig. 4. Correlation between the molecular volume of the ionic liquid anion (V_{IL}) and the observed W nanoparticle size with standard deviations as error bars (from TEM and DLS). IL anions range from BF_4^- (smallest) over trifluoromethylsulfonate (triflate, $CF_3SO_3^-$, TfO^-) to the largest bis(trifluoromethylsulfonyl)amide [$(CF_3SO_2)_2N^-$, Tf_2N^-].[106]

Complete $M(CO)_6$ decomposition from the short, 3 min microwave irradiation was verified by Raman spectroscopy with no (metal-)carbonyl bands between 1750 and 2000 cm^{-1} being observed any more after the microwave treatment (Fig. 5 and Fig. 6).[23]

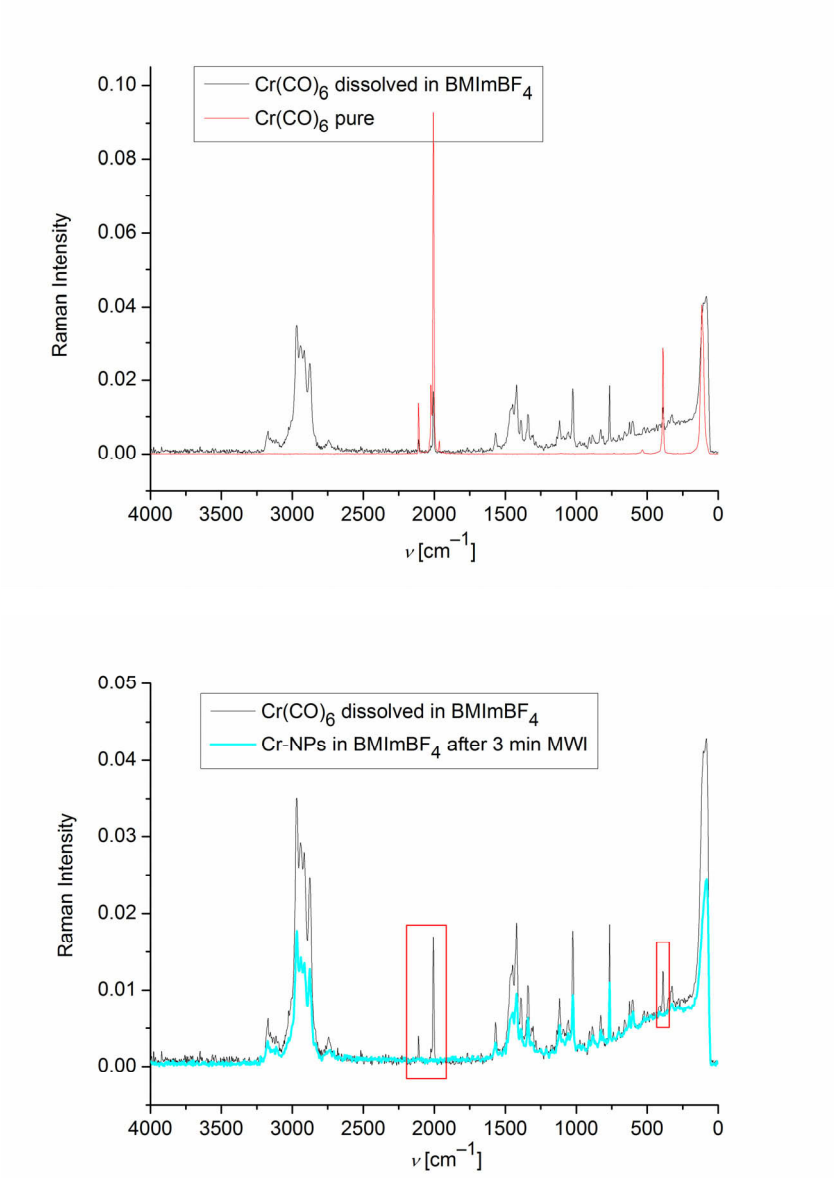

Fig. 5. Raman-FT spectra of pure $Cr(CO)_6$ and dissolved in $BMIm^+BF_4^-$ before (upper part) and after 3 min 10 W microwave irradiation (MWI) dissolved in $BMIm^+BF_4^-$ (lower part). Red boxes highlight the indicative chromium carbonyl bands.[23]

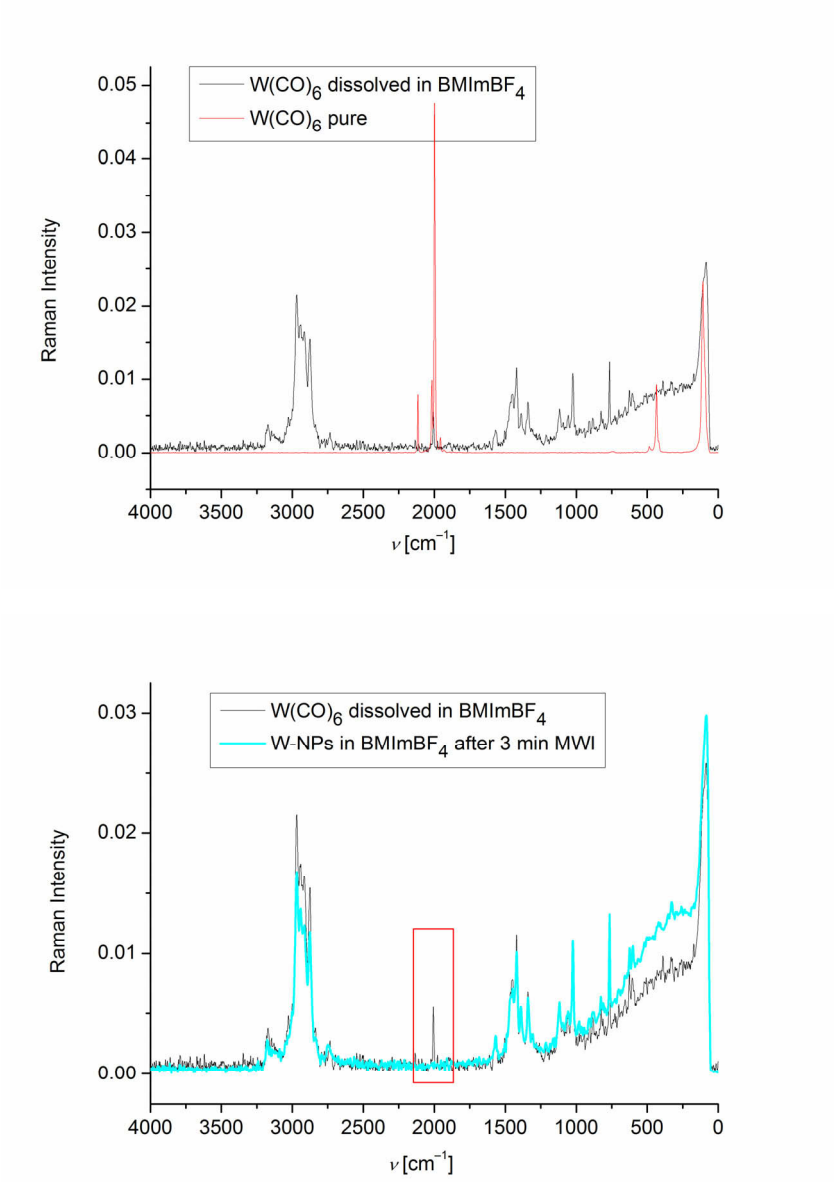

Fig. 6. Raman-FT spectra of pure $W(CO)_6$ and dissolved in $BMIm^+BF_4^-$ before (upper part) and and after 3 min 10 W microwave irradiation dissolved in $BMIm^+BF_4^-$ (lower part). The red box highlights the indicative tungsten carbonyl band.[23]

Table 5. M-NP (M = Cr, Mo, W, Re, Mn, Fe, Ru, Os, Co, Rh and Ir) size and size distribution[a] in $BMIm^+BF_4^-$ [23]

Entry	Metal carbonyl	Microwave decomposition [b]		Photolytic decomposition [c]		Conventional thermal decomposition[d]	
		TEM NP diameter/ nm, (standard deviation σ)	Dynamic light scattering NP median diameter [e]/ nm, (standard deviation σ)	TEM NP diameter/ nm, (standard deviation σ)	Dynamic light scattering NP median diameter [e]/ nm, (standard deviation σ)	TEM NP diameter/ nm, (standard deviation σ)	Dynamic light scattering NP median diameter[e]/ nm, (standard deviation σ)
1	$Cr(CO)_6$	≤ 1.5 (± 0.3) [f]	3.8 (± 0.8)	4.4 (± 1.0)	7.1 (± 0.3)	≤ 1.5 (± 0.3)[g]	3.0 (± 0.6)[g]
2	$Mo(CO)_6$	~1 – 2	4.5 (± 0.8)	~1 – 2 [g]	3.8 (± 1.1) [g]	≤ 1.5 (± 0.3)[g]	2.5 (± 0.6)[g]
3	$W(CO)_6$	3.1 (± 0.8)	5.2 (± 1.2)	< 1	10.8 (± 0.5)	≤ 1.5 (± 0.3)[g]	3.1 (± 0.5)[g]
4	$Mn_2(CO)_{10}$	12.4 (± 3)[h]	29 (± 5.0) [h]	< 1	2.5 (± 0.8)	--	--
5	$Re_2(CO)_{10}$	2.4 (± 0.9)	5.7 (± 1.4)	< 1	7.2 (± 2.2)	--	--
6	$Fe_2(CO)_9$	8.6 (± 3.2)[i]	12.8 (± 0.6) [i]	7.0 (± 3.1) [i]	12.5 (± 0.5) [i]	5.2 (± 1.6)[g]	10.1 (± 2.1)[g]
7	$Ru_3(CO)_{12}$	a) 1.6 (± 0.3)	a) 3.2 (± 0.8)	2.0 (± 0.5) [g]	3.9 (± 1.0) [g]	1.6 (± 0.4)[g]	2.9 (± 0.5)[g]
		b) 1.6 (± 0.3) [j]	b) 3.2 (± 0.8)[j]				
8	$Os_3(CO)_{12}$	0.7 (± 0.2)	2.8 (± 0.7)	2.0 (± 1.0)	2.1 (± 0.4)	2.5 (± 0.4)[g,k]	5.6 (± 1.5)[l]
9	$Co_2(CO)_8$	5.1 (± 0.9)	20 (± 3)	8.1 (± 2.5)	12.6 (± 0.4)	14 (± 8) [g]	--
10	$Rh_6(CO)_{16}$	a) 1.7 (± 0.3)	3.7 (± 0.6)	1.9 (± 0.3)	5.5 (± 0.4)	3.5 (± 0.8) [g]	7.0 (± 1.2) [g]
		b) 1.7 (± 0.3)[j]	3.4 (± 0.5)[j]				
11	$Ir_6(CO)_{16}$	0.8 (± 0.2)	3.3 (± 0.9)	1.4 (± 0.3)	4.1 (± 1.2)	a) 1.1 (± 0.2)[g]	4.1 (± 0.7) [g]
						b) 1.3 (±0.2)[g,m]	3.4 (± 1.0) [g,m]

[a] Median diameters and standard deviations are for a single TEM or DLS experiment. Reproducibility of the particle size and distribution was insured by selected repeated TEM experiments and especially by DLS which was carried out for almost all repeated decomposition reactions, [b]Microwave irradiation of metal carbonyls with 10 W for 3 min unless mentioned otherwise, [c]Photolytic de-composition of metal carbonyls with a 1000 W Hg lamp (200-450 nm wavelength) for 15 min. [d]Thermal decomposition of metal carbonyls from 6-12 h with 180-230 °C depending on the metal carbonyl. [e]Hydrodynamic radius, median diameter from the first 3 measurements at 633 nm. The hydrodynamic radius is roughly 2-3 times the size of the pure kernel cluster. For very small M-NPs (~1 nm) the size of the hydrodynamic radius can even increase to more than 3 times the M-NP radius. The resolution of the DLS instrument is 0.6 nm. Solubility of metal carbonyl precursors in $BMIm^+BF_4^-$ is limited to a maximum value of about 1 wt.% M. Statistical evaluation of the total sample pictures. [f] TEM pictures with particles of median diameter of less than 1.5 nm show electron dense cloudy structures due to scattering by the surrounding IL so that resolution of the TEM is limited and particles below 1.5 nm are hardly resolved. [g]Data from ref. [11,22,106], [h] $Mn_2(CO)_{10}$ was of larger grain size than all the other metal carbonyls which came as fine powders. Also upon grinding in a mortar, $Mn_2(CO)_{10}$ could not be as finely powdered as the other metal carbonyls. [i]TEM/TED analyses of the nanoparticles from the microwave and photolytic decomposition of $Fe_2(CO)_9$ show the presence of iron oxide, Fe_2O_3. Because of the experimental setup rigorous air exclusion is more difficult during the microwave irradiation and photolysis and workup. [j]Microwave decomposition of metal carbonyls with 10 W for 10 min. [k]0.2 wt.% $Os_3(CO)_{12}$ in $BMIm^+BF_4^-$. [l]1 wt.% $Os_3(CO)_{12}$ in $BMIm^+BF_4^-$. [m]18 h decomposition time of 0.5 wt.% $Ir_4(CO)_{12}$ in $BMIm^+BF_4^-$.

Stable manganese and rhenium metal nanoparticles were reproducibly obtained by microwave irradiation or UV photolysis from their metal carbonyl precursors $M_2(CO)_{10}$ in the ionic liquid $BMIm^+BF_4^-$ (Scheme 9, Fig. 7, Table 5).[23]

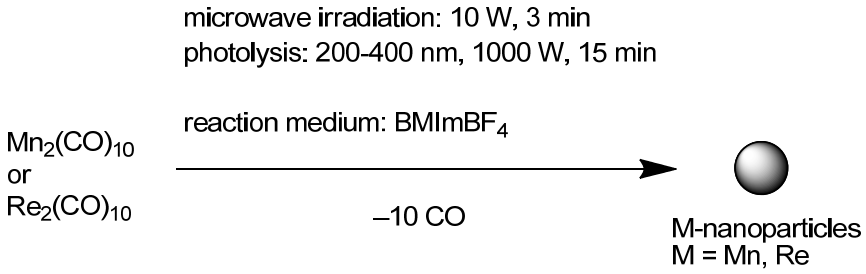

Scheme 9. Formation of Mn and Re nanoparticles by microwave, photolytic or thermal, decomposition of the metal carbonyls $M_2(CO)_{10}$ under argon in the ionic liquid $BMIm^+BF_4^-$.[23]

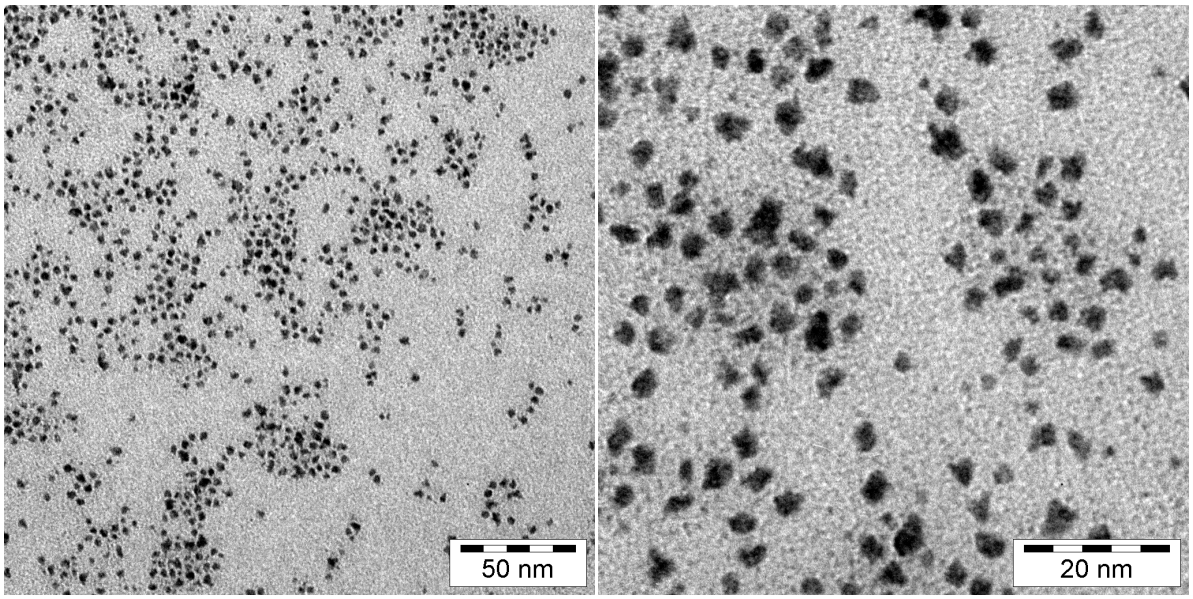

Fig. 7. TEM photograph of Re-NPs from $Re_2(CO)_{10}$ by MWI (∅ 2.4 (± 0.9) nm, entry 5 in Table 5).[23]

Complete $M_2(CO)_{10}$ decomposition from the short, 3 min microwave irradiation was verified by Raman spectroscopy with no (metal-)carbonyl bands between 1750 and 2000 cm^{-1} being observed any more after the microwave treatment (Fig. 8).[23]

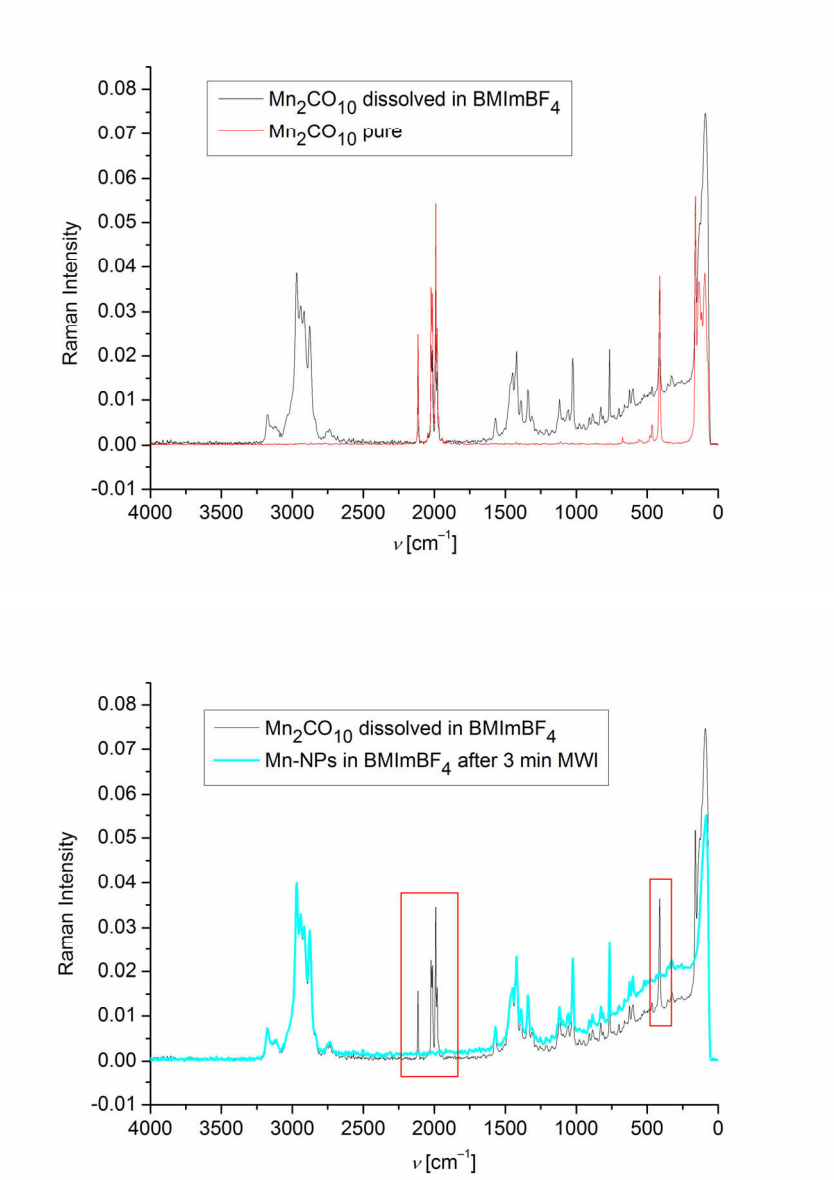

Fig. 8. Raman-FT spectra of pure $Mn_2(CO)_{10}$ and dissolved in $BMIm^+BF_4^-$ (upper part) before and after 3 min 10 W microwave irradiation (MWI) dissolved in $BMIm^+BF_4^-$ (lower part). Red boxes highlight the indicative manganese carbonyl bands.[23]

Stable iron, ruthenium and osmium nanoparticles are obtained reproducibly by microwave irradiation, photolytic or conventional thermal decomposition under argon atmosphere from $Fe_2(CO)_9$, $Ru_3(CO)_{12}$ or $Os_3(CO)_{12}$, dissolved in the ionic liquid $BMIm^+BF_4^-$ and with a very small and uniform size for Ru and Os nanoparticles of about 1.5 nm to 2.5 nm without any additional stabilizers or capping molecules (Scheme 10, Fig. 9-Fig. 11, Table 5).[11,23]

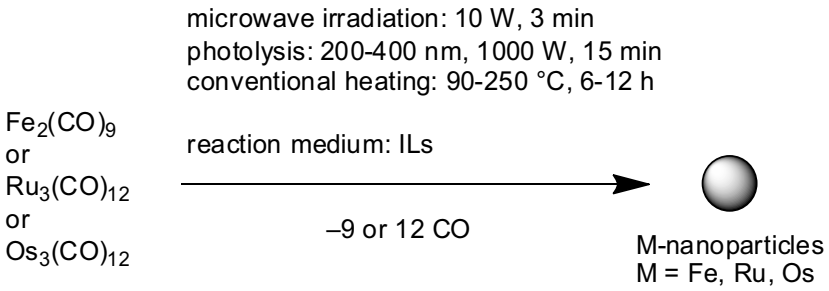

Scheme 10. Formation of Fe, Ru and Os nanoparticles by microwave, photolytic or thermal, decomposition of metal carbonyls $M_x(CO)_y$ under argon in the ionic liquid $BMIm^+BF_4^-$.[11,23]

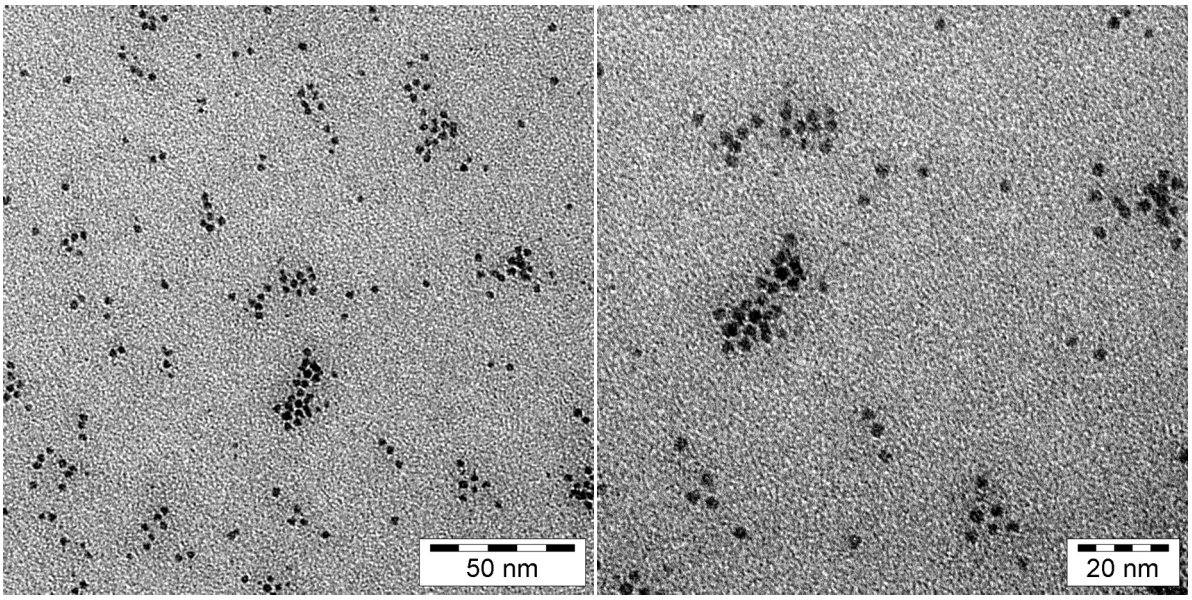

Fig. 9. TEM photographs of Ru-NP from $Ru_3(CO)_{12}$ by photolytic decomposition (0.08 wt.% Ru in $BMIm^+BF_4^-$) (∅ 2.0 (± 0.5) nm, entry 7 in Table 5).[11]

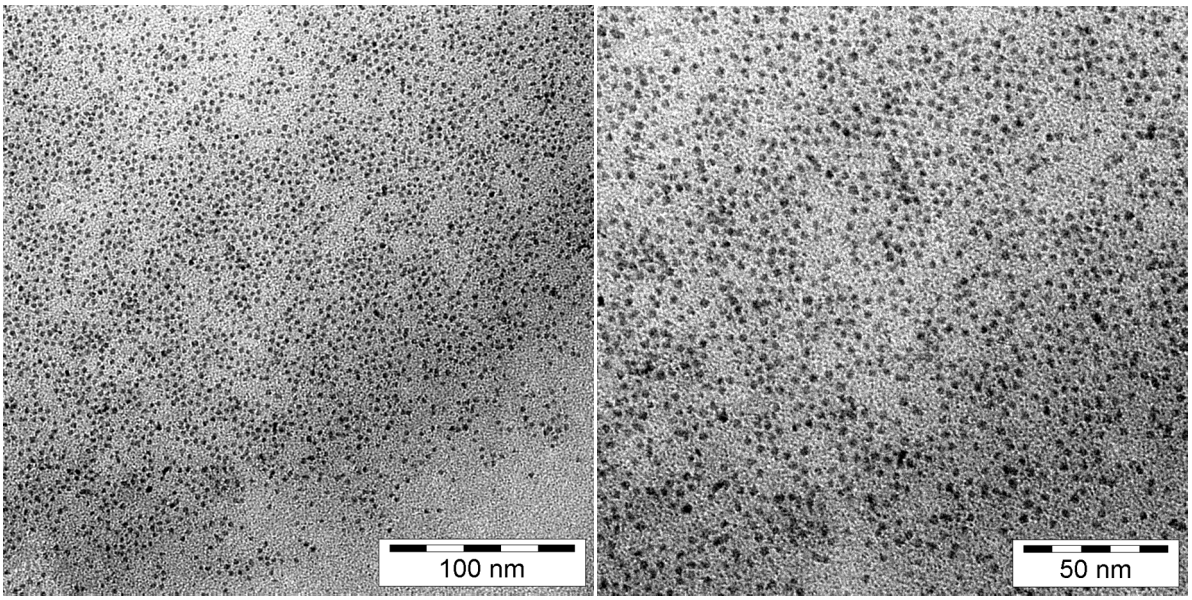

Fig. 10. TEM photographs of Os-NPs from $Os_3(CO)_{12}$ by conventional thermal decomposition (0.2 wt.% Os in $BMIm^+BF_4^-$) (∅ 2.5 (± 0.4) nm, entry 8 in Table 5).[11]

Complete $M_x(CO)_y$ (M = Fe, Ru, Os) decomposition from the short, 3 min microwave irradiation was verified by Raman spectroscopy with no (metal-)carbonyl bands between 1750 and 2000 cm^{-1} being observed any more after the microwave treatment (Fig. 11).[23]

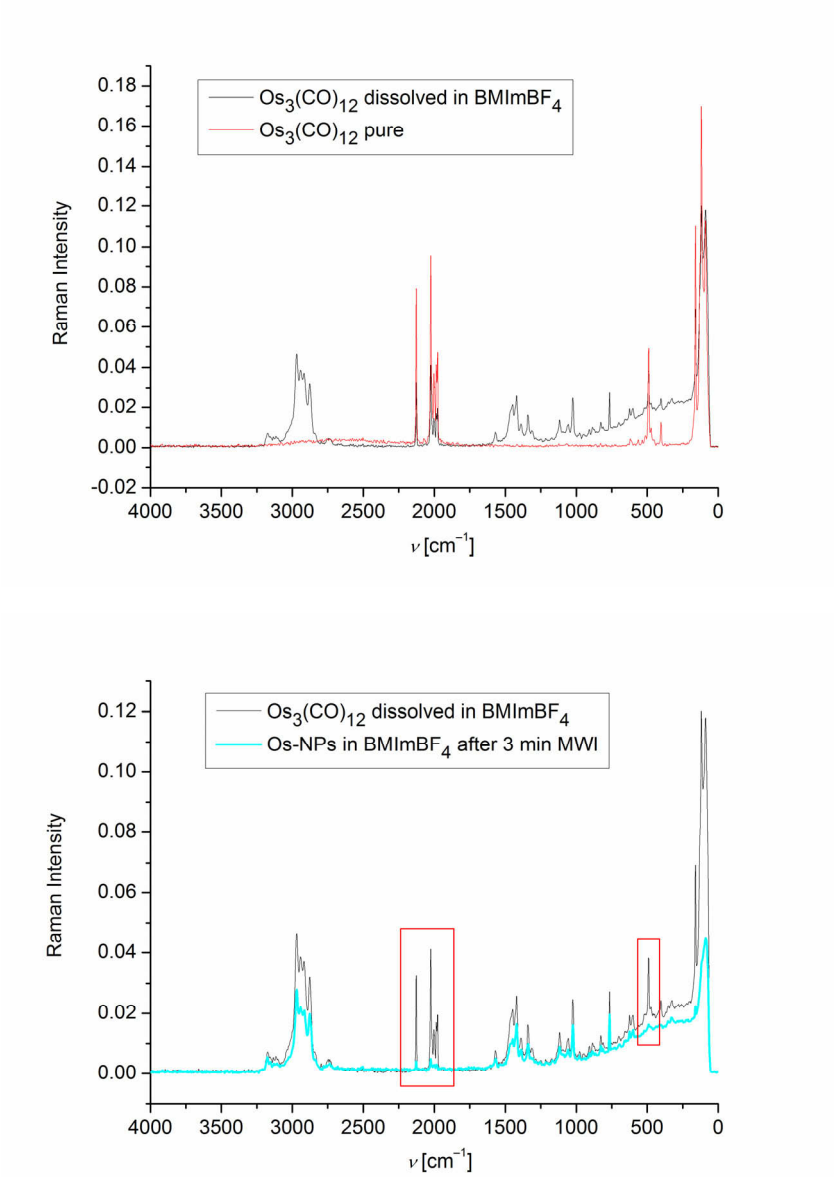

Fig. 11. Raman-FT spectra of pure $Os_3(CO)_{12}$ and dissolved in $BMIm^+BF_4^-$ (upper part) before and after 3 min 10 W microwave irradiation (MWI) dissolved in $BMIm^+BF_4^-$(lower part). The red boxes highlight the indicative osmium carbonyl bands.[23]

The Ru-NP/$BMIm^+BF_4^-$ and other M-NP/IL dispersions were active catalysts in the biphasic liquid-liquid hydrogenation of cyclohexene or benzene to cyclohexane. Even a remarkable partial hydrogenation of benzene to cyclohexene could be achieved with Ru-NP/$BMIm^+PF_6^-$ dispersions.[111] The low miscibility of substrates and products with the IL phase allows for easy separation by simple decantation of the hydrophobic phase.[21] The hydrogenation reaction of cyclohexene was run at 90 °C and 10 bar H_2 to 95% conversion

where the reaction was intentionally stopped as thereafter the decrease in cyclohexene concentration lowered the reaction rate (Fig. 12).[23]

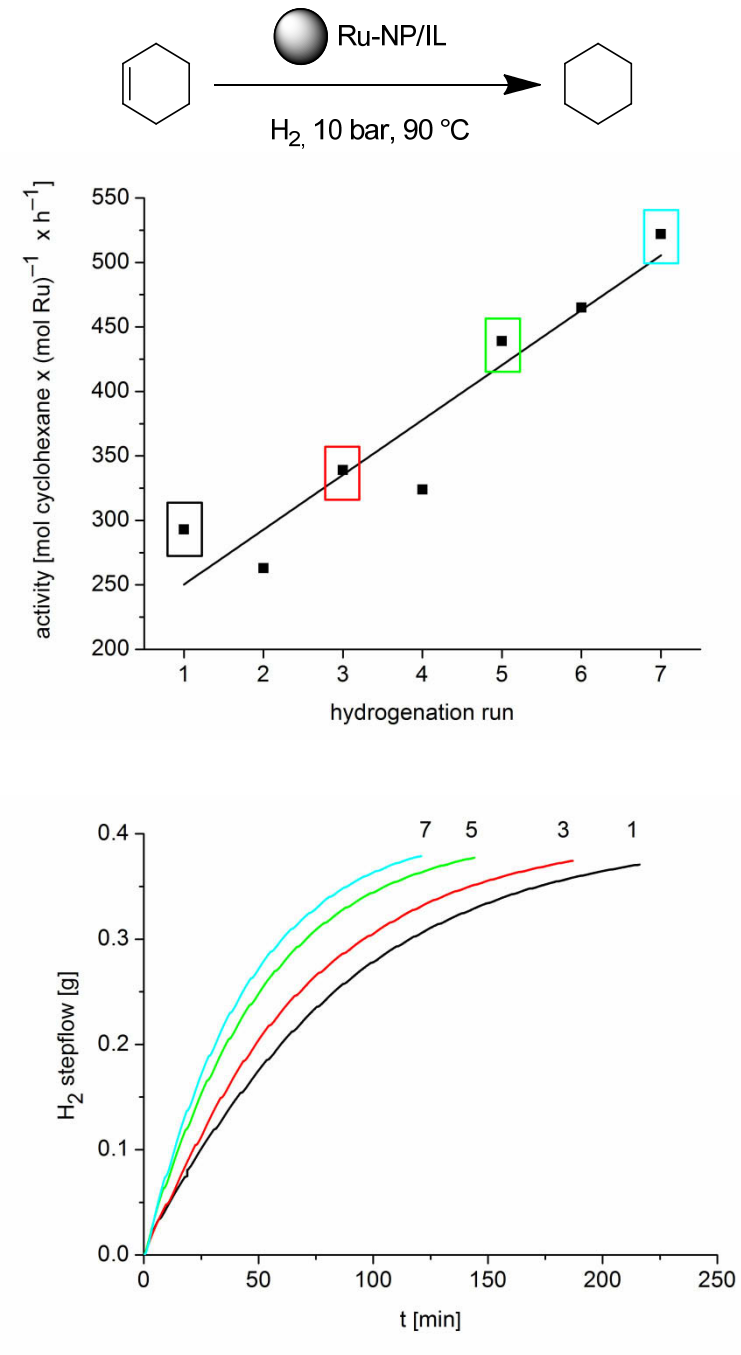

Fig. 12. Activity for seven runs of the hydrogenation of cyclohexene with the same Ru-NP/BMIm^{+}BF$_4^{-}$ catalyst at 90 °C, 10 bar H_2 pressure, run to 95% conversion and H_2 uptake over time for the 1st, 3rd, 5th and 7th hydrogenation run. An H_2 uptake of 0.38 g corresponds to 95% conversion (100% are 0.2 mol or 0.4 g H_2).[23]

Silva, Dupont et al. have prepared cobalt nanoparticles with a size of around 7.7 nm by the decomposition of $Co_2(CO)_8$ in 1-alkyl-3-methylimidazolium Tf_2N^- ionic liquids at 150 °C. These Co-NPs were shown to be effective catalysts for the Fischer-Tropsch (FT) synthesis, yielding olefins, oxygenates, and paraffins (C_7-C_{30}) and could be reused at least three times if they were not exposed to air.[163]

The decomposition of $Co_2(CO)_8$ dispersed in 1-*n*-decyl-3-methylimidazolium bis(trifluoromethylsulfonyl)amide ($DMIm^+Tf_2N^-$) at 150 °C over 1 h afforded a black solution containing Co-NPs with a cubic shape (53 ± 22 nm), together with Co-NPs of irregular shape.[164]

Stable cobalt, rhodium and iridium nanoparticles were obtained reproducibly by thermal decomposition under argon from $Co_2(CO)_8$, $Rh_6(CO)_{16}$ and $Ir_4(CO)_{12}$ dissolved in the ionic liquids $BMIm^+BF_4^-$, $BMIm^+TfO^-$ and $BtMA^+Tf_2N^-$ (Scheme 10, Fig. 13, Table 3).[22] Later it was also shown that an even more rapid and energy-saving decomposition could be achieved with a 10 W microwave irradiation for 3 min of 0.4 ml (0.48 g) of a $BMIm^+BF_4^-$ sample with a 0.5 wt.% M/IL-dispersion (Fig. 14).[23] The very small and uniform nanoparticle size of about 1 to 3 nm for the Co-, Rh- or Ir-NPs in $BMIm^+BF_4^-$ (Table 5) increases with the molecular volume of the ionic liquid anion in $BMIm^+TfO^-$ and $BtMA^+Tf_2N^-$ (Fig. 15). Characterization of the nanoparticles was done by TEM, transmission electron diffraction (TED), X-ray powder diffraction (XRPD) and dynamic light scattering (DLS). The rhodium or iridium nanoparticle/IL systems function as highly effective and recyclable catalysts in the biphasic liquid-liquid hydrogenation of cyclohexene to cyclohexane with activities of up to 1900 mol cyclohexane × $(\text{mol Ir})^{-1} \times h^{-1}$ and 380 mol cyclohexane × $(\text{mol Rh})^{-1} \times h^{-1}$ for and quantitative conversion within 1 h at 4 bar H_2 pressure and 75 °C (Fig. 16).

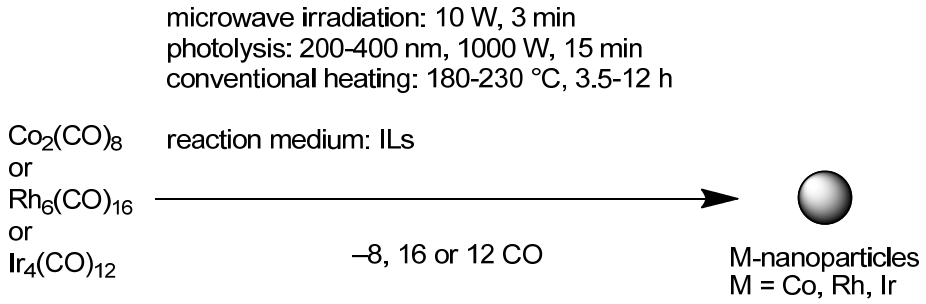

Scheme 11. Formation of Co, Rh and Ir nanoparticles by microwave, photolytic or thermal, decomposition of metal carbonyls $M_x(CO)_y$ under argon in ionic liquids.[22,23]

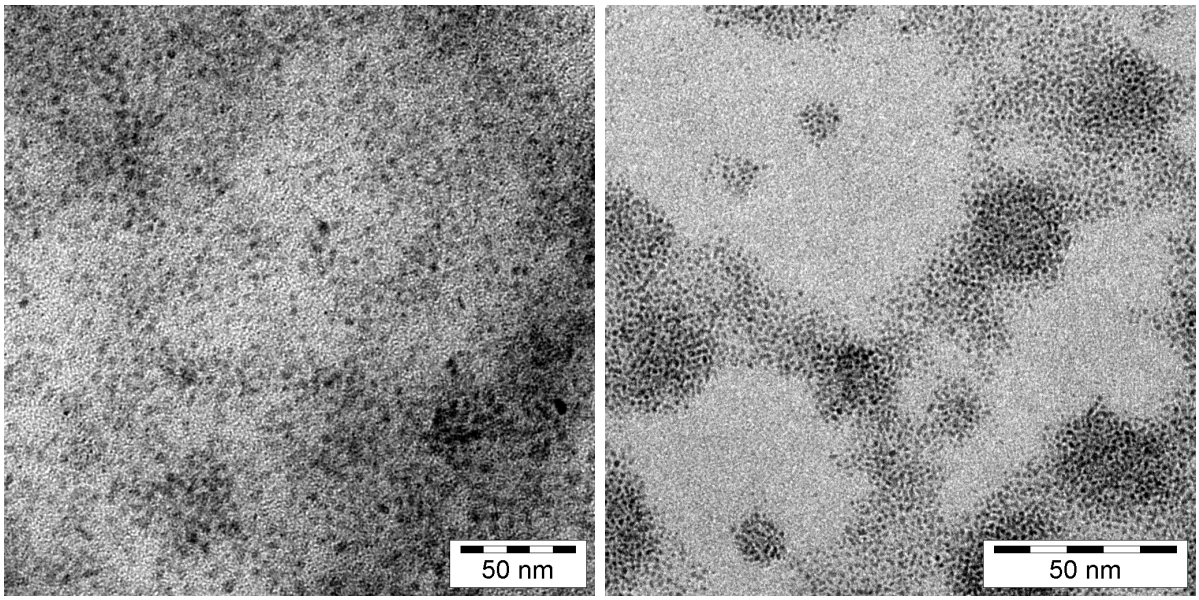

Fig. 13. TEM photographs by conventional thermal decomposition of (left) Rh-NPs from $Rh_6(CO)_{16}$ and (right) (0.5 wt. % Rh in $BMIm^+BF_4^-$) (∅ 3.5 (± 0.8) nm, entry 10 in Table 5) and of (right) Ir-NPs from $Ir_4(CO)_{12}$ (0.5 wt. % Ir in $BMIm^+BF_4^-$, 18 h) (∅ 1.3 (± 0.2) nm, entry 11b in Table 5).[22]

Complete $M_x(CO)_y$ (M = Co, Rh, Ir) decomposition from the short, 3 min microwave irradiation was verified by Raman spectroscopy with no (metal-)carbonyl bands around 2000 cm^{-1} being observed any more after the microwave treatment (Fig. 14).[23]

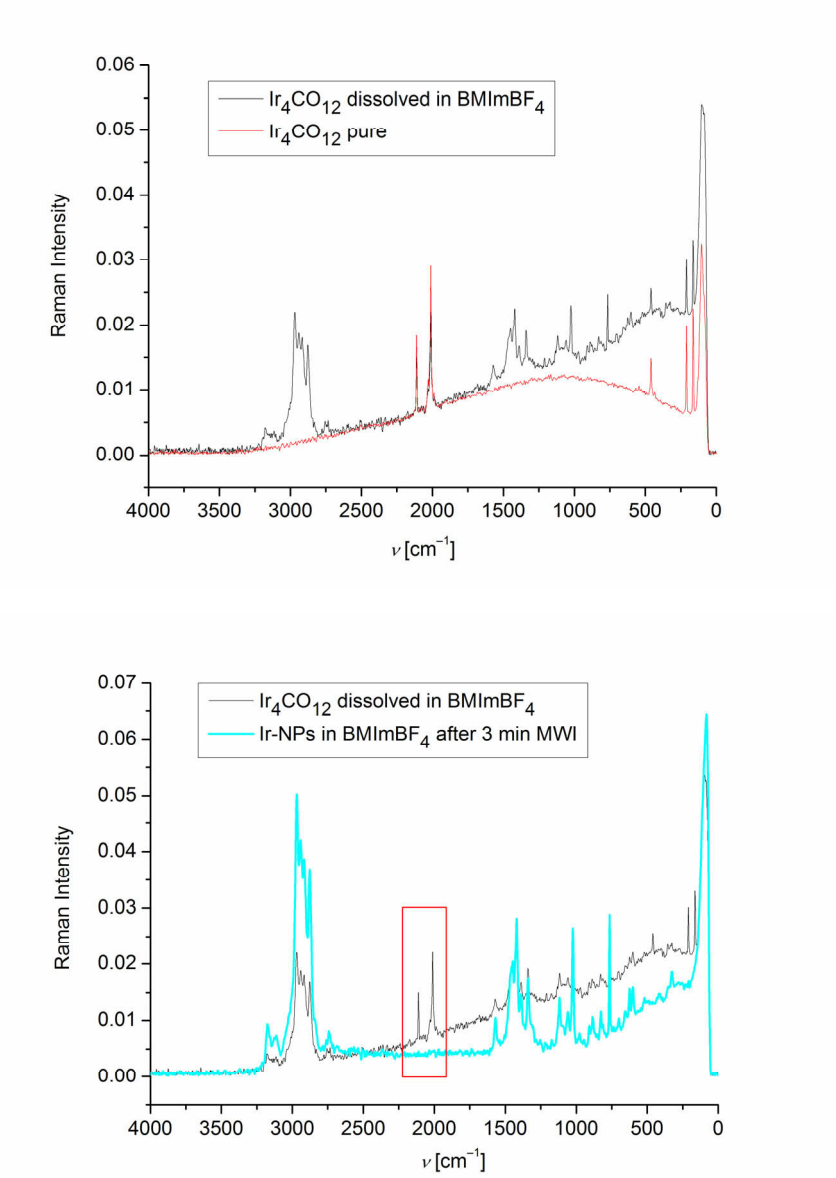

Fig. 14. Raman-FT spectra of pure $Ir_4(CO)_{12}$ and dissolved in $BMIm^+BF_4^-$ (upper part) before and after 3 min 10 W microwave irradiation (MWI) dissolved in $BMIm^+BF_4^-$ (lower part). The red box highlights the indicative iridium carbonyl bands.[23]

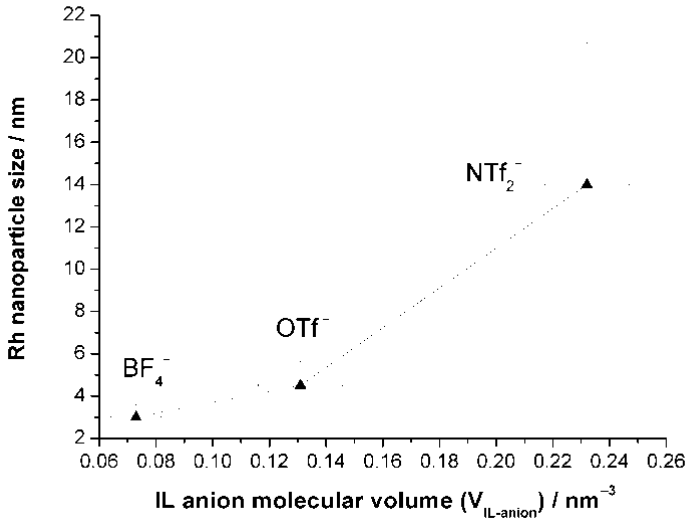

Fig. 15. Correlation between the molecular volume of the ionic liquid anion ($V_{IL\text{-}anion}$) and the observed Rh nanoparticle size with standard deviations as error bars (from TEM). IL anions range from BF_4^- (smallest) over trifluoromethylsulfonate (triflate, $CF_3SO_3^-$, TfO^-) to the largest bis(trifluoromethylsulfonyl)amide [$(CF_3SO_2)_2N^-$, Tf_2N^-].[22]

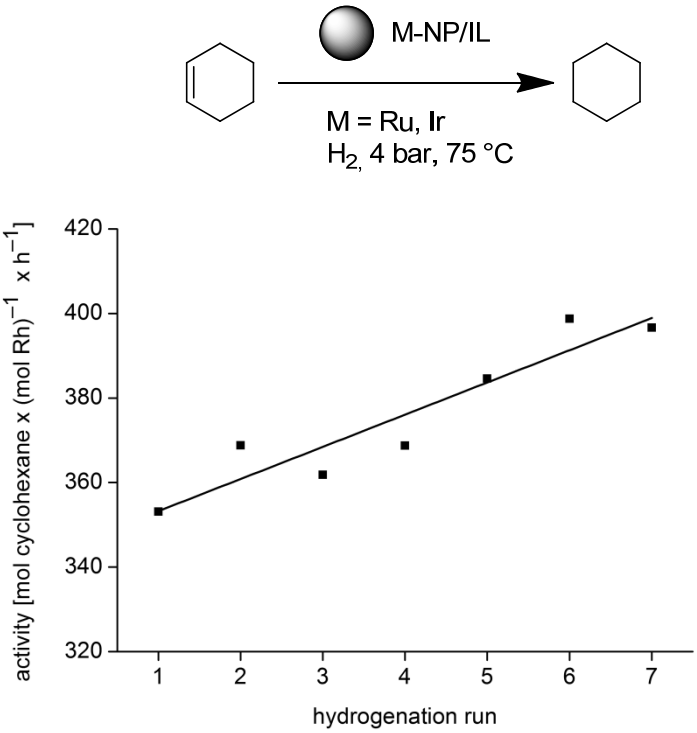

Fig. 16. Activity over seven catalytic cycles for the hydrogenation of cyclohexene with the same Ru-NP/$BMIm^+BF_4^-$ catalyst at 75 °C, 4 bar H_2 pressure and 2.5 h reaction time. An activity of 350 mol product × (mol Ru)$^{-1}$ × h^{-1} corresponds to 88% and an activity of 400 to quantitative (100%) conversion.

2.5 DLVO theory

The classic theory for interaction of two particles in a dispersion is the DLVO (Derjaugin-Landau-Verwey-Overbeek) theory, developed by the research groups of Derjaguin and Landau in the USSR and the group of Vervey and Overbeek in the Netherlands nearly simultaneously in the 1940s. This basic and most commonly theory is considered as a combination of the repulsive Coulomb and the attraction van der Waals forces. Hence DLVO potential is the sum of an effective electrostatic term and a direct van der Waals term.

Some simplifications and thesis are involved in this theory: The surfaces of the particles are flat. The charge density is homogeneous and remains homogenous, even when particles approach each other. Also there is no change of the concentration of the counter ions which cause the electric potential. The solvent itself has only an influence through its dielectric constant.[165]

It is quite clear that the surface of a particle is not flat and the charge density changes when two particles approach each other. It is evident that the theory can only approximate the real-life interactions of two particles. DLVO theory works very well and is the best predictor of the stability of lyophobic colloids. This theory is fundamental for chemists working on and with colloids.[166-168]

It should be pointed that there are two main types of stabilizers for NPs: Electrostatic or "DLVO-type" stabilizers which are considered as point charge stabilizers and "classical" steric stabilizers. Small anions like halides seem to be the closest real-life electrostatic stabilizers.

Concerning nanoparticles and their interactions, the anion is the main focus because anions will bind to the unsaturated surface of the electrophilic NP.[169] Thus, the NPs with their anion layer assume a negative charge and turn into a large multi-negative anion. The repulsion between two such negatively charged NPs is the Coulomb part of the DLVO theory.

The stability of colloids is a balance between Coulomb forces and van der Waals attraction. A measure of the stability of a colloid is the thickness of the Debye layer, which is the sum of the layers of counterions surrounding the particle. The thicker the Debye layer the more stable is the particle because the distance to the next particle is greater and the van der Waals attraction is reduced. Finke et al studied the stability of colloids in different solvents and found that the higher the dielectric constant of the medium the better is the stabilization of the colloid.[97]

The DLVO theory has its limits. It can only be applied to dilute systems (< 5×10^{-2} mol/L). It does not work for higher concentrations. It cannot be applied to ions with multiple charge and sterically stabilized systems.[170] Nowadays the DLVO theory has been supplemented with "extra-DLVO" forces which include effects such as hydrogen bonding, the hydrophobicity and steric interactions.

The van der Waals term is calculated as an integral of interatomic dispersion interactions over the volume of both particles (Eqn.(2)).[165,171]

$$\frac{PMF_{DLVO}^{el}(r)}{k_bT} = L_B Z_1 Z_2 \frac{\exp(\kappa a_1)\exp(\kappa a_2)}{(1+\kappa a_1)(1+\kappa a_2)} \frac{\exp(-\kappa r)}{r} \quad (2)$$

PMF = potential of mean force

L_B = Bjerrum length, $L_B = \frac{e^2}{4\pi\varepsilon_r\varepsilon_o} k_bT$,

κ^{-1} = Debye length

$\kappa^2 = 4\pi L_B \sum_{i=1}^{2} \rho_i Z_i^2$,

ρ_i= the concentration of microion i

Z_i = charge of the colloids 1 and 2

a_i = radius of the colloids

r = distance between the colloids

This term is neglected within the basic model, but it is important for large colloidal particles. To compute the effective electrostatic component, microions are described by point charges and two approximations are made, the Poisson–Boltzmann (PB) approximation (that is, a mean-field treatment of micro ions), and an expansion of the charge density to linear order in the electrostatic potential.

Despite its success, the DLVO theory fails to predict some experimental behaviors. The attraction between equally charged particles in the presence of multivalent counterions is the most surprising one.[172] Numerical simulations within the basic model have remarkably contributed to understand such failure. It has been proven that Poisson–Boltzmann theory cannot predict an attraction, while the PMF computed by simulations can be attractive. Therefore, the attraction can be explained by the correlations between microions, missed within the mean field PB treatment, but present in the simulations. The review by Dijkstra devoted to the simulations of charged colloids summarizes work on this issue.[172]

2.6 Graphene

During the last few years, chemically derived graphene (CDG),[173-176] also called thermally reduced graphite oxide[177-179] or simply graphene, has been rediscovered as an extremely versatile carbon material.[180,181] Because of the functional groups present in CDG the sorption of ions and molecules is possible.[180] This and the high specific surface area of CDG of 400 m^2g^{-1} up to 1500 m^2g^{-1}, make them promising materials for catalytic applications.[180] Metal nanoparticles on carbon materials are of recent interest.[182-188] Pt-, Ru- or Pd-NPs on exfoliated graphene sheets were produced from heating graphite oxide (GO) with the metal complexes $[Pt(NH_3)_4]Cl_2 \times H_2O$, $[Ru(NH_3)_6]Cl_2$ or $[Pd(NH_3)_4]Cl_2 \times H_2O$ under an N_2 atmosphere.[189] Graphene supported MNPs are composite materials[190] that may find applications as chemical sensors,[191] electrodes for fuel cells,[192-194] catalysis,[195-198] or hydrogen storage.[199]

2.7 Organic carbonates

Organic carbonates, such as dimethyl carbonate, diethyl carbonate, ethylene carbonate or propylene carbonate (PC) (Fig. 17) are polar solvents which are available in large amounts and at low prices, have a large liquid temperature range (for PC mp. -49 °C, bp. 243 °C), are of only low (eco)toxicity and are completely biodegradable.[200] PC is an aprotic, highly dipolar solvent, which has a low viscosity[201,202] and is considered a *green* solvent because of its low flammability, volatility and toxicity.[203]

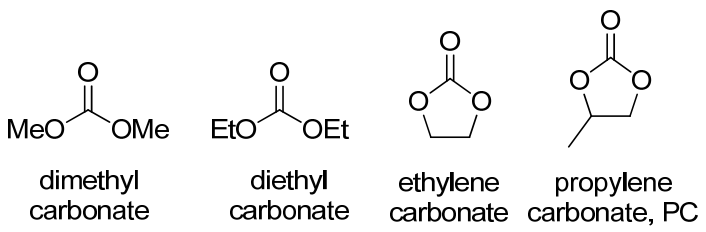

Fig. 17. Selected organic compounds.

Organic carbonates are recognized as solvents in industrial applications such as cleaning, degreasing, paint stripping, gas treating, and textile dyeing.[204] Yet, so far organic carbonates are used primarily for extractive applications and as solvents in electrochemistry.[200] PC is used as a solubilizer and co-solvent in cosmetics,[205] in the FLUOR process for the removal of carbon dioxide from natural gas streams in the oil industry,[206] in lacquer[207] and BASF is using PC for waste removal in the copper wire-coating process.[208] PC is also investigated for Li-ion battery research.[209,210] Reports on metal nanoparticles in organic carbonates are rare and appear to be of accidental coincidence for Pd-NPs.[211-214]

2.8 Trace catalyst

It has recently become more evident that not every component which was originally claimed as catalyst turned out to be the actual active ingredient. In some prominent case trace metal impurities were eventually proven as the actual catalytic species.[215,216] In an early example, traces of nickel compounds which formed unintentional during the cleaning of a V2A steal autoclave and remained in there changed the Ziegler-Aufbau reaction (reaction of $AlEt_3$ with ethylene at 100 °C under pressure to long-chain Al-alkyls) to a clean ethylene dimerization to yield butene. The cause of this unexpected dimerisation was at first unknown and later termed the "nickel effect" after its origin had become clear. In addition, the nickel compounds had required traces of acetylene which were present in technical ethylene for stabilization of the nickel catalyst.[217,218] More recently, a Suzuki cross-coupling which was thought to have occured metal-free was indeed promoted by ppb Pd traces in the Na_2CO_3 or K_2CO_3 bases used for the reaction.[219] Suggested iron-catalyzed cross-coupling reactions with different $FeCl_3$ sources were eventually corrected to ppm-scale copper impurities doing the catalysis.[220] Even with Pd in the ppb range it is possible to carry out a Sonogashira coupling with quantitative conversion.[221] On the other hand, metal traces or dopants are intentionally added to enhance or promote catalytic performance[222,223] or to assist catalyst regeneration.[224]

Researchers in catalysis are aware that impurities left over from previous experiments in their (cleaned) vessels can give activating of desactivating "memory effects" which change

the outcome of a catalytic reaction. Thus, catalytic reactions should be carried out more than once to ensure reproducibility. Surprisingly, a Scifinder search[225] combining the terms "memory effect", "contamination" or "impurity" and "catalysis" did not give any relevant references.

This introduction is part of this cumulative dissertation (**publication 6.3**).

3 AIM OF THIS WORK

The aim of this thesis was to synthesize small and ligand-free “naked” transition metal nanoparticles from their binary carbonyls. The metal nanoparticles should be reproducibly obtainable by an easy and quick synthetic route under as mild conditions as possible. The metal nanoparticles should be kinetically stabilized by a weakly coordinating medium or on a surface without the use of strongly coordinating capping ligands. The use of propylene carbonate (PC) as a liquid medium and polytetrafluoroethylene (PTFE, Teflon) as a surface should be investigated. Both propylene carbonate and Teflon are viewed as environmentally benign, non hazardous, relatively inexpensive and safe-to-handle reagents. Further the catalytic behavior and recyclability of the obtained metal nanoparticles in hydrogenation reactions should be investigated. In the context of *green chemistry* the catalyst systems should be reusable, the conditions for the preparation/synthesis of the catalyst and the conditions of the catalytic reactions should be mild and energy-saving.

4 RESULTS AND DISCUSSION

4.1 Propylene carbonate as stabilizing solvent for transition metal nanoparticles

The metal carbonyl $Mo(CO)_6$, $W(CO)_6$, $Re_2(CO)_{10}$, $Fe_2(CO)_9$, $Ru_3(CO)_{12}$, $Os_3(CO)_{12}$, $Co_2(CO)_8$, $Rh_6(CO)_{16}$ or $Ir_6(CO)_{16}$ was dissolved/suspended under an argon atmosphere in dried and deoxygenated propylene carbonate (PC). Complete decomposition by microwave irradiation of the metal carbonyl in PC was achieved after only 3 minutes using a low power of 50 W under argon (Fig. 18).

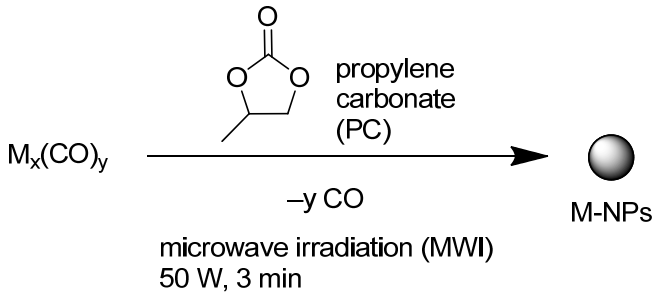

Fig. 18. Microwave decomposition of metal carbonyls to M-NPs in PC.

The resulting orange-red Os-, yellow W-, and dark-brown to black Mo-, Re-, Fe-, Ru-, Co-, Rh- and Ir-NP dispersions were reproducibly obtained through the microwave decomposition route. Complete $M_x(CO)_y$ decomposition from short, 5 min microwave irradiation was verified by Raman spectroscopy with no (metal–)carbonyl bands between 1800 and 2000 cm^{-1} being observed any more after the microwave treatment (Fig. 19).

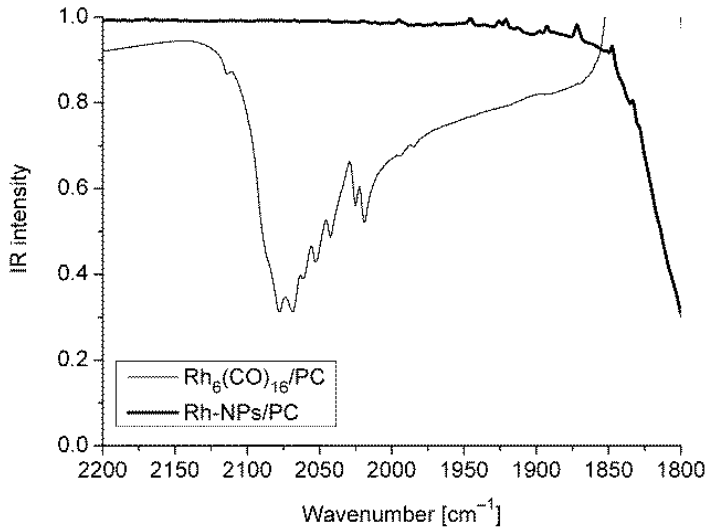

Fig. 19. IR-spectra of $Rh_6(CO)_{16}$/PC (light curve) and the resulting Rh-NP (0.5 wt.%)/PC dispersion (bold curve) after microwave treatment (50 W, 3 min).

The resulting M-NPs were analyzed by TEM (Fig. 20-Fig. 22), transmission electron diffraction (TED), and dynamic light scattering (DLS) for their size and size distribution (Table 6). TED patterns do not show reflections indicative of a crystalline material. It is therefore concluded that the particles obtained from the synthesis are amorphous M-NPs stabilized by PC. Still the diffraction rings match the known d-spacing of the respective metaldiffraction pattern (Table 18-Table 20).

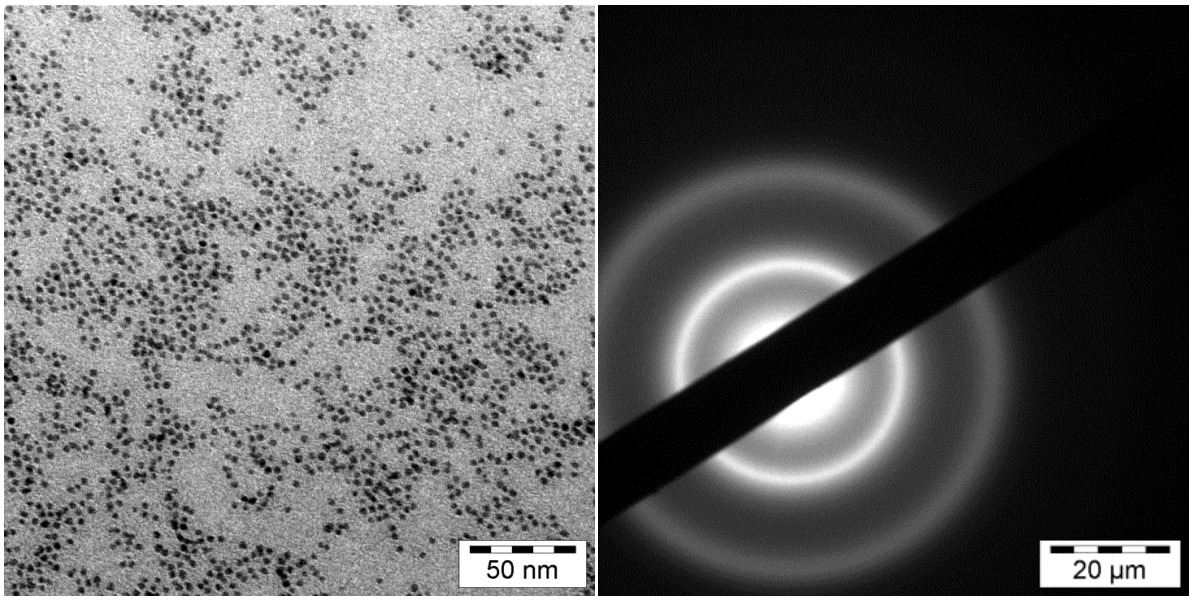

Fig. 20. TEM (left) and TED (right) of Ru-NPs in PC from $Ru_3(CO)_{12}$ (entry 5 in Table 6). The black bar is the beam stopper. The diffraction rings at (Å) 2.10 (very strong), 1.61, 1.26, 1.15 (all weak) match with the d-spacing of the Ru-metal diffraction pattern (see Table 18).

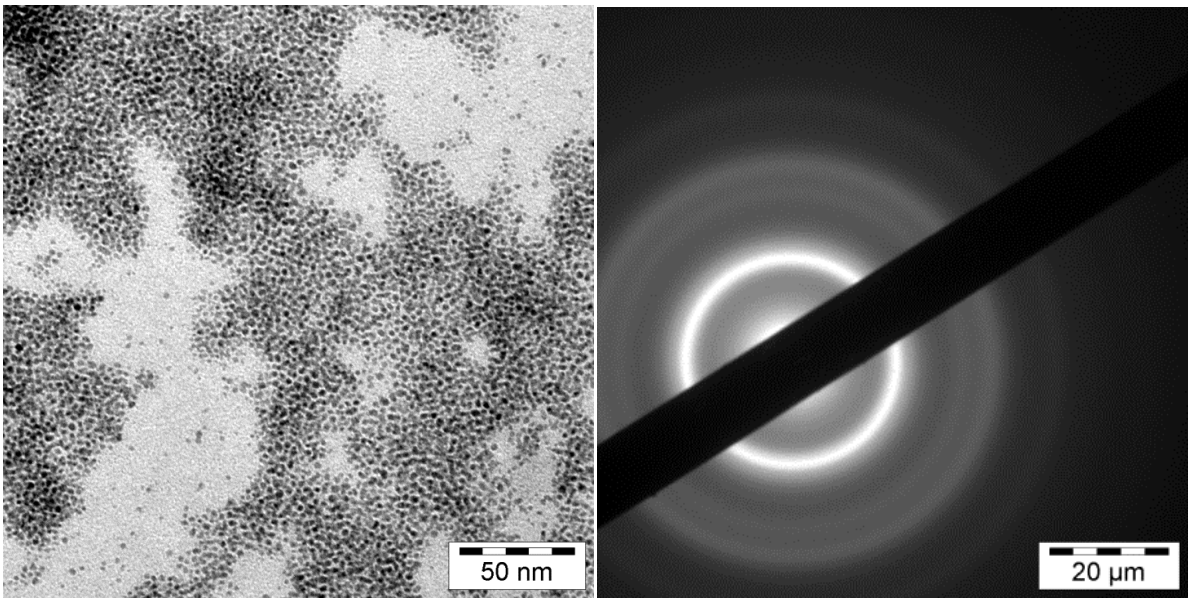

Fig. 21. TEM (left) and TED (right) of Rh-NPs in PC from $Rh_6(CO)_{16}$ (entry 8 in Table 6). The black bar is the beam stopper. Diffraction rings at (Å) 2.23 (very strong), 1.94 (strong), 1.39, 1.17 and 0.89 (weak) match the d-spacing of the Rh-metal diffraction pattern (see Table 19).

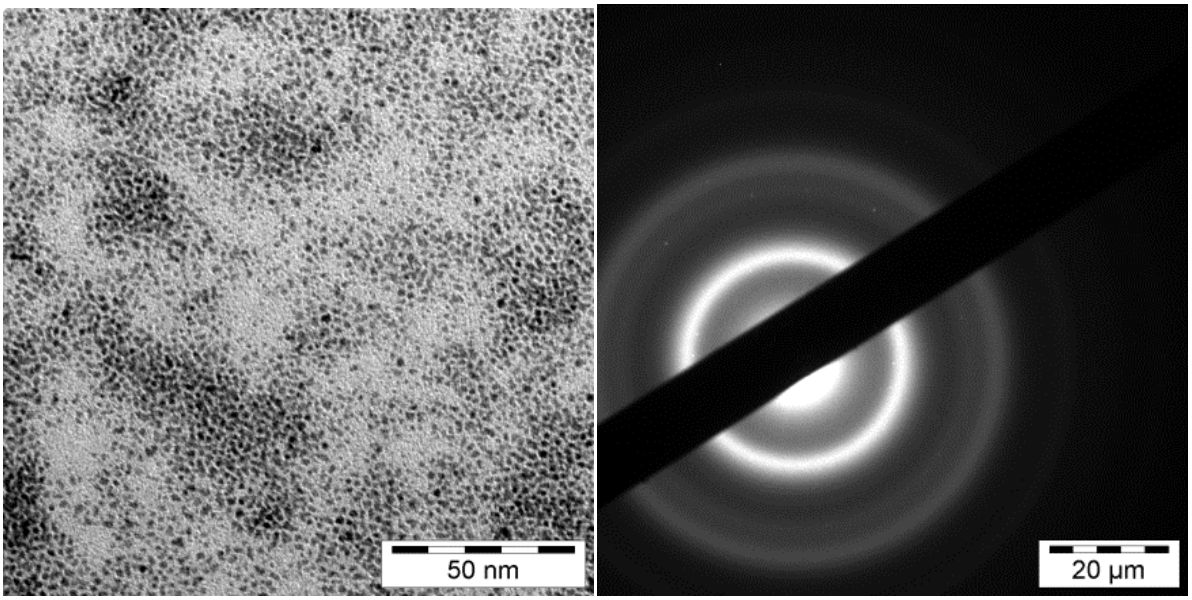

Fig. 22. TEM (left) and TED (right) of Ir-NPs in PC from $Ir_6(CO)_{16}$ (entry 9 in Table 6). The black bar is the beam stopper. The diffraction rings at (Å) 2.25 (strong), 1.38, 1.20 (weak) match with the d-spacing of the Ir-metal diffraction pattern (see Table 20).

The hydrodynamic radius from DLS is roughly two to three times the size of the pure kernel cluster. For very small M-NPs (< 1 nm) the size of the hydrodynamic radius was measured to be more than three times the radius found from TEM. The median M-NP diameter for the microwave-synthesized Mo-, W-, Re-, Ru-, Os-, Rh- and Ir-NPs was between < 1 and 3.0 nm, with a narrow size distribution (TEM data in Table 6). No extra stabilizers or

capping molecules are needed to achieve this small particle size. It is, at present, not trivial to routinely and easily prepare uniform nanoparticles in the size range between < 1-3 nm without strong capping ligands. For the magnetic Fe-NPs and Co-NPs the median diameter was somewhat larger with 2.4 and 6.1 nm, respectively. The M-NP/PC dispersions are stable up to three weeks according to repeated TEM measurements over this time period.

Table 6. M-NP size and size distribution in PC.[a]

entry	Metal carbonyl	TEM Ø (σ) [nm][b]	DLS Ø (σ) [nm][b]
1	$Mo(CO)_6$	2.2 (± 0.5)	3.5 (± 1.1)
2	$W(CO)_6$	2.9 (± 0.6)	3.7 (± 1.4)
3	$Re_2(CO)_{10}$	< 1	1.4 (± 0.5)
4	$Fe_2(CO)_9$	2.4 (± 0.9)	3.2 (± 0.8)
5	$Ru_3(CO)_{12}$	2.7 (± 0.5)	2.6 (± 0.8)
6	$Os_3(CO)_{12}$	3.0 (± 1.5)	4.0 (± 1.2)
7	$Co_2(CO)_8$	6.1 (± 7.4)	6.7 (± 2.2)
8	$Rh_6(CO)_{16}$	2.1 (± 0.6)	2.4 (± 0.8)
9	$Ir_6(CO)_{16}$	1.3 (± 0.5)	6.0 (± 1.6)

[a]0.5 wt.% M-NP/PC dispersion obtained by MWI with 50 W for 3 min. [b]Median diameter (Ø) and standard deviation (σ). See experimental section for TEM and DLS measurement conditions.

Organic carbonates have recently been used as solvents in catalysis, e.g., for platinum-catalyzed hydrosilylation of unsaturated fatty acid esters[226]in palladium-catalyzed substitution reactions,[227] regioselective rhodium-catalyzed hydroformylation[228] and in the asymmetric iridium-catalyzed hydrogenation of olefins.[201,229] Palladium colloids in PC were used to hydrogenate dienesand alkynes[211,212] and for Heck reactions.[213]

The weak interactions between a nanoparticle and organic carbonates could be of interest to develop more efficient catalyst processes. Here the Rh-NPs/PC dispersions have been tested for their catalytic activity in the biphasic liquid–liquid hydrogenation of cyclohexene to cyclohexane (Fig. 23, Table 7). The low miscibility of substrates and products with the PC phase allows for easy separation by simple decantation of the hydrophobic phase. Cyclohexene was chosen as a substrate since it presents a challenge because of its low solubility in PC and is an intermediate in the hydrogenation of benzene to cyclohexane.[230,231]

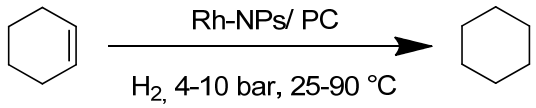

Fig. 23. Hydrogenation of cyclohexene to cyclohexane with Rh-NPs.

Table 7. Hydrogenation of Rh-NPs/PC with different substrates.[a]

entry	substrate	*t* [min]	p_{H2} [bar]	*T* [°C]	conversion [%]	activity [mol product × (mol Rh)$^{-1}$ × h^{-1}]
1	cyclohexene	108	4	75	95 [c]	590
2	cyclohexene	34	4	90	95 [c]	1875
3	cyclohexene	61	10	25	95 [c]	1045
4	1-hexyne [b]	104	10	25	88	51
5	cyclohexene [d]	1440 (= 24h)	4	90	0	0

[a] 10 mL (0.1 mol) cyclohexene or 1.0 mL (1.8 mmol) 1-hexyne; 0.75 mL of the Rh-NP/PC dispersion with 1 wt.% Rh (9 mg, 8.8×10^{-5} mol Rh). [b] 1 mL n-decane was added to provide a biphasic liquid-liquid catalytic system. No n-hexene detected by GC analysis see experimental section. [c] The reaction was intentionally stopped at 95 or 88% conversion as thereafter the decrease in cyclohexene concentration lowered the reaction rate (see Fig. 24). [d] Hydrogenation was carried out with Rh/SR-NPs (see Table 10, entry 3).

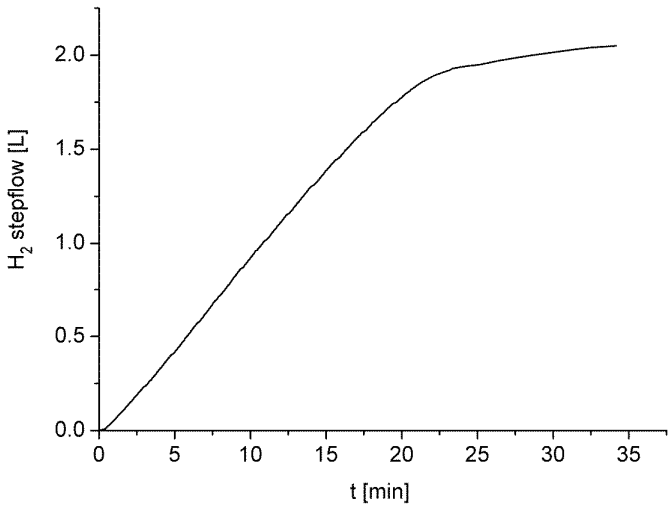

Fig. 24. H_2 uptake (in liter) over time for entry 2 in Table 7: Hydrogenation of cyclohexene (10 ml, 0.1 mol) to cyclohexane with a 0.75 mL of a 1 wt.% Rh-NP/PC dispersion and molar cyclohexene/metal ratio of 88000 at 90 °C, 4 bar H_2 pressure (cf. Table 7). An H_2 uptake of 2.24 L (0.1 mol H_2, ideal gas behavior) corresponds to 100% conversion.

For activity comparison Table 8 and Table 9 summarize related hydrogenation activities for cyclohexene and 1-hexyne with M-NPs in ILs and on supports from the literature. Activities for cyclohexene hydrogenations with Rh-NPs/PC were twice as good than for Ru- or Rh-NP catalysts in ILs[23,111,235] but not as good as for Rh-NPs on supports[232,237,238,284] The lower hydrogenation activities of Ru- and Rh-NPs in ILs are traced to the IL diffusion barrier for H_2 and the substrate, whereas ligand-free NPs on supports have a lower diffusion barrier.

Table 8. Catalyst activities of M-NPs in the 1-hexyne to hexane hydrogenation.

Metal-NP system	p_{H2}	conversion [%]	activity [mol product × (mol Rh)$^{-1}$ × h^{-1}] (= TOF [h^{-1}])	Ref.
Rh/PC	4 bar	88	51	this work
$Pt_2(P_2O_5H_2)_4^{4-}$	20.7 atm	not given	not given	233
1 % Pd/Al_2O_3	1 atm	50	22680, TOF = 6.3 s^{-1}	234

Table 9. Catalyst activities of M-NPs in the cyclohexene to cyclohexane hydrogenation.

Metal NP system	p_{H2}	conversion [%]	activity [mol product × (mol Rh)$^{-1}$ × h^{-1}] (= TOF [h^{-1}])	Ref.
Ru/BMImBF$_4$	10 bar	95	522	23
Ru/BMImBF$_4$	4 bar	> 99	388	235
Ru, solventless	4 atm	> 99	1000	236
Ru/BMImBF$_4$	4 atm	> 99	100	236
Ru/BMImPF$_6$	4 atm	> 99	62	236
Ru/graphene	4 bar	> 99	1570	237
Rh/PC	4 bar	95	1875	this work
Rh/PTFE	4 bar	> 99	32800	this work (section 4.2)
Rh/BMImBF$_4$	10 bar	95	884	23
Rh/graphene	4 bar	> 99	360	237
Rh/attapulgite	30 bar	> 99	2700	284
Rh/silica-coated magnetite NPs	6 atm	> 99	7600	238
Pd/Polygylcerol	40.52	no conv. Given	1190	239
Pt/BMImPF$_6$	4 atm	> 99	156	113
Pt, solventless	4 atm	> 99	833	113
Pt/acetone	4 atm	> 99	833	113
Pt/SiO$_2$	1 bar	no conv. Given	890	240
Pt/SiO$_2$	10 torr cylcohexene, 200 torr H$_2$	no conv. Given	12960	241

The addition of an organic ligand to the bare M-NP surface is generally described as a surface functionalization. However derivatization, coating, or capping are better terms.[126] The post synthetic introduction of an organic capping ligand on the dispersed M-NPs in PC is possible. Surface capping of Rh- or Ru-nanoparticles dispersed in the propylene carbonate was carried out here with 3-mercaptopropionic acid, HS-$(CH_2)_2$-COOH or trioctylphosphine oxide (TOPO). Both 3-mercaptopropionic acid[126] and TOPO[242,243] are well-known stabilizing reagents and both are soluble in propylene carbonate. The transformation of M-NP/PC to M-NP/HS-$(CH_2)_2$-COOH or M-NP/TOPO was done by treating the M-NP/PC dispersion with an excess of HS-$(CH_2)_2$-COOH or TOPO at room temperature over night. The strong affinity between the thiol (-SH) or phospine oxide (-P=O) group and the rhodium or ruthenium nanoparticles replaces the PC protective layer. The ligand-capped nanoparticles are significantly larger (Table 10, Fig. 25-Fig. 28). The use of a protic organic thiol ligand and the unpolar TOPO ligand more than doubles the size of the resulting capped metal nanoparticles (Table 10). The aggregation is a result of the introduction of the capping ligands into the polar PC network. Subsequently the stabilizing property of propylene carbonate towards the M-NPs is weakened and results in further M-NP agglomeration which is driven by the surface-surface interactions.

Table 10. Ligand capped M-NP and size distribution.

				M-NP/ligand in PC	
entry	metal	ligand	M-NP/PC original size from TEM [nm]	TEM Ø (σ) [nm][a]	DLS Ø (σ) [nm][a,b]
1	Rh	HS-$(CH_2)_2$-COOH	2.1 (± 0.6)	9 (±5)	24 (± 17)[c]
2	Rh	TOPO		10 (±5)	30 (± 14)[d]
3	Ru	HS-$(CH_2)_2$-COOH	2.7 (± 0.5)	13 (±4)	6.0 (± 1.5)[c]
4	Ru	TOPO		13 (± 5)	37 (± 12)[d]

[a] Median diameter (Ø) and standard deviation (σ). See experimental section for TEM and DLS measurement conditions. [b]Hydrodynamic radius, median diameter from the measurements at 633 nm. The resolution of the DLS instrument is 0.6 nm. [c]measurement performed in ethanol. [d]measurement performed in chloroform.

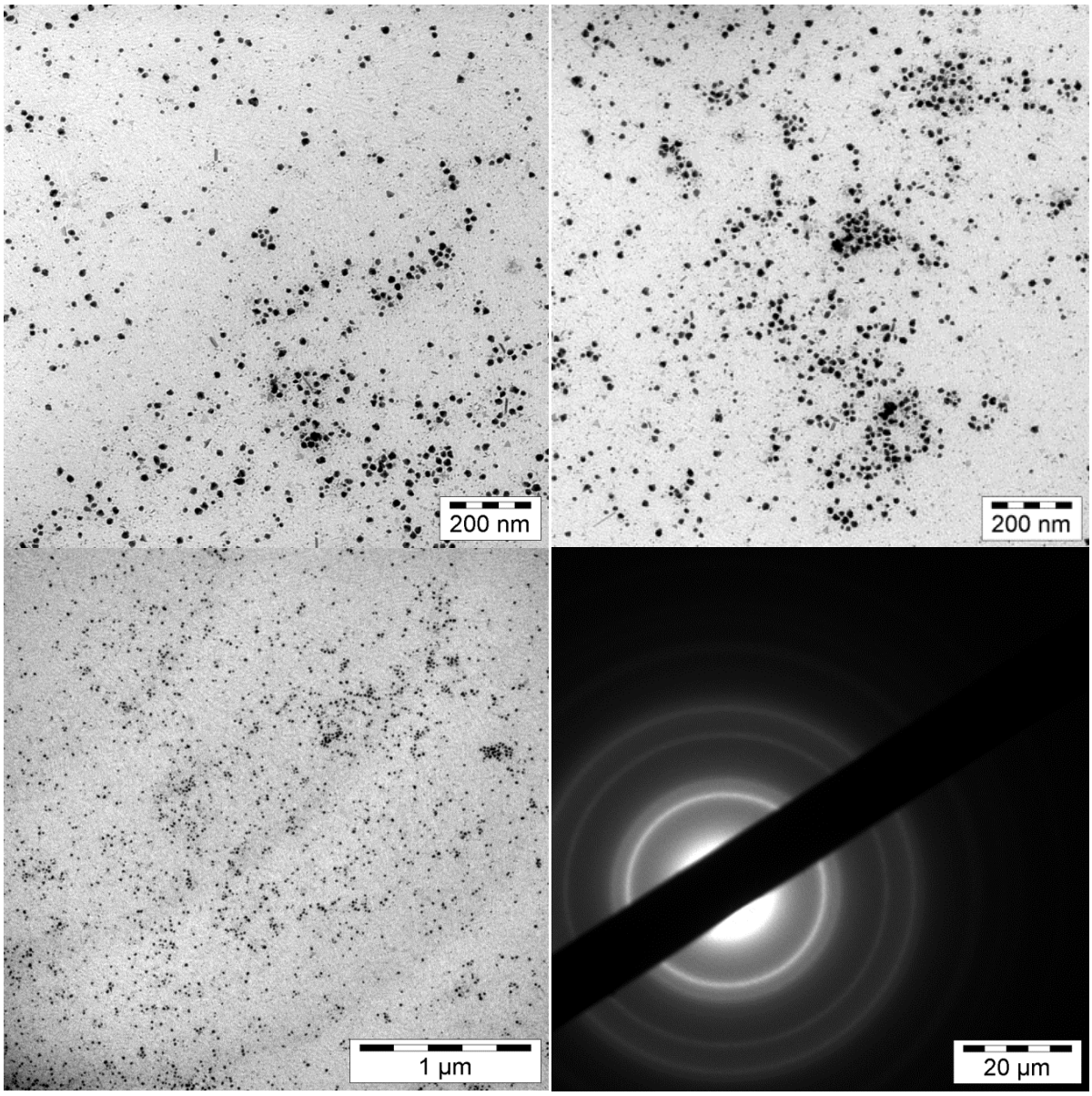

Fig. 25. TEM/TED photographs of Rh-NP/HS-$(CH_2)_2$-COOH from a Rh-NPs/PC dispersion (0.5 wt.%) after thiolation with 3-mercaptopropionic acid, centrifugation and re-dispersion in ethanol (entry 1 in Table 10).

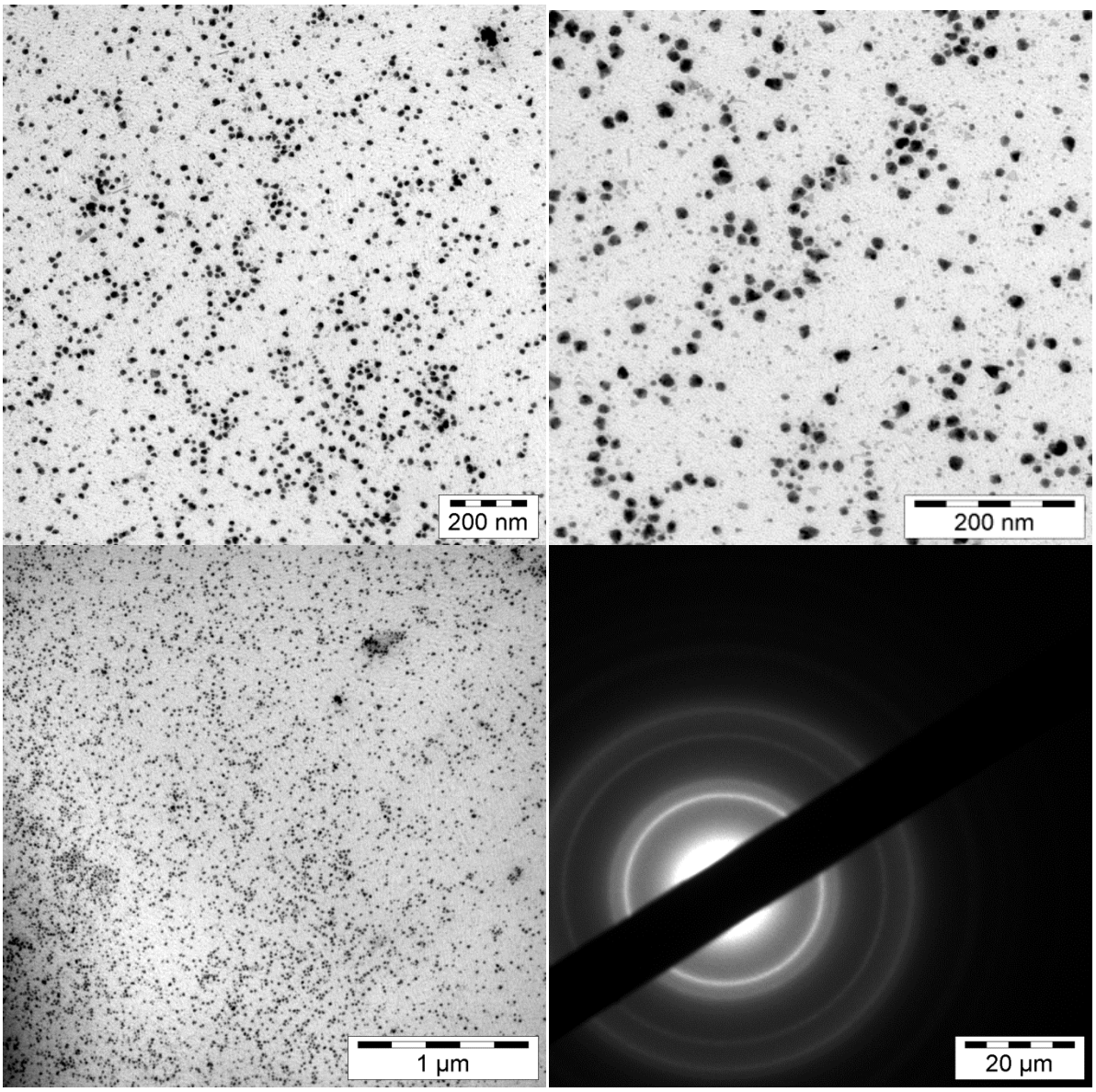

Fig. 26. TEM/TED photographs of Rh-NP/TOPO from a Rh-NPs/PC (0.5 wt.%) after stabilization with TOPO, centrifugation and re-dispersion in chloroform (entry 2 in Table 10).

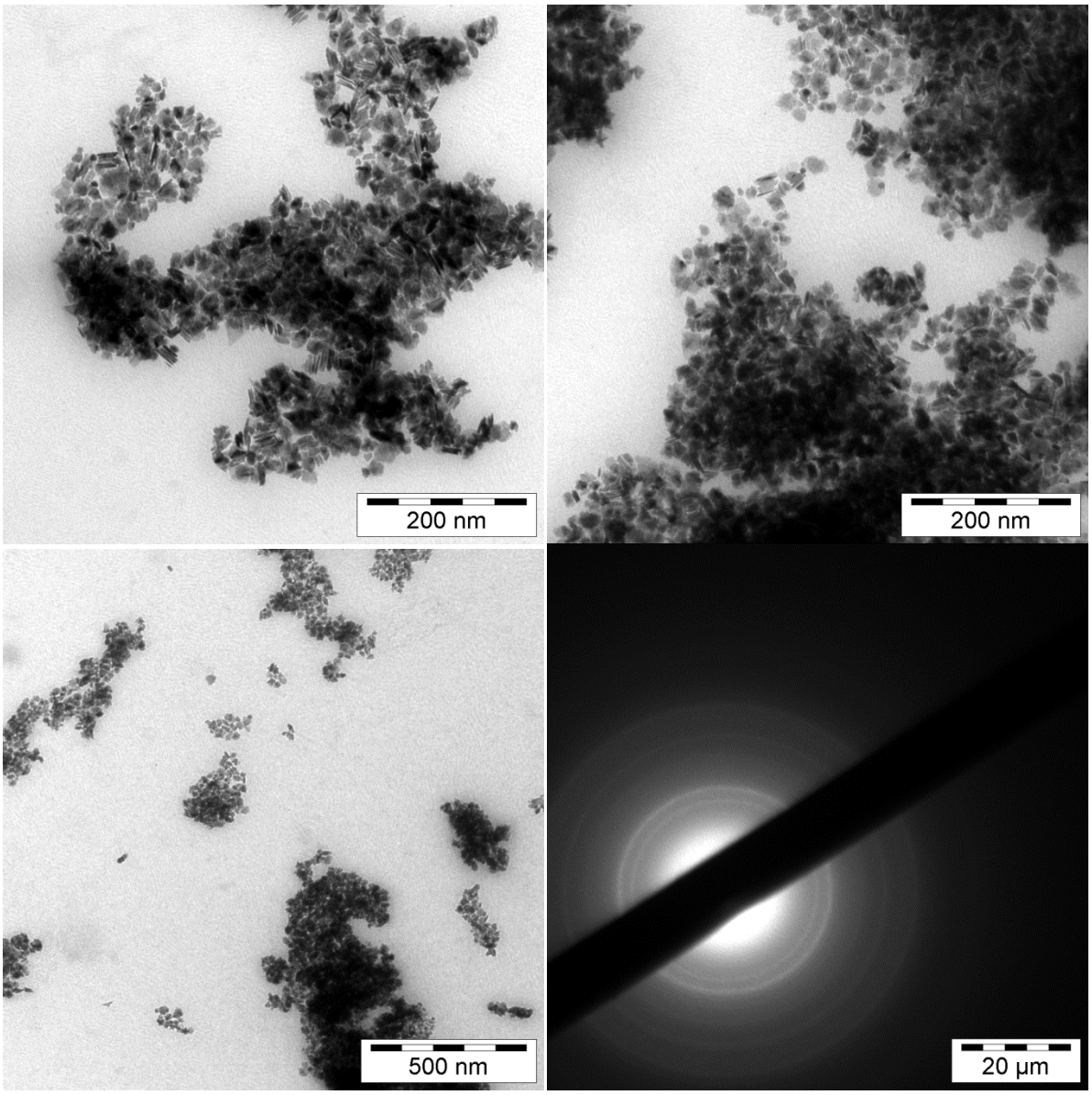

Fig. 27. TEM/TED photographs of Ru-NP/HS-$(CH_2)_2$-COOH from a Ru-NP/PC dispersion (0.5 wt.%) after thiolation with 3-mercaptopropionic acid, centrifugation and re-dispersion in ethanol (entry 3 in Table 10).

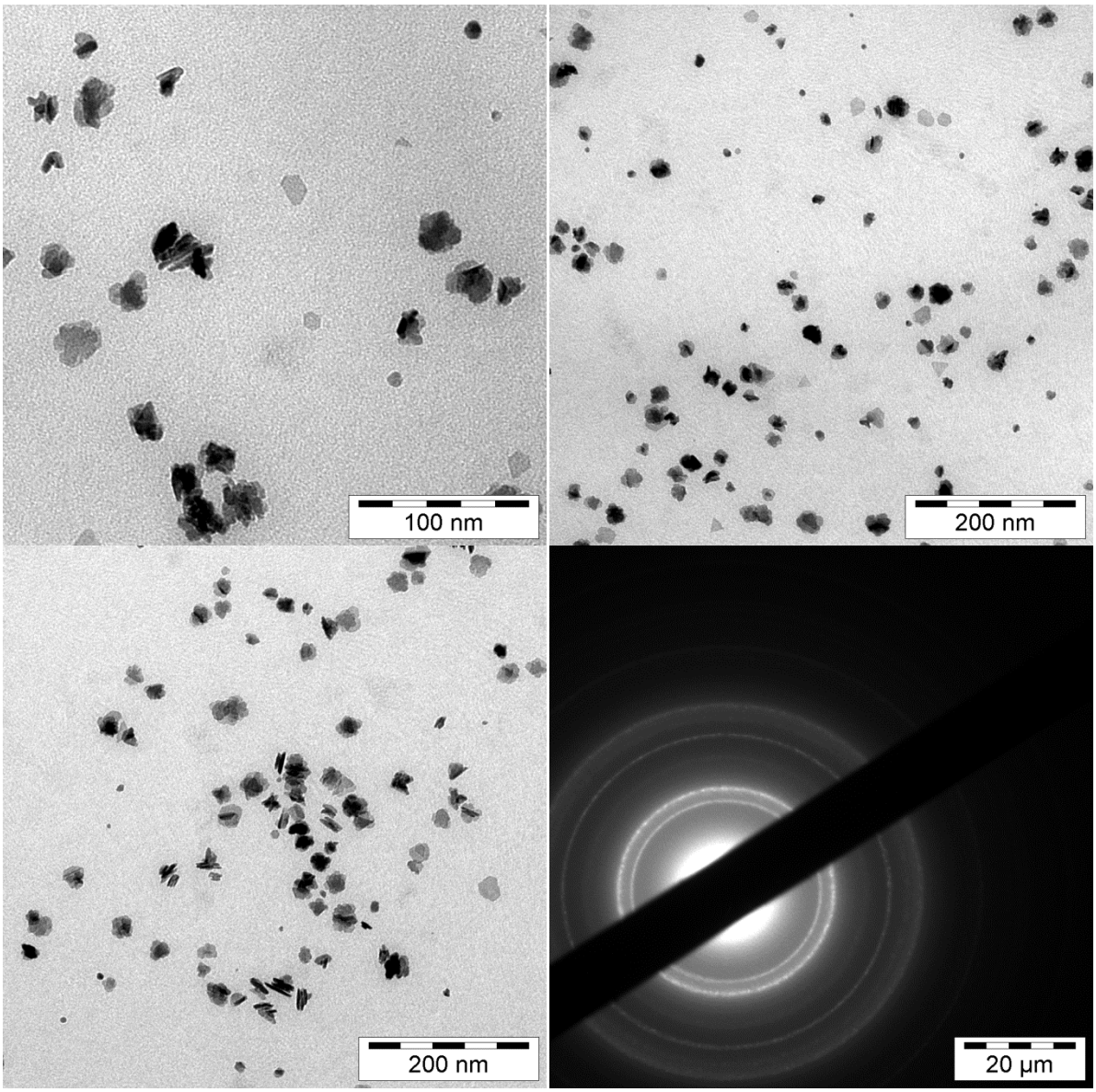

Fig. 28. TEM/TED photographs of Ru-NP/TOPO from a Ru-NP/PC dispersion (0.5 wt.%) stabilized by TOPO, centrifugation and re-dispersion in chloroform (entry 4 in Table 10).

Here a simple, reproducible, and broadly applicable microwave-induced metal carbonyl decomposition for the synthesis of common transition metal nanoparticles in propylene carbonate is shown. The M-NP sizes of about 1 to 3 nm for most of these transition metal nanoparticles are very small and uniform with no extra stabilizers or capping molecules needed to achieve this small particle size in a stable M-NP/PC dispersion. Polar organic carbonates are susceptible for microwave irradiation which, thus, provides a very simple and reproducible way for the rapid (3 min) and energy-saving (50 W power) synthesis of defined and very small M-NPs from their binary metal–carbonyl complexes in PC. The obtained Rh-NP/PC dispersions can be used - without further treatment - as highly active hydrogenation catalysts. In comparison to ionic liquids, PC and other organic carbonates are established

industrial and low-priced solvents.[203] PC appears as an attractive alternative for weakly coordinated, albeit sufficiently stabilized metal nanoparticles

These results are part of this cumulative dissertation (**publication 6.1**).

4.2 Rhodium nanoparticles supported PTFE stirring bars

Here it is shown that a common and frequently used laboratory commodity such as a Teflon-coated magnetic stirring bar can carry on its surface catalytically active metal nanoparticles which are not easily removed. On one hand this is "caveat" on the un-intentional preparation of "catalytically active stirring bars" by nanoparticular metal depositions from previous reactions. On the other hand our simple deposition of rhodium metal nanoparticles (Rh-NPs) on the Teflon surface of a stirring bar (Rh-NPs@stirring bar) yields an easily hand able and re-usable hydrogenation catalyst. This proof-of-concept should be extendable to other metal nanoparticle catalysts. Rhodium was used here as a metal for the proof-of-principle because rhodium is used in many types of catalytic reactions like hydroformylations,[244] C-C bond forming reactions,[245] Pauson-Khand type reactions[246] and hydrogenations.[98,247]

Deposition of Rh-NPs onto a standard Teflon (PTFE)-coated stirring bar is easily achieved by thermal decomposition of $Rh_6(CO)_{16}$ in $BMImBF_4$ through microwave irradiation[23] by immersion of the stirring bar into the Rh-NPs/IL dispersion (Fig. 29).

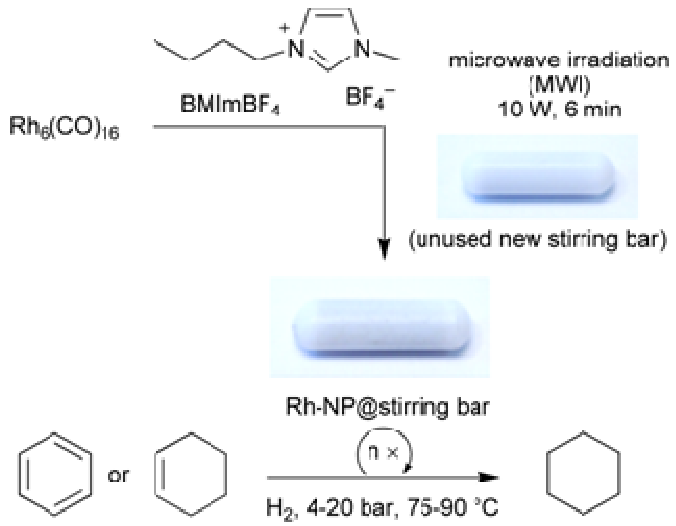

Fig. 29. Preparation of Rh-NP@stirring bar and repeated utilization as hydrogenation catalyst. The photographs show a standard commercial 20 × 6 mm magnetic stirring bar before and after Rh-NPs deposition.

Rh-NPs deposition on the stirring bar is only slightly evident by visual inspection with a naked eye from some minor darkening (Fig. 29). Proof of the Rh-NPs deposits is obtained by scanning electron microscopy (SEM) of the Teflon surface or transmission electron microscopy of Teflon flakes therefrom (Fig. 30). The amount of Rh-NPs@stirring

bar was quantified by AAS to 32 (±8) µg per stirring bar. A Rh-NP size analysis was carried out by transmission electron microscopy (TEM) on Teflon flakes which were cut from the stirring bar (Fig. 30 middle right, down left). Median Rh-NPs diameters were 2.1 (± 0.5) nm and 1.7 (± 0.3) nm after the 10th hydrogenation run.

There are wide ranges of supports described for M-NPs,[10] which can be split into three main categories for solid supports employed for the deposition of M-NPs:

(1) carbonaceous materials, like carbon nanotubes,[248] graphite oxide[249] and graphene[173,180,250]
(2) metal oxides, including silica,[251-253] titania,[254-256] zirconia,[257] and ceria,[253,258] calcium oxide,[259] or magnesia[248,260-262] and
(3) organic polymers, such as polyorgano-phosphazenes,[263] polyvinylpyridine, fibers and dendrimers.[264]

However, very little is known for PTFE as a nanoparticle support.[126,265,266] The immobilization of Fe-NPs on the surface of PTFE nanogranules appears to be a singular example. The chemical properties of bulk PTFE were considered unsuitable for the stabilization of metal containing nanoparticles.[267]

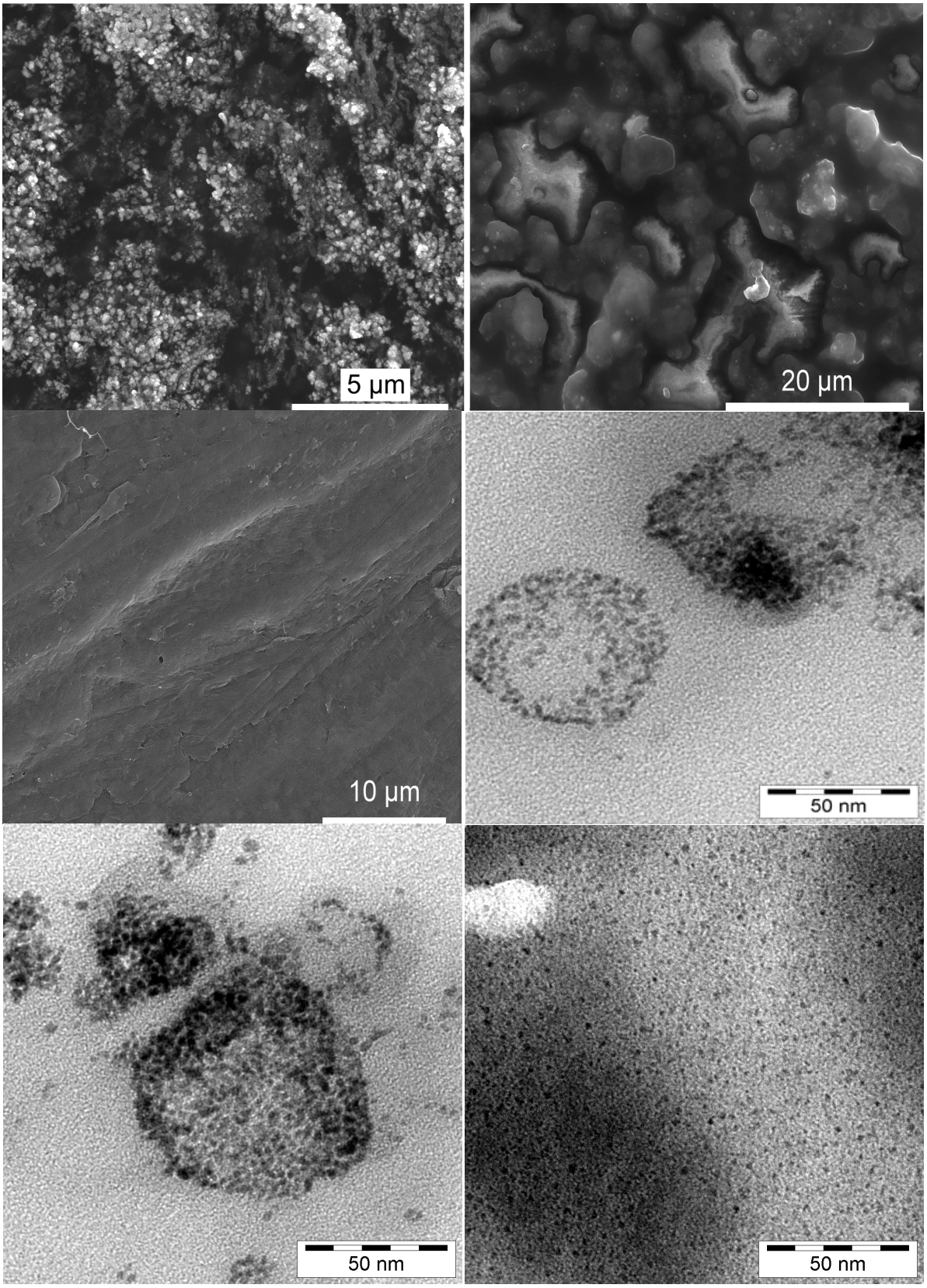

Fig. 30. SEM-pictures of Rh-NPs on a Teflon-coated magnetic stirring bar (Rh-NP@stirring bar) (upper left) and after 10 hydrogenation runs (upper right) in comparison to the blank Teflon surface (middle left). TEM of Teflon flakes from the stirring bar coating for Rh-NP size analysis before catalysis (middle right, down left) and after the 10th catalytic hydrogenation run of cyclohexene (down right).

The caveat: It is evident that PTFE, albeit generally considered a chemically inert material with a non-sticking surface, can support nanoparticular metal deposits. Such nanoparticular deposits can originate from various uses of stirring bars in a laboratory. These M-NP deposits are also not easily removed by washing with organic solvents. If then such a stirring bar with a "colorful past" is used in catalysis experiments the metal nanoparticle deposits can exert an activity while the intended catalysis system is less active or even inactive (akin to the metal impurites in "intended" catalysts noted in the introduction). This possibility is especially problematic because such metal nanoparticle deposits cannot be visually detected.

The chance: The ease of support of metal nanoparticles on a readily available and thermally stable PTFE surface can open new vistas for metal nanoparticle and catalysis research, especially in view of the easy separation of a catalytically acitve magnetic stirring bar akin to the recovery of magnetic nanoparticle catalysts.[268-270]

As a proof-of-concept the Rh-NPs@stirring bar supported magnetic stirring bars were tested for their re-usable catalytic activity in the known hydrogenation of cyclohexene or benzene to cyclohexane under organic-solvent-free conditions where comparative literature data is available (Fig. 7, Fig. 29, Table 12). The hydrogenation reactions were carried out in a stainless steel autoclave equipped with a glass inlay. The autoclave was heated to 75 °C or 90 °C and pressurized with the hydrogen consumption monitored by a Büchi pressflow gas contoller (H_2 uptake over time, Fig. 33, Fig. 34). Near quantitative conversion the reactor was depressurized and the volatile organic components were condensed under vacuum into a clean cold trap. To test for recycling the Rh-NPs@stirring bar was left behind in the autoclave and was re-used by adding fresh substrate. Catalyst recycling was carried out ten times for cyclohexene and three times for benzene. There is an initial increase in activity with recycling from entry 1-3 in Table 11 which was also seen in other hydrogenations with Rh-NPs/IL systems.[22,23] This is probably due to a slow surface restructuring and not due to the rapid formation of Rh–hydride or Rh–heterocyclic carbene (NHC)[271] surface species.[272]

Table 11. Hydrogenation of cyclohexene or benzene to cyclohexane with Rh-NP@stirring bar.[a]

entry	substrate and run	conversion [%]	*t* [min]	activity [mol product × (mol Rh)$^{-1}$ × h^{-1}] (= TOF [h^{-1}])
1	Cyclohexene[b]	> 99	88	14.9 × 10^3
2	2nd run	> 99	49	26.8 × 10^3
3	3rd run	> 99	40	32.8 × 10^3
4	4th run	> 99	48	27.3 × 10^3
5	5th run	> 99	68	19.3 × 10^3
6	6th run	> 99	132	9.9 × 10^3
7	7th run	87[d]	139	8.2 × 10^3
8	8th run	> 99	139	9.4 × 10^3
9	9th run	> 99	161	8.1 × 10^3
10	10th run	80[d]	160	6.6 × 10^3
11	Benzene[c]	85[d]	1474	750
12	2nd run	90	1607	730
13	3rd run	90	2553	460
14	Cyclohexene[e]	78	1440	
15	Cyclohexene[f]	20	1440	
16	Cyclohexene[g]	53	1440	

[a] Conditions: Rh metal 32 µg, 3.1 × 10^{-7} mol. [b]Cyclohexene 0.69 mL, 6.8 mmol, 75 °C, 4 bar H_2. [c]Benzene 0.6 mL, 6.8 mmol; 90 °C, 20 bar H_2. [d]Conversion ceased. [e-g]See Fig. 35 for further details.

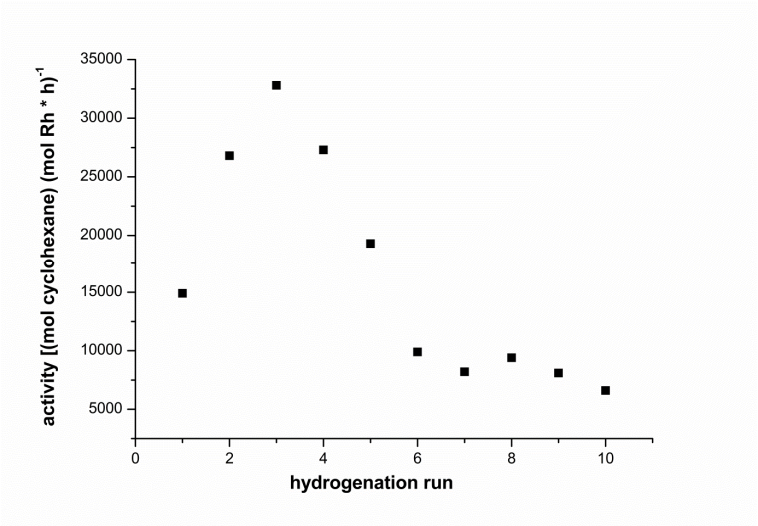

Fig. 31. Activity for 10 runs of the hydrogenation of cyclohexene with the same Rh-NPs@stirring bar and molar cyclohexene/Rh ratio of 2200 at 75 °C, 4 bar H_2 pressure.

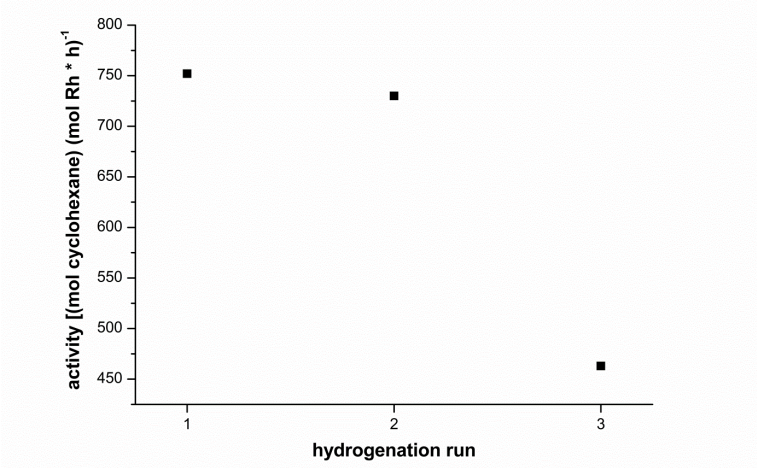

Fig. 32. Activity for 3 runs of the hydrogenation of benzene to cyclohexane with the same Rh-NPs@stirring bar and molar benzene/metal ratio of 2200 at 90 °C, 20 bar H_2 pressure.

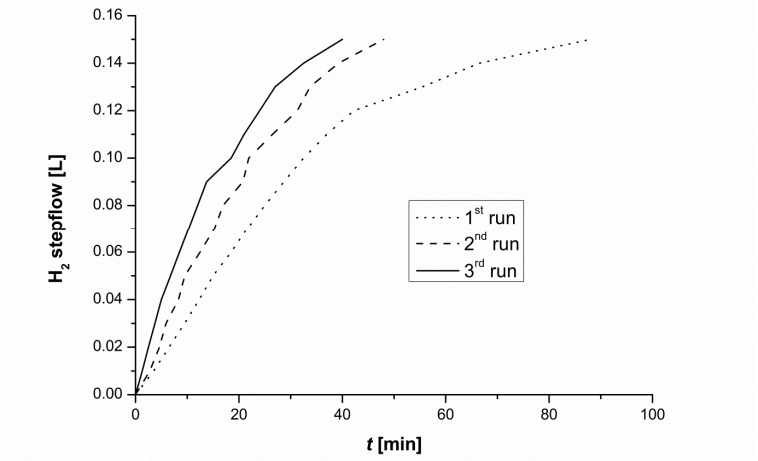

Fig. 33. H_2 uptake over time for the 1st, 2nd and 3rd hydrogenation run of cyclohexene with the same Rh-NPs@stirring bar and molar cyclohexene/Rh ratio of 2200 at 75 °C, 4 bar H_2 pressure. An H_2 uptake of 0.15 L corresponds to > 99% conversion (100% are 6.8 mmol or 0.15 L H_2).

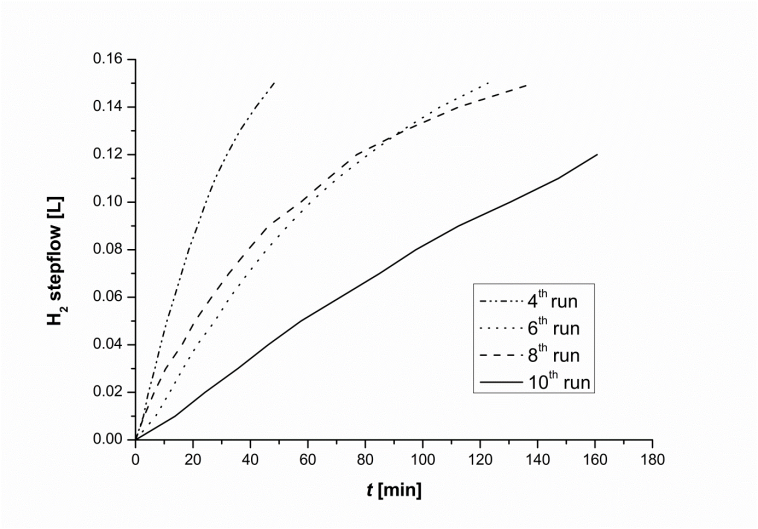

Fig. 34. H_2 uptake over time for the 4th, 6th, 8th and 10th hydrogenation run of cyclohexene to cyclohexane with the same Rh-NPs@stirring bar and molar cyclohexene/Rh ratio of 2200 at 75 °C, 4 bar H_2 pressure. An H_2 uptake of 0.15 L corresponds to > 99% conversion (100% are 6.8 mmol or 0.15 L H_2).

Table 9 and Table 12 summarize related M-NPs (in ILs and on supports) from the literature and their cyclohexene and benzene, respectively, hydrogenation acitivities. For benzene hydrogenation the activity was higher than for most supported M-NP literature systems and only surpassed by Rh-NP/carbon nanofibers (Table 9).

Table 12. Catalyst activities of M-NPs in the benzene to cyclohexane hydrogenation.

Metal	p_{H2}	conversion [%]	activity [mol product × (mol Rh)$^{-1}$ × h^{-1}] (= TOF [h^{-1}])	Ref.
Ru, solventless	4 atm	90	82	236
Ru/BMImBF$_4$	4 atm	30	9	236
Ru/BMImPF$_6$	4 atm	73	20	236
Ru/BMImCF$_3$SO$_3$	4 atm	50	14	236
Ru, solventless	4 atm	> 99	125	236
Ru/HEA-16-Cl[a]	30 bar	> 99	200	273
Rh/PTFE	20 bar	90	750	this work
Rh/BMImPF$_6$	4 atm	> 99	11	98
Rh, solventless	4 atm	> 99	21	98
Rh/acetone	4 atm	> 99	16	98
Rh/graphene	4 bar	99	310	237
Rh/carbon nanofibers	4 atm	>99	7750	274
Rh/HEA-16-Cl[a]	1 atm	> 99	28	275
Ir/BMImPF$_6$	4 atm	> 99	85	98
Ir, solventless	4 atm	> 99	125	98
Ir/acetone	4 atm	> 99	200	98
Pt/BMImPF$_6$	4 atm	46	11	113
Pt, solventless	4 atm	> 99	28	113

[a] HEA-16-Cl = hydroxyethylammonium chloride

In general in M-NP catalysis the active species can be either "heterogeneous" M-NPs in a disperson or on a surface or "homogeneous" atoms or small clusters which leach from the M-NP into the solution.[276] Hence, we cannot exclude, that the Rh-NP@stirring bar functions as a reservoir of such "homogeneous" active atoms or clusters. There is only a minor amount of mechanical abrasion or of leaching of Rh-NPs from the stirring bar

during each catalytic run as was attested by three reproducible experiments outlined in Fig. 35. Abrasion onto the glass surface appears to be more prominent than simple leaching when comparing the resulting activities from stirred (Fig. 35a, Table 11, entry 14) versus non-stirred preparations (Fig. 35b, Table 11, entry 15) before applying the hydrogen pressure. Sizeable conversion can be attested from the abrasion, albeit at prolonged reaction times (24 h, entry 14) when compared to the conversion versus time of Rh-NPs@stirring bar under otherwise identical conditions (entry 1-10).

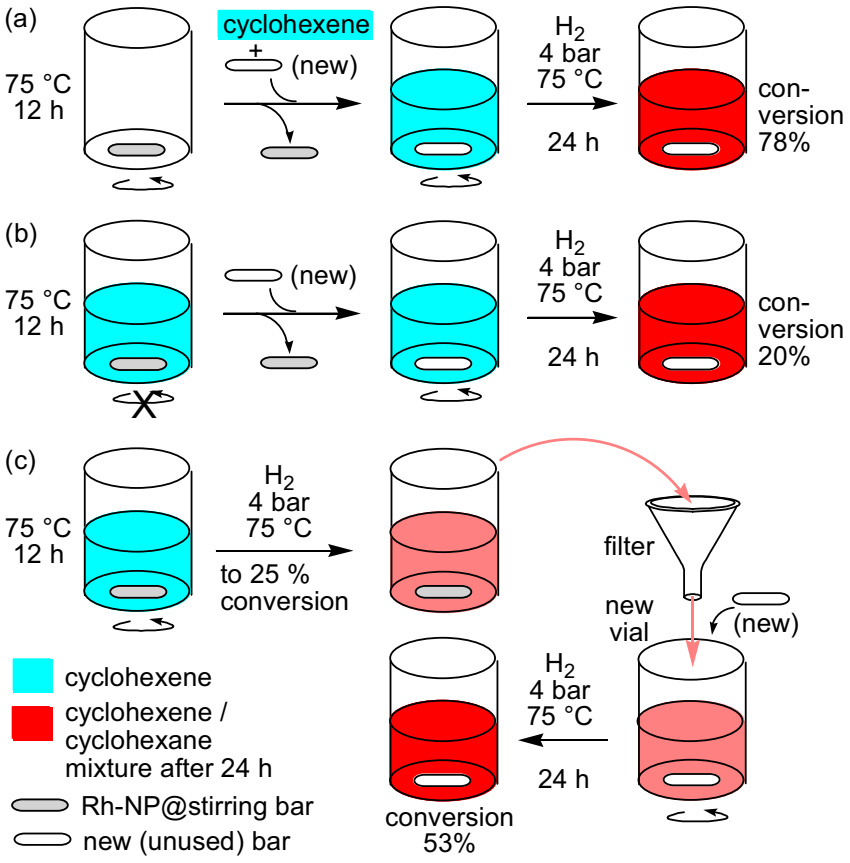

Fig. 35. Experiments to attest the abrasion or leaching from Rh-NPs@stirring bar (carried out twice to ensure reproducibility within experimental error). (a) (Table 11, Entry 14) Stirring of Rh-NPs@stirring bar in the empty glass inlay at 75 °C for 12 h under N_2, followed by removal of the stirring bar, addition of a new (unused) stirring bar, cyclohexene and H_2. A conversion of 78% is reached after 24 h (cf. > 99% with Rh-NPs@stirring 1-2 h, entry 1-5) and indicates some, but little mechanical abrasion of the Rh-NPs from the PTFE surface. (b) (Table 11, Entry 15,) Allowing Rh-NPs@stirring bar to stand in cyclohexene at 75 °C for 12 h under N_2, followed by removal of the stirring bar, addition of a new stirring bar and H_2. A conversion of only 20% after 24 h indicates little leaching from the stirring bar into the cyclohexene substrate. (c) (Table 11, Entry 16) Cyclohexene hydrogenation was run to 25% conversion (within 12 min, monitored by gas uptake). Then, Rh-NPs@stirring bar was removed, the cyclohexene/cyclohexane mixture filtered under argon into a new glass inlay, equipped with a new stirring bar and re-pressurized. Conversion proceeded very slowly to 53% in 24 h, attesting little leaching even under the reaction conditions.

Metal nanoparticle traces can easily be deposited – intentional or unintentional – on the PTFE surface of magnetic stirring bars. Memory effects can derive from unintentional deposits when such stirring bars are employed in catalytic reactions. At the same time it is shown that a lab commodity such as a Teflon-coated magnetic stirring bar can be easily turned into a re-usable, smoothly handable and magnetically removable catalyst system. "Traces" of 32 µg or less of Rh-nanoparticles on the stirring bar surface exert very high hydrogenation activities for cyclohexene or benzene under mild conditions.

These results are part of this cumulative dissertation (**publication 6.2**).

4.3 Rhodium and ruthenium nanoparticles supported Graphene

The fluffy CDG powder (Fig. 36 synthesis according to Fig. 37) can be suspended in the IL 1-butyl-3-methylimidazolium tetrafluoroborate ($BMImBF_4$). The subsequent TEM pictures with M-NPs show single graphene sheets (cf. Fig. 38 and Fig. 39) which suggest that the CDG is dispersed into individual flakes in the IL.

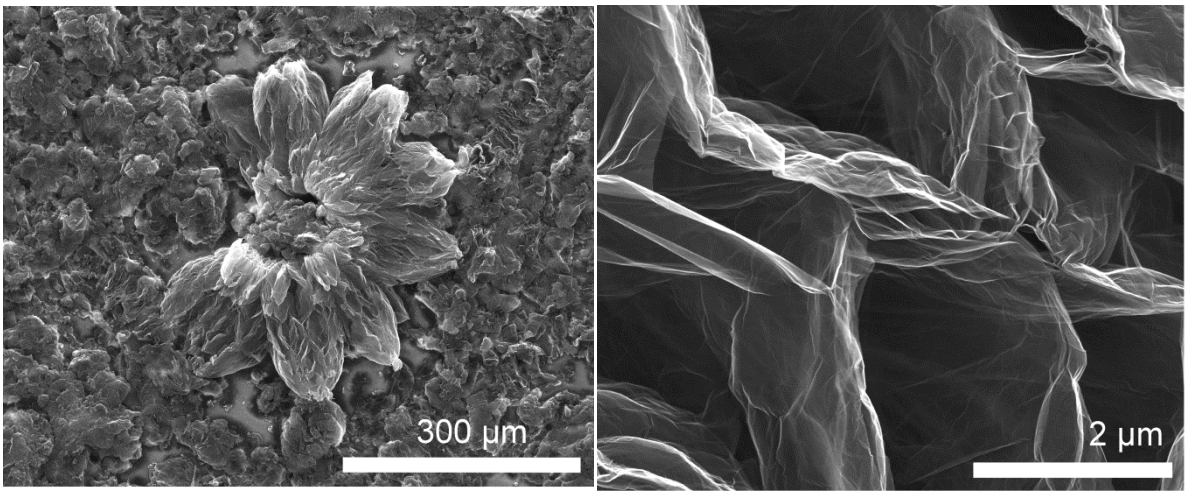

Fig. 36. Scanning electron microscope (SEM) images of CDG from thermally reduced GO, showing the exfoliated sheets at the larger magnification at the right.

The solid metal carbonyl powders $M_x(CO)_y$ (M = Ru, Rh) were added to the CDG slurry in $BMImBF_4$ and suspended under argon atmosphere. The mixture was subjected to microwave 10 irradiation (6 min, 20 W) under argon atmosphere. The M-NP/CDG materials (M = Ru, Rh) can be separated from the IL and unsupported M-NP/IL by centrifugation of the slurry, washing with water and drying in air. Black-grayish flake-like solids of M-NP/CDG were obtained in good yield (Table 13). Defined and small Ru- and Rh-NPs with narrow size distributions (2.2 ± 0.4 nm for Ru, 2.8 ± 0.5 nm for Rh) can be seen on the almost transparent CDG surfaces in the TEM image of the Ru- and Rh-NP/CDG hybrid structures (Fig. 38 and Fig. 39).

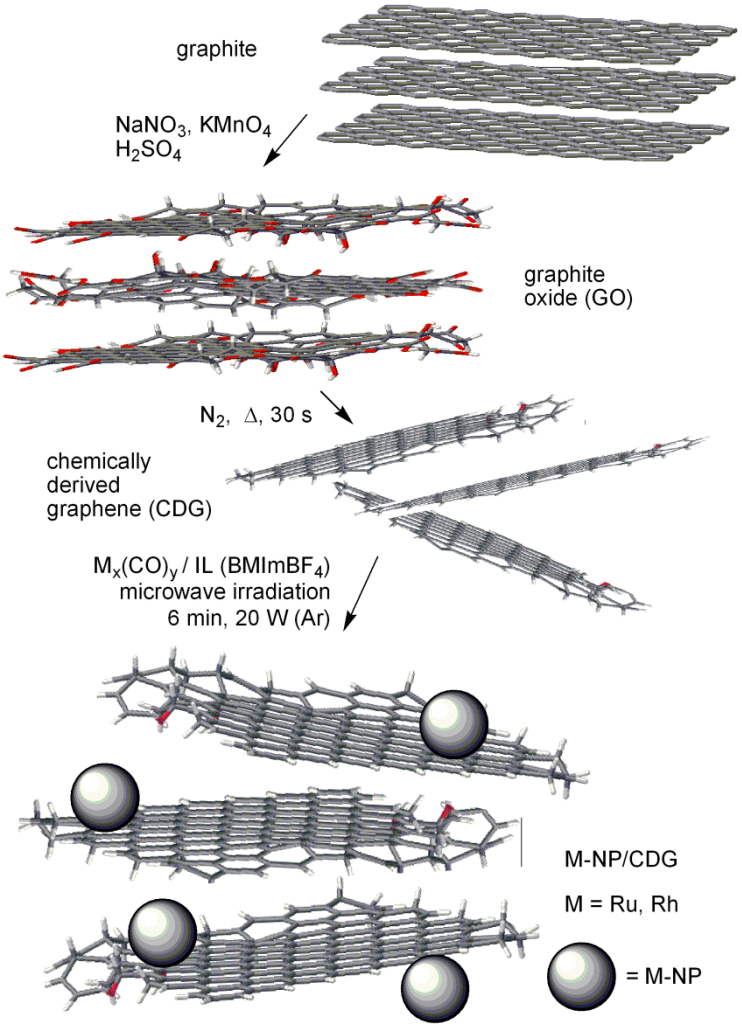

Fig. 37. Synthesis from natural graphite over GO (Hummers and Offeman[277]) to CDG (thermal reduction process [177]) and M-NP/CDG. GO bearing epoxy, hydroxyl, carbonyl and carboxyl groups was heated up to 560 °C and CO, CO_2 and H_2O were eliminated under enormous expansion of the CDG volume. The graphene sheets with mainly hydroxyl, carbonyl group[177,178,278] are exfoliated by the gas release and the specific surface area becomes 510 m²/g in the CDG used here (Fig. 36).

Table 13. M-NP particles sizes and yields of M-NP/CDG.[a]

metal	average diameter Ø [b] [nm]	min Ø [b] [nm]	max Ø[b] [nm]	standard deviation σ [nm]	M load on CDG [c] [%]	M-NP/CDG Yield [mg]	M-NP/CDG Yield [%]
Ru	2.2	1.4	3.6	0.4	17.4	25.0	83
Rh	2.8	1.6	4.4	0.5	17.0	15.7	54

[a] Synthesized by microwave decomposition in $BMImBF_4$ (2.0 ml, 2.4 g, ρ = 1.2 g/ml) with 4.8 mg CDG (0.2 wt% in IL) and 50.6 mg $Ru_3(CO)_{12}$ and 62.5 mg $Rh_6(CO)_{16}$, respectively (1 wt.% metal in IL) under argon. [b] M-NP particle size analysis by transmission electron microscopy (TEM) directly from the M-NP/CDP/IL suspension before work-up. [c] AAS analysis after dissolving the metal with aqua regia.

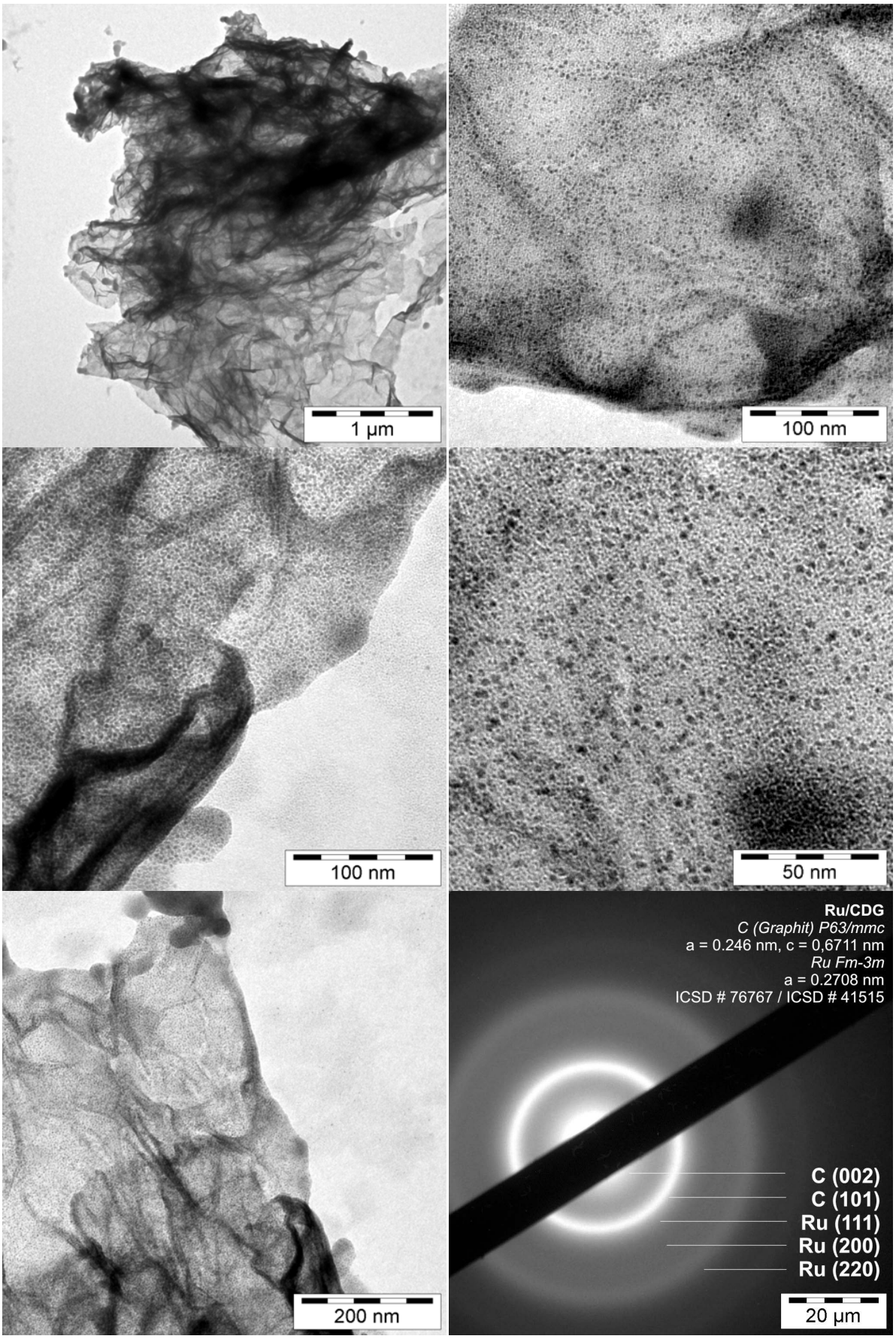

Fig. 38. TEM and TED (transmission electron diffraction) of Ru-NPs supported on CDG from MWI of $Ru_3(CO)_{12}$ in CDG/$BMImBF_4$. The black bar in the TED is the beam stopper (down right). The values match with the d-spacing of Ru metal and graphite.

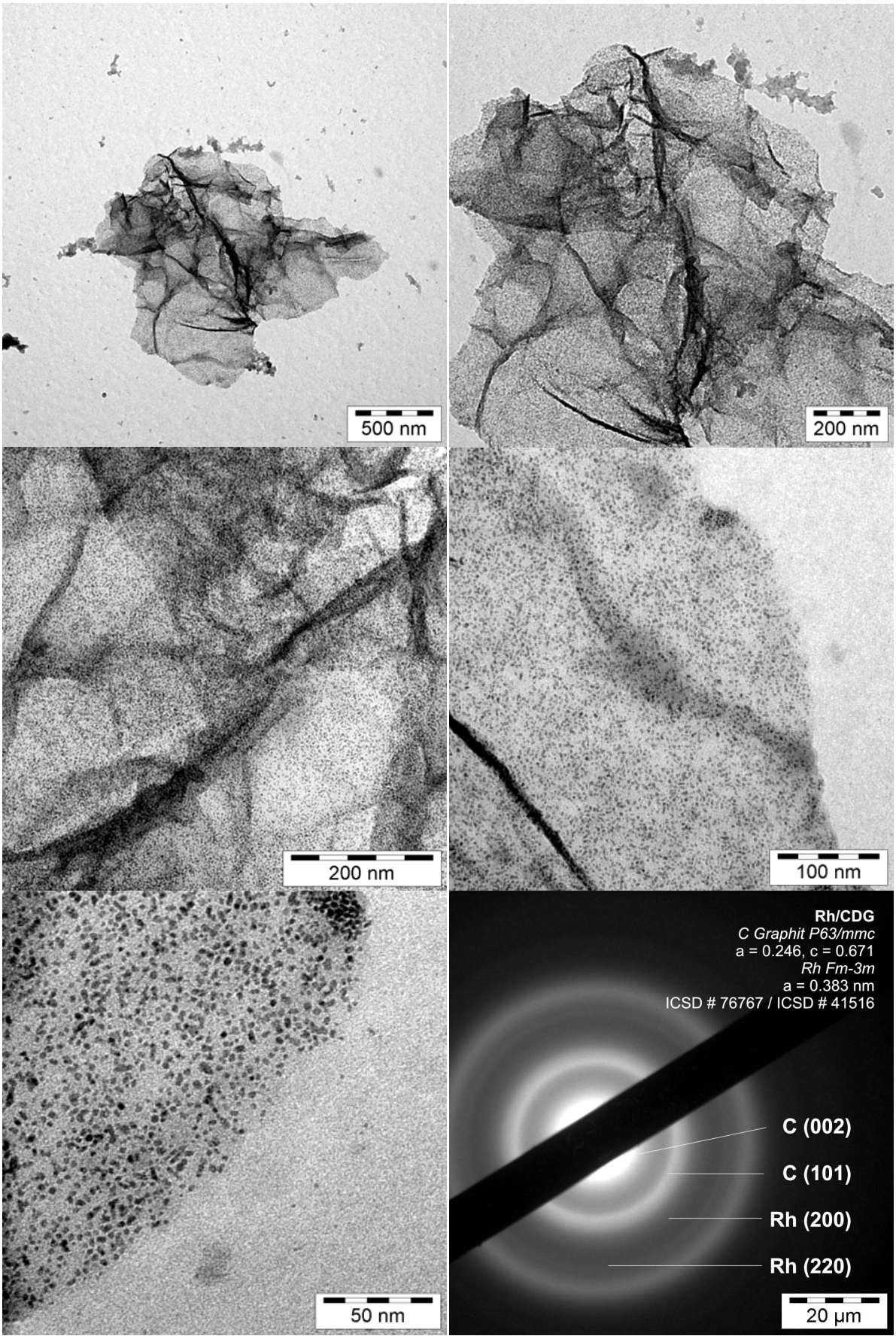

Fig. 39. TEM and TED of Rh-NPs supported on CDG from MWI of $Rh_6(CO)_{16}$ in CDG/$BMImBF_4$. The black bar in the TED is the beam stopper (down right). The d-values match with the d-spacing of Rh metal and graphite.

In a proof-of-principle, the M-NP/CDG materials (M = Rh, Ru) are shown to be catalysts in hydrogenation reactions of cyclohexene and benzene to cyclohexane (Fig. 40). The benzene hydrogenation to cyclohexane is a multi-million ton (IFP–Institute Francais du Petrol) processwith the subsequent oxidation to adipic acid and caprolactam as building blocks for Nylon 6.6 and Nylon 6.[279-283]

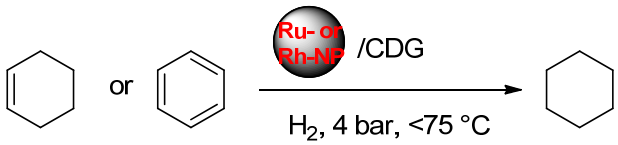

Fig. 40. Hydrogenation of cyclohexene or benzene to cyloclohexane with Ru- or Rh-NPs/CDG under organic-solvent-free conditions.

The M-NP/CDG catalyst (M = Ru, Rh) was suspended in the substrate cyclohexene or benzene without any additional solvent. The hydrogenation reaction times with Ru-NPs/CDG were optimized for near quantitative conversion. For work-up after each catalytic run the organic phase was removed under reduced pressure and condensed in a cold trap for GC analysis. It was possible to re-use the remaining catalyst for repeated runs each with essentially complete conversion (Table 14, Fig. 41). The pressure-normalized cyclohexene hydrogenation activities of Ru-NPs/CDG at 4 bar (~390 mol product × (mol metal)$^{-1}$ × h^{-1} × bar^{-1}) at almost identical > 95% conversions are higher by about one order of magnitude than the activities of similar Ru-NPs/IL systems at 10 bar H_2 pressure (30-53 mol product × (mol metal)$^{-1}$ × h^{-1} × bar^{-1}).[23] With rhodium the normalized activities of ~90 mol product × (mol metal)$^{-1}$ × h^{-1} × bar^{-1} were comparable to those of a Rh-attapulgite (Atta-IL-Rh) catalyst which was prepared by an ionic liquid-assisted immobilization of Rh from complexes, such as $Rh(PPh)^{3+}$, $Rh(COD)(PPh_3)^{2+}$, and $[Rh(COD)(PPh_3)_2]BF_4$ (COD 1,5-cyclooctadiene) on the natural mineral attapulgite. The pressure-normalized activities of Atta-IL-Rh at 30 bar reached ~90 mol product × (mol metal)$^{-1}$ × h^{-1} × bar^{-1} for >99% conversion in 5.5 h.[284] Rh-NPs immobilized on silica-coated magnetite nanoparticles gave high cyclohexene hydrogenation activities between 2500 and 6600 mol product × (mol metal)$^{-1}$ × h^{-1} × bar^{-1} (at 6 bar, 75 °C, >99% conversion) for up to 20 consecutive runs.[238] TEM/TED pictures of Rh-NPs/CDG after 5 consecutive catalytic runs do not show marked changes in Rh-NPs size but a somewhat higher crystallinity is apparent from TED (Fig. 42).

Table 14. Hydrogenation of cyclohexene with M-NP/CDG catalysts.

entry	M-NP/CDG[a]	time[b] [h]	conversion[c] [%]	activity [mol product × (mol metal)$^{-1}$ × h^{-1}] (= TOF [h^{-1}])
1	M = Rh	1.5	99.5	360
2	2nd run	1.5	98.7	357
3	3rd run	1.5	99.3	359
4	4th run	1.5	98.1	355
5	5th run	1.5	99.0	358
6	M = Ru	0.33	97.4	1540
7	2nd run	0.33	99.0	1570
8	3rd run	0.33	98.8	1560
9	4th run	0.33	98.6	1560
10	5th run	0.33	99.1	1570
11	6th run/CS_2[c]	0.33	98.8[b]	1560[c]
12	7th run/CS_2[d]	0.33	47.5[c]	750[d]
13	M=Ru	1	97.8	510
14	M=Ru	0.5	99.6	1040
15	M=Ru	0.3	94.5[e]	1960[e]

[a] The reactions were carried out in steel autoclaves, equipped with glass inlays to eliminate any catalytic influence of the metal surface on the reaction. General conditions 4 bar H_2 and 75°C. 11 mg M-NP/CDG with 17.4 wt% corresponding to 1.89 × 10–5 mol Ru or 17.0 wt% Rh, i.e. 1.82 × 10^{-5} mol Rh, respectively. [b]The hydrogenation reaction times for Ru NP/CDG were optimized for near quantitative conversion. A lower reaction time of 15 min yielded only 94.5% conversion, higher reaction times of 30 min and 1 h showed high conversions of >98% at lower activity [c]Addition of CS_2 (5.59 × 10^{-5} ml, 9.25 × 10^{-7} mol, density 1.266 g/cm^3, M = 46.08 g/mol, corresponding to 0.05 equivalent (5 mol%) of Ru. To work as exactly as possible with these small volumes, the ten-fold amount of CS_2 (5.59 × 10^{-4} ml, 9.25 × 10^{-6} mol) was dissolved in cyclohexene (10 ml, 98.6 mmol) and stirred for 2 minutes. Then 1.0 ml of this cyclohexene/CS_2 mixture was employed in the poisoning hydrogenation experiment. [d]Addition of CS_2 to entry 11 (direct addition of 1.12 µl [1.12 × 10^{-3} ml], 1.85 × 10^{-5} mol) corresponding to 1.0 equivalent (100 mol%) of Ru. [e]Entries 13-15 were experiments to optimize the hydrogenation times for Ru-NP/CDG to 0.33 h (20 min).-A lower reaction time of 15 min yielded only 94.5% conversion, higher reaction times of 30 min and 1 h showed high conversions of >~98% at lower activity.

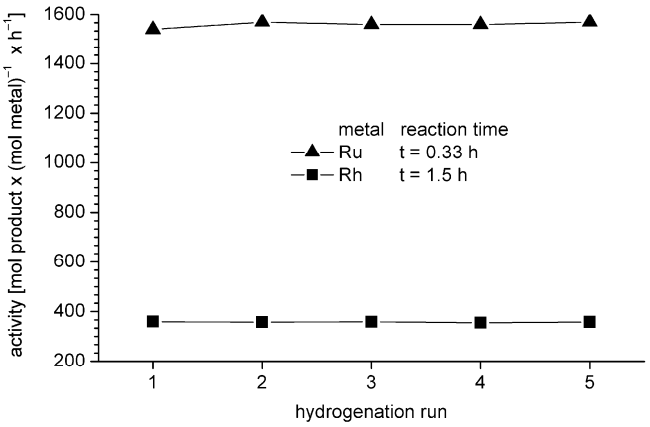

Fig. 41. Activities for the hydrogenation of cyclohexene with the same M-NP/CDG catalyst, entry 1-5 for Rh and entry 6-10 for Ru in Table 14. An even lower reaction time of 15 min for M = Ru gave only 94.5% conversion.

Following the work by Finke et al.[285,286] CS_2 binds strongly to active metal sites and blocks access of the substrates. If it is possible to poison a catalyst completely with << 1 equivalent (<< 100 mol%) of the added ligand per Ru atom, this is strong evidence that it is a heterogeneous catalyst. The reasoning is that in a heterogeneous (colloidal) metal-particle catalyst only a fraction of the metal atoms are on the surface, hence much less than a one molar equivalent of ligand per metal atom will be sufficient to deactivate the catalyst.[286,287] A molecular, homogeneous catalyst needs ≥ 1.0 equivalent of the ligand (per metal atom) for the poisoning. To differentiate between possible homogeneous Ru atom and heterogeneous Ru-NP catalysts we have added CS_2 as a known ruthenium catalyst poison following the work by Finke et al. (see above for explanation).[286,287] For a consecutive catalytic 6th run in the presence of CS_2 (Table 14, entry 11, 0.05 eq., 5 mol% of Ru) we found that CS_2 has only a marginal poisoning effect on the Ru-NPs/CDG catalyst. Even at 1.0 equivalent of CS_2 (100 mol%) to Ru (Table 14, entry 12) still about half of the previous conversion and activity is retained. Failure of Ru-NP/CDG poisoning can be explained with formation of xanthates from alcohols, here the hydroxy-functionalities of CDG and CS_2 (Scheme 12).

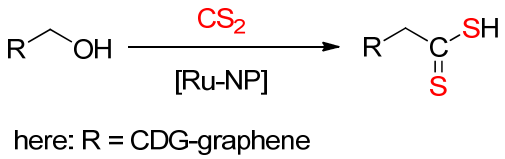

Scheme 12. Xanthate formation. CS_2 capture by the CDG hampers the conclusive evidence from the poisoning experiments.

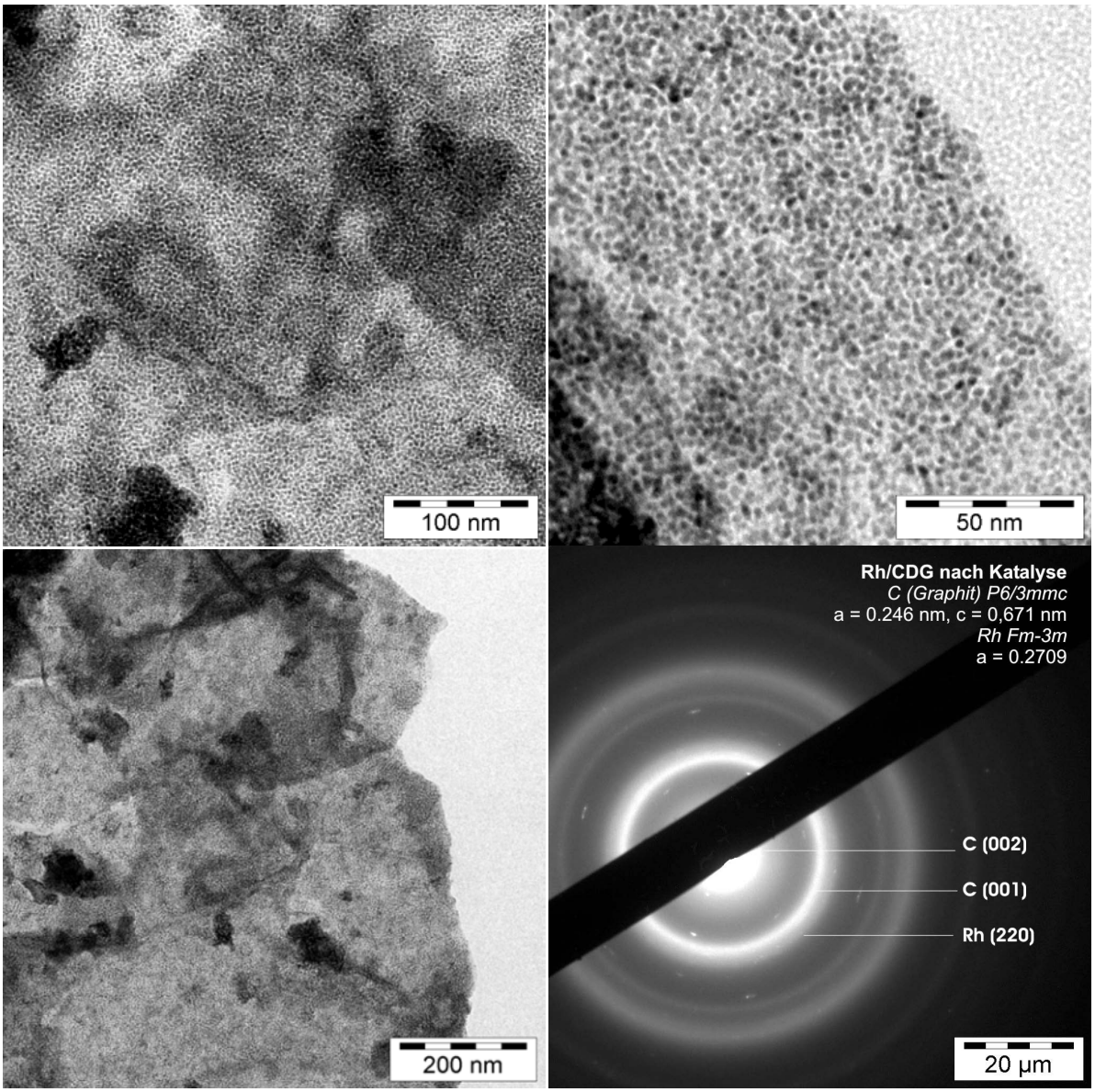

Fig. 42. TEM and TED of Rh-NPs/CDG after five consecutive catalytic hydrogenation runs of cyclohexene (Table 14, entry 5).

A second series of runs for the cyclohexene to cyclohexane hydrogenation proofs that the M-NP/CDG system is catalytic active over 10 runs. No loss of acitivity can be noticed (Table 15).

Table 15. Hydrogenation of cyclohexene with M-NP/CDG catalysts – second series of runs.

entry	M-NP/CDG[a]	*t* [h]	conversion[b] [%]	activity [mol product × (mol Rh)$^{-1}$ × h^{-1}] (= TOF [h^{-1}])
1	M = Rh	1.5	quant.	360
2	2nd run	1.5	quant.	360
3	3rd run	1.5	quant.	360
4	4th run	1.5	quant.	360
5	5th run	1.5	quant.	360
6	6th run	1.5	quant.	360
7	7th run	1.5	quant.	360
8	8th run	1.5	quant.	360
9	9th run	1.5	quant.	360
10	10th run	1.5	quant.	360
11	M = Ru	0.33	quant.	1570
12	2nd run	0.33	quant.	1570
13	3rd run	0.33	quant.	1570
14	4th run	0.33	quant.	1570
15	5th run	0.33	quant.	1570
16	6th run	0.33	quant.	1570
17	7th run	0.33	quant.	1570
18	8th run	0.33	quant.	1570
19	9th run	0.33	quant.	1570
20	10th run	0.33	quant.	1570

[a]The reactions were carried out in steel autoclaves, equipped with glass inlays to eliminate any catalytic influence of the metal surface on the reaction. General conditions 4 bar H_2 and 75 °C. Cyclohexene 0.811 g (1.0 ml, 0.01 mol, density 0.811 g/ml, M = 82.14 g/mol). 11 mg M-NP/CDG with 17.4 wt% Ru corresponding to 1.89×10^{-5} mol Ru or 17.0 wt% Rh, i.e. 1.82×10^{-5} mol Rh, respectively. [b]The hydrogenation reaction times for Ru-NP/CDG were optimized for quantitative conversion. No cyclohexene educt peak was detected by GC analysis on an Agilent Technologies 66890N GC System with a DB-WAX column, length: 30 m, ID [mm]: 0.250, film thickness [μ]: 0.25.

Benzene could be hydrogenated under similar mild conditions to cyclohexane with essentially complete conversion at a temperature of 50 °C, 4 h and 4 bar (Table 16) and a pressure normalized activities of Rh-NP/CDG of ~78 mol product × (mol Rh)$^{-1}$ × h^{-1} × bar^{-1}. This is a much higher activity (TOF) than for other M-NP/IL systems[98,111,113] albeit lower than for Rh-NPs immobilized on silica-coated magnetite nanoparticles. The latter gave high benzene hydrogenation activities between 100 and 180 mol product × (mol Rh)$^{-1}$ × h^{-1} × bar^{-1} (at 6 bar, 75 °C, >99% conversion) for up to 20 consecutive runs.

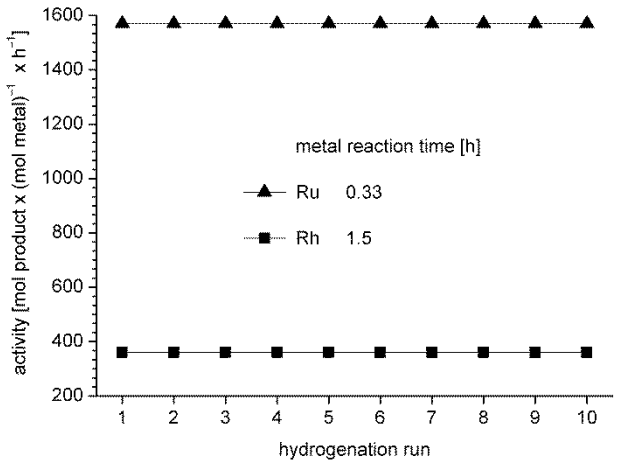

Fig. 43. Activities for the hydrogenation of cyclohexene with the same M-NP/CDG catalyst, entry 1-10 for Rh and entry 11-20 for Ru in Table 14.

Table 16. Hydrogenation of benzene with Rh-NP/CDG catalyst.[a]

entry	*T* [°C]	conversion [%]	activity [mol product × (mol Rh)$^{-1}$ × h^{-1}] (= TOF [h^{-1}])
1	25	72.8	228
2	50	98.8	310
3	75	94.8	297

[a] The reactions were carried out in steel autoclaves, equipped with glass inlays to eliminate any catalytic influence of the metal surface on the reaction. General conditions 4 bar H_2, time 4 h, benzene 0.81 g (0.92 ml, 10.36 mmol), Rh-NP/CDG 5 mg, 17.0 wt.%, 8.26 × 10^{-6} mol Rh, benzene/Rh ratio = 1255.

In summary a simple, rapid and low-energy strategy to deposit small 2-3 nm metal nanoparticles of Ru and Rh with uniform sizes on CDG surfaces, by decomposition of their metal carbonyls under MWI in the IL $BMImBF_4$ is shown. Microwave irradiation provides a very simple and reproducible way for the rapid (6 min) and energy-saving (20 Watt power) synthesis of defined and very small M-NPs from their binary metal carbonyl complexes in ILs. This method should be extendable to other metals with the microwave-induced binary metal carbonyl $M_x(CO)_y$ decomposition and subsequent M-NP deposition on CDG. The obtained hybrid nanomaterials (Rh-NPs/CDG and Ru-NPs/CDG) were shown – without further treatment – to be catalytically active in hydrogenation reactions yielding complete conversion of cyclohexene or benzene to cyclohexane under organic-solvent-free and mild conditions (50-75 °C, 4 bar H_2) with reproducible activities of 1570 mol cyclohexane × (mol Ru)$^{-1}$ x h^{-1} and 310 mol benzene × (mol Rh)$^{-1}$ × h^{-1}. The catalytically active M-NP/CDG-nanocomposite material could be recycled and used for several runs without any loss of activity.

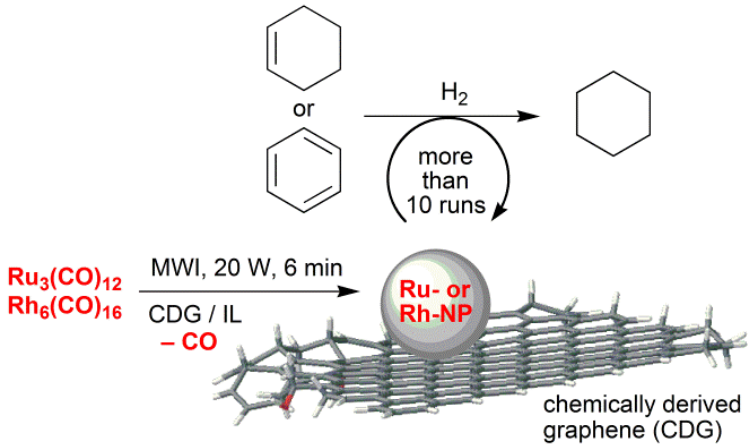

Scheme 13. The use of microwave irradiation for the easy synthesis of transition metal nanoparticles supported on chemically derived graphene (CDG) in ILs. The hybrid nanomaterials Ru-NPs/CDG and Rh-NPs/CDG were active hydrogenation catalysts.

These results are part of this cumulative dissertation (**publication 6.4**).

5 EXPERIMENTAL

5.1 General

5.1.1 Materials

$Mo(CO)_6$, $W(CO)_6$, $Re_2(CO)_{10}$, $Fe_2(CO)_9$, $Ru_3(CO)_{12}$, $Os_3(CO)_{12}$, $Co_2(CO)_8$, $Rh_6(CO)_{16}$ and $Ir_6(CO)_{16}$ were obtained from STREM and Aldrich, Propylene carbonate (PC) (99.7 %, H_2O free), 3-mercaptopropionic acid (> 99 %), TOPO (99 %), 1-hexyne (> 97%), cylcohexene (> 97%), acetone (99% p.a.; particle free) and benzene (> 99 %) from Sigma-Aldrich, $BMImBF_4$ from IoLiTec (H_2O content << 100 ppm; Cl^- content<< 50 ppm).
Literature reported decomposition temperatures are 180 °C for $Mo(CO)_6$ and $W(CO)_6$, 177 °C for $Re_2(CO)_{10}$, above 100 °C for $Fe_2(CO)_9$, 155 °C for $Ru_3(CO)_{12}$ and 224 °C for $Os_3(CO)_{12}$, above 100 °C for $Co_2(CO)_8$, 220 °C for $Rh_6(CO)_{16}$ and 210 °C for $Ir_6(CO)_{16}$.[293]
Stirring bars were obtained by VWR International GmbH, Hilpertstraße 20a, 64295 Darmstadt.

5.1.2 Technics

All manipulations were done using Schlenk techniques under nitrogen since the metal carbonyls salts are hygroscopic and air sensitive. The ILs and PC were dried at high vacuum (10^{-3} mbar) for several days.

Microwave irradiation

For the synthesis of the dispersions a CEM microwave type Discover was used.

5.1.3 Analysis

AAS

Atomic absorption spectrometry (AAS) was performed with Perkin-Elmer AAnalyst 100 (flame AAS), using the software AA WinLab.

DLS

A Malvern Zetasizer Nano-ZS was used for the dynamic light scattering (DLS) measurements working at 633 nm wavelength. Care was taken for choosing the right parameters, such as the index of refraction of the transition metals at their wavelength (Table 17).

Table 17. Parameters for dynamic light scattering.

Element	Index of refraction	Absorption
Molybdenum	3.71	0.1
Tungsten	3.65	0.1
Rhenium	2.93	0.1
Iron	2.87	0.1
Ruthenium	4.79	0.1
Osmium	3.90	0.1
Cobalt	2.26	0.1
Rhodium	2.14	0.1
Iridium	2.53	0.1

FT-IR (Fourier transform infrared)

Measurements were carried out on a Bruker TENSOR 37 IR spectrometer in a range from 4000 to 500 cm^{-1} in a KBr cuvette (thickness 0.05mm).

GC

The cyclohexene or benzene or 1-hexyne to cyclohexane or n-hexane conversion was verified by gas chromatographic (GC) analysis of the product (Perkin Elmer 8500 HSB 6, equipped with a DB-5 film capillary column, 60 m × 0.32 mm, film thickness 25 µm, oven temperature 40 °C, N_2 carrier flow 120 L/min and a flame ionization detector (FID), 250 °C detector temperature). The benzene or cyclohexene or 1-hexyne to cyclohexane or to n-hexane conversion was analyzed by putting a drop of the mixture into a GC sample vial with 1 mL of water. The addition of water as a non-electrolyte can enlarge the activity coefficient of organic components, thereby increase their detection sensitivity through the increase in peak area. The FID does not detect the water itself.[288]

TEM

Transmission electron microscopy (TEM) and transmission electron diffraction (TED) photographs were taken at room temperature from a carbon coated copper grid on a Zeiss LEO 912 transmission electron microscope operating at an accelerating voltage of 120 kV.

Samples were loaded on holey, carbon coated copper grids. The solvents were removed by floating the grids on water for several minutes.

Particles diameters were measured manually using iTEM software tools for manual measurements. Completely automatic measurements, which can be easily performed for well separated particles, fail in the case of heavily clustered particles. For a better comparison of the samples also particles which would have allowed automatic detection were measured manually.

5.1.4 Catalysis

An autoclave with a glass inlay was used. The hydrogenation reactions were carried out in the glass inlay.

The autoclave was conditioned by evacuation and re-filling with nitrogen. All autoclave loading was carried out under nitrogen. Stirring rate was 850 rpm. The autoclave was heated to the desired temperature and set to the desired pressure of H_2 which was kept constant over the reaction time. The H_2 uptake over time was monitored with a Büchi pressflow gas controller. After quantitative or near quantitative conversion was reached (adjudged by the H_2 consumption) the reactor was depressurized, the volatile organic components were condensed under vacuum into a clean cold trap. The catalytic system is left behind in the glass inlay of the autoclave and was re-used by adding fresh substrate.

5.2 Propylene carbonate as stabilizing solvent for transition metal nanoparticles

5.2.1 General

TED

Transmission electron diffraction (TED): d-Spacing, intensity and hkl from STOE WinXPow version 1.10, data base, STOE & Cie GmbH, Darmstadt, Germany, 2002.

Table 18. Diffraction rings of Ru-particles compared with IPDS database, Ru [6-663]

d-Spacing from diffraction rings [Å]	d-spacing [Å] from database	Intensity	hkl
2.10	2.0560	100	101
1.61	1.5808	25	102
not seen	1.3530	25	110
1.26	1.2189	25	103
1.15	1.1299	20	201

Table 19. Diffraction rings of Rh-particles compared with IPDS database, Rh [5-685]

d-Spacing from diffraction rings [Å]	d-spacing [Å] from database	Intensity	hkl
2.23	2.1960	100	111
1.94	1.9020	50	200
1.39	1.3450	26	220
1.17	1.1468	33	311
not seen	1.0979	11	222
not seen	0.9508	7	400
0.89	0.8724	20	331

Table 20. Diffraction rings of Ir-particles compared with IPDS database, Ir [6-598]

d-Spacing from diffraction rings [Å]	d-spacing [Å] from database	Intensity from database	hkl
2.25	2.2170	100	111
1.95	1.9197	50	200
1.38	1.3575	40	220
1.20	1.1574	45	311

In the TED pictures the ring diameters were measured manually using the scale bar in the picture and the d-spacing was then calculated with a TEM specific constant of 79.5 according to: d-spacing (in Å) = 79.5 / diffraction ring diameter (in µm).

DLS

Samples were prepared by dissolution of 0.05 or 0.1 ml of a 0.5 wt.% of the metal dispersion in acetone (99% p.a.; particle free) in a glass cuvette before measurement. Acetone is also capable of stabilizing nanostructured metal clusters.[289,290]

Table 21. DLS measurement of Rh-NPs in different solvents and with different concentrations.[a]

entry	c [g/mL]	solvent	DLS Ø (σ) [nm]
1	0.5	PC	108.8 (± 40.8)
2	0.05	PC	134.0 (± 83.2)
3	0.025	PC	69.7 (± 30.4)
4	0.008	PC	43.6 (± 14.3)
5	0.025	water	82.3 (± 41.9)
6	0.025	acetone	2.4 (± 0.8)

[a] As parent solution a Rh-NPs/PC dispersion (0.5 wt.%) from $Rh_6(CO)_{16}$ was used.

Several measurements with different concentration of Rh-NPs from Rh-NPs/PC dispersions (for synthesis see section 5.2.2) in different solvents have been carried out (Table 21) to determine the particle sizes. The samples in entry 2-4 in Table 21 were diluted in PC. PC and not another solvent was chosen to avoid any effect on the nanoparticles or on the measurements which could brought in by a different solvent with different physical and chemical properties. From entry 1 which is the untreated parent solution (0.5 wt.%) to entry 4

with is a diluted sample the particle sizes decreases, but the results did not match with the result (2.1 (± 0.6) nm) obtained by TEM (see Table 6). Water was used as a dilution solvent in entry 5 and was considered to be unfeasible, because after a few minutes a precipitate appeared on the bottom of the glass cuvette before the measurement was started. Water seems to weaken the protective, stabilizing PC-Layers around the nanoparticles which, thus, are agglomerating to bulk material. Acetone was used as solvent and the results obtained by DLS with acetone used as solvent best fit the results obtained by TEM (see Table 6).

DLS is commonly used for analyses of polymers with particle size larger than nanoparticles. The sizes of nanoparticles (1-5 nm) may not be analyzed precisely because the resolution limit of the DLS is 1 nm. The DLS measurement does not measure the "actual" particle size, but it measures the hydrodynamic diameter *d(H)* as is described by the Stokes-Einstein (Eqn. 3):

$$d\,(H) = \frac{kT}{3\pi\eta D} \quad (3)$$

d (H) = hydrodynamic diameter [nm]
D = translational diffusion coefficient
k = Boltzmann's constant, k = 1.38×10^{23} J/K
T = absolute temperature [k]
η = viscosity of the solvent [kg/(ms)]

The diameter measured in DLS is a value that refers to how a particle diffuses within a fluid so it is referred to as a hydrodynamic diameter. Actually it is not the diameter of a particle, which is measured, but the diameter of a sphere that has the same translational diffusion coefficient (*D*) as the particle. This coefficient *D* depends on the particle size, surface structure, concentration and type of ions in the medium and is calculated via a correlation function during the measurement.[291,292] With these variables a precise investigation of the particle sizes is not possible.

5.2.2 Metal nanoparticle (M-NP) synthesis

Decomposition by means of microwave irradiation was carried out under argon. In a typical reaction, the fine metal carbonyl powder $M_x(CO)_y$ (M = Mo, W, Re, Fe, Ru, Os, Co, Rh, Ir; 19.8 to 9.8 mg, respectively; see Table 22) was dissolved/suspended (≈ 1 h) under an argon atmosphere at room temperature in dried and deoxygenated PC (density: 1.19 g/mL, 1 mL, 1.19 g) for a 0.5 wt.% M-NP/PC dispersion. For the synthesis of a 1 wt.% M-NP/PC dispersion the metal carbonyl $M_x(CO)_y$ (M = Rh; 16.6 mg) was suspended/dissolved (≈ 1 h) under an argon atmosphere at room temperature in dried and deoxygenated PC (1.5 mL, 1.8 g). For the synthesis, the mixture was placed in a microwave (CEM, Discover) under an inert argon atmosphere and the conversion was finished within 3 min at a power of 50 W. For the 1 wt.% dispersions a time of 5 min and a power of 50 W were chosen. Each decomposition reaction was carried out at least twice. Decomposition reactions to produce the Rh-NPs that were used in the catalysis in this work were carried out ten or more times.

Table 22. Microwave decomposition of metal carbonyls in PC with 50 W of power and 3 min reaction time.

Carbonyl $M_x(CO)_y$	Molar mass (g/mol)	Mass% metal in $M_x(CO)_y$	Mass of $M_x(CO)_y$ (mg) in PC	wt.% Metal in 1.19 g (1.0 mL) PC (0.5% = 6.1 mg M)
$Mo(CO)_6$	264.00	36.34	16.8	0.5
$W(CO)_6$	351.90	52.24	11.5	0.5
$Re_2(CO)_{10}$	652.52	57.07	10.5	0.5
$Fe_2(CO)_9$	363.79	30.70	19.8	0.5
$Ru_3(CO)_{12}$	639.33	47.43	12.8	0.5
$Os_3(CO)_{12}$	906.81	62.93	9.8	0.5
$Co_2(CO)_8$	341.94	34.47	17.5	0.5
$Rh_6(CO)_{16}$	1065.62	57.94	10.3	0.5
$Ir_4(CO)_{12}$	1105.00	69.58	8.8	0.5
				in 0.9 g (0.75 mL) PC
$Rh_6(CO)_{16}$	1065.62	57.94	16.6	1.0

5.2.3 Catalysis

The hydrogenation reactions with Rh-NPs/PC were carried out in stainless steel autoclaves connected with an online hydrogenation-consumption monitoring system (Büchi pressflow gas controller, bpc). The autoclave was conditioned by evacuation and re-filling with nitrogen. All autoclave loading was carried out under nitrogen. Each autoclave was equipped with a glass inlay, to eliminate any catalytic influence of the stainless steel surface on the reaction process. A typical experiment used 0.75 mL of the Rh-NPs/PC dispersion with 1 wt.% Rh (9 mg, 8.8×10^{-5} mol Rh) and 10 mL of cyclohexene (0.1 mol, density 0.811 g/ml, M = 82.14 g/mol,) or 1.0 mL of 1-hexyne (1.8 mmol, density 0.72 g/ml, M = 82.14 g/mol). The autoclave was heated to the desired temperature and set to the desired pressure of H_2 which was kept constant over the reaction time. After this time the reactor was depressurized, and the volatile organic components condensed under vacuum (15 min) into a clean cold trap (liquid nitrogen cooled). The Rh-NPs/PC dispersion was left behind.

5.2.3.1 Conditions for cyclohexene hydrogenation

Cyclohexene 10 mL, 0.89 mol (density 0.811 g/ml, M = 82.14 g/mol); Rh metal (9 mg, 8.8×10^{-5} mol); 25-95 °C, 4-10 bar H_2.

5.2.3.2 Conditions for 1-hexyne hydrogenation

1-hexyne (1.0 mL, 1.8 mmol (density 0.72 g/ml, M = 82.11 g/mol); Rh metal (9 mg, 8.8×10^{-5} mol); 25 °C, 10 bar H_2.

5.2.4 Preparation of ligand-capped M-NP in PC

The obtained Rh- and Ru-NPs/PC (0.4 ml, 0.5 wt.%) were stirred with 3-mercaptopropionic acid (2 mL, 3.5×10^{-5} mol) or TOPO (14 mg, 3.5×10^{-5} mol) over night. The ligand-capped M-NPs were collected by centrifugation (2000 rpm, 15 min) and decantation of the clear propylene carbonate phase. The capped M-NPs were dried for several days under high vacuum to remove the PC solvent.

5.3 Rhodium nanoparticles supported PTFE stirring bars

5.3.1 General

Stirring bars (20 × 6 mm) were obtained by VWR International GmbH, Hilpertstraße 20a, 64295 Darmstadt.

Analysis

SEM

Scanning electron microscope (SEM) samples were coated with a thin Au layer (~ 8 nm) and analyzed with a Quanta 250 FEG instrument. The measurements were performed at 3.20^{-4} Pa and at 10 kV voltage using an ETD detector.

AAS

AAS (atomic absorption spectrometry) was performed with Perkin-Elmer AAnalyst 100 (flame AAS), using the software AA WinLab. The rhodium loading on the stirring bar and the rhodium leaching in the catalytic runs was analyzed by AAS. To dissolve the Rh-NPs from the Teflon-coating of the stirring bar it was placed into a conc. HCl/HNO_3 mixture (*aqua regia*, 50 ml) over night. The resulting solution was directly used for the AAS analysis. Analysis of the Rh-NP content on a stirring bar from the above preparations reproducibly gave 32 (± 8) µg of rhodium (± 8 is the standard deviation σ from multiple Rh-content determinations of different stirring bars). After the treatment with *aqua regia* the magnetic stirring bars lost their catalytic properties regarding the hydrogenation of cyclohexene or benzene.

5.3.2 Preparation of Rh-NP/IL dispersion

$Rh_6(CO)_{16}$ (41.42 mg, 3.89×10^{-5} mol) was dissolved/suspended (~1 h) under a nitrogen atmosphere at room temperature in dried and deoxygenated $BMImBF_4$ (2.0 mL, 2.4 g) to give a 1.0 wt.% dispersion. For the synthesis the mixture was placed in a CEM microwave type Discover under inert nitrogen atmosphere and the conversion was finished within 6 minutes at a power of 10 W. $Rh_6(CO)_{16}$ decomposes at 220 °C, so it can easily be handled at room temperature under inert atmosphere.[293]

5.3.3 Preparation of Rh-NP@stirring bar

A brand-new (unused) magnetic stir bar was washed with dried acetone (10 mL) and dried under high vacuum prior to the Rh-NP deposition. Rhodium nanoparticle deposition on PTFE was obtained by stirring the magnetic stirring bar in the Rh-NPs/$BMImBF_4$ dispersion at room temperature under nitrogen for different defined number of 2-8 days. The nanoparticle-loaded stirring bar was removed from the Rh-NPs/$BMImBF_4$ dispersion and stirred in a washing solvent (20 mL) for 15 s to remove the IL, removed with a pincer and dried under vacuum for 30 min. The solvents acetone, water, methanol, *iso*-propanol, tetrahydrofuran and methylene chloride were tested for the washing and removal of the ionic liquid film which adhered to Rh-NP@stirring bar. For each different washing solvent, a cyclohexene hydrogenation run (see section 5.3.4) was carried out to test for the resulting activity. Activities for acetone (p.a), THF or methylene chloride were similar and higher than for acetone (technical), methanol, *iso*-propanol or water. Eventually, THF (p.a) was used as a standard washing solvent for the catalytic recycling experiments.

5.3.4 Catalysis

5.3.4.1 General

Rh-NPs@stirring bars were conditioned after their preparation by using the above-mentioned washing procedure with dried THF (20 mL) for 15 s before the first run to remove the ionic liquid.

An autoclave with a glass inlay was used. The hydrogenation reactions were carried out in the glass inlay. The autoclave was conditioned by evacuation and re-filling with nitrogen. All autoclave loading was carried out under nitrogen. Stirring rate was 850 rpm. The H_2 uptake over time was monitored with a Büchi pressflow gas controller (Büchi pbc). After quantitative or near quantitative conversion was reached (adjudged by the H_2 consumption) the reactor was depressurized, the volatile organic components were condensed under vacuum into a clean cold trap. The Rh-NPs@stirring bar is left behind in the glass inlay of the autoclave and was re-used by adding fresh substrate. Catalyst recycling was carried out ten times for cyclohexene and three times for benzene.

5.3.4.2 Conditions for cyclohexene hydrogenation

Cyclohexene 0.69 mL, 6.8 mmol (density 0.811 g/mL, M = 82.14 g/mol); Rh metal (0.032 mg, 3.1×10^{-7} mol); 75 °C, 4 bar H_2.

5.3.4.3 Conditions for benzene hydrogenation

Benzene 0.60 mL, 6.8 mmol (density 0.88 g/mL, M = 78.11 g/mol); Rh metal (0.032 mg, 3.1 $\times 10^{-7}$ mol); 90 °C, 20 bar H_2. For the slower benzene hydrogenation the reaction was intentionally stopped at 90% conversion (adjudged by the H_2 consumption) as thereafter the decrease in benzene concentration lowered the reaction rate. Thus, the reactor was depressurized after 90 % conversion and the liquid product removed under vacuum and fresh benzene (0.60 mL) was added.

5.3.4.4 Special Experiments

To investigate the possibility of mechanical abrasion or of leaching of Rh-NPs from the stirring bar the following special experiments were performed:

Entry 14 in Table 11– test for mechanical abrasion: Rh-NPs@stirring bar was stirred for 12 h at 75 °C in an empty glass inlay at 850 rpm under N_2. Afterwards this Rh-NPs@stirring bar was replaced by brand-new (untreated) stirring bar. Cyclohexene (0.69 mL) was added and the autoclave was pressurized. Hydrogenation took place at 75 °C and 4 bar H_2. After 24 h the hydrogenation was stopped and the conversion verified by GC.

Entry 15 in Table 11– test for leaching into cyclohexene: Rh-NPs@stirring bar was placed in and allowed to stand for 12 h at 75 °C in cyclohexene (0.69 mL) without stirring under N_2. Afterwards Rh-NPs@stirring bar was replaced by a brand-new (untreated) stirring bar and the autoclave was pressurized. Hydrogenation was carried out at 75 °C and 4 bar H_2. After 24 h the hydrogenation was stopped and the conversion verified by GC.

Entry 16 in Table 11– test for leaching into cyclohexene under hydrogenation conditions: Using the general hydrogenation conditions, the hydrogenation of cyclohexene (0.69 mL) was started at 75 °C and 4 bar H_2 and run until 25 % conversion (which reached after 12 min). The cyclohexane/ cyclohexene mixture was filtered hot at 60 °C under N_2 atmosphere into a new glass inlay equipped with brand-new (untreated) stirring bar. The glass inlay was placed into the autoclave and hydrogenation was resumed at 75 °C by pressurizing to 4 bar H_2. After 24 h the hydrogenation was stopped and the conversion verified by GC.

5.4 Graphene-supported transition metal nanopaticles

5.4.1 General

Energy dispersive X-ray analysis/Scanning electron microscopy (EDX/SEM) were taken on a FEi Quanta 250 FEG, EDX Oxford

Ru-NPs/CDG:

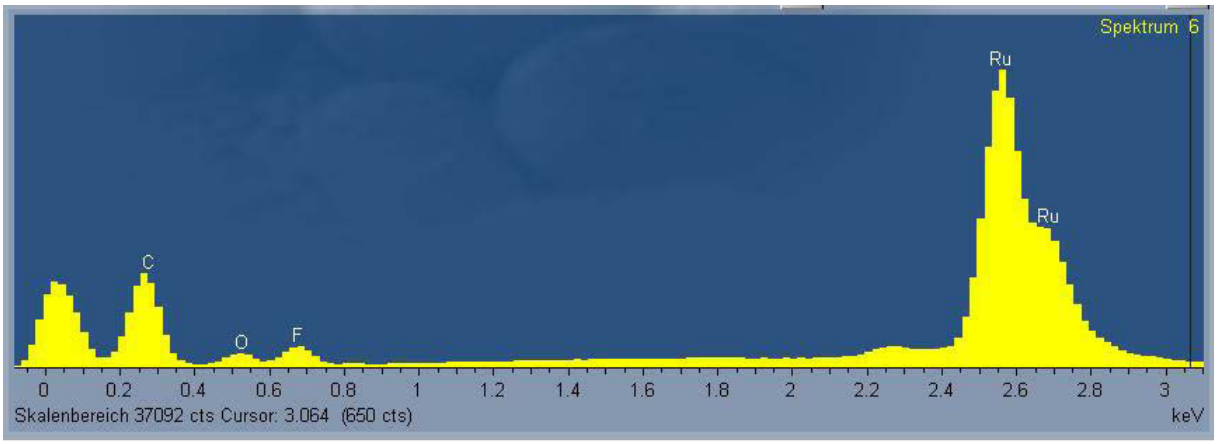

Rh-NPs/CDG:

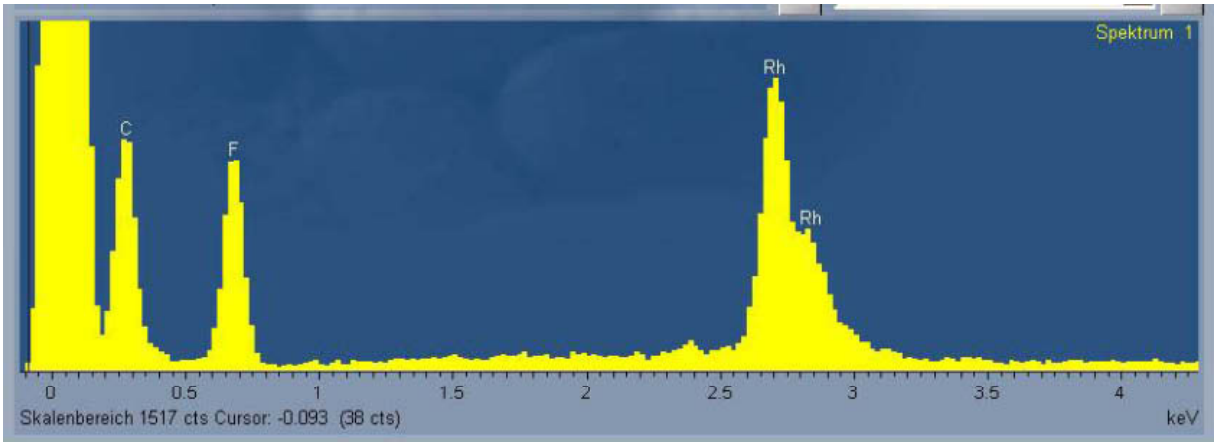

Fig. 44. Energy dispersive X-ray analysis (EDX)-spectra of top-to-bottom Fe-NP/CDG, Ru-NP/CDG and Rh-NP/CDG.

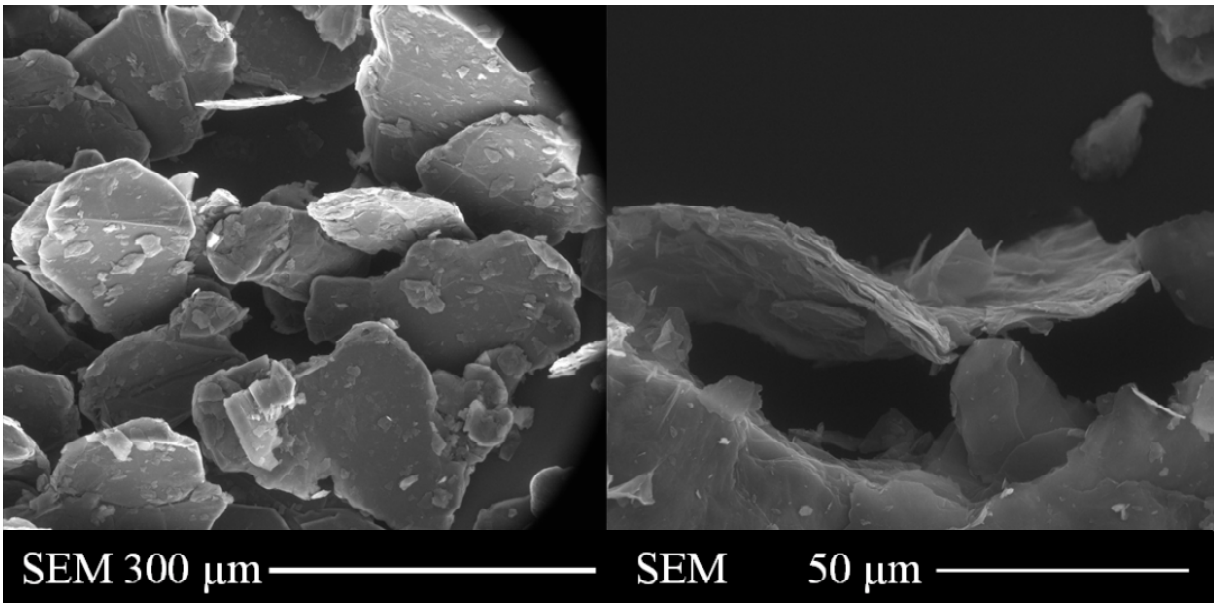

(a) (b)

Fig. 45. Scanning electron micrograph (SEM) of (a) graphite and (b) graphite oxide.

5.4.2 Synthesis of chemically derived graphene ("graphene")-supported transition metal nanoparticles (M-NP/CDG)

In a typical experiment chemically derived graphene (CDG, 4.8 mg, 0.2 wt.% related to 2.4 mg IL) was dissolved/suspended in the dried and degassed (deoxygenated) ionic liquid $BMImBF_4$ (2.0 mL, 2.4 g, density 1.2 g/mL) at room temperature with magnetic stirring for 20 h in a microwave-reaction vial. The solid metal carbonyl powders $M_x(CO)_y$ (M = Ru, Rh; Table 23) were added to the CDG slurry in $BMImBF_4$ (1 wt.% metal, related to 2.4 g $BMImBF_4$) and suspended with magnetic stirring for 18 h under argon atmosphere.

Table 23. Amounts of $M_x(CO)_y$ in the M-NP/CDG synthesis.[a]

Metal carbonyl	Molar mass [g/mol]	Metal mass percent in $M_x(CO)_y$ [%]	$M_x(CO)_y$ mass [mg]	M moles [mmol]	M mass percent in IL [%]	M concentration in IL [mol/ml]
$Ru_3(CO)_{12}$	639.33	47.43	50.6	0.230	1	0.1150
$Rh_6(CO)_{16}$	1065.62	57.94	62.5	0.235	1	0.1175

[a]In $BMImBF_4$ (2.0 mL, 2.4 g, density = 1.2 g/mL) with 4.8 mg CDG.

Then, the stirring bars were removed and the mixture was subjected to microwave irradiation (6 min, 20 W) under argon atmosphere. For workup the slurry was degassed from CO *in vacuo*. Distilled water (6 ml) was added to remove the ionic liquid from the M-NP/CDG

system. The black slurry was centrifuged (2 × 15 min, 2000 rpm, *Hettich Rotina 46*) and the supernatant liquid H_2O/IL phase decanted and discarded. The addition of H_2O, centrifugation and decantation was repeated three times. At last, the residue was again dispersed in water, filtered and dried under vacuum. The dry black-greyish residue formed flakes which could easily be removed from the filter. The primary characterization of the M-NP/CDG composite was carried out by transmission electron microscopy (TEM). The Ru or Rh metal content of the M-NP/CDG samples was determined with AAS by digestion of the sample (15 mg) in hot aqua regia [30 mL, HCl (37 %)/HNO_3 (65 %) 3:1]. After the aqua regia was boiled down, the residue was re-dissolved in HCl (30 ml, 37 %) and boiled down again. The residue was resolved in conc. HCl (37 %) and the solution was filtered to remove particles. Aqua regia was added to a total volume of 25 ml followed by AAS analysis.

5.4.3 Catalysis

5.4.3.1 Hydrogenation of cyclohexene

The hydrogenation reactions of cyclohexene with graphene-supported Ru- and Rh-nanoparticles were carried out in stainless steel autoclaves. The autoclave was conditioned by evacuation and re-filling with argon. All autoclave loading was carried out under argon. Each autoclave was equipped with a glass inlay, to eliminate any catalytic influence of the stainless steel surface on the reaction process, into which the catalyst (Ru-NPs/CDG 11 mg containing 17.4 wt.% Ru or 1.89×10^{-5} mol Ru; Rh-NPs/CDG, 11 mg, containing 17.0 wt.% Rh or 1.82×10^{-5} mol Rh) and the cyclohexene substrate (1.0 ml, density 0.811 g/ml, M = 82.14 g/mol, 0.01 mol) were loaded. The autoclave was heated to 75 °C and pressurized to 4 bar of H_2 which was kept constant over the reaction time. The reaction mixture was stirred for an optimized set time of 1.5 h or 20 min. After this time the reactor was depressurized, and the volatile organic components condensed under vacuum (15 min) into a clean cold trap (liquid nitrogen cooled). Decanting of the organic layer from solid M-NP/CDG was not feasible because the later formed a fine dispersion which did not settle even after a prolonged time. The M-NP/CDG catalyst is left behind in the autoclave and was reused by adding fresh cyclohexene. Organic substrate workup and catalyst recycling was done four times for Ru or Rh. The cyclohexene to cyclohexane conversions were investigated by GC [Perkin Elmer, DB 5 column (60 m × 0.32 mm)].

5.4.3.2 Hydrogenation of benzene

The hydrogenation reactions of benzene with graphene-supported Ru- and Rh-nanoparticles were carried out in stainless steel autoclaves. The autoclave was conditioned by evacuationand re-filling with argon. All autoclave loading was carried out under argon. Each autoclave was equipped with a glass inlay, to eliminate any catalytic influence of the stainless steel surface on the reaction process, into which the catalyst (Rh-NPs/CDG, 5 mg, containing 17.0 wt.% Rh or 8.26×10^{-6} mol Rh) and the benzene substrate (0.92 ml, 0.81 g, 10.36 mmol) were loaded. The autoclave was heated to the desired temperature (25, 50 or 75 °C) and pressurized to 4 bar of H_2 which was kept constant over the reaction time. The reaction mixture was stirred for a set time of 4 h. After this time the reactor was depressurized, and the volatile organic components condensed under vacuum (15 min) into a clean cold trap (liquid nitrogen cooled). Decanting of the organic layer from solid M-NP/CDG was not feasible because the later formed a fine dispersion which did not settle even after a prolonged time. The MNP/CDG catalyst is left behind in the autoclave and was reused by adding fresh benzene. The benzene to cyclohexane conversions were investigated by GC [Perkin Elmer, PEG column (25 m × 0.32 mm)].

5.5 Synthesis of nickel nanoparticles in $BMImBF_4$

Decomposition by means of microwave irradiation was carried out under argon. In a typical reaction, the fine metal salt powder NiX_2 ($X = Cl^-$, Br^-, NO_3^-, OAc^-, $acac^-$); 105.1 to 55.9 mg, respectively; see Table 25 for amounts) was dissolved/suspended (≈ 1 h) under an argon atmosphere at room temperature in dried and deoxygenated $BMImBF_4$ (density: 1.21 g/mL, 2 mL, 1.19 g) and n-butylimidazole (density: 0.948 g/mL, 0.161 mL, 0.152 g) for a 1 wt.% M-NP/$BMImBF_4$ dispersion. The mixture was placed in a microwave (CEM, Discover) under an inert argon atmosphere and decomposition was carried out by microwave irradiation of the metal salt in $BMImBF_4$ using an irradiation time of 4 minutes at a power of 40 W under argon (Fig. 46). Complete decompostition was assumed by analogy with the microwave induced decompsotition of known literature.[23]

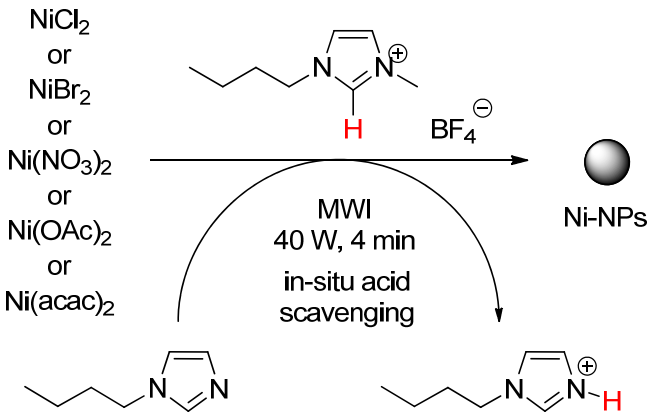

Fig. 46. Formation of Ni-NPs by microwave irradiation, reduction of different metal precursors in $BMImBF_4$ and formation of $HBIm^+Cl^-$.

In the presence of n-butylimidazole (n-BIm), the released HCl is bound as a new imidazolium salt, similar to the IL matrix. During the decomposition process, a white haze of n-butylimidazolium chloride is formed. After cooling to room temperature under argon, a white-yellow precipitate (of n-butylimidazolium chloride) was obtained.[25,126] The white-yellow precipitate was collected by centrifugation (2000 rpm for 10 min) and decanting the supernatant Ni-NP/IL dispersion. It is known that without a scavenger an agglomeration process of the metal-nanoparticles takes place, which is caused by the generated free HCl acid.[25,126] The Ni-NP/IL dispersions were analyzed by TEM (Fig. 47-Fig. 51).

Table 24. Ni-NPs size and size distribution in $BMImBF_4$.[a]

entry	Metal salts	TEM Ø (σ) [nm][b]
1	$NiCl_2$	80.0 (± 22.9)
2	$NiBr_2$	82.8 (± 17.1)
3	$Ni(NO_3)_2$	78.6 (± 17.1)
4	$Ni(OAc)_2$	79.3 (± 31.6)
5	$Ni(acac)_2$	2.7 (± 1.1)

[a]1wt.% Ni-NP/$BMImBF_4$ dispersion obtained by MWI with 40 W for 4 min. [b]Median diameter (Ø) and standard deviation (σ). See experimental section for TEM and DLS measurement conditions.

Table 25. Microwave decomposition of nickel salts to Ni-NPs in $BMImBF_4$ with 40 W of power and 4 min reaction time.

Metal salt	Molar mass (g/mol)	Mass of NiX_2 (mg) in $BMImBF_4$	wt.% metal in 2.42 g (2.0 mL) $BMImBF_4$
$NiCl_2$	129.60	55.9	1
$NiBr_2$	218.50	89.4	1
$Ni(NO_3)_2$	182.70	74.7	1
$Ni(OAc)_2 \times 4\ H_2O$	248.86	101.8	1
$Ni(acac)_2$	256.93	105.1	1

Unless noted otherwise the TEM analyses were carried out on a on a Zeiss LEO 912 transmission electron microscope operating at an accelerating voltage of 120 kV by Dr. Ralf Thomann at the Materials Research Center (FMF), University of Freiburg.

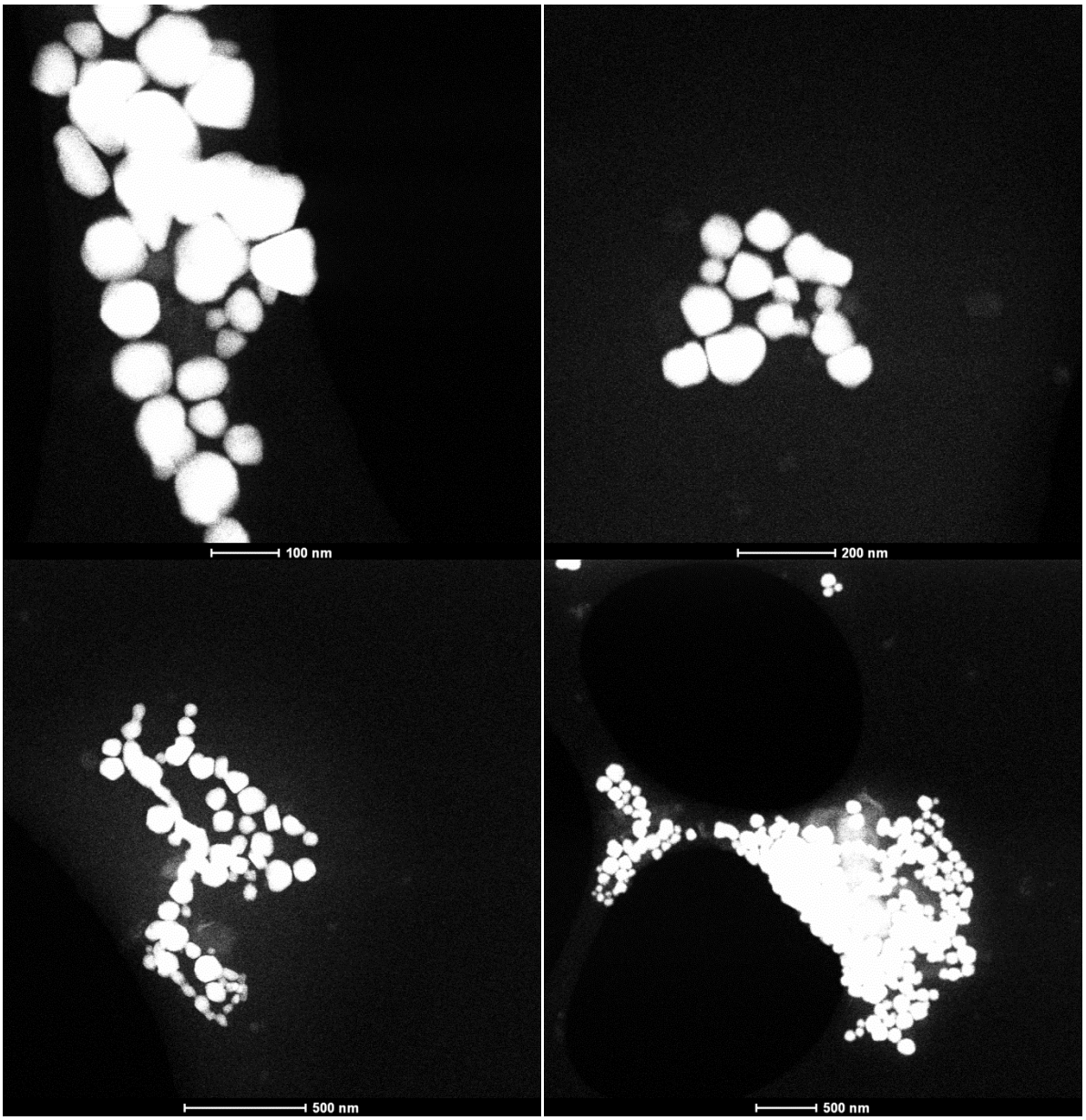

Fig. 47. STEM photographs of Ni-NPs/$BMImBF_4$ dispersion (1 wt.%) from $NiCl_2$ (Table 24, entry 1). STEM studies were carried out on a transmission electron microscope Tecnai F20 at the Research Center Jülich (FZ Jülich) operating at an accelerating voltage of 200 kV by Dipl.-Chem. Hajo Meyer.

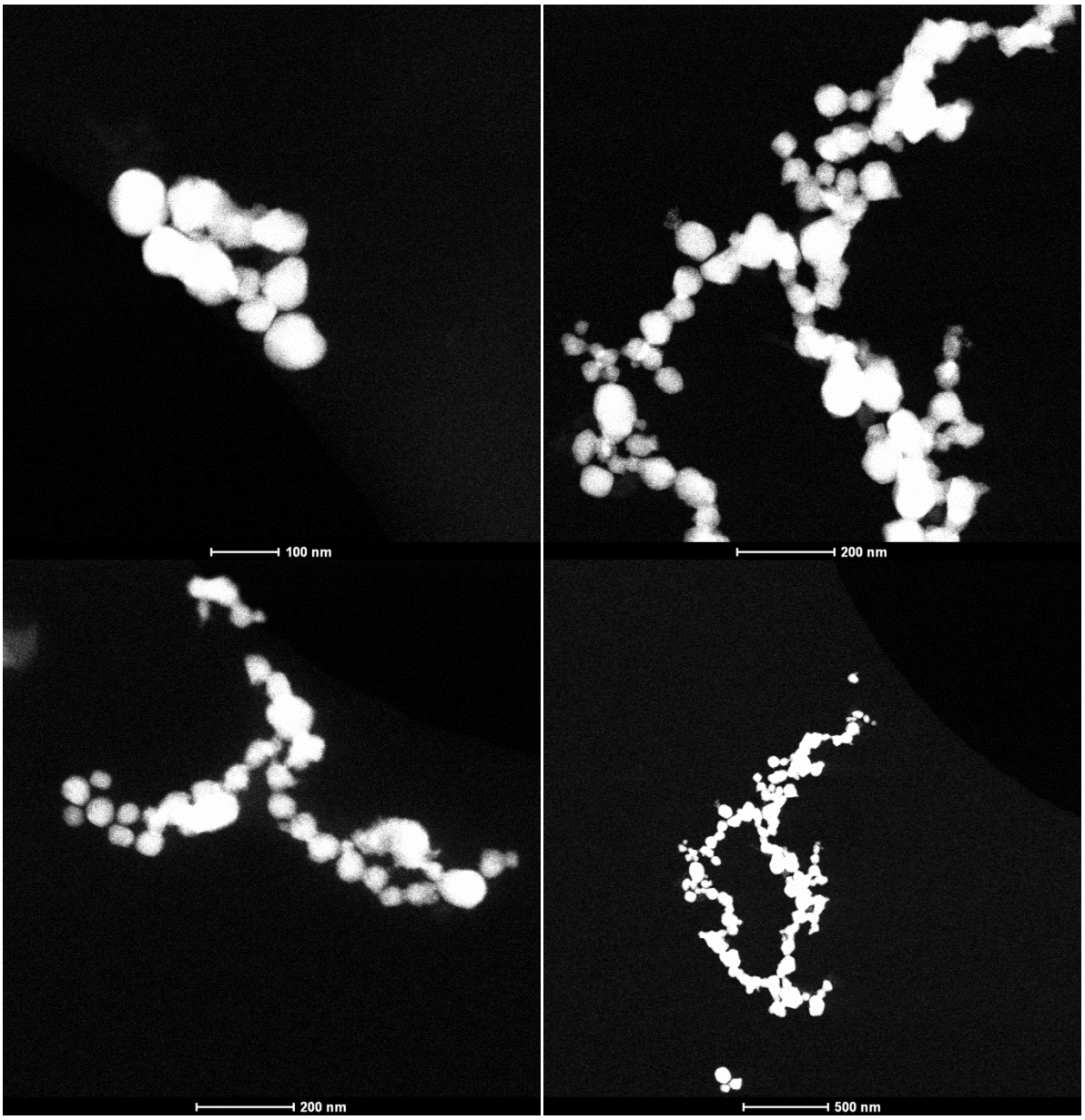

Fig. 48. STEM photographs of Ni-NPs/$BMImBF_4$ dispersion (1 wt.%) from $NiBr_2$ (Table 24, entry 2). STEM studies were carried out on a transmission electron microscope Tecnai F20 at the Research Center Jülich (FZ Jülich) operating at an accelerating voltage of 200 kV by Dipl.-Chem. Hajo Meyer.

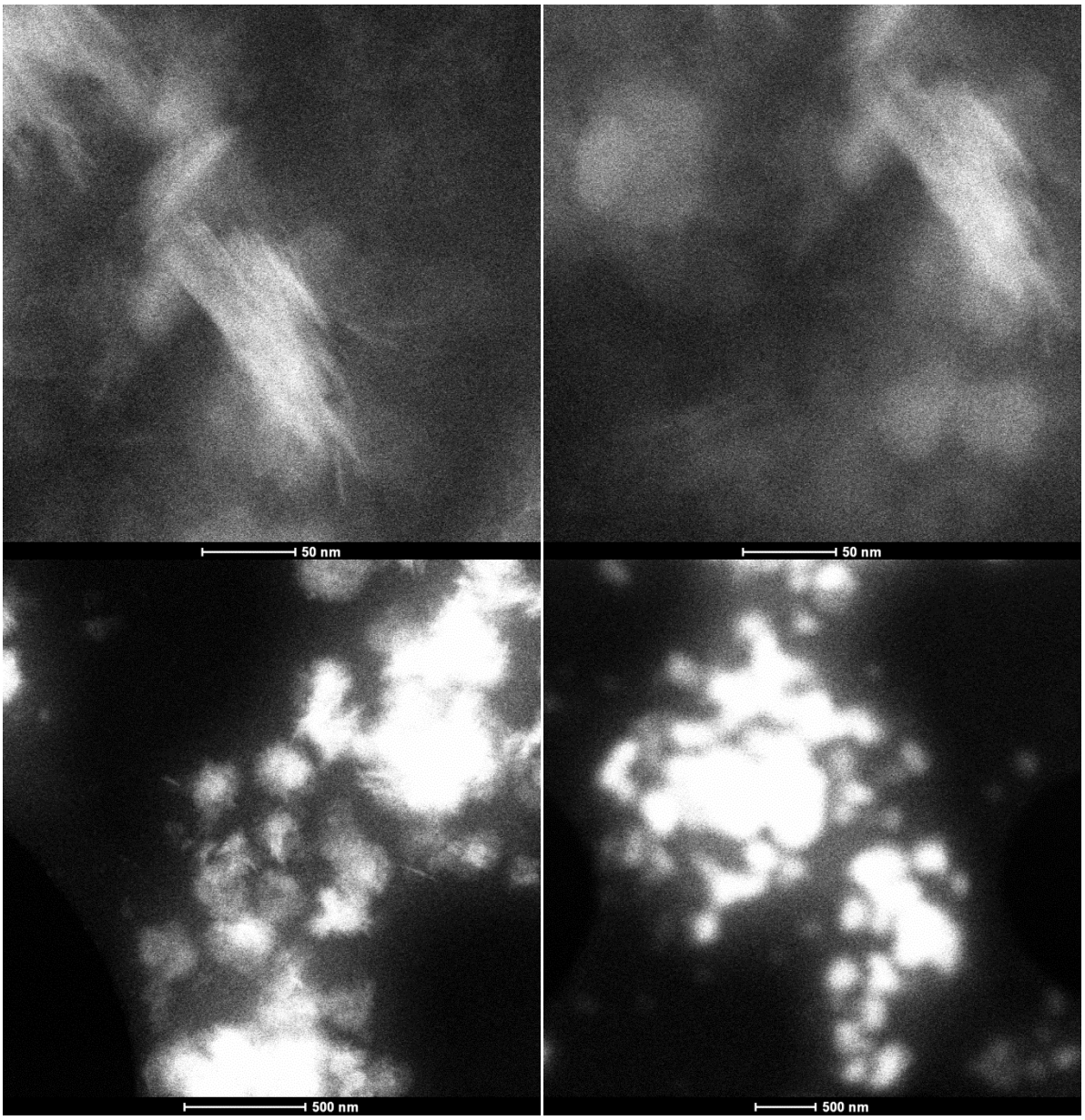

Fig. 49. STEM photographs of Ni-NPs/$BMImBF_4$ dispersion (1 wt.%) from $Ni(NO_3)_2$ (Table 24, entry 3). STEM studies were carried out on a transmission electron microscope Tecnai F20 at the Research Center Jülich (FZ Jülich) operating at an accelerating voltage of 200 kV by Dipl.-Chem. Hajo Meyer.

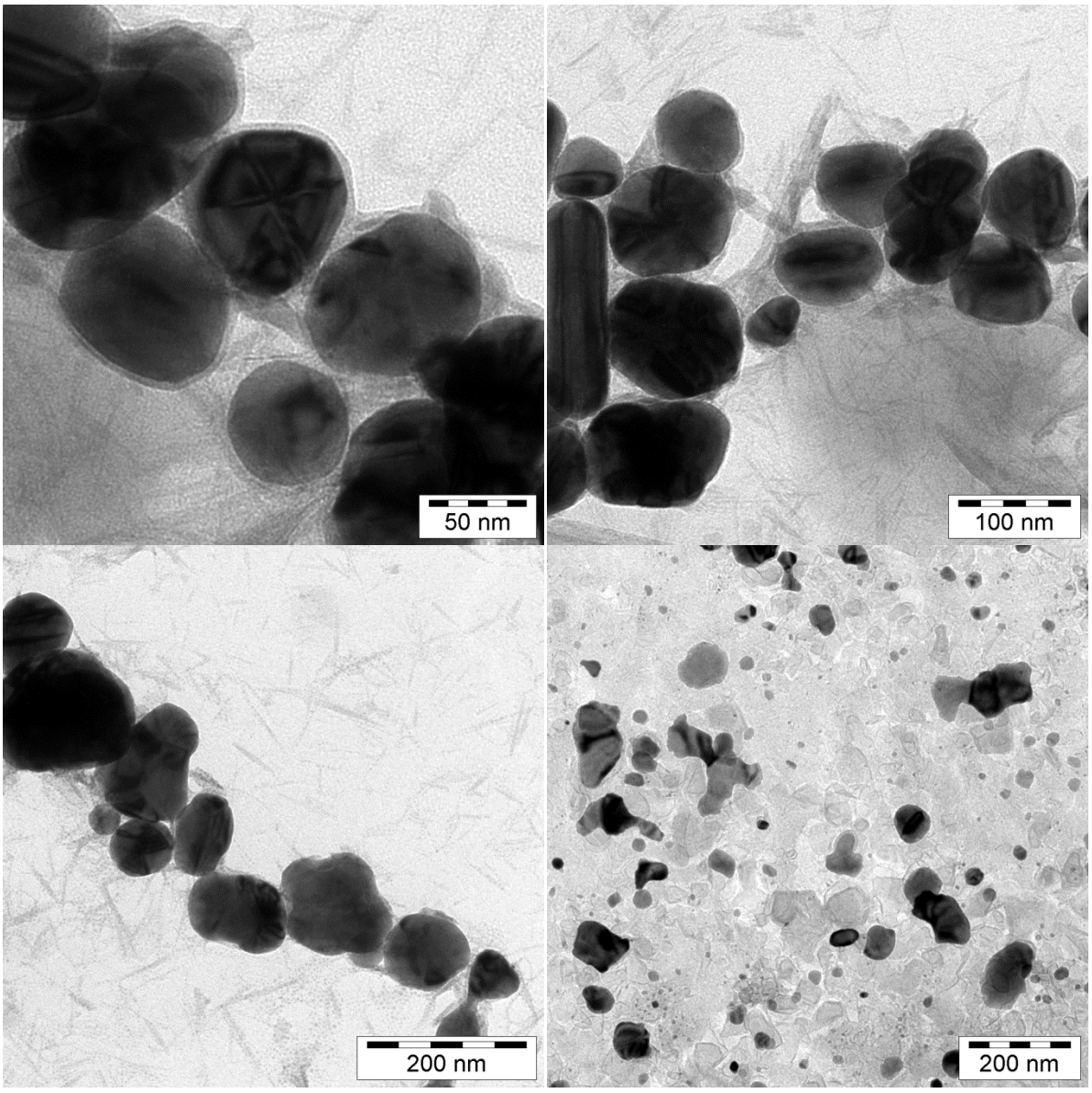

Fig. 50. TEM photographs of Ni-NPs/$BMImBF_4$ dispersion (1 wt.%) from $Ni(OAc)_2$ (Table 24, entry 4).

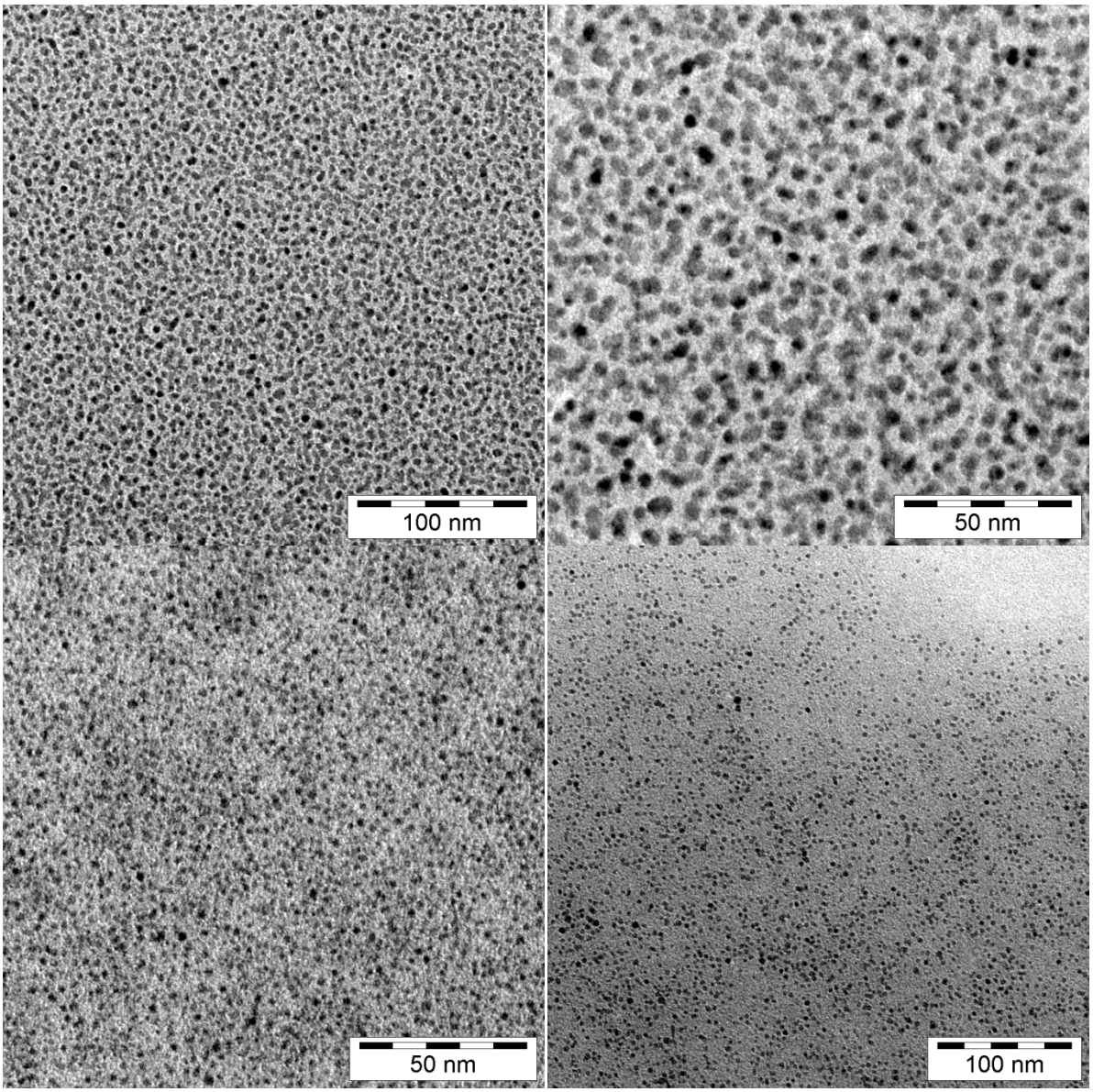

Fig. 51. TEM photographs of Ni-NPs/$BMImBF_4$ dispersion (1 wt.%) from $Ni(acac)_2$ (Table 24, entry 5).

5.6 Synthesis of palladium nanoparticles in $BMImBF_4$

The metal salts K_2PdCl_4 and $Pd(acac)_2$ were dissolved/ suspended under an argon atmosphere in dried and deoxygenated n-butylmethylimidazolium tetrafluoroborate ($BMImBF_4$) (see Table 27 for amount) and n-butylimidazole (density: 0.948 g/mL, 0.088 mL, 0.084 g). Decomposition was carried out by microwave irradiation of the metal salt in $BMImBF_4$ using an irradiation time of 6 minutes a power of 10 W under argon (Fig. 52). Complete decompostition was assumed by analogy with the microwave induced decompsotition of known literature.[23]

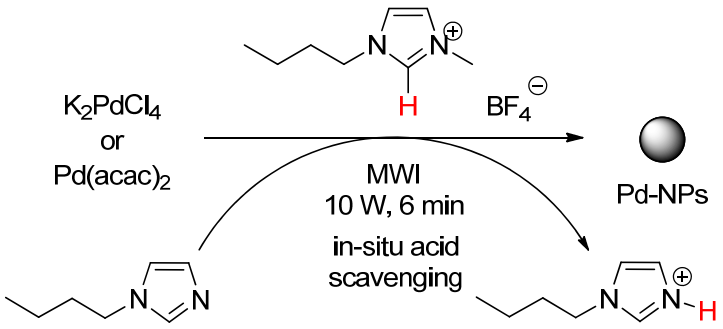

Fig. 52. Formation of Pd-NPs by microwave irradiation with reduction of different metal precursors in $BMImBF_4$ and formation of $HBIm^+Cl^-$.

In the presence of n-butylimidazole, the released HCl is bound as a new imidazolium salt, similar to the IL matrix. During the decomposition process, a white haze of n-butylimidazolium chloride is formed. After cooling to room temperature under argon, a white-yellow precipitate (of n-butylimidazolium chloride) was obtained.[25,126] The white-yellow precipitate was collected by centrifugation (2000 rpm for 10 min) and decanting the supernatant Pd-NP/IL dispersion. It is known that without a scavenger an agglomeration process of the metal-nanoparticles takes place, which is caused by the generated free HCl acid.[25,126] The Pd-NP/IL dispersion was analyzed by TEM (Table 26, Fig. 53, Fig. 54).

Table 26. Pd-NPs size and size distribution in $BMImBF_4$.[a]

entry	Metal salts	TEM Ø (σ) [nm][b]
1	K_2PdCl_4	3.4 (± 1.3)
2	$Pd(acac)_2$	3.0 (± 1.2)

[a]1wt.% Pd-NPs/$BMImBF_4$ dispersion obtained by MWI with 10 W for 6 min. [b]Median diameter (Ø) and standard deviation (σ). See experimental section for TEM and DLS measurement conditions.

Table 27. Microwave decomposition of palladium salts to Pd-NPs in $BMImBF_4$ with 10 W of power and 6 min reaction time.

Metal salt	Molar mass (g/mol)	Mass of Pd salt (mg) in $BMImBF_4$	wt.% metal in 2.42 g (2.0 mL) $BMImBF_4$
K_2PdCl_4	326.43	73.6	1
$Pd(acac)_2$	304.64	69.8	1

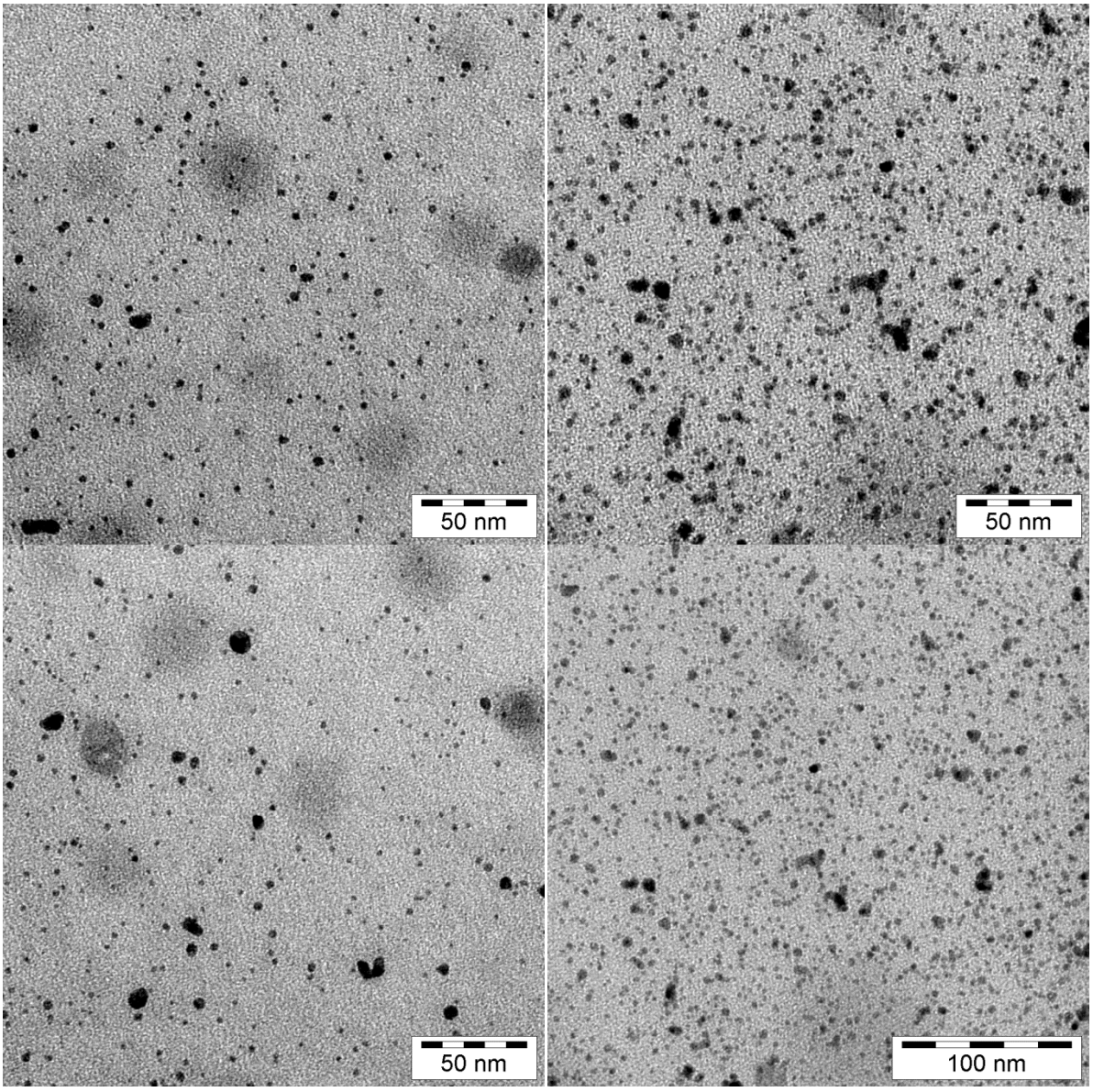

Fig. 53. TEM photographs of Pd-NPs/$BMImBF_4$ dispersion (1 wt.%) from K_2PdCl_4 (Table 26, entry 1).

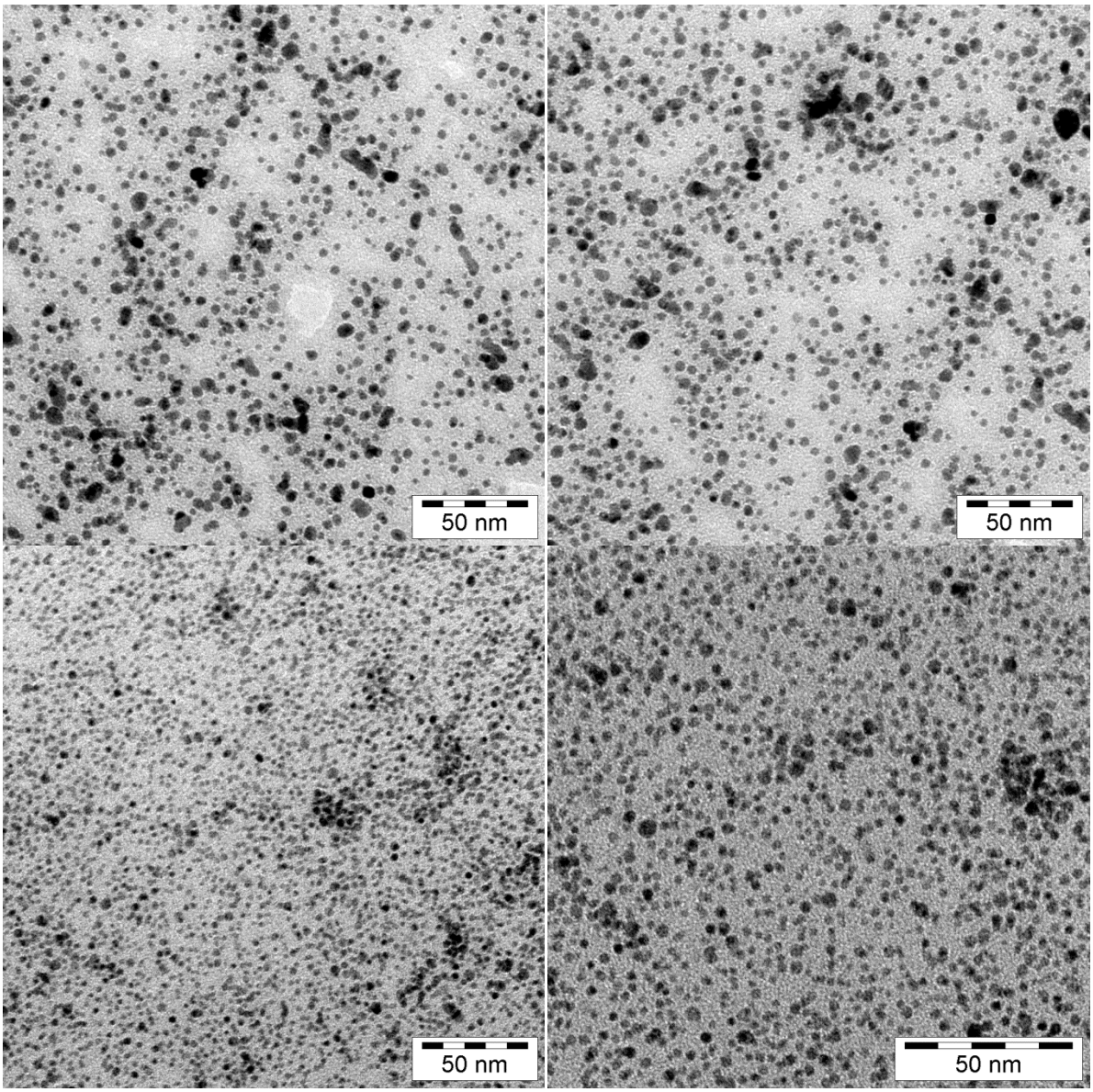

Fig. 54. TEM photographs of Pd-NPs/BMImBF$_4$ dispersion (1 wt.%) from Pd(acac)$_2$ (Table 26, entry 1).

6 PUBLICATIONS

Publications relevant for this cumulative dissertation are enrolled and the estimated contributions are discussed.

6.1 Organic carbonates as stabilizing solvents for transition metal nanoparticles

Christian Vollmer, Ralf Thomann, Christoph Janiak, manuscript submitted to Dalton Transactions

Impact factor: 3.647 (2010)

Contribution:

In the framework of this thesis, I planned and performed the experimental work including the optimization. I wrote the first draft of the manuscript, compiled the supporting information, and was involved in the discussions. GC and DLS analysis were carried out solely by me. The TEM analysis was performed by Dr. Ralf Thomann.

My contribution as a co-author of this paper is approximately 65 %.

6.2 Turning Teflon-coated magnetic stirring bars to catalyst systems with metal nanoparticle trace deposits - A caveat and a chance

Christian Vollmer, Marcel Schröder, Yi Thomann, Ralf Thomann, Christoph Janiak, Appl. Catal. A: Gen. 425-426 (2012) 178-183.

Impact factor: 3.383 (2010)

Contribution:

In the framework of this thesis, I developed the idea to establish this method, planned the experiments, and performed all of the experimental work including the optimization. B. Sc. Marcel Schröder carried out the hydrogenation of benzene under my guidiance during his bachelor thesis. I wrote the first draft of the manuscript, compiled the supporting information, and was involved in the discussions. The TEM and SEM analysis were performed by the co-authors Dr. Yi Thomann and Dr. Ralf Thomann.

My contribution as a co-author of this paper is approximately 55 %.

6.3 Naked metal nanoparticles from metal carbonyls in ionic liquids: Easy synthesis and stabilization

Christian Vollmer, Christoph Janiak, Coord. Chem. Rev. 255 (2011) 2039.

Impact factor: 10.018 (2010)

Contribution:

All the literature research was performed by me. I wrote approximately 60 % of this Review.

My contribution as a co-author of this paper is approximately 60%.

6.4 The use of microwave irradiation for the easy synthesis of graphene-supported transition metal nanoparticle in ionic liquids

Dorothea Marquardt, Christian Vollmer, Ralf Thomann, Peter Steurer, Rolf Mülhaupt, Engelbert Redel, Christoph Janiak, Carbon 49 (2011) 1326.

Impact factor: 4.893 (2010)

Contribution:

In the framework of this thesis, I developed the idea to investigate the catalytic behavior of M-NPs/CDG towards hydrogenation reactions. I planned and put out all of the hydrogenation experiments including the optimization. The GC analysis was done by me. I wrote approximately 50 % of the manuscript and the supporting information. I was involved in all discussions. The immobilization of the M-NPs on CDG was done by Dipl.-Chem. Engelbert Redel and Dipl.-Chem. Dorothea Marquardt, whereby Dipl.-Chem. Dorothea Marquardt was under my guidiance during her diploma thesis at this time. The TEM analysis was performed by Dr. Ralf Thomann.

My contribution as a co-author of this paper is 50 %.

7 SUMMARY AND OUTLOOK

Metal nanoparticles are of high scientific interest because of their broad range of applications in the fields of catalysis, medicine and material science. Synthesis and stabilization of small particles still pose a big challenge.

The aim of this thesis was to obtain reproducible particles with the size smaller than 5 nm originated from their binary carbonyls and to stabilize the particles only with the help of a weak coordinating solvent or by deposition on a surface. Selected metal nanoparticles should be screened for their catalytic activities in hydrogenation reactions. In the context of *green chemistry* the synthesis of the nanoparticles and the following catalysis should be carried out in mild, energy-saving conditions.

In the context of this thesis following aims were accomplished:

1. Spherical nanoparticles of the transition metals molybdenum, tungsten, rhenium, iron, ruthenium, cobalt, rhodium and iridium from their carbonyl precursors in racemic propylene carbonate could be obtained via low and rapid microwave irradiation (5 min, 50 W). The hydrogenation of cyclohexene and 1-hexyne was successful with elemental hydrogen and rhodium nanoparticle in propylene carbonate with activities up to 1875 mol product × $(\text{mol Rh})^{-1}$ × h^{-1}. Rhodium and Ruthenium nanoparticles could be extracted with 3-mercaptopropionic acid or trioctylphosphine oxide (TOPO) from the propylene carbonate phase and were stabilized without a big change in the particle diameter for 3 weeks.
2. Rhodium nanoparticles could be obtained from $Rh_6(CO)_{16}$ in the ionic liquid n-1-butyl-3-methyl-imidazolium tetrafluoroborate ($BMImBF_4$) via low and rapid microwave irradiation (6 min, 10 W). After the deposition of the particles on a PTFE coated, commercially available stirring bar, this “catalytic system” was used for catalytic hydrogenation runs from cyclohexene or benzene to cyclohexane. The activities of the hydrogenation cyclohexene to cyclohexane decreased in ten runs from 14.9×10^3 to 6.6×10^3 mol product × $(\text{mol Rh})^{-1}$ × h^{-1}. The activities of the hydrogenation from benzene to cylohexane slowly decreased in three runs from von 750 auf 460 mol product × $(\text{mol Rh})^{-1}$ × h^{-1}.
3. Chemical derived graphene was synthesized from natural graphite over graphite oxide (Hummers and Offeman) and a following thermal reduction process. Rhodium and Ruthenium nanoparticles were obtained from their carbonyl precursors in the ionic

liquid $BMImBF_4$ and deposited onto chemical derived graphene (CDG) and the M-NP/CDG-system was used for hydrogenation runs from cyclohexene or benzene to cyclohexane with elemental hydrogen. The activities remained constant in ten runs from cyclohexene to cyclohexane of 1570 mol product × $(\text{mol Rh})^{-1}$ × h^{-1}. The activities of Rh-NPs/CDG were examined during the hydrogenation of benzene to cylcohexane at different temperatures (25, 50, 75 °C). The highest activity of 310 mol product × $(\text{mol Rh})^{-1}$ × h^{-1} was measured at 50 °C.

Prospective investigations could be focused on other transition metals, especially metals, which are also commonly used as hydrogenation catalyst, like palladium, platinum and nickel, from other organic and inorganic precursors. With these "catalytic systems" a broad range of subtrates could be hydrogenated, for instance aromatic compounds, alkenes, alkynes, α,β-unsaturated ketones/aldehyds and carbonyl-compounds in general.

With the above described methods it should be possible to synthesize bimetallic nanoparticles.

Beside catalytic hydrogenations, the "catalytic systems" should be investigated on other catalytic reactions, for instance: Palladium is also known as a catalyst for a broad range of C-C coupling reactions, platinum is known as a good catalyst for hydrosilylation reactions and cobalt is an established catalyst for Fischer-Tropsch reactions.

In the case of racemic propylene carbonate, other organic carbonates, cyclic, non-cyclic and enantiopure, for instance dimethyl carbonate or ethylene carbonate or *S*-propylene carbonate, should be investigated as media to synthesize metal nanoparticles. The dispersions should be also tested in different catalytic reactions.

8 REFERENCES

[1] A.H. Lu, E.L. Salabas, F. Schüth, Angew. Chem. Int. Ed. 46 (2007) 1222.

[2] A. Gedanken, Ultrasonics Sonochemistry 11 (2004) 47.

[3] C.N.R. Rao, S R.C. Vivekchand, K. Biwas, A. Govindaraj, Dalton Trans. (2007) 3728.

[4] Y. Mastai, A. Gedanken in: C.N.R. Rao, A. Müller, A.K. Cheetham (editors), Chemistry of Nanomaterials, Wiley-VCH, Weinheim, vol. 1, 2004, 113.

[5] D. Mahajan, E.T. Papish, K. Pandya, Ultrasonics Sonochemistry 11 (2004) 385.

[6] J. Park, J. Joo, S.G. Kwon, Y. Jang, T. Hyeon, Angew. Chem. Int. Ed. 46 (2007) 4630.

[7] D. Astruc, F. Lu, J.R. Aranzaes, Angew. Chem. Int. Ed. 44 (2005) 7852.

[8] C. Pan, K. Pelzer, K. Philippot, B. Chaudret, F. Dassenoy, P. Lecante, M.-J Casanove, J. Am. Chem. Soc. 123 (2001) 7584.

[9] J.D. Aiken III, R.G. Finke, J. Am. Chem. Soc. 121 (1999) 8803.

[10] R.J. White, R. Luque, V.L. Budarin, J.H. Clark, D.J. Macquarrie, Chem. Soc. Rev. 38 (2009) 481.

[11] J. Krämer, E. Redel, R. Thomann, C. Janiak, Organometallics 27 (2008) 1976.

[12] K. Ueno, H. Tokuda, M. Watanabe, Phys. Chem. Chem. Phys. 12 (2010) 1649.

[13] J. Dupont, J.D. Scholten, Chem. Soc. Rev. 39 (2010) 1780.

[14] J. Dupont, J. Brazil Chem. Soc. 15 (2004) 341.

[15] M.-A. Neouze, J. Mater. Chem. 20 (2010) 9593.

[16] C.S. Consorti, P.A.Z. Suarez, R.F. de Souza, R.A. Burrow, D.H. Farrar, A.J. Lough, W. Loh, L.H.M. da Silva, J. Dupont, J. Phys. Chem. B 109 (2005) 4341.

[17] J. Dupont, P.A.Z. Suarez, R.F. de Souza, R.A. Burrow, J.-P. Kintzinger, Chem. Eur. J. 6 (2000) 2377.

[18] R.A. Sheldon, Chem. Commun. (2008) 3352.

[19] P. Wasserscheid, T.Welton, Ionic Liquid in Synthesis, Wiley-VCH, Weinheim, vol. 1, 2007, 93.

[20] P. Wasserscheid, W. Keim, Angew. Chem. Int. Ed. 39 (2000) 3773.

[21] C. van Doorslaer, Y. Schellekens, P. Mertens, K. Binnemanns, D. De Vos, Phys. Chem. Chem. Phys. 12 (2010) 1741.

[22] E. Redel, J. Krämer, R. Thomann, C. Janiak, J. Organomet. Chem. 694 (2009) 1069.

[23] C. Vollmer, E. Redel, K. Abu-Shandi, R. Thomann, H. Manyar, C. Hardacre, C. Janiak, Chem. Eur. J. 16 (2010) 3849.

[24] V. Parvulescu, C. Hardacre, Chem Rev. 107 (2007) 2615.

[25] D. Astruc, Nanoparticles and Catalysis, Wiley-VCH, Weinheim, 2008, 211.

[26] K.P.C. Vollhardt, N.E. Schore, Organische Chemie, Wiley-VCH, Weinheim, vol. 3, 2000, 981.

[27] B.M. Trost, Science 254 (1991) 1471.

[28] B.M. Trost, Angew. Chem. Int. Ed. 34 (1995) 259.

[29] P.T. Anastas, J.C. Warner, Green Chemistry: Theory and Practice, Oxford University Press, New York, 1998.

[30] J.H. Clarke, Green Chem. 1 (1999) 1.

[31] P.J. Dunn, Chem. Soc. Rev. 41 (2012) 1452.

[32] R.A. Sheldon, I. Arend, U. Hanefeld, Green Chemistry and Catalysis, Wiley-VCH, Weinheim, 2007, 1.

[33] R.B.N. Baig, R.S. Varma, Chem. Soc. Rev. 41 (2012) 1559.

[34] P.T. Anastas, J. B. Zimmerman, Sustainability Science and Engineering Defining Principles, Elsevier, Amsterdam, vol. 1, 2006, 11.

[35] S.L.Y. Tang, R.L. Smith, M. Poliakoff, Green Chem. 7 (2005) 761.

[36] R.A. Sheldon, Chem. Soc. Rev. 41 (2012) 1437.

[37] H. Weingärtner, Angew. Chem. Int. Ed. 47 (2008) 654.

[38] D. Xiao, J.R. Rajian, A. Cady, S. Li, R.A. Bartsch, E.L. Quitevis, J. Phys. Chem. B 111 (2007) 4669.

[39] I. Krossing, J.M. Slattery, C. Daguenet, P.J. Dyson, A. Oleinikova, H. Weingärtner, J. Am. Chem. Soc. 128 (2006) 13427.

[40] K.R. Seddon, Chem. Soc. Rev. 37 (2008) 123.

[41] P. Bonhôte, A.-P. Dias, N. Papageorgiou, K.K. Kalyanasundaram, M. Grätzel, Inorg. Chem. 35 (1996) 1168.

[42] J.M. Pringle, J. Golding, K. Baranyai, C.M. Forsyth, B.B. Deacon, J.L. Scott, D.R. Mc Farelane, New J. Chem. 27 (2003) 1504.

[43] P. Migowski, D. Zanchet, G. Machado, M.A. Gelesky, S.R. Teixeira, J. Dupont, Phys. Chem. Chem. Phys. 12 (2010) 6826.

[44] J.J. Jodry, K. Mikami, Tetrahedron Lett. 45 (2004) 4429.

[45] T.J. Gannon, G. Law, R.P. Watson, A.J. Carmichael, K.R. Seddon, Langmuir 15 (1999) 8429.

[46] J.N.A Canongia Lopes, M.F.C. Gomes, A.A.H. Padua, J. Phys. Chem. B 110 (2006) 16816.

[47] G. Law, R. P. Watson, A. J. Carmichael, K. R. Seddon, Phys. Chem. Chem. Phys. 3 (2001) 2879.

[48] J.N.A. Canongia Lopes, A.A.H. Pádua, J. Phys. Chem. B 110 (2006) 3330.

[49] D.G.E. Kerfoot, X. Nickel, E. Wildermuth, H. Stark, G. Friedrich, F.L. Ebenhöch, B. Kühborth, J. Silver, R. Rituper, Iron Compounds, in Ullmann's Encyclopaedia of Industrial Chemistry, Wiley, 5th edn (online), 2008.

[50] T. Hyeon, Chem. Commun. (2003) 927.

[51] P.H. Hess, P.H. Parker, Jr., J. Appl. Polym. Sci. 10 (1966) 1915.

[52] J.R. Thomas, J. Appl. Phys. 37 (1966) 2914.

[53] E. Papirer, P. Horny, H. Balard, R. Anthore, C. Petipas, A. Martinet, J. Colloid Interface Sci. 94 (1983) 207.

[54] E. Papirer, P. Horny, H. Balard, R. Anthore, C. Petipas, A. Martinet, J. Colloid Interface Sci. 94 (1983) 220.

[55] K. S. Suslick, M. Fang, T. Hyeon, J. Am. Chem. Soc. 118 (1996) 11960.

[56] O.A. Platonova, L.M. Bronstein, S.P. Solodovnikov, I.M. Yanovskaya, E.S. Obolonkova, P.M. Valetsky, E. Wenz, M. Antonietti, Colloid Polym. Sci. 275 (1997) 426.

[57] G.H. Lee, S.H. Huh, H.I. Jung, J. Mol. Struct. 400 (1998) 141.

[58] D.P. Dinega, M.G. Bawendi, Angew. Chem. Int. Ed. 38 (1999) 1788.

[59] M. Giersig, M. Hilgendorff, J. Phys. D: Appl. Phys. 32 (1999) L111.

[60] U. Wiedwald, M. Spasova, E.L. Salabas, M. Ulmeanu, M. Farle, Z. Frait, A. Fraile Rodriguez, D. Arvanitis, N.S. Sobal, M. Hilgendorff, M. Giersig, Phys. Rev. B 68 (2003) 064424.

[61] J. van Wonterghem, S. Mørup, S.W. Charles, S. Wells, J. Villadsen, Phys. Rev. Lett. 55 (1985) 410.

[62] J. van Wonterghem, S. Mørup, S.W. Charles, S. Wells, J. Colloid Interface Sci. 121 (1988) 558.

[63] C. Pathmamanoharan, N.L. Zuiverloon, A.P. Philipse, Progr. Colloid Polym. Sci. 115 (2000) 141.

[64] A. Goossens, L.J. de Jongh, K. Butter, A.P. Philipse, M.W.J. Crajé, A.M. van der Kraan, Hyperfine Interact. 141/142 (2002) 381.

[65] K. Butter, P.H.H. Bomans, P.M. Frederik, G.J. Vroege, A.P. Philipse, Nat. Mater. 2 (2003) 88.

[66] E. Bauer-Grosse, G. Le Caër, Phil. Mag. B 56 (1987) 485.

[67] S.H. Huh, S.J. Oh, Y.N. Kim, G.H. Lee, Rev. Sci. Instrum. 70 (1999) 4366.

[68] S.-J. Park, S. Kim, S. Lee, Z.G. Khim, K. Char, T. Hyeon, J. Am. Chem. Soc. 122 (2000) 8581.

[69] S. Sun, C.B. Murray, D. Weller, L. Folks, A. Moser, Science 287 (2000) 1989.

[70] M. Chen, D.E. Nikles, J. Appl. Phys. 91 (2002) 8477.

[71] M. Chen, D.E. Nikles, Nano Lett. 2 (2002) 211.

[72] J.-I. Park, J. Cheon, J. Am. Chem. Soc. 123 (2001) 5743.

[73] V.F. Puntes, K.M. Krishnan, P. Alivisatos, Appl. Phys. Lett. 78 (2001) 2187.

[74] T. Hyeon, S.S. Lee, J. Park, Y. Chung, H.B. Na, J. Am. Chem. Soc. 123 (2001) 12798.

[75] S.-W. Kim, S.U. Son, S.S. Lee, T. Hyeon, Y.K. Chung, Chem. Commun. (2001) 2212.

[76] N.A.D. Burke, H.D.H. Stöver, F.P. Dawson, Chem. Mater. 14 (2002) 4752.

[77] K. Butter, A.P. Philipse, G.J. Vroege, J. Magn. Magn. Mater. 252 (2002) 1.

[78] M. Rutnakornpituk, M.S. Thompson, L.A. Harris, K.E. Farmer, A.R. Esker, J.S. Riffle, J. Connolly, T.G. St. Pierre, Polymer 43 (2002) 2337.

[79] F.S. Diana, S.-H. Lee, P.M. Petroff, E.J. Kramer, Nano Lett. 3 (2003) 891.

[80] H. Bönnemann, W. Brijoux, R. Brinkmann, N. Matoussevitch, H. Waldöfner, N. Palina, H. Modrow, Inorg. Chim. Acta 350 (2003) 617.

[81] H. Bönnemann, R.A. Brand, W. Brijoux, H.-W. Hofstadt, M. Frerichs, V. Kempter, W. Maus-Friedrichs, N. Matoussevitch, K.S. Nagabhushana, F. Voigts, V. Caps, Appl. Organometal. Chem. 19 (2005) 790.

[82] S. Behrens, H. Bönnemann, N. Matoussevitch, A. Gorschinski, E. Dinjus, W. Habicht, J. Bolle, S. Zinoveva, N. Palina, J. Hormes, H. Modrow, S. Bahr V. Kempter, J. Phys.: Condens. Matter 18 (2006) S2543.

[83] N. Matoussevitch, A. Gorschinski, W. Habicht, J. Bolle, E. Dinjus, H. Bönnemann, S. Behrens, J. Magn. Magn. Mater. 311 (2007) 92.

[84] Y. Yin, R.M. Rioux, C.K. Erdonmez, S. Hughes, G.A. Somorjai, A.P. Alivisatos, Science 304 (2004) 711.

[85] M. Zubris, R.B. King, H. Garmestani, R. Tannenbaum, J. Mater. Chem. 15 (2005) 1277.

[86] A. Hütten, D. Sudfeld, I. Ennen, G. Reiss, K. Wojczykowski, P. Jutzi, J. Magn. Magn. Mater. 293 (2005) 93.

[87] D. Sudfeld, I. Ennen, A. Hütten, U. Golla-Schindler, H. Jaksch, G. Reiss, D. Meißner, K. Wojczykowski, P. Jutzi, W. Saikaly, G. Thomas, J. Magn. Magn. Mater. 293 (2005) 151.

[88] B.D. Korth, P. Keng, I. Shim, S.E. Bowles, C. Tang, T. Kowalewski, K.W. Nebesny, J. Pyun, J. Am. Chem. Soc. 128 (2006) 6562.

[89] R.A. Mercuri, Chem. Abstr. 148 (2007) 37461.

[90] R.A. Mercuri, Chem. Abstr. 146 (2007) 233646.

[91] J.S. Gergely, E.S. Marston, S. Subramoney, L. Zhang, Chem. Abstr. 146 (2007) 433242.

[92] C. Gürler, M. Feyen, S. Behrens, N. Matoussevitch, A.M. Schmidt, Polymer 49 (2008) 2211.

[93] N. Doan, K. Kontturi, C. Johans, J. Colloid Interface Sci. 350 (2010) 126.

[94] A. Taubert, Z. Li, Dalton Trans. (2007) 723.

[95] E. Redel, R. Thomann, C. Janiak, Inorg. Chem. 47 (2008) 14.

[96] T. Gutel, J. Garcia-Anton, K. Pelzer, K. Philippot, C.C. Santini, Y. Chauvin, B. Chaudret, J.-M. Basset, J. Mater. Chem. 17 (2007) 3290.

[97] L.S. Ott, R.G. Finke, Inorg. Chem. 45 (2006) 8382.

[98] G.S. Fonseca, A.P. Umpierre, P.F.P. Fichtner, S.R. Teixeira, J. Dupont, Chem. Eur. J. 9 (2003) 3263.

[99] Z. Li, A. Friedrich, A. Taubert, J. Mater. Chem. 18 (2008) 1008.

[100] P. Migowski, G. Machado, S.R.Teixeira, M.C.M. Alves, J. Morais, A. Traverse, J. Dupont, Phys. Chem. Chem. Phys. 9 (2007) 4814.

[101] J.M. Zhu, Y.H. Shen, A.J. Xie, L.G. Qiu, Q. Zhang, X.Y. Zhang, J. Phys. Chem. C 111 (2007) 7629.

[102] M.A. Firestone, M.L. Dietz, S. Seifert, S. Trasobares, D.J. Miller, N.J. Zaluzec, Small 1 (2005) 754.

[103] K. Peppler, M. Polleth, S. Meiss, M. Rohnke, J.Z. Janek, Phys. Chem. 220 (2006) 1507.

[104] A. Safavi, N. Maleki, F. Tajabadi, E. Farjami, Electrochem. Commun. 9 (2007) 1963.

[105] K. Kim, C. Lang, P.A. Kohl, J. Electrochem. Soc. 152 (2005) E9.

[106] E. Redel, R. Thomann, C. Janiak, Chem. Commun. 15 (2008) 1789.

[107] G. Schmid, Nanoparticles, Wiley-VCH, Weinheim, vol. 2, 2010, 215.

[108] M. Antonietti, D. Kuang, B. Smarly, Y. Zhou, Angew. Chem. Int. Ed. 43 (2004) 4988.

[109] F. Endres, M. Bukowski, R. Hempelmann, H. Natter, H. Angew. Chem., Int. Ed. 42 (2003) 3428.

[110] Y.J. Zhu, W.W. Wang, R.J. Qi, X.L. Hu, Angew. Chem., Int. Ed. 43 (2004) 1410.

[111] E.T. Silveira, A.P. Umpierre, L.M. Rossi, G. Machado, J. Morais, G.V. Soares, I.J.R. Baumvol, S.R. Teixeira, R.F.P. Fichtner, J. Dupont, Chem. Eur. J. 10 (2004) 3734.

[112] J. Dupont, G.S. Fonseca, A.P. Umpierre, P.F.P. Fichtner, S.R. Teixeira, J. Am. Chem. Soc. 124 (2002) 4228.

[113] C.W. Scheeren, G. Machado, J. Dupont, P.F.P. Fichtner, S.R. Texeira, Inorg. Chem. 42 (2003) 4738.

[114] A.I. Bhatt, A. Mechler, L.L. Martin, A.M. Bond, J. Mater. Chem. 17 (2007) 2241.

[115] H. Itoh, K. Naka, Y. Chujo, J. Am. Chem. Soc. 126 (2004) 3026.

[116] H.S. Schrekker, M.A. Gelesky, M.P. Stracke, C.M.L. Schrekker, G. Machado, S.R. Teixeira, J.C. Rubim, J. Dupont, J. Colloid Interface Sci. 316 (2007) 189.

[117] R.A. Alvarez-Puebla, E. Arceo, P.J.G. Goulet, J.J. Garrido, R.F. Aroca, J. Phys. Chem. B 109 (2005) 3787.

[118] E.J.W. Verwey, J.T.G. Overbeek , Theory of the Stability of Lyophobic Colloids, Dover Publications Mineola, New York, 1999, 106.

[119] E. Redel, J. Krämer, R. Thomann, C. Janiak, GIT Labor-Fachzeitschrift, April 2008, 400.

[120] A.N. Shipway, E. Katz, I. Willner, ChemPhysChem 1 (2000) 18.

[121] T. Cassagneau, J. H. Fendler, J. Phys. Chem. B 103 (1999) 1789.

[122] C.D. Keating, K.K. Kovaleski, M.J. Natan, J. Phys. Chem. B. 102 (1998) 9404.

[123] M.N. Kobrak, H. Li, Phys. Chem. Chem. Phys. 12 (2010) 1922.

[124] L.S. Ott, R.G. Finke, Coord. Chem. Rev. 251 (2007) 1075.

[125] B.L. Bhargava, S. Balasubramanian, M.L. Klein, Chem. Commun. (2008) 3339.

[126] E. Redel, M. Walter, R. Thomann, C. Vollmer, L. Hussein, H. Scherer, M. Krüger, C. Janiak, Chem. Eur. J. 15 (2009) 10047.

[127] R.G. Pearson, Chemical Hardness: Application from Molecules to Solids, Wiley-VCH, Weinheim, 1997, 1.

[128] T.A. Baker, C.M. Friend, E. Kaxiras, J. Am. Chem. Soc. 130 (2008) 3720-3721.

[129] K.-S. Kim, D. Demberelnyamba, H. Lee, Langmuir 20 (2004) 556-560.

[130] S. Gao, H. Zhang, X. Wang, W. Mai, C. Peng, L. Ge, Nanotechnology 16 (2005) 1234.

[131] R. Marcilla, D. Mecerreyes, I. Odriozola, J.A. Pomposo, J. Rodriguez, I. Zalakain, I. Mondragon, Nano 2 (2007) 169.

[132] M.A. Gelesky, A.P. Umpierre, G. Machado, R.R.B. Correia, W.C. Magno, J. Morais, G. Ebeling, J. Dupont, J. Am. Chem. Soc. 127 (2007) 4588.

[133] G.S. Fonseca, G. Machado, S.R. Teixeira, G.H. Fecher, J. Morais, M.C.M. Alves, J. Dupont, J. Colloid Interface Sci. 301 (2006) 193.

[134] M. Ruta, G. Laurenczy, P.J. Dyson, L. Kiwi-Minsker, J. Phys. Chem. C 112 (2008) 17814.

[135] H. Zhang, H. Cui, Langmuir 25 (2009) 2604.

[136] C.W. Scheeren, J.B. Domingos, G. Machado, J. Dupont, J. Phys. Chem. C 112 (2008) 16463.

[137] E. Redel, M. Walter, R. Thomann, L. Hussein, M. Krüger, C. Janiak, Chem. Commun. 46 (2010) 1159.

[138] J. Turkevich, P.C. Stevenson, J. Hillier, Discuss. Faraday Soc. 11 (1951) 55.

[139] H.R. Ryu, L. Sanchez, H.A. Keul, A. Raj, M.R. Bockstaller, Angew. Chem. Int. Ed. 47 (2008) 7639.

[140] Y. Hatakeyama, S. Takahashi, K. Nishikawa, J. Phys. Chem. C. 114 (2010) 11098.

[141] T. Kameyama, Y. Ohno, T. Kurimoto, K.-I. Okazaki, T. Uematsu, S. Kuwabata, T. Torimoto, Phys. Chem. Chem. Phys. 12 (2010) 1804.

[142] T. Suzuki, K.-I. Okazaki, S. Suzuki, T. Shibayama, S. Kuwabata, T. Torimoto, Chem. Mater. 22 (2010) 5209.

[143] R.R. Deshmukh, R. Rajagopal, K.V. Srinivasan, Chem. Commun. (2001) 1544.

[144] M.H.G. Prechtl, J.D. Scholten, J. Dupont, Molecules 15 (2010) 3441.

[145] V. Calo, A. Nacci, A. Monopoli, S. Laera, N. Coffi, J. Org. Chem. 68 (2003) 2929.

[146] L. Xu, W. Chen, J. Xiao, Organometallics 19 (2000) 1123.

[147] K. Anderson, S.C. Fernández, C. Hardacre, P.C. Marr, Inorg. Chem. Commun. 7 (2004) 73.

[148] J.D. Scholten, G. Ebeling, J. Dupont, Dalton Trans. (2007) 5554.

[149] M. Harada, Y. Kimura, K. Saijo, T. Ogawa, S. Isoda, J. Colloid Interface Sci. 339 (2009) 373.

[150] A. Imanishi, M. Tamura, S. Kuwabata, Chem. Commun. (2009) 1775.

[151] P. Roy, R. Lynch, P. Schmuki, Electrochem. Commun. 11 (2009) 1567.

[152] C. Fu, Y. Kuang, Z. Huang, X. Wang, N. Du, J. Chen, H. Zhou, Chem. Phys. Lett. 499 (2010) 250.

[153] S.Z. El Abedin, F. Endres, Electrochim. Acta 54 (2009) 5673.

[154] L. Yu, H. Sun, J. He, D. Wang, X. Jin, X. Hu, G.Z. Chen, Electrochem. Commun. 9 (2007) 1374.

[155] D. Bogdal, Microwave-Assisted Organic Synthesis, Oxford, Elsevier, 2005, 47.

[156] A.L. Buchachenko, E.L. Frankevich, Chemical Generation and Reception of Radio- and Microwaves, Wiley-VCH, Weinheim, 1993, 11.

[157] V.K. Ahluwulia, Alternative Energy Processes in Chemical Synthesis, Alpha Science International LTD, Oxford, 2008, 1.

[158 J. Berlan, P. Giboreau, S. Lefeuvre, C. Marchand, Tedrahedron Lett. 32 (1991) 2363.

[159 F. Langa, P. de la Cruz, A. de la Hoz, A. Diez-Barra, Contemp. Org. Synth. 4 (1997) 373.

[160] L. Perreux, A. Loupy, Tetrahedron 57 (2001) 9199.

[161] A. Stadler, C.O. Kappe, J. Chem. Soc. Perkin Trans. 2 (2000) 1363.

[162] A. Stadler, C.O. Kappe, Eur. J. Org. Chem. (2001) 919.

[163] D.O. Silva, J.D. Scholten, M.A. Gelesky, S.R. Teixeira, A.C.B. Dos Santos, E.F. Souza-Aguiar, J. Dupont, ChemSusChem 1 (2008) 291.

[164] M. Scariot, D.O. Silva, J.D. Scholten, G. Machado, S.R. Teixeira, M.A. Novak, G. Ebeling, J. Dupont, Angew. Chem. Int. Ed. 47 (2008) 9075.

[165] V. Dahirel, M. Jardat, Curr. Opin. Colloid Interafce Sci. 15 (2010) 2.

[166] B.W. Ninham, Adv. Colloid Interface Sci. 83 (1999) 1.

[167] J.-P. Hansen, H. Löwen, Annu. Reb. Phys. Chem. 51 (2000) 209.

[168] T. Liu, Langmuir 26 (2010) 9202.

[169] R.G. Finke in: D.L. Feldheim, C.A. Foss Jr. (editors), Metal Nanoparticle: Synthesis, Characterization and Applications, Marcel Dekker, Inc., New York, 2002, 17.

[170] M. Boström, D.R.W. Williams, B.W. Ninham, Phys. Rev. Lett. 87 (2001) 168103.

[171] J. Lyklema, Fundamentals of Interface and Colloid Science, Elsevier, London, 2005.

[172] M. Dijkstra, Curr. Opin. Colloid Interface Sci. 6 (2001) 372.

[173] G.M. Scheuermann , L. Rumi, P. Steurer, W. Bannwarth, R. Mülhaupt, J. Am. Chem. Soc. 131 (2009) 8262.

[174] S. Stankovich, D.A. Dikin, G.H.B. Dommett, K.M. Kohlhaas, E.J. Zimney, E.A. Stach, R.D. Piner, S.T. Nguyen, R.S. Ruoff, Nature 442 (2006) 282.

[175] A.K. Geim, K.S. Novoselov, Nature Mater. 6 (2007) 183.

[176] D. Li, R.B. Kaner, Science 320 (2008) 1170.

[177] P. Steurer, R. Wissert, R. Thomann, R. Mülhaupt, Macromol. Rapid Commun. 30 (2009) 316.

[178] M.J. McAllister, J.-L. Li, D.H. Adamson, H.C. Schniepp, A.A. Abdala, J. Liu, M. Herrera-Alonso, D.L. Milius, R. Car, R.K. Prud'homme, I.A. Aksay Chem. Mater. 19 (2007) 4396.

[179] H.C. Schniepp, J.L. Li, M.J. McAllister, H. Sai, M. Herrera-Alonso, D.H. Adamson, R.K. Prud'homme, R. Car, D.A. Saville, I.A. Aksa J. Phys.Chem. B 110 (2006) 8535.

[180] G. Goncalves, P.A.A.P. Marques, C.M. Granadeiro, H.I.S. Nogueira, M.K. Singh, J. Grácio, Chem. Mater. 21 (2009) 4796.

[181] H.P. Boehm, E. Stumpp, Carbon 45 (2007) 1381.

[182] H.B. Li, W.J. Kang, B.J. Xi, Y. Yan, H.Y. Bi, Y.C. Zuhu, Y. Qian, Carbon 48 (2010) 464.

[183] H. Park, J.S. Kim, B.G. Choi, S.M. Jo, D.Y. Kim, W.H. Hong, S.-Y. Jang, Carbon 48 (2010) 1325.

[184] D.N. Ventura, R.A. Stone, K.S. Chen, H.H. Hariri, K.A. Riddle, T.J. Fellers, C.S. Yun, G.F. Strouse, H.W. Kroto, S.F.A. Acquah, Carbon 48 (2010) 987.

[185] S. Kudo, T. Maki, K. Miura, K. Mae, Carbon 48 (2010) 1186.

[186] K. Scholz, J. Scholz, A.J. McQuilla, G. Wagner, O. Klepel, Carbon 48 (2010) 1788.

[187] Y.H. Kim, Y.T. Kim, H. Kim, D. Lee, Carbon 48 (2010) 2072.

[188] V. Tzitzios, V. Georgakilas, E. Oikonomou, M. Karakassides, D. Petridis, Carbon 44 (2006) 848.

[189] K. Gotoh, K. Kawabata, E. Fujii, K. Morishige, T. Kinumoto, Y. Miyazaki, H. Ishida, Carbon 47 (2009) 2120.

[190] J. Li, C.Y. Liu, Eur. J. Inorg. Chem. (2010) 1244.

[191] M.P.N. Bui, S. Lee, K.N. Han, X.H. Pham, C.A. Li, J. Choo, G.H. Seong, Chem. Commun. (2009) 5549.

[192] W.Z. Li, M. Waje, Z.W. Chen, P. Larsen, Y.S. Yan, Carbon 48 (2010) 995.

[193] G. Lee, J.H. Shim, H. Kang, K.M. Nam, H. Song, J.T. Park, Chem. Commun. (2009) 5036.

[194] B. Seger, P.V. Kamat, J. Phys. Chem. 113 (2009) 7990.

[195] L. Dong, R.R.S. Gari, Z. Li, M.M. Craig, S. Hou, Carbon 48 (2010) 781.

[196] B. Karimi, F. Kabiri Esfahani, Chem. Commun. (2009) 5555.

[197] M. Sun, J. Zhang, Q. Zhang, Y. Wang, H. Wan, Chem. Commun. (2009) 5174.

[198] L. Armelao, D.B.D. Amico, R. Braglia, F. Calderazzo, F. Garbassi, G. Marra, A. Merigo, DaltonTrans. (2009) 5559.

[199] I.V. Lightcap, T.H. Kosel, P.V. Kamat, Nano Lett. 10 (2010) 577.

[200] B. Schäffner, F. Schäffner, S.P. Verevkin, A. Börner, Chem. Rev. 110 (2010) 4554.

[201] J. Bayardon, J. Holz, B. Schäffner, V. Andrushko, S. Verevkin, A. Preetz , A. Börner, Angew. Chem. Int. Ed. 46 (2007) 5971.

[202] S.P. Verevkin, V.N. Emel'yanenko, A.V. Toktonov, Y. Chernyak, B. Schäffner, A. Börner, J. Chem. Thermodynamics 40 (2008) 1428.

[203] B. Schäffner, S.P. Verevkin, A. Börner, Chem. Unserer Zeit 43 (2009) 12.

[204] J. H. Clements, J. Ind. Eng. Chem. Res. 42 (2003) 663.

[205] A. Ansmann, B. Boutty, M. Dierker, Chem. Abstr. 149 (2008) 17219.

[206] A.L. Kohl, P.A. Buckingham, Oil Gas J. 58 (1960) 146.

[207] J. Xia, M.E. Ragsdale, E.B. Stephens, Chem. Abstr. 136 (2001) 38897.

[208] S. Schmidt, Chem. Abstr. 142 (2004) 375279.

[209] R. Jasinski, J. Electroanal. Chem. 15 (1967) 89.

[210] K.K.D. Ehinon, S. Naille, R. Dedryvère, P.-E. Lippens, J.-C. Jumas, D. Gonbeau, Chem. Mater. 20 (2008) 5388.

[211] A. Behr, H. Schmidke, Chem.-Ing.-Tech. 65 (1993) 568.

[212] A. Behr, N. Döring, S. Durowicz-Heil, B. Ellenberg, C. Kozik, C. Lohr, H. Schmidke, Fat Sci. Technol. 95 (1993) 2.

[213] M. Reetz, G. Lohmer, Chem. Commun. (1996) 1921.

[214] J. Demel, J. Čejka, S. Bakardjieva, P. Štěpnička, J. Mol. Catal. A: Chem. 263 (2007) 259.

[215] I. Thomé, A. Nijs, C. Bolm, Chem. Soc. Rev. 41 (2012) 979.

[216] J.M. Crow, Chemistry World, 46 May 2011.

[217] G. Wilke, Angew. Chem. Int. Ed. 42 (2003) 5000.

[218] K. Fischer, K. Jonas, P. Misbach, R. Stabba, G. Wilke, Angew. Chem. Int. Ed. 12 (1973) 943.

[219] R.K. Arvela, N.E. Leadbeater, M.S. Sangi, V.A. Williams, P. Granados, R.D. Singer, J. Org. Chem. 70 (2005) 161.

[220] S.L. Buchwald, C. Bolm, Angew. Chem. Int. Ed. 48 (2009) 5586.

[221] Z. Gonda, G.L. Tolnai, Z. Novák, Chem. Eur. J. 16 (2010) 11822.

[222] K. Yoshida, N. Begum, S.-I. Ito, K. Tomishige, Appl. Catal. A 358 (2009) 186.

[223] K. Nishida, I. Atake, D. Li, T. Shishido, Y. Oumi, T. Sano, K. Takehira, Appl. Catal. A 337 (2008) 48.

[224] D. Li, I. Atake, T. Shishido, Y. Oumi, T. Sano, K. Takehira, Appl. Catal. A 332 (2007) 98.

[225] Scifinder search performed November 2011.

[226] A. Behr, F. Naendrup, D. Obst, Adv. Synth. Catal. 344 (2002) 1142.

[227] B. Schäffner, J. Holz, S.P. Verevkin, A. Börner, ChemSusChem, 1 (2008) 249.

[228] A. Behr, D. Obst, B. Turkowski, J. Mol. Catal. A: Chem. 226 (2005) 215.

[229] B. Schäffner, V. Andrushko, J. Bayardon, J. Holz, A. Börner, Chirality, 21 (2009) 857.

[230] H.-E. Elias, Makromoleküle, Wiley-VCH, Weinheim, 2001, Vol. 3, 368.

[231] B.K. Hodnett, Heterogeneous Catalytic Oxidations, Wiley-VCH, Weinheim. 2000, 240; P.T. Anastas, J.C. Warner, Green Chemistry: Theory and Practice, Oxford University Press, New York, 1998.

[232] C. Vollmer, M. Schröder, Y. Thomann, R. Thomann, C. Janiak, Appl. Catal. A (2012) in press. http://dx.doi.org/10.1016/j.apcata.2012.03.017

[233] J. Lin, C.U. Pittman, *J.* Orgmet. Chem. 512 (1996) 69.

[234] J.A. Anderson, J. Mellor, R.P.K. Wells, J. Catal. 261 (2009) 208.

[235] L. M. Rossi, G. Machado, P. F. P. Fichtner, S.R. Teixeira, J. Dupont, Catal. Lett. 92 (2004) 149.

[236] E.T. Silveira, A.P. Umpierre, L.M. Rossi, G. Machado, J. Morais, I.L.R. Baumvol, S.R. Teixeira, P.F.P. Fichtner, J. Dupont, Chem. Eur. J. 10 (2004) 3734.

[237] D. Marquardt, C. Vollmer, R. Thomann, P. Steurer, R. Mülhaupt, E. Redel, C. Janiak, Carbon 49 (2011) 1326.

[238] M.J. Jacinto, P.K. Kiyohara, S.H. Masunaga, R.F. Jardim, L.M. Rossi, Applied Catalysis A: Gen. 338 (2008) 52.

[239] R. Sablong, U. Schlotterbeck, D. Vogt, S. Mecking, Adv. Synth. Catal. 345 (2003) 333.

[240] L. Armelao, D.B.D. Amico, R. Braglia, F. Calderazzo, F. Garbassi, G. Marra, A. Merigo, Dalton Trans. (2009) 5559.

[241] R.M. Rioux, B.B. Hsu, M.E. Grass, H. Song, G.A. Somorjai, Catal Lett. 126 (2008) 10.

[242] C. Pan, K. Pelzer, K. Philippot, B. Chaudret, F. Dassenoy, P. Lecante, M.-J. Casanove, J. Am Chem. Soc. 124 (2001) 7584.

[243] T. Cassagneau, T. E. Mallouk, J.H. Fendler, J. Am. Chem. Soc. 120 (1998) 7848.

[244] M.-N. Birkholz, Z. Freixa, P.W.N.M. van Leeuwen, Chem. Soc. Rev. 38 (2009) 1099.

[245] K. Fagnou, M. Lautens, Chem. Rev. 103 (2003) 169.

[246] N. Jeong, B.K. Sung, J.S. Kim, S.B. Park, S.D. Seo, J.Y. Shin, K.Y. In, Y.K. Choi, Pure Appl. Chem. 74 (2002) 85.

[247] X. Cui, K. Burgess, Chem. Rev. 105 (2005) 3272.

[248] G.G. Wildgoose, C.E. Banks, R. G. Compton, Small 2 (2006) 182.

[249] P.M. Ajayan, B.I. Yakobson, Nature 441 (2006) 818.

[250] C.N.R.Rao, K. Biswas, K.S. Subrahmanyam, A. Govindaraj, J. Mater. Chem. 19 (2009) 2457.

[251] A.R. McDonald, C. Müller, D. Vogt, G.P M. van Klink, G. van Koten, Green Chem. 10 (2008) 424.

[252] R.A. May, B.L. Iversen, B.D. Chandler, J. Am. Chem. Soc. 125 (2003) 14832.

[253] G. Glaspell, H.M.A. Hassan, A. Elzatahry, V. Abdalsayed, M.S. El-Shall, Top. Catal. 47 (2008) 22.

[254] N. Perkas, Z. Zhong, J. Grinblat, A. Gedanken, Catal. Lett. 120 (2008) 19.

[255] M. Haruta, Chem. Record. 3 (2003) 75.

[256] L. Guczi, A. Beck, A. Horvath, Z. Koppany, G. Stefler, K. Frey, I. Sajo, O. Geszti, D. Bazin, J. Lynch, J. Mol. Catal. A: Chem. 204 (2004) 545.

[257] S. Pröckl, W. Kleist, M.A. Gruber, K. Köhler, Angew. Chem. Int. Ed. 43 (2004) 1881.

[258] S. Senkan, M. Kahn, S. Duan, A. Ly, C. Ledholm, Catal. Today 117 (2006) 291.

[259] K. Mori, T. Hara, T. Mizugaki, K. Ebitani, K. Kaneda, J. Am. Chem. Soc. 126 (2004) 10657.

[260] X. Yang, X. Zhang, Y. Ma, Y. Huang, Y. Wang, Y. Chen, J. Chem. Mater. 19 (2009) 2710.

[261] Y. Si, E.T. Samulski, Chem. Mater. 20 (2008) 6792.

[262] P. Pfeifer, K. Schubert, M.A. Liauw, G. Emig, Appl. Catal. A 270 (2004) 165.

[263] N. Panziera, P. Pertici, L. Barazzone, A.M. Caporusso, G. Vitulli, P. Salvadori, S. Borsacchi, M. Geppi, C.A. Veracini, G. Martra, L. Bertinetti, J. Catal. 246 (2007) 351.

[264] D. Astruc, F. Lu, J.R. Aranzaes, Angew. Chem. Int. Ed. 44 (2005) 7852.

[265] K. Grytsenko, Y. Kolomzarov, O. Lytvyn, V. Strelchuk, V. Ksianzou, S. Schrader, H. Beyer, B. Servet, S. Enouz-Vedrenne, G. Garry, R.D. Schulze, J. Friedrich, Adv. Sci. Lett. 3 (2010) 308.

[266] Z. Jia, Y. Yang, B. Fan, Appl. Mechanics Mater. 29-32 (2010) 395.

[267] M.S. Korobov, G.Yu. Yurkov, A.V. Kozinkin, Yu.A. Koksharov, I.V. Pirog, S.V. Zubkov, V.V. Kitaev, D.A. Sarychev, V.M. Buznik, A.K. Tsvetnikov, S.P. Gubin, Inorg. Mater. 40 (2004) 31.

[268] T. Zeng, W.-W. Chen, C.M. Cirtiu, A. Moores, G. Song, C.-J. Li, Green Chem. 12 (2010) 570.

[269] M. Rossier, F.M. Koehler, E.K. Athanassiou, R.N. Grass, B. Aeschlimann, D. Güntherm, W.J. Stark, J. Mater. Chem. 19 (2009) 8239.

[270] D. Guin, B. Baruwati, S.V. Manorama, Org. Lett. 9 (2007) 1419.

[271] J.M. Praetorius, C.M. Crudden, Dalton Trans. (2008) 4079.

[272] G. Ertl, H. Knözinger, J. Weitkamp in: Handbook of Heterogenous Catalysis, Wiley-VCH, Weinheim, Vol. 9, 2008.

[273] A. Nowicki, V. Le Boulaire, A. Roucoux, Adv. Synth. Catal. 349 (2007) 2326.

[274] Y. Motoyama, M. Takasaki, S.-H. Yoon, I. Mochida, H. Nagashami, Org. Lett. 11 (2009) 5042.

[275] F. Lu, J. Liu, J. Xu, J. Mol. Catal. A: Chem. 271 (2007) 6.

[276] L. Durán Pachón, G. Rothenberg, Appl. Organometal. Chem. 22 (2008) 288.

[277] W.S. Hummers, R.E. Offeman, J. Am. Chem. Soc. 80 (1958) 1339.

[278] Z. Li, W. Zhang, Y. Luo, J. Yang , J.G. Hou, J. Am. Chem. Soc. 131 (2009) 6320.

[279] H. Brunner in: B. Cornils, W.A. Herrmann (editors), Applied Homogeneous catalysis with organometallic compounds, Wiley-VCH, Weinheim, vol. 1, 2000, 209.

[280] G.W. Parshall, S.D. Ittel, Homogeneous catalysis, Wiley-VCH, New York, 1992.

[281] M.G. Clerici, M. Ricci, G. Strukul in: G.P. Chiusoli, P.M. Maitlis (editors), Metal-catalysis in industrial organic processes, RSC Publishing, Cambridge, 2006, 28.

[282] H.-G. Elias, Makromoleküle, Wiley-VCH, Weinheim, 2000, vol. 3, 155.

[283] A. Behr, Angewandte homogene Katalyse, Wiley-VCH, Weinheim, 2008, 408.

[284] S. Miao, Z. Liu, Z. Zhang, B. Han, Z. Miao, K. Ding, G. An, Phys. Chem. C 111 (2007) 2185.

[285] Y. Lin, R.G. Finke Inorg. Chem. 33 (1994) 4891.

[286] B.J. Hornstein, J.D. Aikon III, R.G. Finke, Inorg. Chem. 41 (2002) 1625.

[287] J.A. Widegren, M.A. Bennett, R.G. Finke, J. Am. Chem. Soc. 125 (2002) 10301.

[288] H. Hachenberg, K. Beringer, Die Headspace-Gaschromatographie als Analysen- und Meßmethode, Vieweg, Braunschweig/Wiesbaden, Germany, 1996, 32.

[289] K.J. Klabunde, G. Cárdenas-Trivino in: A. Fürstner, Active Metals: Preparation, Characterization, Applications, VCH-Wiley, Weinheim, 1996, 247, 263, 264.

[290] G. Cárdenas, S. Salinas, R. Oliva, Colloid Polym Sci. 282 (2003) 41; G. Cárdenas, R. Segura, J. Morales, H. Soto, C.A. Lima, Mater. Res. Bull. (35) 2000 1251; K. Cheng, Q. Chen, Z. Wu, M. Wang, H. Wang, CrystEngComm 13 (2011) 5394.

[291] B.N. Khlebtsov, N.G.Khlebtsov, Colloid J. 73 (2011)118.

[292] R. Pecora, Dynamic Light Scattering. Applications of Photon Correlation Spectroscopy, Plenum, New York-London, 1985.

[293] A.F. Hollemann, N. Wiberg, Lehrbuch der anorganischen Chemie, 33 ed, de Gruyter, Berlin, 1985, 1159.

9 ATTACHEMENT

This cumulative dissertation is based on the following published, accepted or submitted publications (in the reverse chronological order) which are attached:

4. *"Organic carbonates as stabilizing solvents for transition metal nanoparticles"*
Christian Vollmer, Ralf Thomann, Christoph Janiak, manuscript submitted to Dalton Transactions

3. *"Turning Teflon-coated magnetic stirring bars to catalyst systems with metal nanoparticle trace deposits - A caveat and a chance"*
Christian Vollmer, Marcel Schröder, Yi Thomann, Ralf Thomann, Christoph Janiak, Appl. Cat. A: Gen. 425-426 (2012) 178-183.

2. *"Naked metal nanoparticles from metal carbonyls in ionic liquids: Easy synthesis and stabilization"*
Christian Vollmer, Christoph Janiak, Coord. Chem. Rev. 255 (2011) 2039-2057.

1. *"The use of microwave irradiation for the easy synthesis of graphene-supported transition metal nanoparticles in ionic liquids"*
Dorothea Marquardt, Christian Vollmer, Ralf Thomann, Peter Steurer, Rolf Mülhaupt, Engelbert Redel, Christoph Janiak, Carbon 49 (2011) 1326-1332.

Journal Name

Dynamic Article Links ►

Cite this: DOI: 10.1039/c0xx00000x

www.rsc.org/xxxxxx

ARTICLE TYPE

Organic carbonates as stabilizing solvents for transition-metal nanoparticles†

Christian Vollmer,[a] Ralf Thomann[b] and Christoph Janiak*[a]

Received (in XXX, XXX) Xth XXXXXXXXX 20XX, Accepted Xth XXXXXXXXX 20XX
DOI: 10.1039/b000000x

Biodegradable, non-toxic, "green" and inexpensive propylene carbonate (PC) solvent is shown to function as a stabilizing medium for the synthesis of weakly-coordinated transition-metal nanoparticles. Kinetically stable nanoparticles (M-NPs) with a small and uniform particle size (typically < 5±1 nm) have been reproducibly obtained by easy, rapid (3 min) and energy-saving 50 W microwave irradiation under an argon atmosphere from their metal–carbonyl precursors in PC. The M-NP/PC dispersions are stable for up to three weeks according to repeated TEM studies over this time period. The rhodium nanoparticle/PC dispersion is a highly active and easily recyclable catalyst for the biphasic liquid–liquid hydrogenation of cyclohexene to cyclohexane with activities of up to and 1875 (mol product)□(mol Rh)$^{-1}$□h^{-1} and near quantitative conversion at 4 to 10 bar H_2 and 90□°C. From the PC dispersion the M-NPs can be coated with organic capping ligands such as 3-mercaptopropionic acid or trioctylphosphine oxide for further stabilization.

Introduction

Organic carbonates, such as dimethyl carbonate, diethyl carbonate, ethylene carbonate or propylene carbonate (PC) (Fig. 1) are polar solvents which are available in large amounts and at low prices, have a large liquid temperature range (for PC mp. -49 °C, bp. 243 °C), are of only low (eco)toxicity and are completely biodegradable.[1] Propylene carbonate (PC) is an aprotic, highly dipolar solvent, which has a low viscosity[2,3] and is considered a *green* solvent because of its low flammability, volatility and toxicity.[4]

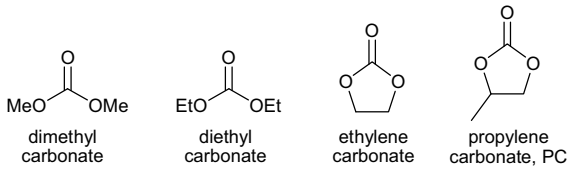

Fig. 1 Selected organic carbonates

Organic carbonates are recognized as solvents in industrial applications such as cleaning, degreasing, paint stripping, gas treating, and textile dyeing.[5] Yet, so far organic carbonates are used primarily for extractive applications and as solvents in electrochemistry.[1] PC is used as a solubilizer and co-solvent in cosmetics,[6] in the FLUOR process for the removal of carbon dioxide from natural gas streams in the oil industry,[7] in lacquer[8] and BASF is using PC for waste removal in the copper wire-coating process.[9] PC is also investigated for Li-ion battery research.[10,11]

Here we show that PC can function as a solvent for metal nanoparticle synthesis and stabilization without the need for additional capping ligands. Metal nanoparticles (M-NPs) are of significant interest for technological applications in several areas of science and industry, especially in catalysis due to their high activity.[12,13,14,15] The controlled and reproducible synthesis of defined and stable M-NPs with a small size distribution is important.[16,17,18,19,20] Very small M-NPs tend to aggregate because of their high surface energy and large surface area. To avoid this agglomeration, M-NPs need to be stabilized either by organic donor ligands,[21,22,23,24] ionic liquids[15,25,26,27,] or by deposition on solid supports.[28,29,30]

Reports on metal nanoparticles in organic carbonates are rare and appear to be of accidental coincidence for Pd-NPs.[31,32,33,34] Here we demonstrate that PC can generally stabilize small M-NPs (<5 nm).

Results and discussion

M-NP synthesis and characterization

The metal carbonyl $Mo(CO)_6$, $W(CO)_6$, $Re_2(CO)_{10}$, $Fe_2(CO)_9$, $Ru_3(CO)_{12}$, $Os_3(CO)_{12}$, $Co_2(CO)_8$, $Rh_6(CO)_{16}$ or $Ir_6(CO)_{16}$ was dissolved/ suspended under an argon atmosphere in dried and deoxygenated propylene carbonate (PC). Complete decomposition by microwave irradiation of the metal carbonyl in PC was achieved after only 3 minutes using a low power of 50 W under argon (Fig. 2).

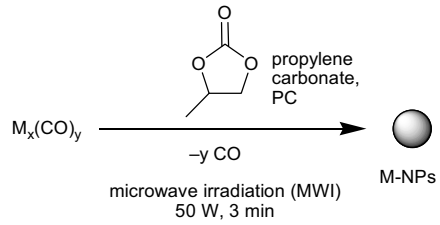

Fig. 2 Microwave decomposition of metal carbonyls to M-NPs in PC.

The resulting orange-red Os-, yellow Mn- and W-, and dark-brown to black Mo-, Re-, Ru-, Co-, Rh- and Ir-NP dispersions were reproducibly obtained through the microwave decomposition route. Complete $M_x(CO)_y$ decomposition from short, 5 min microwave irradiation was verified by Raman spectroscopy with no (metal–)carbonyl bands between 1800 and 2000 cm^{-1} being observed any more after the microwave treatment (Fig. 3).

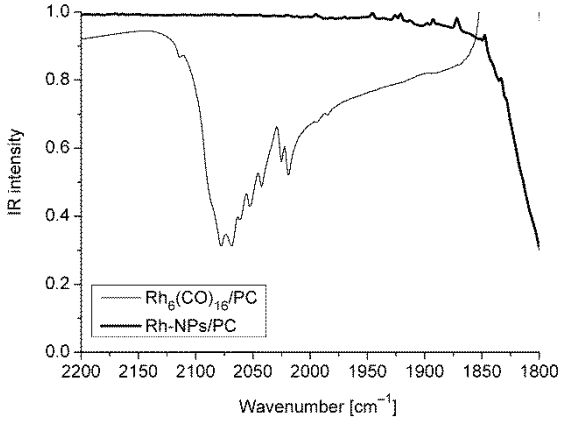

Fig. 3 IR-spectra of $Rh_6(CO)_{16}$/PC (light curve) and the resulting Rh-NP (0.5 wt.%)/PC-dispersion (bold curve) after microwave treatment (50 W, 3 min).

The resulting M-NPs were analyzed by transmission electron microscopy (TEM; Figures 4-6), selected area electron diffraction (SAED), and dynamic light scattering (DLS) for their size and size distribution (Table 1). SAED patterns do not show reflections indicative of a crystalline material. We therefore conclude that the particles obtained from the synthesis are amorphous M-NPs stabilized by PC. Still the diffraction rings match the known d-spacing of the respective metal diffraction pattern (see Tables S3-S5 in ESI†).

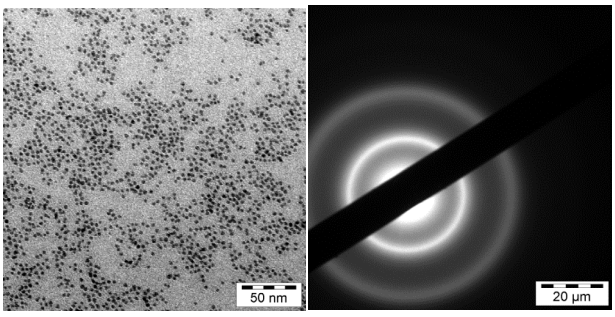

Fig. 4 TEM (left) and SAED (right) of Ru-NPs in PC from $Ru_3(CO)_{12}$ (entry 5 in Table 1). The black bar is the beam stopper. The diffraction rings at (Å) 2.10 (very strong), 1.61, 1.26, 1.15 (all weak) match with the d-spacing of the Ru-metal diffraction pattern (see Table S3).

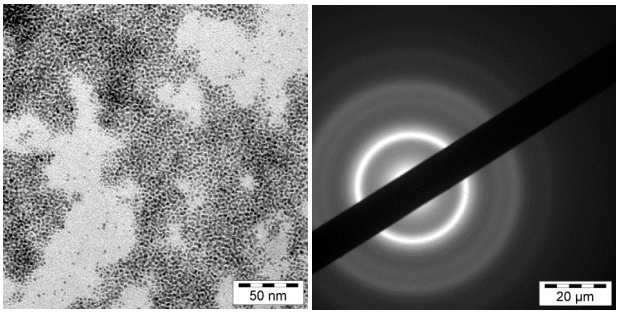

Fig. 5 TEM (left) and SAED (right) of Rh-NPs in PC from $Rh_6(CO)_{16}$ (entry 8 in Table 1). The black bar is the beam stopper. Diffraction rings at (Å) 2.23 (very strong), 1.94 (strong), 1.39, 1.17 and 0.89 (weak) match the d-spacing of the Rh-metal diffraction pattern (see Table S4).

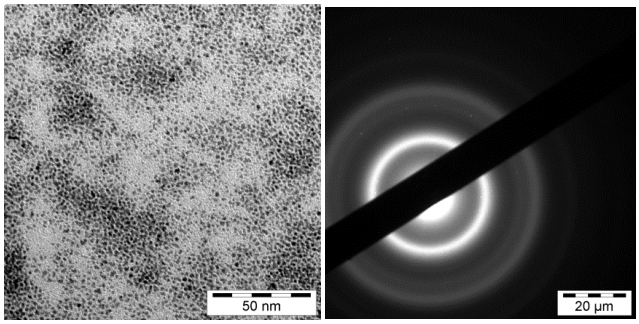

Fig. 6 TEM (left) and TED (right) of Ir-NPs in PC from $Ir_6(CO)_{16}$ (entry 9 in Table 1). The black bar is the beam stopper. The diffraction rings at (Å) 2.25 (strong), 1.38, 1.20 (weak) match with the d-spacing of the Ir-metal diffraction pattern (see Table S5).

The hydrodynamic radius from DLS is roughly two to three times the size of the pure kernel cluster. For very small M-NPs (<1 nm) the size of the hydrodynamic radius was measured to be more than three times the radius found from TEM. The median M-NP diameter for the microwave-synthesized Mo-, W-, Re-, Ru-, Os-, Rh- and Ir-NPs was between <1 and 3.0 nm, with a narrow size distribution (TEM data in Table 1). No extra stabilizers or capping molecules are needed to achieve this small particle size. It is, at present, not trivial to routinely and easily prepare uniform nanoparticles in the size range between <1-3 nm without strong capping ligands. For the magnetic Fe-NPs and Co-NPs the median diameter was somewhat larger with 2.4 and 6.1 nm, respectively. The M-NP/PC dispersions are stable up to three weeks according to repeated TEM measurements over this time period.

Table 1 M-NP size and size distribution in PC.[a]

Entry	Metal carbonyl	TEM Ø (σ) [nm][b]	DLS Ø (σ) [nm][b]
1	$Mo(CO)_6$	2.2 (± 0.5)	3.5 (± 1.1)
2	$W(CO)_6$	2.9 (± 0.6)	3.7 (± 1.4)
3	$Re_2(CO)_{10}$	< 1	1.4 (± 0.5)
4	$Fe_2(CO)_9$	2.4 (± 0.9)	3.2 (± 0.8)
5	$Ru_3(CO)_{12}$	2.7 (± 0.5)	2.6 (± 0.8)
6	$Os_3(CO)_{12}$	3.0 (± 1.5)	4.0 (± 1.2)
7	$Co_2(CO)_8$	6.1 (± 7.4)	6.7 (± 2.2)
8	$Rh_6(CO)_{16}$	2.1 (± 0.6)	2.4 (± 0.8)
9	$Ir_6(CO)_{16}$	1.3 (± 0.5)	6.0 (± 1.6)

[a] 0.5 wt.□% M-NP/PC dispersions obtained by MWI with 50 W for 3 min. [b] Median diameter (Ø) and standard deviation (σ). See experimental section for TEM and DLS measurement conditions.

Hydrogenation of cyclohexene and 1-hexyne

Organic carbonates have recently been used as solvents in catalysis, e.g., for platinum-catalyzed hydrosilylation of unsaturated fatty acid esters[35] in Pd-catalyzed substitution reactions,[36] regioselective rhodium-catalyzed hydroformylation[37] and in the asymmetric iridium-catalyzed hydrogenation of olefins.[2,38] Palladium collids in PC were used to hydrogenate dienes and alkynes[31,32] and for Heck-reactions.[33] The weak interactions between a nanoparticle and organic carbonates could be of interest to develop more efficient catalyst processes.

Here we tested the Rh-NP/PC dispersions for their catalytic activity in the biphasic liquid–liquid hydrogenation of cyclohexene to cyclohexane (Fig. 7, Table 2). The low miscibility of substrates and products with the PC phase allows for easy separation by simple decantation of the hydrophobic phase. Cyclohexene was chosen as a substrate since it presents a challenge because of its low solubility in PC and is an intermediate in the hydrogenation of benzene to cyclohexane.[39,40]

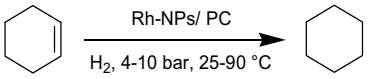

Fig. 7 Hydrogenation of cyclohexene to cyclohexane with Rh-NPs.

Table 2 Hydrogenation of Rh-NPs/PC with different substrates.[a]

Entry	Substrate	t [min]	p_{H2} [bar]	T [°C]	Conversion [%]	activity [mol product x (mol Rh)$^{-1}$ x h^{-1}]
1	cyclohexene	108	4	75	95 [c]	590
2	cyclohexene	34	4	90	95 [c]	1875
3	cyclohexene	61	10	25	95 [c]	1045
4	1-hexyne [b]	104	10	25	88	51
5	cyclohexene [d]	1440 (=24h)	4	90	0	0

[a] 10 mL (0.1 mol) cyclohexene or 1.0 mL (1.8 mmol) 1-hexyne; 0.75 mL of the Rh-NP/PC dispersion with 1 wt.% Rh (9 mg, 8.8×10^{-5} mol Rh). [b] 1 mL n-decane was added to provide a biphasic liquid-liquid catalytic system. No n-hexene detected by GC analysis see experimental section. [c] The reaction was intentionally stopped at 95 or 88% conversion as thereafter the decrease in cyclohexene concentration lowered the reaction rate (see Fig. S5 in ESI†). [d] Hydrogenation was carried out with Rh/SR-NPs (see Table 3, entry 3).

For activity comparison Table S6 and S7 in ESI† summarize related hydrogenation activities for cyclohexene and 1-hexyne with M-NPs in ILs and on supports from the literature. Activities for cyclohexene hydrogenations with Rh-NPs/PC were twice as good than for Ru- or Rh-NP catalysts in ILs[26,41,42,] but not as good as for Rh-NPs on supports[30,43,44,45] (Table S5 in ESI†). The lower hydrogenation activities of Ru- and Rh-NPs in ILs are traced to the IL diffusion barrier for H_2 and the substrate. Whereas ligand-free NPs on supports have a lower diffusion barrier.

Rh- and Ru-NPs surface capping

The addition of an organic ligand to the bare M-NP surface is generally described as a surface functionalization. However derivatization, coating, or capping are better terms.[46] The post synthetic introduction of an organic capping ligand on the dispersed M-NPs in PC is possible. Surface capping of Rh- or Ru-nanoparticles dispersed in the propylene carbonate was carried out here with 3-mercaptopropionic acid, HS-$(CH_2)_2$-COOH or trioctylphosphine oxide (TOPO). Both 3-mercaptopropionic acid[46] and TOPO[47,48] are well-known stabilizing reagents and both are soluble in propylene carbonate. The transformation of M-NP/PC to M-NP/HS-$(CH_2)_2$-COOH or M-NP/TOPO was done by treating the M-NP/PC dispersion with an excess of HS-$(CH_2)_2$-COOH or TOPO at room temperature over night. The strong affinity between the thiol (-SH) or phospine oxide (-P=O) group and the rhodium or ruthenium nanoparticles replaces the PC protective layer. The ligand-capped nanoparticles are significantly larger (Table 3, Fig. 8, Fig. 9, see Fig. S1-S4 in ESI† for additional TEM pictures).

The use of a protic organic thiol ligand and the unpolar TOPO ligand more than doubles the size of the resulting capped metal nanoparticles (Table 3). The aggregation is a result of the introduction of the capping ligands into the polar PC network. Subsequently the stabilizing property of propylene carbonate towards the M-NPs is weakened and results in further M-NP agglomeration which is driven by the surface-surface interactions.

Table 3 Ligand capped M-NP size and size distribution.

Entry	Metal	Ligand	M-NP/PC original size from TEM [nm]	M-NP/ligand in PC TEM Ø (σ) [nm][a]	M-NP/ligand in PC DLS Ø (σ) [nm] [a,b]
1	Rh	HS-$(CH_2)_2$-COOH	2.1 (± 0.6)	9 (±5)	24 (± 17) [c]
2	Rh	TOPO		10 (±5)	30 (± 14) [d]
3	Ru	HS-$(CH_2)_2$-COOH	2.7 (± 0.5)	13 (±4)	6.0 (± 1.5) [c]
4	Ru	TOPO		13 (± 5)	37 (± 12) [d]

[a] Median diameter (Ø) and standard deviation (σ). See experimental section for TEM and DLS measurement conditions. [b] Hydrodynamic radius, median diameter from the measurements at 633 nm. The resolution of the DLS instrument is 0.6 nm. [c] measurement performed in ethanol. [d] measurement performed in chloroform.

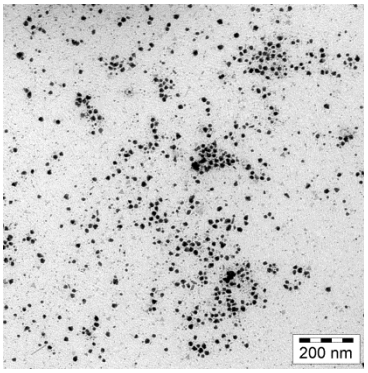

Fig. 8 TEM of Rh-NP/HS-$(CH_2)_2$-COOH from propylene carbonate after thiolation with 3-mercaptopropionic acid, centrifugation and re-dispersion in ethanol.

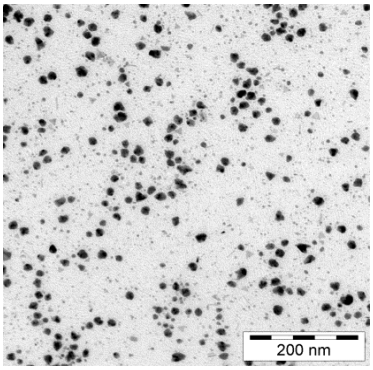

Fig. 9 TEM of Rh-NP/TOPO from propylene carbonate after stabilization with TOPO, centrifugation and re-dispersion in chloroform.

Conclusion

We describe here a simple, reproducible, and broadly applicable microwave-induced metal carbonyl decomposition for the synthesis of common transition-metal nanoparticles in propylene carbonate, PC. The M-NP sizes of about 1 to 3 nm for most of these transition-metal nanoparticles are very small and uniform with no extra stabilizers or capping molecules needed to achieve this small particle size in a stable M-NP/PC dispersion. Polar organic carbonates are susceptible for microwave irradiation which, thus, provides a very simple and reproducible way for the rapid (3 min) and energy-saving (50 W power) synthesis of defined and very small M-NPs from their binary metal–carbonyl complexes in PC. The obtained Rh-NP/PC dispersions can be used - without further treatment - as highly active hydrogenation catalysts. In comparison to ionic liquids, PC and other organic carbonates are established industrial and low-priced solvents.[4] PC appears as an attractive alternative for weakly coordinated, albeit sufficiently stabilized metal nanoparticles.

Acknowledgement. Financial support through DFG grant Ja466/17-1 is gratefully acknowledged.

Experimental section

Materials and instrumentation for M-NP synthesis: $Mo(CO)_6$, $W(CO)_6$, $Re_2(CO)_{10}$, $Fe_2(CO)_9$, $Ru_3(CO)_{12}$, $Os_3(CO)_{12}$, $Co_2(CO)_8$, $Rh_6(CO)_{16}$, and $Ir_6(CO)_{16}$ were obtained from Strem and Aldrich, racemic propylene carbonate (PC) from Sigma-Aldrich (purity 99.7 %, H_2O free). Cyclohexene (> 99%), 1-hexyne (> 97%), 3-mercaptopropionic acid (> 99%), *n*-decane (p.A., purity >99.5□%) and trioctylphosphine oxide (99%) were obtained from Sigma–Aldrich and used without further purification. All synthesis experiments were carried out with Schlenk techniques under argon since the metal carbonyls are hygroscopic and air sensitive. The PC was dried under high vacuum (10^{-3} mbar) for several days.

FT-IR (Fourier transform infrared) measurements were carried out on a Bruker TENSOR 37 IR spectrometer in a range from 4000 to 500 cm^{-1} in a KBr cuvette (thickness 0.05mm).

Transmission electron microscopy (TEM) photographs were taken at room temperature on a *Zeiss LEO* 912 TEM operating at an accelerating voltage of 120 kV. Samples were deposited on 200 µm carbon-coated copper grids.

A Malvern Zetasizer Nano-ZS was used for the *dynamic light scattering (DLS) measurements* working at 633 nm wavelength. Care was taken for choosing the right parameters, such as the index of refraction of the transition metals at their wavelength (Table S2). Samples were prepared by dissolution of 0.05 or 0.1 ml of a 0.5 wt.% of the metal dispersion in acetone (99% p.a.; particle free) in a glass cuvette before measurement. Acetone is also capable of stabilizing nanostructured metal clusters.[49,50]

Metal nanoparticle (M-NP) synthesis: Decomposition by means of microwave irradiation was carried out under argon. In a typical reaction, the fine metal carbonyl powder $M_x(CO)_y$ (M = Mo, W, Re, Fe, Ru, Os, Co, Rh, Ir; 19.8 to 9.8 mg, respectively; see Table S1 in ESI†) was dissolved/suspended (≈ 1 h) under an argon atmosphere at room temperature in dried and deoxygenated PC (density: 1.19 g/mL, 1 mL, 1.19 g) for a 0.5 wt.□% M-NP/PC dispersion. For the synthesis of a 1 wt□% M/PC dispersion the metal carbonyl $M_x(CO)_y$ (M = Rh; 16.6 mg) was suspended/dissolved (≈ 1 h) under an argon atmosphere at room temperature in dried and deoxygenated PC (1.5 mL, 1.8 g). For the synthesis, the mixture was placed in a microwave (CEM, Discover) under an inert argon atmosphere and the conversion was finished within 3 min at a power of 50 W. For the 1 wt.% dispersions a time of 5 min and a power of 50 W were chosen. Each decomposition reaction was carried out at least twice. Decomposition reactions to produce the Rh-NPs that were used in the catalysis in this work were carried out ten or more times.

Catalysis: The hydrogenation reactions with Rh-NPs/PC were carried out in stainless steel autoclaves connected with an online hydrogenation-consumption monitoring system (Büchi pressflow gas controller, bpc). The autoclave was conditioned by evacuation and re-filling with nitrogen. All autoclave loading was carried out under nitrogen. Each autoclave was equipped with a glass inlay, to eliminate any catalytic influence of the stainless steel surface on the reaction process. A typical experiment used 0.75 mL of the Rh-NP/PC dispersion with 1 wt.% Rh (9 mg, 8.8×10^{-5} mol Rh) and 10 mL of cyclohexene (0.1 mol, density 0.811 g/ml, M = 82.14 g/mol,) or 1.0 mL of 1-hexyne (1.8 mmol, density 0.72 g/ml, M = 82.14 g/mol). The autoclave was heated to the desired temperature and set to the desired pressure of H_2 which was kept constant over the reaction time. After this time the reactor was depressurized, and the volatile organic components condensed under vacuum (15 min) into a clean cold trap (liquid nitrogen cooled). The Rh-NP/PC dispersion was left behind. The conversions were investigated by gas chromatography using a Perkin Elmer headspace GC HS6 with a DB 5 column (60 m × 0.32 mm film thickness 25 µm) oven temperature 40 °C, N_2 carrier flow 120 L/min) and a flame ionization detector (FID, 250 °C detector temperature). The conversion was analyzed by adding a drop of the mixture into a GC sample vial with 1 ml of water. The addition of water as a non-electrolyte can enlarge the activity coefficient of organic components, thereby increase their detection sensitivity through the increase in peak area. The FID does not detect the water itself.[51]

Preparation of ligand-capped M-NP in PC: The obtained Rh- and Ru-NPs/PC (0.4 ml, 0.5 wt.%) were stirred with 3-mercaptopropionic acid (2 mL, 3.5×10^{-5} mol) or TOPO (14 mg, 3.5×10^{-5} mol) over night. The ligand-capped M-NPs were collected by centrifugation (2000 rpm, 15 min) and decantation of the clear propylene carbonate phase. The capped M-NPs were

dried for several days under high vacuum to remove the PC solvent.

Notes and references

[a] *Institut für Anorganische Chemie und Strukturchemie, Heinrich-Heine-Universität Düsseldorf 1, D-40204 Düsseldorf, Germany. Fax: +49 211 81 12287; Tel: + 49 211 81 12286; E-mail: janiak@uni-duesseldorf.de*
[b] *Freiburger Material Forschungszentrum (FMF) and Institut für Makromolekulare Chemie, Universität Freiburg, Stefan-Meier-Str. 21-31, 79104 Germany. Tel: +49 761 2035379; E-mail: ralf.thomann@fmf.uni-freiburg.de*

† Electronic Supplementary Information (ESI) available: additional TEMs, DLS and SAED parameters, catalytic activity with comparative activity data from literature. See DOI: 10.1039/b000000x/

1 B. Schäffner, F. Schäffner, S. P. Verevkin and A. Börner, *Chem. Rev.*, 2010, **110**, 4554-4581.
2 J. Bayardon, J. Holz, B. Schäffner, V. Andrushko, S. Verevkin, A. Preetz and A. Börner, *Angew. Chem. Int. Ed*. 2007, **46**, 5971-5974.
3 S. P. Verevkin, V. N. Emel'yanenko, A. V. Toktonov, Y. Chernyak, B. Schäffner and A. Börner, *J. Chem. Thermodynamics* 2008, **40**, 1428-1432.
4 B. Schäffner, S. P. Verevkin and A. Börner, *Chem. Unserer Zeit*, 2009, **43**, 12-21.
5 J. H. Clements, *J. Ind. Eng. Chem. Res.*, 2003, **42**, 663-674.
6 A. Ansmann, B. Boutty and M. Dierker, *Chem. Abstr.* 2008, **149**, 17219.
7 A. L. Kohl and P. A. Buckingham, *Oil Gas J*., 1960, **58**, 146.
8 J. Xia, M. E. Ragsdale and E. B. Stephens, *Chem. Abstr.*, 2001, **136**, 38897.
9 S. Schmidt, *Chem. Abstr.*, 2004, **142**, 375279.
10 R. Jasinski, *J. Electroanal. Chem*., 1967, **15**, 89-91.
11 K. K. D. Ehinon, S. Naille, R. Dedryvère, P.-E. Lippens, J.-C. Jumas and D. Gonbeau, *Chem. Mater.*, 2008, **20**, 5388-5398.
12 V. I. Pârvulescu and C. Hardacre, *Chem. Rev.*, 2007, **107**, 2615-2665.
13 A. Seyed-Razavi, I. K. Snook and A. S. Barnard, *J. Mater. Chem.*, 2010, **20**, 416-421;
14 Y. Teow, P. V. Asharani, M. P. Hande and S. Valiyaveettil, *Chem. Comm.*, 2011, **47**, 7025-7038.
15 J. Dupont and J. D. Scholten, *Chem. Soc. Rev*., 2010, **39**, 1780-1804.
16 A.-H. Lu, E. L. Salabas and F. Schüth, *Angew. Chem. Int. Ed.*, 2007, **46**, 1222-1244.
17 A. Gedanken, *Ultrasonics Sonochem.,* 2004, **11**, 47-55.
18 C. N. R. Rao, S.R.C. Vivekchand, K. Biswas and A. Govindaraj, *Dalton Trans.*, 2007, 3728-3749.
19 Y. Mastai, A. Gedanken, in: C. N. R. Rao, A. Müller, A. K. Cheetham (Eds.), Chemistry of Nanomaterials, vol. 1, Wiley-VCH, Weinheim, 2004, p. 113.
20 J. Park, J. Joo, S. G. Kwon, Y. Jang and T. Hyeon, *Angew. Chem. Int. Ed*., 2007, **46**, 4630-4660.
21 L. D. Pachón and G. Rothenberg, *Appl. Organometal. Chem.* 2008, **22**, 288-299.
22 P. Graf, A. Mantion, A. Foelske, A. Shkilnyy, A. Măsić, A. F. Thünemann and A. Taubert, *Chem. Eur. J.*, 2009, **15**, 5831-5844.
23 G. Salas, C. C. Santini, K. Philippot, V. Collière, B. Chaudret, B. Fenet and P. F. Fazzini, *Dalton Trans*., 2011, **40**, 4660-4668.
24 C. Pan, K. Pelzer, K. Philippot, B. Chaudret, F. Dassenoy, P. Lecante and M.-J. Casanove, *J. Am. Chem. Soc*., 2011, **123**, 7584-7593.
25 A. Taubert and Z. Li, *Dalton Trans.*, 2007, 723-727; E. Redel, R. Thomann and C. Janiak, *Inorg. Chem.*, 2008, **47**, 14-16; E. Redel, R. Thomann and C. Janiak, *Chem. Commun.*, 2008 1789-1791; E. Redel, J. Krämer, R. Thomann and C. Janiak, *J. Organomet. Chem.*, 2009, **694**, 1069-1075; E. Redel, M. Walter, R. Thomann, L. Hussein, M. Krüger and C. Janiak, *Chem. Commun.*, 2010, **46**, 1159-1161.
26 C. Vollmer, E. Redel, K. Abu-Shandi, R. Thomann, H. Manyar, C. Hardacre and C. Janiak, *Chem. Eur. J*., 2010, **16**, 3849-3858.
27 C. Vollmer and C. Janiak, *Coord. Chem. Rev*., 2011, **255**, 2039-2057.
28 R. J. White, R. Luque, V. L. Budarin, J. H. Clark and D. J. Macquarrie, *Chem. Soc. Rev.*, 2009, **38**, 481-494.
29 B. Inceesungvorn, J. López-Castro, J. J. Calvino, S. Bernal, F. C. Meunier, C. Hardacre, K. Griffin and J. J. Delgado, *Appl. Catal. A*, 2011, **391**, 187-193.
30 D. Marquardt, C. Vollmer, R. Thomann, P. Steurer, R. Mülhaupt, E. Redel and C. Janiak, *Carbon*, 2011, **49**, 1326-1332.
31 A. Behr and H. Schmidke, *Chem.-Ing.-Tech.*, 1993, **65**, 568-569.
32 A. Behr, N. Döring, Susanne Durowicz-Heil, B. Ellenberg, C. Kozik, C. Lohr and H. Schmidke, *Fat Sci. Technol.*, 1993, **95**, 2-12.
33 M. Reetz and G. Lohmer, *Chem. Commun.*, 1996, 1921-1922.
34 J. Demel, J. Čejka, S. Bakardjieva and P. Štěpnička, *J. Mol. Catal. A: Chem.*, 2007, **263**, 259-265.
35 A. Behr, F. Naendrup and D. Obst, *Adv. Synth. Catal.*, 2002, 344, 1142-1145.
36 B. Schäffner, J. Holz, S. P. Verevkin and A. Börner, *ChemSusChem*, 2008, **1**, 249-253.
37 A. Behr, D. Obst and B. Turkowski, *J. Mol. Catal. A: Chem.*, 2005, **226**, 215-219.
38 B. Schäffner, V. Andrushko, J. Bayardon, J. Holz and A. Börner, *Chirality*, 2009, **21**, 857-861.
39 H.-E. Elias in *Makromoleküle*, Vol. 3, Wiley-VCH, Weinheim, 2001, pp. 368-454.
40 B. K. Hodnett in *Heterogeneous Catalytic Oxidations,* Wiley-VCH, Weinheim. 2000, pp. 240-263.
41 E. T. Silveira, A. P. Umpierre, L. M. Rossi, G. Machado, J. Morais, I. L. R. Baumvol, S. R. Teixeira, P. F. P. Fichtner and J. Dupont, *Chem. Eur. J.*, 2004, **10**, 3734-3740.
42 L. M. Rossi, G. Machado, P. F. P. Fichtner and S. R. Teixeira, J. Dupont, *Catal. Lett.*, 2004, **92**, 149-155.
43 S. Miao, Z. Liu, Z. Zhang, B. Han, Z. Miao, K. Ding, G. An, *J. Phys. Chem. C*, 2007, **111**, 2185-2190.
44 M. J. Jacinto, P. K. Kiyohara, S. H. Masunaga, R. F. Jardim and L. M. Rossi, *Appl. Catal. A*, 2008, **338**, 52-57.
45 C. Vollmer, M. Schröder, Y. Thomann, R. Thomann, C. Janiak, *Appl. Catal. A*, 2012, in press. http://dx.doi.org/10.1016/j.apcata.2012.03.017
46 E. Redel, M. Walter, T. Thomann, C. Vollmer, L. Hussein, H. Scherer, M. Krüger, C. Janiak, *Chem. Eur. J.* 2009, **15**, 10047-10059.
47 C. Pan, K. Pelzer, K. Philippot, B. Chaudret, F. Dassenoy, P. Lecante and M.-J. Casanove, *J. Am Chem. Soc.*, 2001, **124**, 7584-7593.
48 T. Cassagneau, T. E. Mallouk and J. H. Fendler, *J. Am. Chem. Soc.*, 1998, **120**, 7848-7859.
49 K. J. Klabunde and G. Cárdenas-Trivino, in Active Metals: Preparation, Characterization, Applications, ed. A. Fürstner, VCH, Weinheim, 1996, pp. 247, 263, 264.
50 G. Cárdenas, S. Salinas and R. Oliva, *Colloid Polym Sci.*, 2003, **282**, 41-47; G. Cárdenas, R. Segura, J. Morales, H. Soto and C. A. Lima, *Mater. Res. Bull.*, 2000, **35**, 1251–1259; K. Cheng, Q. Chen, Z. Wu, M. Wang and H. Wang, *CrystEngComm*, 2011, **13**, 5394–5400
51 H. Hachenberg and K. Beringer, *Die Headspace-Gaschromatographie als Analysen- und Meßmethode,* Vieweg, Braunschweig/ Wiesbaden, Germany, 1996, pp. 32–35.

Applied Catalysis A: General 425–426 (2012) 178–183

Contents lists available at SciVerse ScienceDirect

Applied Catalysis A: General

journal homepage: www.elsevier.com/locate/apcata

Turning Teflon-coated magnetic stirring bars to catalyst systems with metal nanoparticle trace deposits – A caveat and a chance

Christian Vollmer[a], Marcel Schröder[a], Yi Thomann[b], Ralf Thomann[b], Christoph Janiak[a,*]

[a] Institut für Anorganische Chemie und Strukturchemie, Universität Düsseldorf, Universitätsstr. 1, D-40225 Düsseldorf, Germany
[b] Freiburger Material Forschungszentrum (FMF) and Institut für Makromolekulare Chemie, Universität Freiburg, Stefan-Meier-Str. 21-31, 79104 Freiburg, Germany

ARTICLE INFO

Article history:
Received 13 February 2012
Received in revised form 8 March 2012
Accepted 10 March 2012
Available online 19 March 2012

Keywords:
Metal nanoparticles
Rhodium
Teflon surface
Trace metal
Hydrogenation
Stirring bar

ABSTRACT

It could be an unintentional effect to deposit metal nanoparticles on a simple Teflon-coated magnetic stirring bar. Rhodium nanoparticles, as an example, were reproducibly deposited onto a standard, commercial Teflon-coated magnetic stirring bar by easy and rapid microwave-assisted decomposition of the metal carbonyl precursor $Rh_6(CO)_{16}$ in the ionic liquid 1-*n*-butyl-3-methyl-imidazolium tetrafluoroborate. Such metal nanoparticle deposits are not easy to remove from the Teflon surface by simple washing procedures and present active catalysts which one is not necessarily aware of. Barely visible metal-nanoparticle deposits on a stirring bar can act as trace metal impurities in catalytic reactions. As a proof-of-principle the rhodium-nanoparticle deposits of 32 μg or less Rh metal on a 20 mm × 6 mm magnetic stirring bar were shown to catalyze the hydrogenation reaction of neat cyclohexene or benzene to cyclohexane with quantitative conversion. Rhodium-nanoparticle-coated stirring bars were easily handable, separable and re-usable catalyst system for the heterogeneous hydrogenation with quantitative conversion and very high turnover frequencies of up to 32,800 mol cyclohexene × (mol Rh)$^{-1}$ × h^{-1} under organic-solvent-free conditions.

1. Introduction

It has recently become more evident that not every component which was originally claimed as catalyst turned out to be the actual active ingredient. In some prominent cases trace metal impurities were eventually proven as the actual catalytic species [1,2]. In an early example, traces of nickel compounds which formed unintentional during the cleaning of a V2A steal autoclave and remained in there changed the Ziegler–Aufbau reaction (reaction of $AlEt_3$ with ethylene at 100 °C under pressure to long-chain Al-alkyls) to a clean ethylene dimerization to yield butene. The cause of this unexpected dimerization was at first unknown and later termed the "nickel effect" after its origin had become clear. In addition, the nickel compounds had required traces of acetylene which were present in technical ethylene for stabilization of the nickel catalyst [3,4].

More recently, a Suzuki cross-coupling which was thought to have occurred metal-free was indeed promoted by ppb Pd traces in the Na_2CO_3 or K_2CO_3 bases used for the reaction [5]. Suggested iron-catalyzed cross-coupling reactions with different $FeCl_3$ sources were eventually corrected to ppm-scale copper impurities doing the catalysis [6]. Even with Pd in the ppb range it is possible to carry out a Sonogashira coupling with quantitative conversion [7].

On the other hand, metal traces or dopants are intentionally added to enhance or promote catalytic performance [8,9] or to assist catalyst regeneration [10].

Researchers in catalysis are aware that impurities left over from previous experiments in their (cleaned) vessels can give activating of desactivating effects which change the outcome of a catalytic reaction. Thus, catalytic reactions should be carried out more than once to ensure reproducibility. Surprisingly, a Scifinder search [11] combining the terms "memory effect", "contamination" or "impurity" and "catalysis" did not give any relevant references.

Here we show that a common and frequently used laboratory commodity such as a Teflon-coated magnetic stirring bar can carry on its surface catalytically active metal nanoparticles which are not easily removed. On one hand this is "caveat" on the unintentional preparation of "catalytically active stirring bars" by nanoparticular metal depositions from previous reactions. On the other hand our simple deposition of rhodium metal nanoparticles (Rh-NPs) on the Teflon surface of a stirring bar (Rh-NPs@stirring bar) yields an easily handable and re-usable hydrogenation catalyst. This proof-of-concept should be extendable to other metal nanoparticle catalysts. Rhodium was used here as a metal for the proof-of-principle because rhodium is used in many types of

* Corresponding author. Tel.: +49 211 81 12286; fax: +49 211 81 12287.
E-mail address: janiak@uni-duesseldorf.de (C. Janiak).

0926-860X/$ – see front matter © 2012 Elsevier B.V. All rights reserved.
doi:10.1016/j.apcata.2012.03.017

catalytic reactions like hydroformylations [12], C—C bond forming reactions [13], Pauson–Khand type reactions [14] and hydrogenations [15,16].

2. Experimental

2.1. Materials and methods

$Rh_6(CO)_{16}$ was obtained by Acros, the ionic liquid (IL) 1-*n*-butyl-3-methylimidazolium tetrafluoroborate ($BMImBF_4$) from IoLiTec (H_2O content $\ll$ 100 ppm; Cl^- content $\ll$ 50 ppm).

New stirring bars with the dimensions (length × width) 20 mm × 6 mm were obtained from VWR International GmbH, Hilperstraße 20a, 64295 Darmstadt, Germany and had not been used for any reactions before. Solvents were of technical quality (acetone) or of p.a. quality (acetone, methanol, *iso*-propanol, tetrahydrofuran (THF), methylene chloride).

All manipulations were done using Schlenk techniques under nitrogen since the metal carbonyls salts are hygroscopic and air sensitive. The ILs were dried at high vacuum (10^{-3} mbar) for several days.

AAS (atomic absorption spectrometry) was performed with Perkin-Elmer AAnalyst 100 (flame AAS), using the software AA WinLab.

Transmission electron microscopy (TEM) photographs were taken at room temperature from a carbon coated copper grid on a Zeiss LEO 912 transmission electron microscope operating at an accelerating voltage of 120 kV. Samples were loaded on holey, carbon coated copper grids. The Rh-NP samples were prepared by cutting Teflon flakes from the stirring bar. Median Rh-NP diameters of Rh-NPs@stirring bar were 2.1 (±0.5) nm. The Rh-NPs@stirring bar after 10 hydrogenation runs of cyclohexene had a size of 1.7 (±0.3) nm (cf. Fig. 2). Particle diameters were measured manually using iTEM software tools for manual measurements. Completely automatic measurements, which can be easily performed for well separated particles, fail in the case of heavily clustered particles. For a better comparison of the samples also particles which would have allowed automatic detection were measured manually.

Scanning electron microscopy (SEM) samples were coated with a thin Au layer (~8 nm) and analyzed with a Quanta 250 FEG instrument. The measurements were performed at 3.20^{-4} Pa and at 10 kV voltage using an ETD detector.

2.2. Preparation of Rh-NP/IL dispersion

$Rh_6(CO)_{16}$ (41.42 mg, 3.89×10^{-5} mol) was dissolved/suspended (~1 h) under a nitrogen atmosphere at room temperature in dried and deoxygenated $BMImBF_4$ (2.0 mL, 2.4 g) to give a 1.0 wt.% dispersion. For the synthesis the mixture was placed in a CEM microwave type Discover under inert nitrogen atmosphere and the conversion was finished within 6 min at a power of 10 W. $Rh_6(CO)_{16}$ decomposes at 220 °C, so it can easily be handled at room temperature under inert atmosphere [17].

2.3. Preparation of Rh-NP@stirring bar

A brand-new (unused) magnetic stir bar was washed with dried acetone (10 mL) and dried under high vacuum prior to the Rh-NP deposition. Rhodium nanoparticle deposition on PTFE was obtained by stirring the magnetic stirring bar in the Rh-NP/$BMImBF_4$ dispersion at room temperature under nitrogen for different defined number of 2–8 days. The nanoparticle-loaded stirring bar was removed from the Rh-NP/$BMImBF_4$ dispersion and stirred in a washing solvent (20 mL) for 15 s to remove the IL, removed with a pincer and dried under vacuum for 30 min.

The solvents acetone, water, methanol, *iso*-propanol, tetrahydrofuran and methylene chloride were tested for the washing and removal of the ionic liquid film which adhered to Rh-NP@stirring bar. For each different washing solvent, a cyclohexene hydrogenation run (see Section 2.4) was carried out to test for the resulting activity. Activities for acetone (p.a.), THF or methylene chloride were similar and higher than for acetone (technical), methanol, *iso*-propanol or water. Eventually, THF (p.a.) was used as a standard washing solvent for the catalytic recycling experiments.

The rhodium loading on the stirring bar and the rhodium leaching in the catalytic runs was analyzed by AAS. To dissolve the Rh-NPs from the Teflon-coating the stirring bar was placed into a conc. HCl/HNO_3 mixture (*aqua regia*, 50 mL) over night. The resulting solution was directly used for the AAS analysis. Repeated analyses of the Rh-NP content on a stirring bar from the above preparations reproducibly gave 32(±8) μg of rhodium (±8 is the standard deviation σ from multiple Rh-content determinations of different stirring bars). Hence, the Rh-NP loading does not depend on the time variation for deposition within 2–8 days. After the treatment with *aqua regia* the magnetic stirring bars lost their catalytic properties for the hydrogenation of cyclohexene or benzene.

2.4. Catalysis

2.4.1. General

Rh-NP@stirring bars were conditioned after their preparation by using the above-mentioned washing procedure with dried THF (20 mL) for 15 s before the first run to remove the ionic liquid.

An autoclave with a glass inlay was used. The hydrogenation reactions were carried out in the glass inlay. The autoclave was conditioned by evacuation and re-filling with nitrogen. All autoclave loading was carried out under nitrogen. Stirring rate was 850 rpm. The H_2 uptake over time was monitored with a Büchi pressflow gas controller (Büchi pbc). After quantitative or near quantitative conversion was reached (adjudged by the H_2 consumption) the reactor was depressurized, the volatile organic components were condensed under vacuum into a clean cold trap. The Rh-NPs@stirring bar was left behind in the glass inlay of the autoclave and was reused by adding fresh substrate. Catalyst recycling was carried out ten times for cyclohexene and three times for benzene.

The cyclohexene or benzene to cyclohexane conversion was verified by gas chromatographic (GC) analysis of the product (Perkin-Elmer 8500 HSB 6, equipped with a DB-5 film capillary column, 60 m × 0.32 mm, film thickness 25 μm, oven temperature 40 °C, N_2 carrier flow 120 L/min and a flame ionization detector (FID), 250 °C detector temperature). The benzene or cyclohexene to cyclohexane conversion was analyzed by putting a drop of the mixture into a GC sample vial with 1 mL of water. The addition of water as a non-electrolyte can enlarge the activity coefficient of organic components, thereby increase their detection sensitivity through the increase in peak area. The FID does not detect the water itself [18].

2.4.2. Conditions for cyclohexene hydrogenation

Cyclohexene 0.69 mL, 6.8 mmol (density 0.811 g/mL, M = 82.14 g/mol); Rh metal (0.032 mg, 3.1×10^{-7} mol); 75 °C, 4 bar H_2.

2.4.3. Conditions for benzene hydrogenation

Benzene 0.60 mL, 6.8 mmol (density 0.88 g/mL, M = 78.11 g/mol); Rh metal (0.032 mg, 3.1×10^{-7} mol); 90 °C, 20 bar H_2. For the slower benzene hydrogenation the reaction was intentionally stopped at 90% conversion (adjudged by the H_2 consumption) as thereafter the decrease in benzene concentration lowered the reaction rate. Thus, the reactor was depressurized

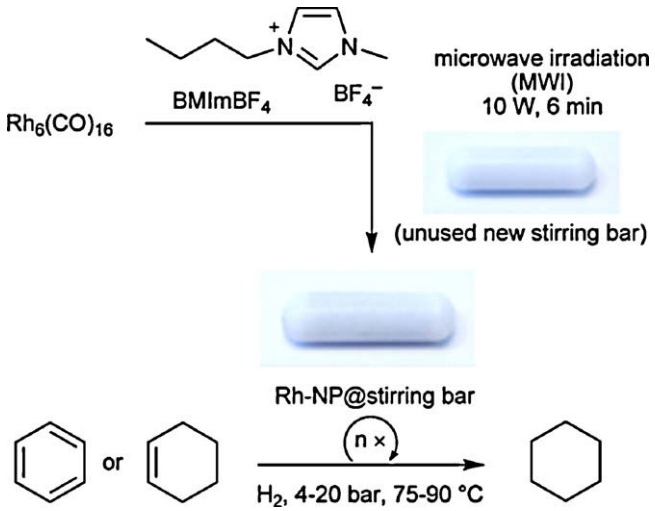

Fig. 1. Preparation of Rh-NP@stirring bar and repeated utilization as hydrogenation catalyst. The photographs show a standard commercial 20 mm × 6 mm magnetic stirring bar before and after Rh-NP deposition.

after 90% conversion and the liquid product removed under vacuum and fresh benzene (0.60 mL) was added.

2.4.4. Special experiments

To investigate the possibility of mechanical abrasion or of leaching of Rh-NPs from the stirring bar the following special experiments were performed. In each case the hydrogenation was carried out at 75 °C and 4 bar H_2 and was stopped after 24 h to verify the conversion by GC.

Entry 14 in manuscript Table 1 – *test for mechanical abrasion:* Rh-NPs@stirring bar was stirred for 12 h at 75 °C in an empty glass inlay at 850 rpm under N_2. Afterwards this Rh-NPs@stirring bar was replaced by a brand-new (untreated) stirring bar. Cyclohexene (0.69 mL) was added and the autoclave was pressurized with H_2.

Entry 15 in manuscript Table 1 – *test for leaching into cyclohexene:* Rh-NPs@stirring bar was placed in and allowed to stand for 12 h at 75 °C in cyclohexene (0.69 mL) without stirring under N_2. Afterwards Rh-NPs@stirring bar was replaced by a brand-new (untreated) stirring bar and the autoclave was pressurized with H_2.

Entry 16 in manuscript Table 1 – *test for leaching into cyclohexene under hydrogenation conditions:* Using the general hydrogenation conditions, the hydrogenation of cyclohexene (0.69 mL) was run until 25% conversion (which was reached after 12 min). The cyclohexane/cyclohexene mixture was filtered hot at 60 °C under N_2 atmosphere into a new glass inlay equipped with a brand-new (untreated) stirring bar. The glass inlay was placed into the autoclave and hydrogenation was resumed.

3. Results and discussion

Deposition of Rh-NPs onto a standard Teflon (PTFE)-coated stirring bar is easily achieved by thermal decomposition of $Rh_6(CO)_{16}$ in $BMImBF_4$ through microwave irradiation [19] and immersion of the stirring bar into the Rh-NP/IL dispersion (Fig. 1).

Rh-NP deposition on the stirring bar is only slightly evident by visual inspection with a naked eye from some minor darkening (Fig. 1). Proof of the Rh-NP deposits is obtained by scanning electron microscopy (SEM) of the Teflon surface or transmission electron microscopy of Teflon flakes therefrom (Fig. 2). The amount of Rh-NP@stirring bar was quantified by AAS to 32(±8) μg per stirring bar. A Rh-NP size analysis was carried out by transmission electron microscopy (TEM) on Teflon flakes which were cut from the stirring bar (Fig. 2d and e). Median Rh-NP diameters were 2.1 (±0.5) nm and 1.7 (±0.3) nm after the 10th hydrogenation run.

Syntheses and applications of transition-metal nanoparticles (M-NPs) are of contemporary interest in several areas of science [20–23] including catalysis [24]. The efficient stabilization of M-NPs requires surface-coordinating ligands [25,26] ionic liquids [27–30] or deposition onto solid surfaces [25,31,32]. There are wide ranges of supports described for M-NPs (see Supplementary data), however, very little is known for PTFE as a nanoparticle support [33–35]. The immobilization of Fe-NPs on the surface of PTFE nanogranules appears to be a singular example. The chemical properties of bulk PTFE were considered unsuitable for the stabilization of metal containing nanoparticles [36].

The caveat: It is evident that PTFE, albeit generally considered a chemically inert material with a non-sticking surface, can support nanoparticular metal deposits. Such nanoparticular deposits can originate from various uses of stirring bars in a laboratory. These M-NP deposits are also not easily removed by washing with common organic solvents or with water (see Section 2.3). If then such a stirring bar with a "colorful past" is used in catalysis experiments the metal nanoparticle deposits can exert an activity while the intended catalysis system is less active or even inactive (akin to the metal impurities in "intended" catalysts noted in the introduction). This possibility is especially problematic because such metal nanoparticle deposits cannot be visually detected.

The chance: The ease of support of metal nanoparticles on a readily available and thermally stable PTFE surface can open new vistas for metal nanoparticle and catalysis research, especially in view of the easy separation of a catalytically active magnetic stirring bar akin to the recovery of magnetic nanoparticle catalysts [37–39].

As a proof-of-concept the Rh-NP@stirring bar supported magnetic stirring bars were tested for their re-usable catalytic activity in the known hydrogenation of cyclohexene or benzene to cyclohexane under organic-solvent-free conditions where comparative literature data is available (Fig. 1, Table 1 and Tables S1 and S2 in Supplementary data). The hydrogenation reactions were carried out in a stainless steel autoclave equipped with a glass inlay. The autoclave was heated to 75 °C or 90 °C and pressurized with the hydrogen consumption monitored by a Büchi pressflow gas controller (H_2 uptake over time, see Figs. S3 and S4 in Supplementary data). Near quantitative conversion the reactor was depressurized and the volatile organic components were condensed under vacuum into a clean cold trap. To test for recycling the Rh-NPs@stirring bar was left behind in the autoclave and was re-used by adding fresh substrate. Catalyst recycling was carried out ten times for cyclohexene and three times for benzene. There is an initial increase in activity with recycling from entry 1 to 3 in Table 1 which was also seen in other hydrogenations with Rh-NP/IL systems [19,40]. This is probably due to a slow surface restructuring and not due to the rapid formation of Rh–hydride or Rh–heterocyclic carbene (NHC) [41] surface species [42].

Activities for cyclohexene hydrogenations with Rh-NP@stirring bar were 5–10 times higher than for other supported Ru-, Rh-, Pd- or Pt-NP catalysts in ILs [19,43–45] or on supports [46–50] (Table S1 in Supplementary data). For benzene hydrogenation the activity was higher than for most M-NP literature systems [16,43,46,51,52] and only surpassed by Rh-NP/carbon nanofibers [53] (Table S2 in Supplementary data). The lower hydrogenation activities of Ru- and Rh-NPs in ILs are traced to the IL diffusion barrier for H_2 and the substrate. For the supported Rh-NP catalysts the average nanoparticle size deposited here on the stirring bar was found to be considerably smaller (2.1 ± 0.5 nm) than the size given for other supports (2.8–5 nm) [46–48] (Table S1 in Supplementary data).

In general in M-NP catalysis the active species can be either "heterogeneous" M-NPs in a dispersion or on a surface or

Table 1
Hydrogenation of cyclohexene or benzene to cyclohexane with Rh-NP@stirring bar.[a]

Entry	Substrate and run	Conversion [%]	Time [min]	Activity (TOF) [mol product × (mol Rh)$^{-1}$ × h^{-1}]
1	Cyclohexene[b]	>99	88	14.9×10^3
2	2nd run	>99	49	26.8×10^3
3	3rd run	>99	40	32.8×10^3
4	4th run	>99	48	27.3×10^3
5	5th run	>99	68	19.3×10^3
6	6th run	>99	132	9.9×10^3
7	7th run	87[d]	139	8.2×10^3
8	8th run	>99	139	9.4×10^3
9	9th run	>99	161	8.1×10^3
10	10th run	80[d]	160	6.6×10^3
11	Benzene[c]	85[d]	1474	750
12	2nd run	90	1607	730
13	3rd run	90	2553	460
14	Cyclohexene[e]	78	1440	
15	Cyclohexene[e]	20	1440	
16	Cyclohexene[e]	53	1440	

[a] Conditions: Rh metal 32 μg, 3.1×10^{-7} mol.
[b] Cyclohexene 0.69 mL, 6.8 mmol, 75 °C, 4 bar H_2.
[c] benzene 0.6 mL, 6.8 mmol; 90 °C, 20 bar H_2.
[d] Conversion ceased.
[e] See Section 2.4.4 for further details.

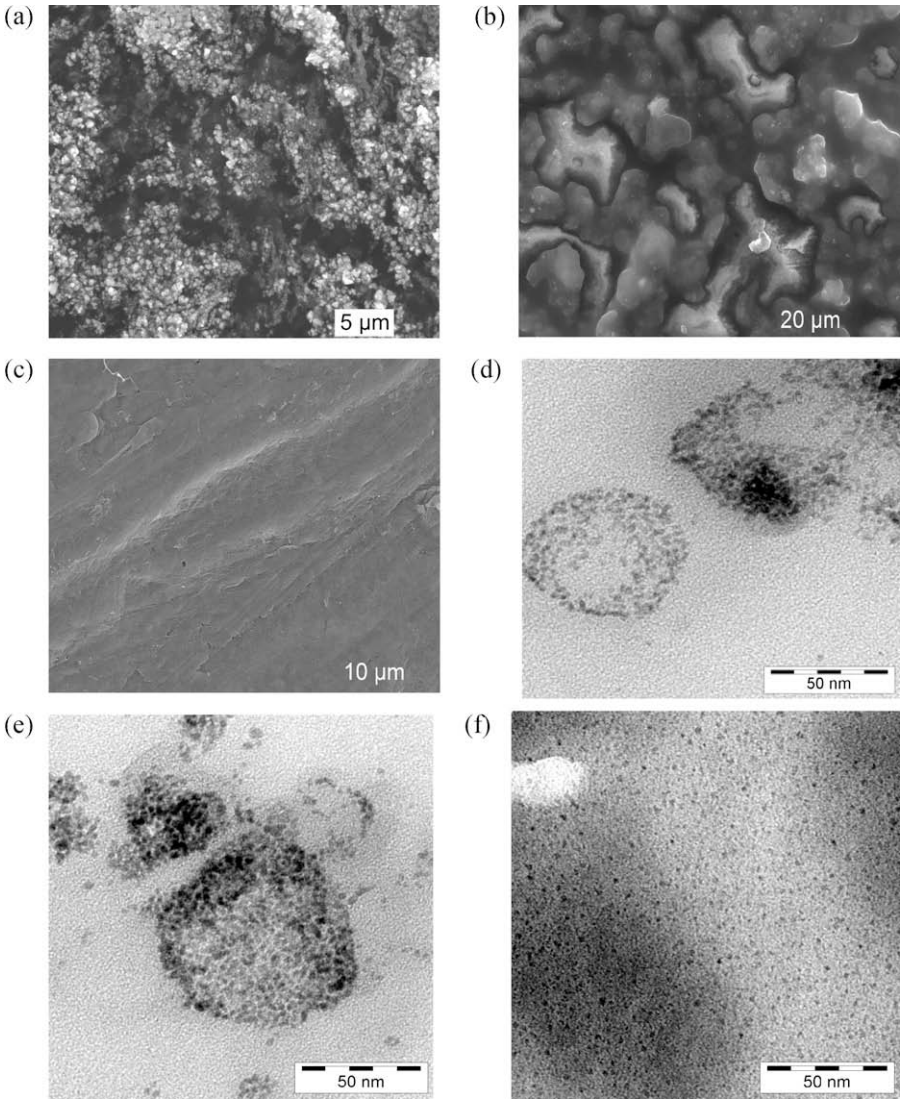

Fig. 2. SEM-pictures of Rh-NPs on a Teflon-coated magnetic stirring bar (Rh-NP@stirring bar) (a) and after 10 hydrogenation runs (b) in comparison to the blank Teflon surface (c). TEM of Teflon flakes from the stirring bar coating for Rh-NP size analysis before catalysis (d, e) and after the 10th catalytic hydrogenation run of cyclohexene (f).

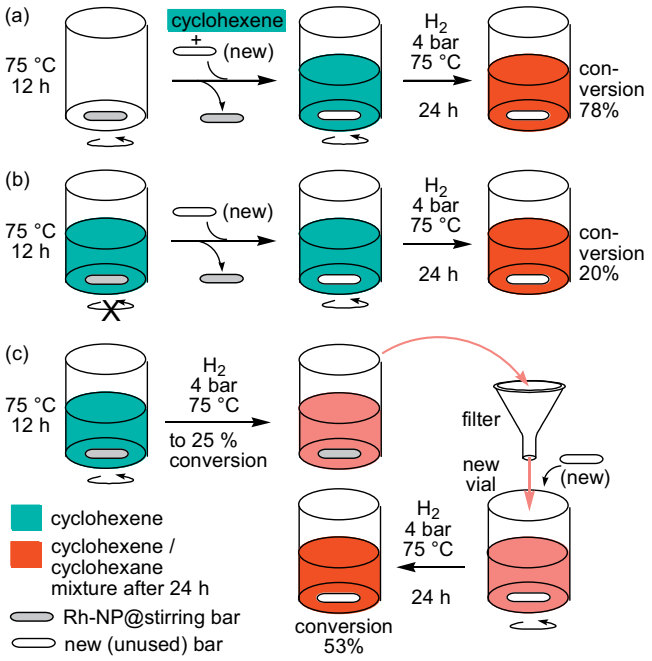

Fig. 3. Experiments to attest the abrasion or leaching from Rh-NPs@stirring bar (carried out twice to ensure reproducibility within experimental error). (a) (Entry 14, Table 1) Stirring of Rh-NP@stirring bar in the empty glass inlay at 75 °C for 12 h under N_2, followed by removal of the stirring bar, addition of a new (unused) stirring bar, cyclohexene and H_2. A conversion of 78% is reached after 24 h (cf. > 99% with Rh-NP@stirring bar in 1–2 h, entry 1–5) and indicates some, but little mechanical abrasion of the Rh-NPs from the PTFE surface. (b) (Entry 15, Table 1) Allowing Rh-NP@stirring bar to stand in cyclohexene at 75 °C for 12 h under N_2, followed by removal of the stirring bar, addition of a new stirring bar and H_2. A conversion of only 20% after 24 h indicates little leaching from the stirring bar into the cyclohexene substrate. (c) (Entry 16, Table 1) Cyclohexene hydrogenation was run to 25% conversion (within 12 min, monitored by gas uptake). Then, Rh-NP@stirring bar was removed, the cyclohexene/cyclohexane mixture filtered under argon into a new glass inlay, equipped with a new stirring bar and re-pressurized. Conversion proceeded very slowly to 53% in 24 h, attesting little leaching even under the reaction conditions.

"homogeneous" atoms or small clusters which leach from the M-NP into the solution [25]. Hence, we cannot exclude, that the Rh-NP@stirring bar functions as a reservoir of such "homogeneous" active atoms or clusters. There is only a minor amount of mechanical abrasion or of leaching of Rh-NPs from the stirring bar during each catalytic run as was attested by three reproducible experiments outlined in Fig. 3. Abrasion onto the glass surface appears to be more prominent than simple leaching when comparing the resulting activities from stirred (Fig. 3a, entry 14 in Table 1) versus non-stirred preparations (Fig. 3b, entry 15 in Table 1) before applying the hydrogen pressure. Sizeable conversion can be attested from the abrasion, albeit at prolonged reaction times (24 h, entry 14) when compared to the conversion versus time of Rh-NP@stirring bar under otherwise identical conditions (entry 1–10). If one would want to avoid abrasion the stirring bar could be loaded into containments of a mechanical stirrer, such as designed by Mouljin, van Leeuwen et al. for loading catalyst-impregnated monolith blocks to give an immobilized homogeneous rotating catalyst (ROTACAT) [54,55].

4. Conclusions

Metal nanoparticle traces can easily be deposited – intentional or un-intentional – on the PTFE surface of magnetic stirring bars. Activating or desactivating effects can derive from un-intentional deposits when such stirring bars are employed in catalytic reactions. At the same time we show that a lab commodity such as a Teflon-coated magnetic stirring bar can be easily turned into a re-usable, smoothly handable and magnetically removable catalyst system. "Traces" of 32 μg or less of Rh-nanoparticles on the stirring bar surface exert very high hydrogenation activities for cyclohexene or benzene under mild conditions.

Acknowledgements

This work was supported by DFG grant Ja466/17-1.

Appendix A. Supplementary data

Supplementary data associated with this article can be found, in the online version, at doi:10.1016/j.apcata.2012.03.017.

References

[1] I. Thomé, A. Nijs, C. Bolm, Chem. Soc. Rev. 41 (2012) 979–987.
[2] J.M. Crow, Chem. World (May) (2011) 46–49.
[3] G. Wilke, Angew. Chem. Int. Ed. 42 (2003) 5000–5008.
[4] K. Fischer, K. Jonas, P. Misbach, R. Stabba, G. Wilke, Angew. Chem. Int. Ed. 12 (1973) 943–953.
[5] R.K. Arvela, N.E. Leadbeater, M.S. Sangi, V.A. Williams, P. Granados, R.D. Singer, J. Org. Chem. 70 (2005) 161–168.
[6] S.L. Buchwald, C. Bolm, Angew. Chem. Int. Ed. 48 (2009) 5586–5587.
[7] Z. Gonda, G.L. Tolnai, Z. Novák, Chem. Eur. J. 16 (2010) 11822–11826.
[8] K. Yoshida, N. Begum, S.-i. Ito, K. Tomishige, Appl. Catal. A 358 (2009) 186–192.
[9] K. Nishida, I. Atake, D. Li, T. Shishido, Y. Oumi, T. Sano, K. Takehira, Appl. Catal. A 337 (2008) 48–57.
[10] D. Li, I. Atake, T. Shishido, Y. Oumi, T. Sano, K. Takehira, Appl. Catal. A 332 (2007) 98–109.
[11] Scifinder search performed November 2011.
[12] M.-N. Birkholz, Z. Freixa, P.W.N.M. van Leeuwen, Chem. Soc. Rev. 38 (2009) 1099–1118.
[13] K. Fagnou, M. Lautens, Chem. Rev. 103 (2003) 169–196.
[14] N. Jeong, B.K. Sung, J.S. Kim, S.B. Park, S.D. Seo, J.Y. Shin, K.Y. In, Y.K. Choi, Pure Appl. Chem. 74 (2002) 85–91.
[15] X. Cui, K. Burgess, Chem. Rev. 105 (2005) 3272–3296.
[16] G.S. Fonseca, A.P. Umpierre, P.F.P. Fichtner, S.R. Teixeira, J. Dupont, Chem. Eur. J. 9 (2003) 3263–3269.
[17] A.F. Hollemann, N. Wiberg, Lehrbuch der anorganischen Chemie, 102nd ed., de Gruyter, Berlin, 2007, pp. 1781–1782.
[18] H. Hachenberg, K. Beringer, Die Headspace-Gaschromatographie als Analysen- und Meßmethode, Vieweg, Braunschweig/Wiesbaden, Germany, 1996, pp. 32–35.
[19] C. Vollmer, E. Redel, K. Abu-Shandi, R. Thomann, H. Manyar, C. Hardacre, C. Janiak, Chem. Eur. J. 16 (2010) 3849–3858.
[20] V.I. Pârvulescu, C. Hardacre, Chem. Rev. 107 (2007) 2615–2665.
[21] C. Vollmer, C. Janiak, Coord. Chem. Rev. 255 (2011) 2039–2057.
[22] A. Seyed-Razavi, I.K. Snook, A.S. Barnard, J. Mater. Chem. 20 (2010) 416–421.
[23] Y. Teow, P.V. Asharani, M.P. Hande, S. Valiyaveettil, Chem. Commun. 47 (2011) 7025–7038.
[24] J. Dupont, J.D. Scholten, Chem. Soc. Rev. 39 (2010) 1780–1804.
[25] L. Durán Pachón, G. Rothenberg, Appl. Organomet. Chem. 22 (2008) 288–299.
[26] P. Graf, A. Mantion, A. Foelske, A. Shkilnyy, A. Măsić, A.F. Thünemann, A. Taubert, Chem. Eur. J. 15 (2009) 5831–5844.
[27] E. Redel, M. Walter, R. Thomann, L. Hussein, M. Krüger, C. Janiak, Chem. Commun. 46 (2010) 1159–1161.
[28] E. Redel, R. Thomann, C. Janiak, Chem. Commun. (2008) 1789–1791.
[29] A. Taubert, Z. Li, Dalton Trans. (2007) 723–727.
[30] H. Olivier-Bourbigou, L. Magna, D. Morvan, Appl. Catal. A 373 (2010) 1–56.
[31] R.J. White, R. Luque, V.L. Budarin, J.H. Clark, D.J. Macquarrie, Chem. Soc. Rev. 38 (2009) 481–494.
[32] B. Inceesungvorn, J. López-Castro, J.J. Calvino, S. Bernal, F.C. Meunier, C. Hardacre, K. Griffin, J.J. Delgadob, Appl. Catal. A 391 (2011) 187–193.
[33] E. Redel, M. Walter, R. Thomann, C. Vollmer, L. Hussein, H. Scherer, M. Krüger, C. Janiak, Chem. Eur. J. 15 (2009) 10047–10059.
[34] K. Grytsenko, Y. Kolomzarov, O. Lytvyn, V. Strelchuk, V. Ksianzou, S. Schrader, H. Beyer, B. Servet, S. Enouz-Vedrenne, G. Garry, R.D. Schulze, J. Friedrich, Adv. Sci. Lett. 3 (2010) 308–312.
[35] Z. Jia, Y. Yang, B. Fan, Appl. Mech. Mater. 29–32 (2010) 395–400.
[36] M.S. Korobov, G.Yu. Yurkov, A.V. Kozinkin, Yu.A. Koksharov, I.V. Pirog, S.V. Zubkov, V.V. Kitaev, D.A. Sarychev, V.M. Buznik, A.K. Tsvetnikov, S.P. Gubin, Inorg. Mater. 40 (2004) 31–40.
[37] T. Zeng, W.-W. Chen, C.M. Cirtiu, A. Moores, G. Song, C.-J. Li, Green Chem. 12 (2010) 570–573.
[38] M. Rossier, F.M. Koehler, E.K. Athanassiou, R.N. Grass, B. Aeschlimann, D. Günther, W.J. Stark, J. Mater. Chem. 19 (2009) 8239–8243.
[39] D. Guin, B. Baruwati, S.V. Manorama, Org. Lett. 9 (2007) 1419–1421.
[40] E. Redel, J. Krämer, R. Thomann, C. Janiak, J. Organomet. Chem. 694 (2009) 1069–1075.
[41] J.M. Praetorius, C.M. Crudden, Dalton Trans. (2008) 4079–4094.

[42] G. Ertl, H. Knözinger, J. Weitkamp, Handbook of Heterogeneous Catalysis, vol. 9, Wiley-VCH, Weinheim, 2008.
[43] E.T. Silveira, A.P. Umpierre, L.M. Rossi, G. Machado, J. Morais, I.L.R. Baumvol, S.R. Teixeira, P.F.P. Fichtner, J. Dupont, Chem. Eur. J. 10 (2004) 3734–3740.
[44] L.M. Rossi, G. Machado, P.F.P. Fichtner, S.R. Teixeira, J. Dupont, Catal. Lett. 92 (2004) 149–155.
[45] C.W. Scheeren, G. Machado, J. Dupont, P.F.P. Fichtner, S.G. Texeira, Inorg. Chem. 42 (2003) 4738–4742.
[46] D. Marquardt, C. Vollmer, R. Thomann, P. Steurer, R. Mülhaupt, E. Redel, C. Janiak, Carbon 49 (2011) 1326–1332, Ru-NPs and Rh-NPs on graphene.
[47] S. Miao, Z. Liu, Z. Zhang, B. Han, Z. Miao, K. Ding, G. An, J. Phys. Chem. C 111 (2007) 2185–2190, Rh-NPs on attapulgite support.
[48] M.J. Jacinto, P.K. Kiyohara, S.H. Masunaga, R.F. Jardim, L.M. Rossi, Appl. Catal. A 338 (2008) 52–57, Rh-NPs on silica-coated magnetite NPs.
[49] L. Armelao, D.B.D. Amico, R. Braglia, F. Calderazzo, F. Garbassi, G. Marra, A. Merigo, Dalton Trans. (2009) 5559–5566, Pt-NPs on SiO_2.
[50] R.M. Rioux, B.B. Hsu, M.E. Grass, H. Song, G.A. Somorjai, Catal. Lett. 126 (2008) 10–19, Pt-NPs on SiO_2.
[51] F. Lu, J. Liu, J. Xu, J. Mol. Catal. A: Chem. 271 (2007) 6–13.
[52] A. Nowicki, V. Le Boulaire, A. Roucoux, Adv. Synth. Catal. 349 (2007) 2326–2330.
[53] Y. Motoyama, M. Takasaki, S.-H. Yoon, I. Mochida, H. Nagashami, Org. Lett. 11 (2009) 5042–5045.
[54] R.K. Edvinsson, M.J.J. Houterman, T. Vergunst, E. Grolman, J.A. Moulijn, AIChE J. 44 (1998) 2459–2464.
[55] A.J. Sandee, R.S. Ubale, M. Makkee, J.N.H. Reek, P.C.J. Kamer, J.A. Moulijn, P.W.N.M. van Leeuwen, Adv. Synth. Catal. 343 (2001) 201–206.

Coordination Chemistry Reviews 255 (2011) 2039–2057

Contents lists available at ScienceDirect

Coordination Chemistry Reviews

journal homepage: www.elsevier.com/locate/ccr

Review

Naked metal nanoparticles from metal carbonyls in ionic liquids: Easy synthesis and stabilization

Christian Vollmer, Christoph Janiak*

Institut für Anorganische Chemie und Strukturchemie, Heinrich-Heine-Universität Düsseldorf, Universitätsstrasse 1, D-40225 Düsseldorf, Germany

Contents

ARTICLE INFO

Article history:
Received 1 December 2010
Accepted 6 March 2011
Available online 16 March 2011

Keywords:
Metal nanoparticle
Ionic liquid
Metal carbonyl
Synthesis
Stabilization
Catalysis

ABSTRACT

An overview with more than 160 references on the synthesis and stabilization of metal nanoparticles (M-NPs) from metal carbonyls, metal salts in ionic liquids (ILs) and in particular from metal carbonyls in ionic liquids is given. The synthesis of M-NPs can proceed by chemical reduction, thermolysis, photochemical decomposition, electroreduction, microwave and sonochemical irradiation. Commercially available metal carbonyls $M_x(CO)_y$ are elegant precursors as they contain the metal atoms already in the zero-valent oxidation state needed for M-NPs. No extra reducing agent is necessary. The side product CO is largely given off to the gas phase and removed from the dispersion. The microwave induced thermal decomposition of metal carbonyls $M_x(CO)_y$ in ILs provides an especially rapid and energy-saving access to M-NPs because of the ILs significant absorption efficiency for microwave energy due to their high ionic charge, high polarity and high dielectric constant. The electrostatic and steric properties of ionic liquids allow for the stabilization of M-NPs without the need of additional stabilizers, surfactants or capping ligands and are highlighted by pointing to the DLVO (Derjaugin–Landau–Verwey–Overbeek) and extra-DLVO theory. Examples for the direct use of M-NP/IL dispersions in hydrogenation catalysis of cyclohexene and benzene are given.

1. Introduction

Metal nanoparticles (M-NPs) are of significant interest for technological applications in several areas of science and industry, especially in catalysis due to their high activity. The controlled and reproducible synthesis of defined and stable M-NPs with a small size distribution is very important for a range of applications [1–5]. Note that through the years metal nanoparticles were also referred to as nanophase metal clusters, metal nanocrystals and metal colloids. In the following we primarily use the term (metal) nanoparticles for simplicity. Small (< 5 nm) M-NPs are only kinetically stable and will combine to thermodynamically favored larger metal particles via agglomeration. This M-NP tendency for aggregation is due to the high surface energy and the large surface area. To avoid this agglomeration, M-NPs need to be stabilized with strongly coordinating protective ligand layers which provide electrostatic and/or steric protection like polymers and surfactants [6–8]. Ionic liquids (ILs) can be an alternative to such ligand layers (Scheme 1). ILs may be seen to act as a "novel nanosynthetic template" [9] that stabilize

* Corresponding author. Tel.: +49 211 81 12286.
E-mail address: janiak@uni-duesseldorf.de (C. Janiak).

0010-8545/$ – see front matter © 2011 Elsevier B.V. All rights reserved.
doi:10.1016/j.ccr.2011.03.005

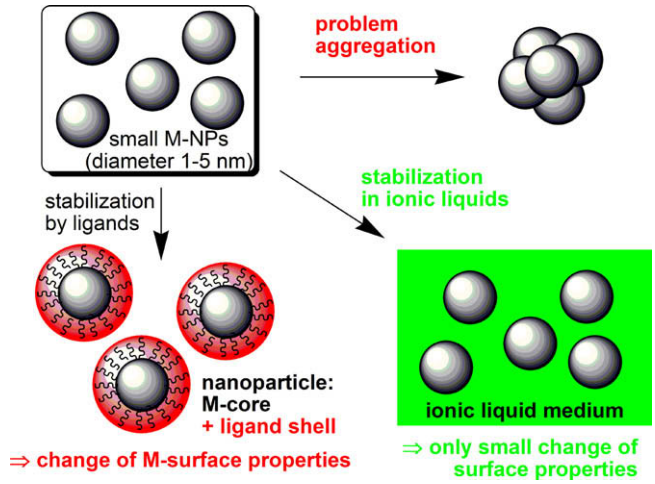

Scheme 1. Stabilization of metal nanoparticles (M-NP) through protective ligand stabilizers or in ionic liquids (IL). For the use of color in this graphic the reader is referred to the web version of the article.

M-NPs on the basis of their ionic nature [10], high polarity, high dielectric constant and supramolecular network (see Section 2) without the need of additional protective ligands (cf. Scheme 3) [11–15].

In the absence of strongly coordinating protective ligand layers, M-NPs in ILs should be effective catalysts. The IL network contains only weakly coordinating cations and anions (see Scheme 2) that bind less strongly to the metal surface and, hence, are less deactivating, than the commonly employed capping or protective ligands. The combination of M-NPs and ILs can be considered a *green catalytic system* because it can avoid the use of organic solvents. ILs are interesting in the context of green catalysis [16] which requires that catalysts be designed for easy product separation from the reaction products and multi-time efficient reuse/recycling [17–19]. Firstly, the very low vapor pressure of the IL and designable low miscibility of ILs with organic substrates allows for a facile separation of volatile products by distillation or removal in vacuum. Secondly, the IL is able to retain the M-NPs for catalyst reuse and recycling. For example, Dupont and coworkers recycled a M-NP/IL system quite easily and reused it several times without any significant changes in catalytic activity [11]. In recent reports of Rh- or Ru-NP/IL in hydrogenation reactions, the catalytic activity did not decrease upon repeated reuse [20,21]. A sizable number of catalytic reactions have successfully been carried out in ILs [22]. Generally, the catalytic properties (activity and selectivity) of dispersed M-NPs indicate

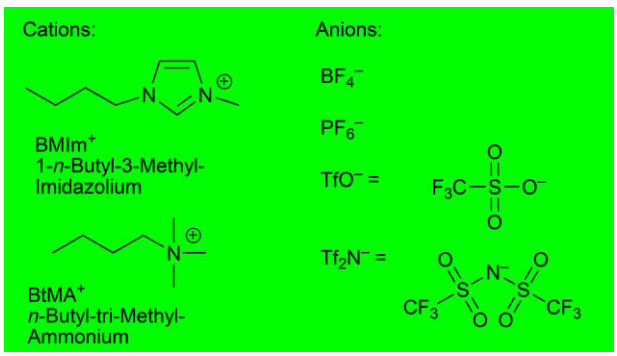

Scheme 2. Typical cations and anions of most common commercially available ILs. $BMIm^+$ is also abbreviated as BMI in the literature.

that they possess pronounced surface-like (multi-site) rather than single-site-like character [23,24].

In the following we give a brief introduction into the relevant properties of ionic liquids (Section 2) followed by an overview on the use of metal carbonyls for the synthesis of metal nanoparticles (Section 3). We then combine the synthesis of metal nanoparticles by various methods with ionic liquids as the matrix or medium for their preparation (Section 4). The theory for the treatment of particle dispersions, the DLVO (Derjaugin–Landau–Verwey–Overbeek) theory is then briefly discribed in Section 5.

2. Ionic liquids (ILs)

Ionic liquids are salts which are composed of charged inorganic and organic ion pairs. By definition their melting point is below 100 °C, more typically ILs are liquid at room temperature [18,25]. Such room temperature ionic liquids are occasionally abbreviated as RTILs [26]. ILs are liquid under standard ambient conditions because the liquid state is thermodynamically favorable, due to the large size and conformational flexibility of the ions involved, which leads to small lattice enthalpies and large entropy changes that favor melting [27]. ILs are characterized and set apart from other solvents by their physical properties like high charge density, high polarity, high dielectric constant and supramolecular network formation (Scheme 3) [14]. Typical IL cations include 1-alkyl-3-methylimidazolium, tetraalkylammonium, 1-alkylpyridinium and oxazolium. Typical anions for ILs are halide anions, tetrafluoroborate BF_4^-, hexafluorophosphate PF_6^-, tetrahalogenidoaluminate AlX_4^-, trifluoromethylsulfonate (triflate) $CF_3SO_3^-$ (TfO^-) or bis(trifluoromethylsulfonyl)amide [also named *N*-bis(trifluoromethanesulfonyl)imide, $(CF_3SO_2)_2N^-$, Tf_2N^-] (Scheme 2) [22,28].

The desired properties of the IL can be designed through judicious combination of anions and cations which presents an advantage over other solvent systems for the various envisioned IL applications. For instance: ILs containing Tf_2N^- offer low viscosity and high electrochemical and thermal stability [29]. If bis(*trifluoro*methylsulfonyl)amide Tf_2N^- is replaced by bis(methylsulfonyl)amide, viscosity increases and stability decreases [30]. This variety leads to a high interest towards ILs as new *green* reusable reaction media, especially in the field of catalysis [23].

Scattering experiments on ILs provided important information on the structure of ionic liquids which are not liquids in the conventional sense, but may rather be considered as mesophases [15]. Strictly speaking, however, ILs are not mesophases since they are isotropic liquids and just posses mesophases when they are liquid crystals. ILs are a class of substances that have an organizational behavior intermediate between isotropic liquids and liquid crystals. ILs have an intrinsic "nanostructure" which is caused by electrostatic, hydrogen bonding and van der Waals interactions [12,25]. The mesoscopic structure of imidazolium ionic liquids in particular can be described in part as a supramolecular three-dimensional hydrogen-bonded network (Scheme 3a) [12,14,15]. Pure 1,3-dialkylimidazolium ionic liquids can be described as a hydrogen-bonded [12,14,15] polymeric supramolecular network of the type $\{[(RR'Im)_x(A)_{x-n}]^{n+}[(RR'Im)_{x-n}(A)_x]^{n-}\}_n$ where RR′Im is the 1,3-dialkylimidazolium cation and A the anion. This structural pattern is not only seen in the solid phase but is also maintained to a great extent in the liquid phase. The introduction of other molecules and macromolecules proceeds with a disruption of the hydrogen bonding network and in some cases can generate nano-structures with polar and non-polar regions where inclusion-type compounds can be formed [11,12]. When mixed with other molecules or M-NPs, ILs

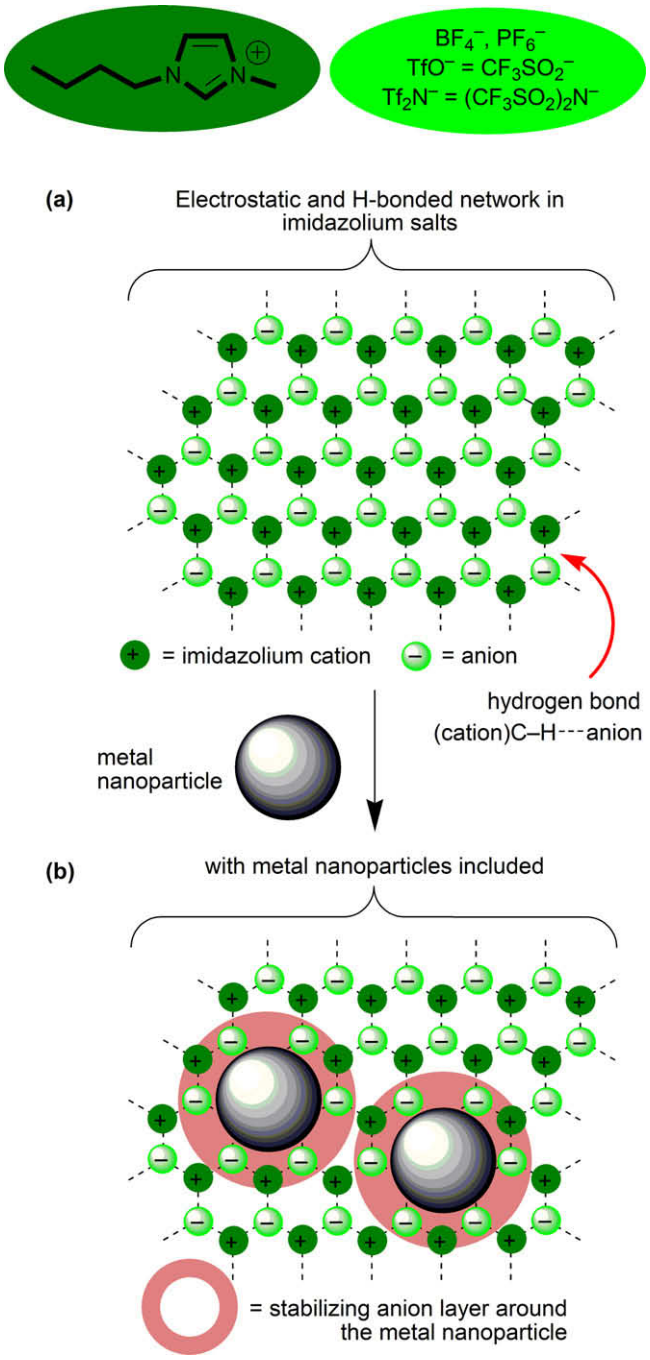

Scheme 3. (a) Schematic network structure in 1,3-dialkylimidazolium-based ionic liquids. (b) The inclusion of metal nanoparticles (M-NPs) in the supramolecular IL network with electrostatic and steric (=*electrosteric*) stabilization is indicated through the formation of the suggested primary anion layer forming around the M-NPs. For the use of color in this graphic the reader is referred to the web version of the article.

become nanostructured materials with polar and nonpolar regions [31–33].

Ionic liquids are nanostructural liquid media [34]. Nanometer-scale structuring in room-temperature ILs was observed by molecular simulation for ionic liquids belonging to the 1-alkyl-3-methylimidazolium family with hexafluorophosphate or with bis(trifluoromethylsulfonyl)amide as the anions. For ionic liquids with alkyl side chains longer than or equal to C_4, aggregation of the alkyl chains in nonpolar domains was observed. These domains permeate a three-dimensional network of charged or polar ionic channels formed by anions and by the imidazolium rings of the cations (cf. Scheme 3(a)). As the length of the alkyl chain increases, the nonpolar domains become larger and more connected and cause swelling of the ionic network, in a manner analogous to systems exhibiting microphase separation [34]. In other words, ILs are nanostructurally organized with nonpolar regions arising from clustering of the alkyl chains and ionic networks arising from charge ordering of the anions and imidazolium rings of the cations [26]. The combination of undirected Coulomb forces and directed hydrogen bonds leads to a high attraction of the IL building units. This is the basis for their (high) viscosity, negligible vapor pressure and three-dimensional constitution. The IL network properties should be well suited for the synthesis of defined nano-scaled metal colloid structures (see Scheme 3) [11–13].

3. Synthesis of metal nanoparticles (M-NPs) from metal carbonyls

The use of binary metal carbonyls for the synthesis of metal nanoparticles is sensible and logical. Metal carbonyls are commercially available (Table 1). $Fe(CO)_5$ and $Ni(CO)_4$ are industrially produced on a multi-ton scale [35]. Compounds $M_x(CO)_y$ are easily purifyable and handable, even if care should be exerted for the possible liberation of poisonous CO. The metal carbonyls contain the metal atoms already in the zero-valent oxidation state needed for M-NPs. No reducing agent is necessary. The side product CO is largely given off to the gas phase and removed from the dispersion. Contamination from by- or decomposition products, which are otherwise generated during the M-NP synthesis (see Section 4), are greatly reduced. Thus, metal carbonyls were used early on for the preparation of M-NPs. It will be evident from the following examples (see also Table 2) that all these metal nanoparticles which were prepared in the condensed phase needed stabilization through additional ligands, like dispersants, surfactants or through passivation with a metal-oxide shell. Also the majority of the work uses the metal carbonyls $Fe(CO)_5$ and $Co_2(CO)_8$. The following excerpts from the literature are roughly arranged in chronological order according to the year of publication (see also Table 2 for further examples). Much of the work on Fe- or Co-NPs at large is devoted to their magnetism [36].

In early reports Hess and Parker [37] and Thomas [38] described processes for preparing metallic cobalt particles of uniform size in the 10–1000 Å range (0.1–100 nm). Dicobalt octacarbonyl $Co_2(CO)_8$ was thermally decomposed in typically toluene solutions of dispersant polymers, such as methyl methacrylate-ethyl acrylate-vinylpyrrolidone terpolymers, high-purity polystyrene, styrene-acrylonitrile polymers, polyacrylonitril, chloropolyethylene sulfonamide, polyester and polyether urethanes to form stable colloids of discrete particles which are separated by polymer coatings. Variation of polymer composition, molecular weight and solvent result in a variation of particle size and colloid stability. Preparation of single-domain ferromagnetic cobalt particles with good magnetic properties was possible through a balance between dispersant polymer, solvent, and the growing metal particle [37].

Papirer et al. prepared a stable suspension of metallic cobalt particles in an organic solvent (ferrofluid) by decomposition of $Co_2(CO)_8$ [39,40]. The cobalt particles originate from the thermolysis of the dicobalt octacarbonyl solution in the presence of a chosen surface active agent. The reaction temperature, the nature of the solvent and of the surfactant, the weight ratio of carbonyl and surfactant, and the initial concentration of the cobalt carbonyl solution were varied. Spherical particles, of a narrow size distribution, are obtained when the decomposition of $Co_2(CO)_8$ is carried out in an aromatic solvent above 110 °C and in the presence of a sur-

Table 1
Binary metal carbonyls.[a]

Group Metal	5 V, Nb, Ta	6 Cr, Mo, W	7 Mn, Tc, Re	8 Fe, Ru, Os	9 Co, Rh, Ir	10 Ni, Pd, Pt
Mononuclear complexes	$V(CO)_6$	**$Cr(CO)_6$** **$Mo(CO)_6$** **$W(CO)_6$**		**$Fe(CO)_5$** $Ru(CO)_5$ $Os(CO)_5$		**$Ni(CO)_4$**
Polynuclear complexes			**$Mn_2(CO)_{10}$** $Tc_2(CO)_{10}$ **$Re_2(CO)_{10}$**	**$Fe_2(CO)_9$** **$Fe_3(CO)_{12}$** $Ru_2(CO)_9$ **$Ru_3(CO)_{12}$** $Os_2(CO)_9$ **$Os_3(CO)_{12}$**	**$Co_2(CO)_8$** **$Co_4(CO)_{12}$** **$Rh_4(CO)_{12}$** **$Rh_6(CO)_{16}$** **$Ir_4(CO_{12})$**	

[a] Metal carbonyls given in bold were confirmed to be commercially available, e.g., from Aldrich, ABCR or Acros.

factant possessing a long hydrocarbon chain and a strong ionic group (sulfonate). The decomposition in toluene, in which ethyl (2-hexyl) sodium sulfo-succinate is dissolved, leads to particles of about 70 Å in diameter. When a ferrofluid is being formed, an initial and rapid evolution of CO corresponding to the formation of $Co_4(CO)_{12}$ is recorded. Part of this compound is insoluble in the reaction medium and appears to be a regulating intermediate. After this short initial stage the rate of decomposition of $Co_4(CO)_{12}$ slows down and becomes practically constant. Later the CO formation is accelerated again and finally it decreases as the reaction goes to completion. This S-shaped curve which describes the decomposition of $Co_2(CO)_8$ is always observed when a ferrofluid is in progress of formation [39]. The diameters of the particles, and the number of growing particles have been measured using also small-angle X-ray scattering and magnetic methods. The presence of microreactors in the reaction medium and a diffusion controlled growth mechanism are seen as the responsible two factors for the formation of particles of very narrow size distribution [40].

Lee et al. produced nanoparticles of iron, chromium, molybdenum and tungsten by laser decomposition of the corresponding metal carbonyls with a 10.6 μm CO_2 laser in the presence of Ar and SF_6 [41]. Argon helped to increase the purity of the metal clusters by suppressing the formation of $(M)_x(CO)_y$ for M = Fe, Cr, Mo, W. SF_6 acted as an infrared photosensitizer, which initially absorbed the 10.6 μm IR photons from the CO_2 laser and transferred its energy to a metal carbonyl via collisions. The M-NP size distributions were narrow and the average diameter was 6, 3.5, 2 and ~1 nm for Fe, Cr, Mo and W clusters, respectively, as determined by TEM. The structure is body-centered cubic (bcc) for both Fe and Cr clusters, face-centered cubic (fcc) for Mo clusters, and amorphous for W clusters as determined from the X-ray diffraction patterns (note that all the bulk metals have bcc structure). The cluster size (n) in one cluster of average diameter was estimated by assuming a spherical shape such that n = (cluster volume/atomic volume) × packing fraction = $(r/r_0)^3 f$, with r the cluster radius, r_0 the atomic radius and f the packing fraction (0.68 for bcc and 0.74 for fcc). Considering the cluster sizes (n = 9630, 1870, 230 and ~30 for Fe-, Cr-, Mo- and W-NPs, respectively) estimated from their average diameters, it was found likely that there exists a structural transition from fcc to bulk bcc with increasing cluster size in these metal clusters [41].

Giersig and Hilgendorff prepared cobalt nanoparticles by thermolysis of $Co_2(CO)_8$ in Ar-saturated toluene as an organic carrier at 110 °C in the presence of two different surfactants. The surfactants

Table 2
Additional examples for M-NP syntheses from metal carbonyls.

Metal	Metal carbonyl	Solvent	M-NP size: range or average diameter (standard deviation) [nm]	Remarks, stabilizer	Reference
Fe	$Fe(CO)_5$	Octanol or hexadecane	3–8 (amorphous)	Sonochemical decomposition; stabilized by polyvinylpyrrolidone (PVP) or oleic acid	[75]
Fe	$Fe(CO)_5$	Trioctylphosphine oxide (TOPO)	2 (monodisperse, spherical)	Thermal decomposition, rod-shaped particles stabilized by TOPO; rod-shaped Fe-NPs from the controlled growth of the monodisperse spherical NPs	[76]
Fe	$Fe(CO)_5$	Decalin	2–10 (variation by the $Fe(CO)_5$/PIB ratio)	Stabilized by modified polyisobutylene (PIB); NP characterization also by magnetic measurements (fastoxidation in air); linear structures of the larger particles (by cryo-TEM) because of magnetic interaction	[77]
Co	$Co_2(CO)_8$	Toluene or THF	3–5	Thermal decompostition, stabilized by polystyrene(PS)-poly-4-vinyl-pyridine (PVP)	[78]
Co	$Co_2(CO)_8$	Trioctylphosphine oxide	20	Thermal decomposition, stabilized by TOPO; new structure of elemental cobalt (ε-cobalt)	[79]
$CoPt_3$	$Co_2(CO)_8$, $Pt(hfac)_2$	Hot toluene or nonane	1.8(1)	Thermal decomposition, stabilized by oleic acid or dodecane isocyanide; alloy nanoparticles	[80]
FeCo	$Co_2(CO)_8$, $Fe(CO)_5$	1,2-Dichlorobenzene	1–11	FeCo-alloyed nanoparticles, thermal decomposition, stabilized by oleic acid and trioctyl-phosphane oxide	[81,82]

used were sodium bis 2-(ethyl-hexyl)sulfosuccinate and oleoyl-sarcosine. The magnetic nanoparticles were then ordered into a two-dimensional array using a magnetophoretic technique. The quality of the ordering was observed by electron microscopy and the lattice constants determined by electron diffraction. Cobalt particles condense into a hexagonal close packed array [42]. These arrays of monodisperse colloidal 11.4 nm Co nanoparticles were investigated by multifrequency ferromagnetic resonance and X-ray magnetic circular dichroism (XMCD) to determine the ratio of orbital-to-spin magnetic moment as $\mu_L/\mu_S^{eff} = 0.24 \pm 0.06$ by XMCD [43].

Van Wonterghem, Mørup et al. [44,45], Pathmamanoharan et al. [46], Gossens et al. [47] and Butter, Philipse et al. [48] formed iron nanoparticles by thermolysis of $Fe(CO)_5$ in decalin with modified polyisobutene and oleic acid as stabilizers. The magnetic Fe-NPs are fairly monodisperse even for particle radii below 10 nm. The particle size can be increased by seeded growth, and the particle shape can be changed by using a mercaptan stabilizer, which leads to rod-like iron colloids. The thermal decomposition of iron pentacarbonyl in a mixture of decalin and sarkosyl-O (*n*-oleyoyl sarcosine) has been studied by Moessbauer spectroscopy. With the X-ray diffraction it was shown that the sample contained small particles of a metallic glass (amorphous material). Annealing of the particles at 523 K resulted in crystallization of the particles into a mixture of α-Fe and Fe_5C_2 [44]. Fe^{2+} was found in all samples. After some time of reaction, a new iron carbonyl complex appeared. During the final stages of the reaction, this intermediate carbonyl complex decomposed, and ultrafine particles of an amorphous $Fe_{100-x}C_x$ alloy were formed [45]. Moessbauer spectroscopy also showed that the Fe-NPs with $r = 5.3$, 6.9 and 8.2 nm are dominated by the broadened sextuplet with $H_{eff} = 262$ kOe similar to that found in the sarcosyl and oleic acid stabilized colloids. This hyperfine field characterizes $Fe_{1-x}C_x$ species with $x \approx 0.25$ by comparison with sputtered amorphous $Fe_{1-x}C_x$ films [49]. In addition, a small contribution of a sextuplet with $H_{eff} = 496$ kOe characterizing an Fe(III) oxidic contribution is visible in the spectra of the Fe-NPs with $r = 5.3$ and 6.9 nm. This Fe(III) oxidic contribution is absent for the largest NP with $r = 8.2$ nm, while the spectrum of the NPs with the smallest radius ($r = 2.1$ nm) turned out to be completely oxidic [47].

Huh et al. combined a thermal decomposition of metal carbonyls with a collision induced clustering. Metal carbonyls $Fe(CO)_5$ and $Mo(CO)_6$ were thermally decomposed with a hot filament and the resultant bare metal atoms underwent collisions to produce high purity Fe, Mo, and alloy Fe/Mo nanometer size metal particles [50].

By thermal decomposition of $Fe(CO)_5$ with simultaneous reduction of platinum acetylacetonate $Pt(acac)_2$ in the presence of oleic acid and oleyl amine Sun, Murray et al. synthesized monodisperse iron–platinum nanoparticles [51]. Chen and Nikles used this procedure for the preparation of FePd and FeCoPt alloy nanoparticles with very narrow size distribution, using $Fe(CO)_5$, $Pd(acac)_2$ or $Pt(acac)_2$ and $Co(acac)_2$ [52,53].

Puntes et al. reported the synthesis of monodisperse ε-Co nanoparticles with spherical shapes and sizes ranging from 3 to 17 nm by the rapid pyrolysis of a dicobalt octacarbonyl solution in dichlorobenzene in the presence of a surfactant mixture composed of oleic acid, lauric acid and trioctylphosphine. The size distribution and the shape of the nanocrystals were controlled by varying the surfactant (oleic acid, phosphonic oxides and acids, etc.) its concentration, and the reaction temperature [54].

Hyeon et al. utilized a high-temperature (300 °C) aging of an iron-oleic acid metal complex, which was in turn prepared by the thermal decomposition of iron pentacarbonyl in the presence of oleic acid at 100 °C to generate monodisperse iron nanoparticles. The Fe-NP particle size ranged from 4 to 20 nm. The resulting iron nanoparticles were then transformed to monodisperse γ-Fe_2O_3 nanocrystallites by controlled oxidation using trimethylamine oxide as a mild oxidant [55]. With a similar procedure Kim, Hyeon et al. prepared cobalt nanoparticles from $Co_2(CO)_8$, oleic acid, trioctylphosphine and dioctyl ether under reflux. The Co-NPs were applied as recyclable catalysts for Pauson–Khand reactions, which involve the cycloaddition of alkynes, alkenes and carbon monoxide to cyclopentenones [56].

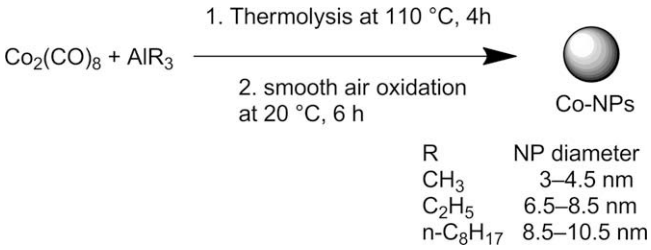

Scheme 4. Thermolysis of $Co_2(CO)_8$ in the presence of aluminium alkyls to Co-NPs and smooth air oxidation for surface passivation.

Burke et al. prepared polymer-coated iron nanoparticles by the thermal decomposition of $Fe(CO)_5$ in the presence of ammonia and polymeric dispersants [57]. The dispersants consist of polyisobutylene (PIB), polyethylene, or polystyrene chains functionalized with tetraethylenepentamine, a short polyethyleneimine chain. Inorganic-organic core–shell nanoparticles were formed with all three types of dispersants. With the PIB dispersants, the particle size is determined, in part, by the iron pentacarbonyl loading, increasing from 8 ± 1 nm for a 1:1 $Fe(CO)_5$/dispersant ratio to 20 ± 4 nm for a 5.5:1 ratio [57].

Rutnakornpituk et al. use copolymers as micelles in toluene to serve as nanoreactors for the thermal decomposition of $Co_2(CO)_8$ to superparamagnetic Co-NP dispersions. The steric stabilizers are poly[dimethylsiloxane-*b*-(3-cyanopropyl)methylsiloxane-*b*-dimethylsiloxane] (PDMS-PCPMS-PDMS) triblock copolymers in poly(dimethylsiloxane) carrier fluids. The nitrile groups on the PCPMS central blocks are thought to adsorb onto the particle surface. The Co-NP size could be controlled by adjusting the Co-to-copolymer ratio. TEM showed non-aggregated Co-NPs with narrow size distributions and evenly surrounded by the copolymer sheaths [58].

Diana et al. synthesized cobalt nanoparticles within inverse micelles of polystyrene-*block*-poly(2-vinylpyridine) copolymer in toluene by the pyrolysis of $Co_2(CO)_8$ at 115 °C [59]. The nanoparticle structure at different reaction times was investigated using transmission electron microscopy and Fourier transform infrared spectroscopy (FT-IR). At early reaction stages, the nanoparticles were noncrystalline from TEM; and FT-IR showed that the precursor was only partially decomposed. After 15 min of reaction, the nanoparticles became crystalline, forming chains due to magnetic interactions. The noncrystalline nanoparticles could be crystallized upon heating to 420 °C on grids in the transmission electron microscope. This produced nearly monodisperse single nanocrystals inside each micelle, with limited aggregation, but such annealing led to the degradation of the polymer [59].

Bönnemann et al. obtained monodisperse Co, Fe, and FeCo nanoparticles through thermal decomposition of the metal carbonyls $Co_2(CO)_8$, $Fe(CO)_5$ or $Fe(CO)_5/Co_2(CO)_8$ in the presence of aluminium alkyls (AlR_3), as air-stable magnetic metal nanoparticles after surface passivation [60–63]. After decomposition the metal particles were treated with synthetic air through a thin capillary (*smooth oxidation*) (Scheme 4) to yield particles stable in air under ambient conditions for over 1 year, as confirmed by magnetic measurements.

The aluminium alkyl acts as a catalyst, activating the thermal decomposition of the metal carbonyl as well as the surface

passivation during the *smooth oxidation*. The resulting particles strongly depend on the alkyl chain length *R* of the aluminium alkyl and the $Co_2(CO)_8$ to AlR_3 ratio. Monodisperse Co nanoparticles, 3–4.5, 6.5–8.5 and 8.5–10.5 nm in diameter, were obtained for $Al(CH_3)_3$, $Al(C_2H_5)_3$ and $Al(C_8H_{17})_3$, respectively. The particles were characterized by electron microscopy (SEM, TEM), electron spectroscopy (MIES, UPS, and XPS) and X-ray absorption spectroscopy (EXAFS). EXAFS measurements showed that this preparation pathway provides long-term stable zerovalent magnetic cobalt particles [62]. The chemical nature of the surfactant used exerts a significant influence on the stability and the local electronic and geometric structure of the analyzed nanoparticles [61]. With the help of surfactants, for instance oleic acid or cashew nut shell liquid, the metal particles can be peptized in organic solvents like toluene or kerosene, resulting in magnetic fluids. The saturation of magnetization, *Ms*, of the fluids was determined by specific magnetization. The sizes and structure of the particles were investigated by transmission electron microscopy, and Moessbauer analysis showed that the core of the particles was metallic or alloyed, respectively. The particle surface termination was studied by X-ray photoelectron and Auger electron spectroscopy [61]. The particles were also peptized by surfactants to form stable magnetic fluids in various organic media and water, exhibiting a high volume concentration and a high saturation magnetization. In view of potential biomedical applications of the particles, several procedures for surface modification are possible, including peptization by functional organic molecules, silanization, and *in situ* polymerization [62]. Other procedures for surface modification of these pre-stabilized, metallic Co-NPs include direct anchoring of surface-active functional groups and biocompatible dextran layers as well as silica and polymer coatings. As a result, individually coated nanoparticles as well as microspheres can be obtained [63].

Yin et al. (2004) formed a Pt@CoO yolk–shell nanostructure in which a platinum nanocrystal of a few nanometers was encapsulated in a CoO shell [64]. This was achieved by first reducing platinum acetylacetonate with a longchain polyol to form uniform platinum nanoparticles in the presence of surfactants such as oleic acid, oleylamine, and trioctylphosphine. The size of the platinum particles was tuned from 1 to 10 nm, depending on the concentration of surfactants. $Co_2(CO)_8$ was then injected into the hot solution and decomposed to form a conformal coating on the platinum nanocrystals. Oxidation of the Pt@Co nanocrystals was performed a few minutes after introduction of the cobalt carbonyl by blowing a stream of O_2/Ar mixture into the colloidal solution at 455 K [64].

Zubris et al. describe the synthesis of iron and cobalt alloy nanoparticles by the co-decomposition of iron and cobalt carbonyl precursors in the presence of polystyrene as a surface stabilizing agent [65]. The decomposition kinetics of $Fe(CO)_5$ and $Co_2(CO)_8$ were established and controlled. The results suggest that $Fe(CO)_5$ decomposition is a higher-order process (not first-order as previously assumed), with a complicated intermediate mechanism. Equal initial concentrations of both precursors generated nanoalloys with a crystalline core–shell dense morphology, while precursor concentrations corresponding to initial equal rates of decomposition generated polycrystalline nanoalloys with a diffuse morphology [65].

Korth et al. synthesized polystyrene (PS)-coated cobalt nanoparticles by the thermolysis of $Co_2(CO)_8$ in the presence of end-functional polymeric surfactants in refluxing 1,2-dichlorobenzene [66]. A mixture of amine and phosphine oxide PS surfactants (4:1 wt ratio) was used in the thermolysis of $Co_2(CO)_8$ to prepare polymer-coated cobalt nanoparticles, where the ligating end group passivated the colloidal surface. The combination of both amine and phosphine oxide ligands on the PS chain was necessary to yield uniform ferromagnetic nanoparticles. These polymer-coated cobalt nanoparticles (PS-Co) were then characterized using TEM, atomic force microscopy (AFM), and magnetic force microscopy (MFM) to determine particle size and morphology of magnetic colloids and nanoparticle chains [66].

It is obvious that the use of metal carbonyls for M-NP preparation will also be noted in the patent literature. An example is given by Mercuri, describing "a process for producing nano-scale metal particles which includes feeding at least one metal carbonyl into a reactor vessel; exposing the metal carbonyl to a source of energy sufficient to decompose the metal carbonyl to produce nano-scale metal particles; and depositing or collecting the metal nanoparticles. Oxygen is fed into the reactor vessel to partially oxidize the nanoscale metal particles produced by decomposition of the decomposable moiety. The nanoscale metal particles are then brought onto an end-use substrate which are intended to be employed, such as the aluminium oxide or other components of an automotive catalytic converter, or the electrode or membrane of a fuel cell or electrolysis cell" [67,68].

Gergely et al. describe "a process for preparing superparamagnetic transition metal nanoparticles by introducing into a gas stream a hydrocarbon and a transition metal carboxyl wherein the transition metal carbonyl is introduced downstream from the hydrocarbon; wherein at the point of introduction of the hydrocarbon the gas stream is as a plasma, and wherein at the point of introduction of the transition metal carbonyl the gas stream is at a temperature of at least 1000 °C, followed by quenching to form C-coated transition metal nanoparticles; and wherein the gas stream consists essentially of at least one inert gas and H" [69].

Gürler et al. showed that hydroxyfunctional cobalt nanoparticles can be obtained in a single step by thermal decomposition of $Co_2(CO)_8$ in the presence of ricinolic acid as a functional surfactant. The chemisorbed ricinolic acid through the carboxylic acid group served to introduce hydroxyl groups that serve as an initiator for the ring-opening polymerization of 3-caprolactone to give the desired hybrid cobalt/polycaprolactone brush particles [70].

Doan et al. investigated the oxidation of Co nanoparticles stabilized with various ligands in an autoclave [71]. Tridodecylamine stabilized Co nanoparticles with different sizes (8, 22 and 36 nm) were prepared by thermal decomposition of $Co_2(CO)_8$ in dodecane. The oxidation of the particles was studied by introducing oxygen into the autoclave and following the oxygen consumption with a pressure meter. Tridodecylamine capped particles were initially oxidized at a high rate, however, the oxidation layer quickly inhibited further oxidation. The thickness of the oxide layer estimated from the oxygen consumption was 0.8 nm for all three particle sizes showing that the oxidation is size independent in the studied particle size range. The tridodecylamine ligand was exchanged for various long chain carboxylic acids followed by subsequent oxidation. With the carboxylic acids the formed oxide layer does not inhibit further oxidation as effectively as in the case of tridodecylamine. TEM studies show that tridodecylamine capping leads to particles with a metal core surrounded by an oxide layer, while particles capped with long chain carboxylic acids form hollow cobalt oxide shells [71].

Howard and coworkers used a carbonyl metallate $Na_2Fe(CO)_4$ (Collman's reagent) and $Pt(acac)_2$ to synthesize bimetallic fcc and face-centered tetragonal (fct) FePt nanoparticles in hydrocarbon solvents with the size of 3 nm stabilized by oleic acid [72].

Another way to generate bimetallic FePt nanoparticles is the decomposition of the bimetallic cluster $Pt_3Fe_3(CO)_{15}$ by sonication in toluene, oleic acid and oleylamine. The resulting nanoparticles had a size of 2 nm [73].

Robinson et al. used the bimetallic carbonyl metallate cluster anions $[FeCo_3(CO)_{12}]^-$, $[Fe_3Pt_3(CO)_{15}]^{2-}$, $[FeNi_5(CO)_{13}]^{2-}$ and $[Fe_4Pt(CO)_{16}]^{2-}$ as precursors and obtained the bimetallic $FeCo_3$, FePt, $FeNi_5$ and Fe_4Pt, respectively, particles by thermal decompo-

sition in 1,2-dichlorobenzene with the average diameters of 7.0, 4.4, 2.6 and 3.2 nm, respectively. The size variation is due to the use of different stabilizers like oleic acid, myristic acid or hexadecyl amine [74].

The aforementioned examples together with reviews on the chemical synthesis of metal nanoparticles [36] illustrate the wide applicability of commercial $Fe(CO)_5$ and $Co_2(CO)_8$ for the preparation of iron- and cobalt-containing nanoparticles (additional examples are given in Table 2). Yet, it is also evident that the utilization of metal carbonyls in nanoparticle synthesis is largely limited to these two carbonyl compounds. This may in part be due to the strong interest in magnetic M-NPs. It also becomes clear that the prepared M-NPs need a protecting layer to prevent aggregation to larger particles or oxidation.

4. Synthesis of metal nanoparticles (M-NPs) in ionic liquids (ILs)

Metal nanoparticles can be synthesized in ionic liquids [83] through chemical reduction [21,84–89] or decomposition [90–93], by means of photochemical reduction [94,95] or electro-reduction [96–98] of metal salts where the metal atom is in a formally positive oxidation state and by decomposition of metal carbonyls with zero-valent metal atoms [9,20,21,99] without the need of extra stabilizing molecules or organic solvents [6,11,13,100,101].

A myriad of M-NPs have been prepared in ILs from compounds with the metal in a formally positive oxidation state M^{n+}. Such M-NPs then include, for example, the main-group metals and metalloids Al [102], Te [103], and the transition metals Ru [104], Rh [87], Ir [105], Pt [106], Ag [84,107], Au [108] (cf. Table 3).

The inclusion of metal nanoparticles in the supramolecular ionic liquid network brings with it the needed electrostatic and steric (=*electrosteric*) stabilization through the formation of an ion layer forming around the M-NPs. The type of this ion layer, hence, the mode of stabilization of metal nanoparticles in ILs is still a matter of some discussion [13,109]. Aside from the special case of thiol-, ether-, carboxylic acid-, amino-, hydroxyl- and other functionalized ILs (see Scheme 5 and accompanying text) one could decide between IL-cation or -anion coordination to the NP surface. Schrekker and co-workers proposed electrostatic stabilization of a negatively charged surface of Au-NPs by parallel coordination mode of the imidazolium cation on the basis of surface-enhanced Raman spectroscopy (SERS) studies [110]. This proposal was supported by Alvarez-Puebla and co-workers who found a negative zeta potential of M-NPs prepared by chemical reduction processes which indicated a negative charge of such NPs in aqueous solutions [111].

According to DLVO (Derjaugin–Landau–Verwey–Overbeek) theory (see Section 5) [112], ILs provide an electrostatic protection in the form of a "protective shell" for M-NPs [100,113–117]. DLVO theory predicts that the first inner shell must be anionic and the anion charges should be the primary source of stabilization for the electrophilic metal nanocluster [112]. DLVO theory treats anions as ideal point charges. Real-life anions with a molecular volume would be better classified as "*electrosteric* stabilizers" meaning to combine both the *electro*static and the *steric* stabilization. However, the term "electrosteric" is contentious and ill-defined [118]. The stabilization of metal nanoclusters in ILs could, thus, be attributed to "extra-DLVO" forces [118] which include effects from the network properties of ILs such as hydrogen bonding, the hydrophobicity and steric interactions [2,119].

Density functional theory (DFT) calculations in a gas phase model favor interactions between IL anions, such as BF_4^-, instead of imidazolium cations and Au_n clusters ($n = 1, 2, 3, 6, 19, 20$). This suggests a Au···F interaction and anionic Au_n stabilization in fluorous

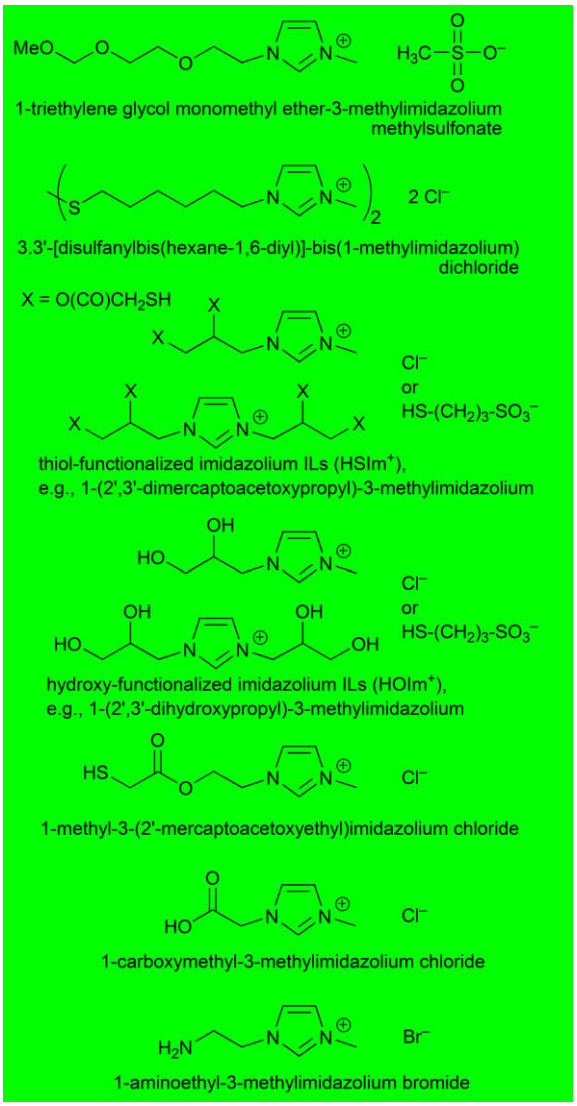

Scheme 5. Examples of functionalized imidazolium-ILs [108–110,124–126].

ILs. A small and Au-concentration dependent ^{19}F NMR chemical shift difference (not seen in ^{11}B- or ^1H NMR) for Au-NP/$BMIm^+BF_4^-$ supports the notion of a BF_4^--fluorine···Au-NP contact seen as crucial for the NP stabilization in dynamic ILs [120]. The DFT study used the binding energy (BE) of different IL-ions, free bases and the Cl^- anion to gold clusters of various sizes as a relative measure for the interaction strength.

The BE is defined as the difference of the relaxed energies of the gas phase anions and the Au_n clusters to the energy of their adduct (Eq. (1)) [120,121].

$$BE = E(\text{anion}) + E(Au_n) - E(\text{anion adduct to } Au_n) \quad (1)$$

Fig. 1 shows the Au_n–IL anion binding configurations and the variation of the BE with cluster size n. Fig. 2 illustrates Au_n–substrate binding configurations and the variation of the BE with cluster size n for BF_4^- in comparison with other common substrate ligands. The BE of $BMIm^+$ is very weak and not shown here (see in Refs. [120,121]). BE comparison with chloride, citrate, PH_3 and H_2O illustrates the critical influence of the ionic charge and electron delocalization from the ligand to Au_n (Fig. 2). The softer the anion or ligand, that is, the more charge transfer or electron delocalization (according to Pearsons hard-soft concept and the

Table 3
Examples of M-NPs prepared in ILs by chemical reduction.

Metal	Metal salt precursor	Reducing agent	IL[a]	M-NP size, average diameter (standard deviation) [nm]	Reference
Ru	Ru(COD)(COT)[b]	H_2	$BMIm^+Tf_2N^-$	0.9–2.4	[85]
	Ru(COD)(COT)[b]	H_2	$BMIm^+BF_4^-$, $BMIm^+PF_6^-$, $BMIm^+TfO^-$	2.6(4)	[104]
Rh	$RhCl_3{\cdot}3H_2O$	H_2	$BMIm^+PF_6^-$	2.0–2.5	[87]
	$[Rh(COD)\text{-}\mu\text{-}Cl]_2$[b]	H_2 + laser radiation	$BMIm^+PF_6^-$	7.2(1.3)	[127]
Ir	$[Ir(COD)Cl]_2$[b]	H_2	$BMIm^+BF_4^-$, $BMIm^+PF_6^-$, $BMIm^+TfO^-$	2–3	[128]
	$[Ir(COD)_2]BF_4$, $[Ir(COD)Cl]_2$[b]	H_2	1-alkyl-3-methyl-Im$^+BF_4^-$	Irregular 1.9(4), 3.6(9)	[89]
Pd	H_2PdCl_4	$NaBH_4$	$HSCO_2Im^+Cl^-$[c]	Nanowires	[125]
	$PdCl_2$	H_2 + laser radiation	$BMIm^+PF_6^-$	4.2(8)	[127]
	$Pd(acac)_2$	H_2	$BMIm^+PF_6^-$	10(2)	[91]
Pt	$Na_2Pt(OH)_6$	$NaBH_4$	$HSIm^+A^-$ or $HOIm^+A^-$[d]	3.2(1.1), 2.2(2), 2.0(1)	[124]
	H_2PtCl_6	$NaBH_4$	$CMMIm^+Cl^-$[e], $AEMIm^+Br^-$[f]	2.5	[109]
	PtO_2	H_2	$BMIm^+BF_4^-$, $BMIm^+PF_6^-$	2–3	[129]
Ag	$AgBF_4$	H_2	$BMIm^+BF_4^-$	2.8	[85]
			$BMIm^+PF_6^-$	4.4	[85]
			$BMIm^+TfO^-$	8.7	[85]
			$BtMA^+Tf_2N^-$	26.1	[85]
Au	$KAuCl_4$	$SnCl_2$	$BMIm^+BF_4^-$	2.6–200	[121]
	$HAuCl_4$	Na_3citrate/$NaBH_4$	$EMIm^+EtSO_4^-$	9.4	[131]
		Na_3citrate	$EMIm^+EtSO_4^-$	3.9	[131]
		Ascorbic acid	$EMIm^+EtSO_4^-$	Nanorods	[131]
	$HAuCl_4{\cdot}3H_2O$	$H_2NNH_2{\cdot}H_2O$ (hydrazine monohydrate)	$TriMIm^+MeSO_3^-$[g]	~7.5	[110]
	$HAuCl_4$	$NaBH_4$	$ShexMIm^+Cl^-$[h]	5.0	[108]
	$HAuCl_4$	$NaBH_4$	$HSIm^+A^-$ or $HOIm^+A^-$[d]	3.5(7), 3.1(5), 2.0(1)	[124]
	$HAuCl_4$	$NaBH_4$	$CMMIm^+Cl^-$[e], $AEMIm^+Br^-$[f]	3.5	[109]
	$HAuCl_4$	Na_3citrate	$CMMIm^+Cl^-$[e], $AEMIm^+Br^-$[f]	23–98	[109]
	$HAuCl_4$	Cellulose	$BMIm^+Cl^-$	300–800	[88]

[a] Common ILs: $BMIm^+BF_4^-$, $BMIm^+PF_6^-$, $BMIm^+TfO^-$ = 1-*n*-butyl-3-methylimidazolium tetrafluoroborate, hexafluorophosphate, trifluoromethylsulfonate, $BtMA^+Tf_2N^-$ *n*-butyl-trimethylammonium bis(trifluoromethylsulfonyl)amide (cf. Scheme 2); $EMIm^+EtSO_4^-$ = 1-ethyl-3-methylimidazolium ethylsulfate.
[b] COD = 1,5-cyclooctadiene, COT = 1,3,5-cyclooctatriene.
[c] $HSCO_2Im^+Cl^-$ = 1-methyl-3-(2′-mercaptoacetoxyethyl)imidazolium chloride (cf. Scheme 5).
[d] $HSIm^+A^-$ = thiol-functionalized imidazolium ILs, e.g., 1-(2′,3′-dimercaptoacetoxypropyl)-3-methylimidazolium, $HOIm^+A^-$ = hydroxy-functionalized imidazolium ILs, e.g., 1-(2′,3′-dihydroxypropyl)-3-methylimidazolium, A^- = Cl^- or HS-$(CH_2)_3$-SO_3^- (cf. Scheme 5).
[e] $CMMIm^+Cl^-$ = 1-carboxymethyl-3-methylimidazolium chloride (cf. Scheme 5).
[f] $AEMIm^+Br^-$ = 1-aminoethyl-3-methylimidazolium bromide (cf. Scheme 5).
[g] $TriMIm^+MeSO_3^-$ = 1-triethylene glycol monomethyl ether-3-methylimidazolium methylsulfonate (cf. Scheme 5).
[h] $ShexMIm^+Cl^-$ = 3.3′-[disulfanylbis(hexane-1,6-diyl)]-bis(1-methylimidazolium) dichloride.

nephelauxetic series) [122] to Au_n is possible, the better the stabilizing effect. H_2O as a hard and neutral ligand offers the least stabilization, hence, reduction of gold salts by $SnCl_2$ in water led immediately to the red purple solution (known as the Purple of Cassius). Remarkably, the relatively soft chloride anion shows the largest BE in agreement with the strong covalent binding of chloride ions to the Au(1 1 1) surface found in recent DFT simulations [123].

The DFT calculations also indicate a weak covalent part in this Au···F interaction. Free imidazole bases (e.g., 1-methylimidazole) show similar binding energies. The Cl^- anions have the highest binding energy and can therefore be expected to bind to the NP if present in the solution. At the same time no significant binding of the $BMIm^+$ or MIm^+ imidazolium cations is found. These findings support the model of preferred interaction between anions and Au-NPs, but also confirm the importance to consider a possible presence of Cl^- anions in the ionic liquid solution [120,121].

Compared with the non-functionalized imidazolium-ILs (cf. Scheme 2), functionalized imidazolium-ILs stabilize aqueous dispersed metal NPs much more efficiently because of the special functional group. Thiol-functionalized [108,124,125], ether-functionalized [110], carboxylic acid-functionalized [109], amino-functionalized [109,126], and hydroxyl-functionalized [124] imidazolium-ILs (Scheme 5) have been used to synthesize aqueous dispersed noble, primarily gold metal NPs.

4.1. Chemical reduction

The reduction of metal salts is the most utilized method to generate NPs in solution and also in ILs in general. Many different types of reducing agents are used, like gases (H_2), organic (citrate, ascorbic acid, imidazolium cation of IL) and inorganic ($NaBH_4$, $SnCl_2$) agents (Table 3).

Molecular hydrogen (H_2) is often taken as clean reductant. Dupont et al. used $RhCl_3{\cdot}3H_2O$ as a precursor in $BMIm^+PF_6^-$ for the formation of Rh-NPs. For Ir-NPs the precursor $[Ir(COD)Cl]_2$ (COD = 1,5-cyclooctadiene) was reduced with H_2. The formation to M-NPs was carried out at 75 °C and 4 bar hydrogen pressure. Transmission electron microscopy (TEM) analysis showed the particle sizes of 2.0–2.5 nm [87]. Redel et al. used hydrogen and $AgBF_4$ for the synthesis of Ag-NPs in different ILs. A correlation between the IL-anion molecular volume and the NP size was noted. The larger the volume of the IL-anion the larger is the size of the Ag-NPs. Thereby it was possible to form Ag-NPs in sizes from 2.8 to 26.1 nm with a narrow size distribution [84].

Different researchers used hydrogen as a reagent not to reduce the metal but to reduce (hydrogenate) the ligands COD and COT (COT = 1,3,5-cyclooctatriene) of an Ru(0) organometallic precursor [85,104]. They dissolved Ru(COD)(COT) in imidazolium based ILs and heated the mixture under 4 bar of hydrogen under different conditions. Both organic ligands were reduced to cyclooctane and thereby dissociate from the already zero-valent metal atom. Cyclooctane can then be removed under reduced pressure.

It is also possible to use less-noble metals for the reduction of noble metals. The reduction of $KAuCl_4$ by $SnCl_2$ leads to the formation of Au-NPs [121]. By variation of the molar Au(III):Sn(II) ratio it was possible to synthesize Au-NPs in different sizes in a stop-and-go, stepwise and "ligand-free" nucleation, nanocrystal growth process which can be stopped and resumed at different color steps

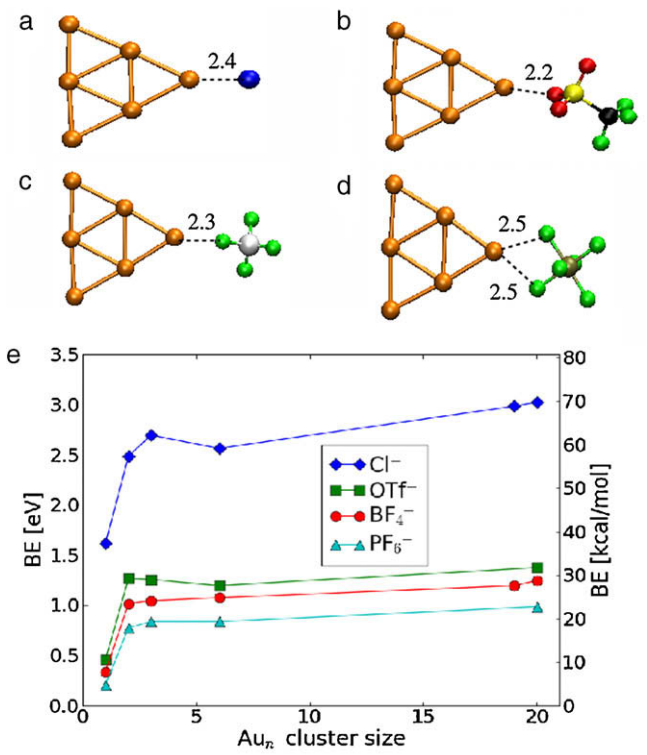

Fig. 1. Relaxed configurations of Au_6 bound to (a) Cl^-, (b) TfO^-, (c) BF_4^- and (d) PF_6^-. The bond lengths are given in Å. (e) Binding energy. All the anions show a similar behavior in their BE: the BE to a single gold atom $n = 1$ is quite low and more than doubles for Au_2 ($n = 2$). Increasing the cluster size to $n = 20$ does not change the BE substantially anymore, i.e., the BE is already saturated for Au_2. The chloride anion shows the largest BE of all anions and can, hence, be expected to be bound to the clusters if it is present in the dispersion [120].

and Au-NP sizes from 2.6 to 200 nm. This stepwise Au-NP formation was possible because the IL apparently acted as a *kinetically* stabilizing, dynamic molecular network in which the reduced Au^0 atoms and clusters can move by diffusion and cluster together, as verified by TEM analysis [121].

A well-known method to generate Au-NPs was already established by Turkevich et al. in 1951 [130]. The reducing agent was citrate. Bockstaller and coworkers used this method and carried out the reduction in the imidazolium-based IL 1-ethyl-3-methylimidazolium ethyl-sulfate ($EMIm^+EtSO_4^-$). Afterwards it was possible to give these particles different shapes by adding Ag(I) [131].

Taubert et al. reacted $HAuCl_4$ with cellulose [88]. Thereby cellulose has two roles: first, cellulose is the reducing agent for Au(III). Second, cellulose acts as a morphology- and size-directing agent, which drives the crystallization towards polyhedral particles or thick plates. The gold particle morphologies and sizes mainly depend on the reaction temperature. With this route it was possible to synthesize plates with a thickness from 300 nm at 110 °C to 800 nm at 200 °C.

Gold nanoparticles of 1–4 nm size could be prepared by sputter deposition of the metal onto the surface of the ionic liquid $BMIm^+BF_4^-$ to generate nanoparticles in the liquid with no additional stabilizing agents [132]. Likewise, Au-NPs were prepared by sputter deposition of Au metal in $BMIm^+PF_6^-$. The size of Au nanoparticles was increased from 2.6 to 4.8 nm by heat treatment at 373 K [133]. Sputter deposition of indium in the ionic liquids $BMIm^+BF_4^-$, $EMIm^+BF_4^-$, (1-allyl)$MIm^+BF_4^-$ and (1-allyl)(3-ethyl)$Im^+BF_4^-$ could produce stable In metal nanoparticles whose surface was covered by an amorphous In_2O_3 layer to form In/In_2O_3 core/shell particles. The size of the In core was tunable from ca. 8 to 20 nm by selecting the IL [134].

Mudring and coworkers evaporated elemental Cu powder under high vacuum (10^{-6} torr) into the IL 1-butyl-3-methylimidazolium hexafluorophosphate and generated Cu nanoparticles with the size of 3 nm. Au nanoparticles were prepared with the same evaporation method. Depending on the different ILs which were used, nanoparticles from 4 to 50 nm were generated. This method made it also possible to produce Cu/ZnO nanocomposites [135].

Dupont et al. prepared Au-NPs with the size of 3–5 nm from gold foil by sputtering deposition onto several imidazolium-based ILs. [136].

In the presence of imidazolium-based ILs Pd-NPs from palladium(II) salts could be synthesized without the need for an additional reducing agent. It is suggested that formation of *N*-heterocyclic Pd-carbene complexes takes place as an intermediate preceding the formation of Pd-NPs (Scheme 6) which can then catalyze Suzuki C–C coupling reactions [92,137]. Pd-carbene complexes are able to catalyze the Heck reaction [138,139].

Deshmukh et al. used $Pd(OAc)_2$ or $PdCl_2$ in the imidazolium-based ILs BBImBr or $BBImBF_4$ to irradiate the mixtures with

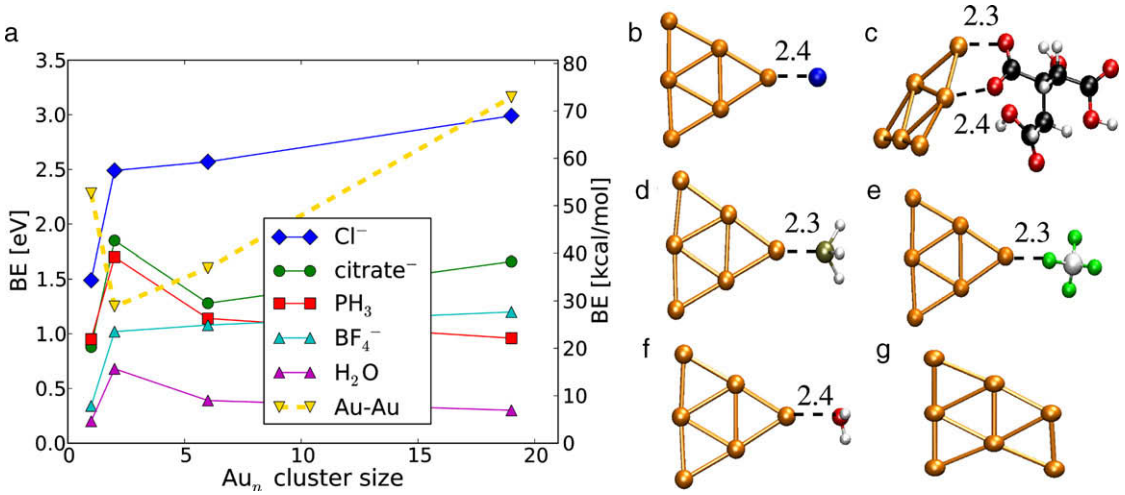

Fig. 2. (a) Binding energies (BE) and Au-atom addition energies depending on the cluster size. (b–f) Relaxed configurations of Au_6 bound to (b) Cl^-, (c) citrate$^-$ ($C_6H_7O_7^-$), (d) PH_3, (e) BF_4^- and (f) H_2O. (g) Relaxed configuration of Au_7. The bond lengths are given in Å [121].

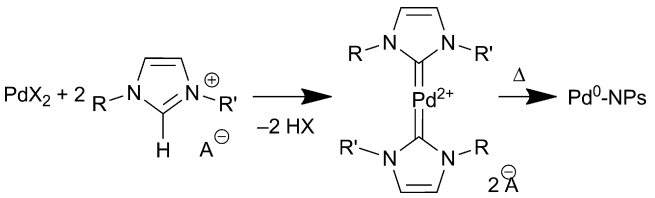

Scheme 6. Reduction of Pd(II)-species with an imidazolium-based IL through intermediate formation of Pd-carbene complexes. Decomplexation and reduction occurs during heating.

ultrasound for 1 h. The Pd-NPs were nearly spherical and a size of 20 nm was observed [92].

Anderson, Marr et al. formed Pd-NPs with a diameter of ~1 nm from $Pd(OAc)_2$ in $BMIm^+Tf_2N^-$ simply by heating to 80 °C in the presence of PPh_3 [93].

Ruta et al. synthesized monodisperse Pd nanoparticles of 5 and 10 nm through reduction of $Pd(acac)_2$ dissolved in the hydroxyl-functionalized butyl-3-methylimidazolium bis(trifluoromethylsulfonyl)amide IL $HOBMIm^+Tf_2N^-$ by simple heating in the absence of an additional reducing agent [91].

D/H exchange reactions at C2, C4 and C5 of the imidazolium cation in catalytic hydrogenation reactions promoted by classical Ir(I) colloid precursors and Ir-NPs in deuterated imidazolium ILs supported the participation of carbene species in this media [140].

Also by thermal decomposition, albeit from an Ni(0) source, Ni nanoparticles with 4.9(9) to 5.9(1.4) nm average diameter (standard deviation) were prepared from the bis(1,5-cyclooctadiene)nickel(0) organometallic precursor dissolved in 1-alkyl-3-methylimidazolium bis(trifluoromethylsulfonyl)amide ionic liquids [90].

Carboxylic acid- and amino-functionalized ionic liquids $CMMIm^+Cl^-$ = 1-carboxylmethyl-3-methylimidazolium chloride and $AEMIm^+Br^-$ = 1-aminoethyl-3-methylimidazolium bromide (cf. Scheme 5) were used as the stabilizer for the synthesis of gold and platinum metal nanoparticles in aqueous solution. Smaller Au-NPs (3.5 nm) and Pt-NPs (2.5 nm) were prepared with $NaBH_4$ as the reductant. Larger gold nanospheres (23, 42, and 98 nm) were synthesized using different quantities of trisodium citrate reductant. The morphology and the surface state of the metal nanoparticles were characterized by high-resolution transmission electron microscopy, UV–vis spectroscopy, and X-ray photoelectron. X-ray photoelectron spectra indicated that binding energies of C 1s and N 1s from ionic liquids on the surface of metal nanoparticles shifted negatively compared with that from pure ionic liquids. The mechanism of stabilization is proposed to be due to the interactions between imidazolium ions/functional groups in ionic liquids and metal atoms. The imidazolium ring moiety of ionic liquids might interact with the π-electronic nanotube surface by virtue of cation–π and/or π–π interactions, and the functionalized group moiety of ionic liquids might interact with the metal NPs surface [109].

4.2. Photochemical reduction

Photochemical methods for the synthesis of M-NPs present a rather clean procedure because contaminations by reducing agents are excluded.

Zhu et al. used $HAuCl_4{\cdot}4H_2O$ in a mixed solution of $BMIm^+BF_4^-$ and acetone (ratio 10:1) and irradiated the salt for 8 h with a UV light at a wavelength of 254 nm. The UV light turns the acetone into a free radical, which then reduces the cationic Au(III) to Au-NPs. The obtained Au nanosheets were about 4 μm long and 60 nm thick [94].

Firestone et al. used this route to form Au-NPs from $HAuCl_4$ in the IL 1-decyl-3-methyl-imidazolium chloride in water. The irradiation was carried out with 254 nm UV light for 30–70 min. The obtained Au-NPs were analyzed by scanning electron microscopy (SEM). The nanorods had different shapes and morphologies. The sizes varied between 100 and 1000 nm [95].

Harada et al. used a high-pressure mercury lamp to irradiate $AgClO_4$ in a mixture of an IL, water and Tween 20 (polyoxyethylene sorbitan monolaurate). Benzoin was used as photoactivator. The average diameters of Ag-NPs prepared in water/$BMIm^+BF_4^-$ and water/$OMIm^+BF_4^-$ (1-octyl-3-methylimidazolium) microemulsions were 8.9 and 4.9 nm, respectively [141].

4.3. Electroreduction

Another clean route to prepare nanoparticles is electroreduction as only electrons are used as the reducing agent. It should be noted, however, that the size of the metal nanoparticles from electroreduction is often above the 100 nm definition limit for nanoparticles.

Imanishi et al. used a low-energy electron beam irradiation to synthesize Au-NPs from a $NaAuCl_4{\cdot}2H_2O$ precursor in the IL $BMIm^+Tf_2N^-$. The obtained particles had a large size of 122 nm [142].

It is also possible to deposit particles on supporting material. Roy et al. prepared Ag-NPs from $AgBF_4$ in $BMIm^+BF_4^-$ on TiO_2. The electroreduction was performed in the high vacuum chamber of a SEM. The resulting Ag-NPs arranged themselves in a dendritic network structure [143].

Fu et al. reduced graphene oxide (GO) and $HAuCl_4$ simultaneously in $BMIm^+PF_4^-$ at a potential of −2.0 V. The obtained Au-NPs on the electrochemical reduced graphene had a size of 10 nm [144].

El Abedin and Endres used Ag(TfO) as a source of silver. The precursor was electrochemically reduced in 1-ethyl-3-methylimidazolium trifluoromethylsulfonate, $EMIm^+TfO^-$. The prepared Ag nanowires were 3 μm long and 200 nm wide [145].

CuCl as precursor was used by Lu et al. and reduced in a cavity microelectrode in $BMIm^+PF_6^-$. The electrode potential was varied. The smallest particles had a size of 10 nm and were obtained at an electrode potential of −1.8 V [146].

4.4. Metal carbonyl precursors for metal nanoparticles in ILs

As pointed out in Section 3 metal carbonyls contain the metal atoms already in the zero-valent oxidation state needed for the metal nanoparticles. No reducing agent is necessary. The side product CO is largely given off to the gas phase and removed from the M-NP/IL dispersion. The M-NP synthesis in IL from $M_x(CO)_y$ is generally carried out without any additional stabilizers, surfactants or capping molecules which is different from the use of metal carbonyls for the M-NP syntheses described in Section 3. Metal carbonyls can be decomposed to metal nanoparticles in ILs by conventional thermal heating, UV-photolysis or microwave irradiation (MWI) (Fig. 3a–c).

ILs are an especially attractive media for microwave reactions and have significant absorption efficiency for microwave energy because of their high ionic charge, high polarity and high dielectric constant [18]. Microwave heating is extremely rapid. Microwaves are a low-frequency energy source that is remarkably adaptable to many types of chemical reactions [147]. Microwave radiation can interact directly with the reaction components: the reactant mixture absorbs the microwave energy and localized superheating occurs resulting in a fast and efficient heating time [148,149]. Using microwaves is a fast way to heat reactants compared with conventional thermal heating. Any presumptions about abnormal "microwave effects" [150–152] have been proven wrong in the

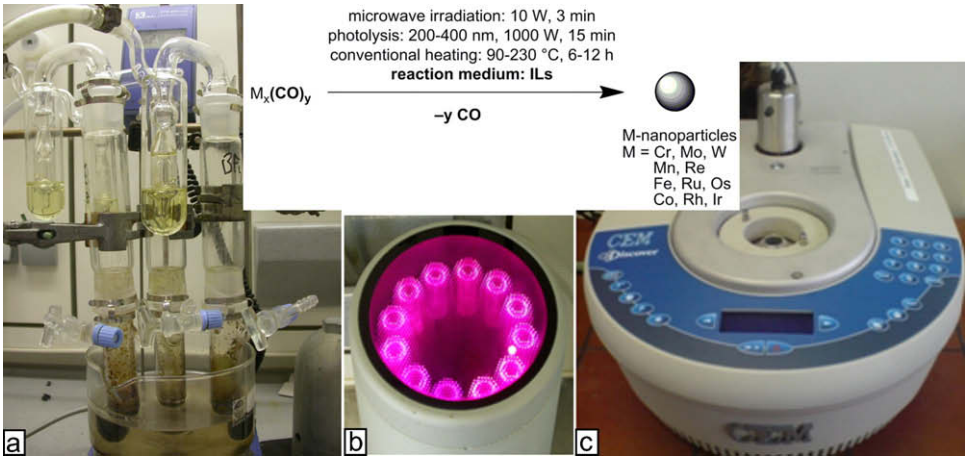

Fig. 3. (a) Setup for conventional thermal heating of $M_x(CO)_y$/IL dispersions under argon, (b) UV reactor, (c) commercial laboratory microwave reactor.

meantime [153,154]. Moreover, microwave reactions are also an "instant on/instant off" energy source, significantly reducing the risk of overheating reactions [147,148].

Metal nanoparticles (M-NPs) were reproducibly obtained by easy, rapid (3 min) and energy-saving 10 Watt microwave irradiation (MWI) under an argon atmosphere from their metal carbonyl precursors $M_x(CO)_y$ in ILs. This MWI synthesis was compared to UV-photolytic (1000 W, 15 min) or conventional thermal decomposition (180–250 °C, 6–12 h) of $M_x(CO)_y$ in ILs. The MWI-obtained nanoparticles have a very small (<5 nm) and uniform size and are prepared without any additional stabilizers or capping molecules as long-term stable M-NP/IL dispersions [characterization by transmission electron microscopy (TEM), transmission electron diffraction (TED) and dynamic light scattering (DLS)].

Stable chromium, molybdenum and tungsten nanoparticles could be obtained reproducibly by thermal or photolytic decomposition under argon from their mononuclear metal carbonyl precursors $M(CO)_6$ (M = Cr, Mo, W) suspended in the ionic liquids $BMIm^+BF_4^-$, $BMIm^+TfO^-$ and $BtMA^+Tf_2N^-$ (Scheme 7) [99]. Later an even more rapid and energy-saving decomposition could be achieved with a 10 W microwave irradiation for 3 min of 0.4 ml (0.48 g) of a $BMIm^+BF_4^-$ sample with a 0.5 wt.% M/IL-dispersion [21]. The resulting Cr-, Mo- and W-NPs were of very small and uniform size of 1–1.5 nm in $BMIm^+BF_4^-$ (Table 4) which increases with the molecular volume of the ionic liquid anion to ~30–100 nm in $BtMA^+Tf_2N^-$ (Fig. 4). Characterization was done by TEM, dynamic light scattering (DLS) and transmission electron diffraction (TED) analysis [99].

Complete $M(CO)_6$ decomposition from the short, 3 min microwave irradiation was verified by Raman spectroscopy with no (metal-)carbonyl bands between 1750 and 2000 cm^{-1} being observed any more after the microwave treatment (Fig. 5) [21].

Stable manganese and rhenium metal nanoparticles were reproducibly obtained by microwave irradiation or UV photolysis from their metal carbonyl precursors $M_2(CO)_{10}$ in the ionic liquid 1-butyl-3-methylimidazolium tetrafluoroborate ($BMIm^+BF_4^-$) (Scheme 8, Fig. 6, Table 4) [21].

Complete $M_2(CO)_{10}$ decomposition from the short, 3 min microwave irradiation was verified by Raman spectroscopy with no (metal-)carbonyl bands between 1750 and 2000 cm^{-1} being observed any more after the microwave treatment (Fig. 7) [21].

Stable iron, ruthenium and osmium nanoparticles are obtained reproducibly by microwave irradiation, photolytic or conventional thermal decomposition under argon atmosphere from $Fe_2(CO)_9$, $Ru_3(CO)_{12}$ or $Os_3(CO)_{12}$, dissolved in the ionic liquid $BMIm^+BF_4^-$ and with a very small and uniform size for Ru and Os nanoparticles of about 1.5–2.5 nm without any additional stabilizers or capping molecules (Scheme 9, Figs. 8–10, Table 4) [9,21].

Complete $M_x(CO)_y$ (M = Fe, Ru, Os) decomposition from the short, 3 min microwave irradiation was verified by Raman spectroscopy with no (metal-)carbonyl bands between 1750 and 2000 cm^{-1} being observed any more after the microwave treatment (Fig. 10) [21].

The Ru-NP/$BMIm^+BF_4^-$ and other M-NP/IL dispersions were active catalysts in the biphasic liquid–liquid hydrogenation of cyclohexene or benzene to cyclohexane. Even a remarkable partial hydrogenation of benzene to cyclohexene could be achieved with

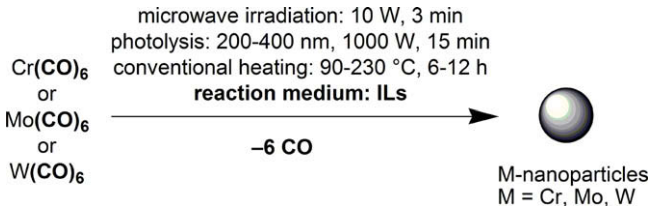

Scheme 7. Formation of Cr, Mo and W nanoparticles by microwave, photolytic or thermal decomposition of metal carbonyls $M(CO)_6$ under argon in ionic liquids [21,99].

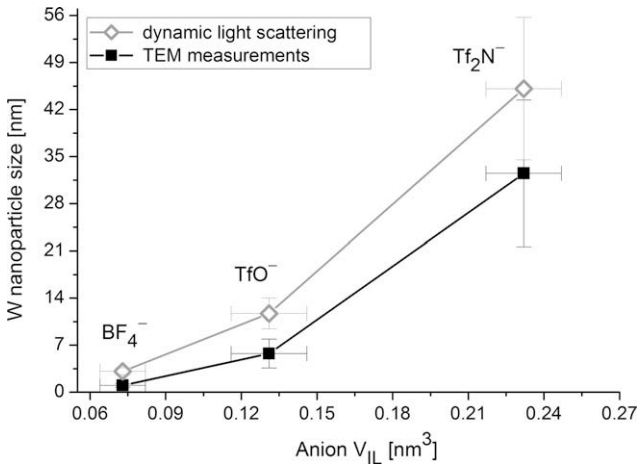

Fig. 4. Correlation between the molecular volume of the ionic liquid anion (V_{IL}) and the observed W nanoparticle size with standard deviations as error bars (from TEM and dynamic light scattering). IL anions range from BF_4^- (smallest) over trifluoromethylsulfonate (triflate, $CF_3SO_3^-$, TfO^-) to the largest bis(trifluoromethylsulfonyl)amide [$(CF_3SO_2)_2N^-$, Tf_2N^-] [99].

nd Ir) size and size distribution in $BMIm^+BF_4^-$ [21].[a]

Microwave decomposition[b]		Photolytic decomposition[c]		Conventional thermal decomposition[d]	
TEM NP diameter/nm (standard deviation σ)	Dynamic light scattering NP median diameter[e]/nm (standard deviation σ)	TEM NP diameter/nm (standard deviation σ)	Dynamic light scattering NP median diameter[e]/nm (standard deviation σ)	TEM NP diameter/nm (standard deviation σ)	Dynamic light scattering NP median diameter[e]/nm (standard deviation σ)
≤1.5 (±0.3)[f]	3.8 (±0.8)	4.4 (±1.0)	7.1 (±0.3)	≤1.5 (±0.3)[g]	3.0 (±0.6)[g]
~1–2	4.5 (±0.8)	~1–2[g]	3.8 (±1.1)[g]	≤1.5 (±0.3)[g]	2.5 (±0.6)[g]
3.1 (±0.8)	5.2 (±1.2)	<1	10.8 (±0.5)	≤1.5 (±0.3)[g]	3.1 (±0.5)[g]
12.4 (±3)[h]	29 (±5.0)[h]	<1	2.5 (±0.8)	–	–
2.4 (±0.9)	5.7 (±1.4)	<1	7.2 (±2.2)	–	–
8.6 (±3.2)[i]	12.8 (±0.6)[i]	7.0 (±3.1)[i]	12.5 (±0.5)[i]	5.2 (±1.6)[g]	10.1 (±2.1)[g]
(a) 1.6 (±0.3) (b) 1.6 (±0.3)[j]	(a) 3.2 (±0.8) (b) 3.2 (±0.8)[j]	2.0 (±0.5)[g]	3.9 (±1.0)[g]	1.6 (±0.4)[g]	2.9 (±0.5)[g]
0.7 (±0.2)	2.8 (±0.7)	2.0 (±1.0)	2.1 (±0.4)	2.5 (±0.4)[g,k]	5.6 (±1.5)[l]
5.1 (±0.9)	20 (±3)	8.1 (±2.5)	12.6 (±0.4)	14 (±8)[g]	–
(a) 1.7 (±0.3) (b) 1.7 (±0.3)[j]	3.7 (±0.6) 3.4 (±0.5)[j]	1.9 (±0.3)	5.5 (±0.4)	3.5 (±0.8)[g]	7.0 (±1.2)[g]
0.8 (±0.2)	3.3 (±0.9)	1.4 (±0.3)	4.1 (±1.2)	(a) 1.1 (±0.2)[g] (b) 1.3 (±0.2)[g,m]	4.1 (±0.7)[g]3.4 (±1.0)[g,m]

re for a single TEM or DLS experiment. Reproducibility of the particle size and distribution was insured by selected repeated TEM experiments and especially by DLS which was n reactions. Solubility of metal carbonyl precursors in $BMIm^+BF_4^-$ is limited to a maximum value of about 1 wt.% M.

ls with 10 W for 3 min unless mentioned otherwise.

s with a 1000 W Hg lamp (200–450 nm wavelength) for 15 min.

rom 6 to 12 h with 180–230 °C depending on the metal carbonyl.

n the first three measurements at 633 nm. Only the first three scans are somewhat reliable, because the laser light used for the measurements induces clustering of the nanoparticles mic radius is roughly 2–3 times the size of the pure kernel cluster. For very small M-NPs (~1 nm) the size of the hydrodynamic radius can even increase to more than 3 times the nt is 0.6 nm.

ter of less than 1.5 nm show electron dense cloudy structures due to scattering by the surrounding IL so that resolution of the TEM is limited and particles below 1.5 nm are hardly

he other metal carbonyls which came as fine powders. Also upon grinding in a mortar, $Mn_2(CO)_{10}$ could not be as finely powdered as the other metal carbonyls.

the microwave and photolytic decomposition of $Fe_2(CO)_9$ show the presence of iron oxide, Fe_2O_3. Because of the experimental setup rigorous air exclusion is more difficult during orkup.

ls with 10 W for 10 min.

$_2$ in $BMIm^+BF_4^-$.

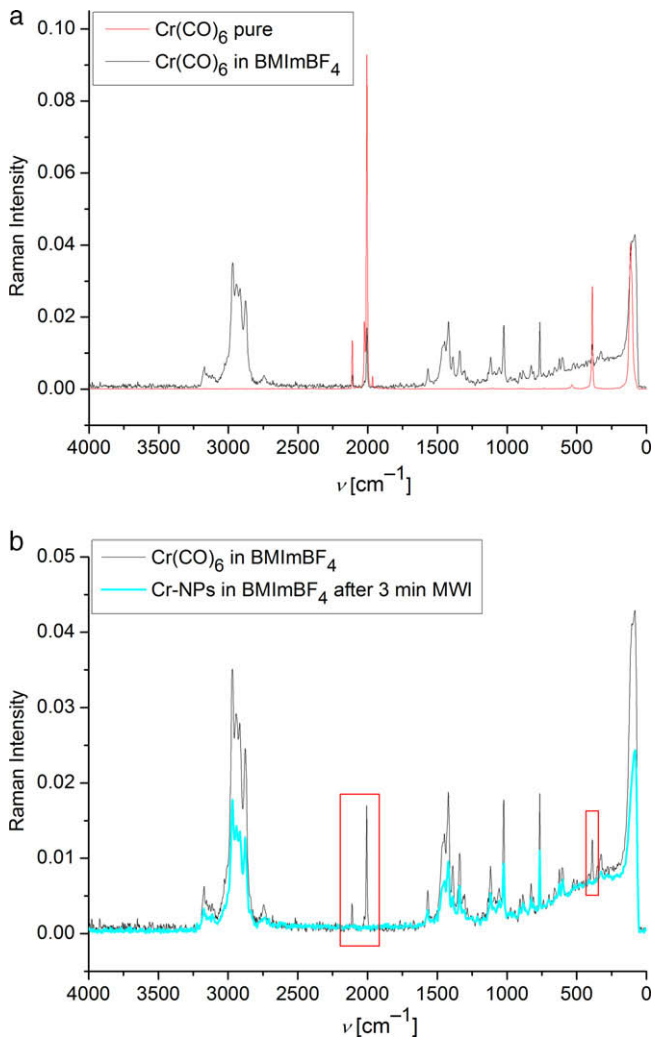

Fig. 5. Raman-FT spectra. Top: pure $Cr(CO)_6$ and $Cr(CO)_6$ in $BMIm^+BF_4^-$; bottom: $Cr(CO)_6$ in $BMIm^+BF_4^-$ before and after 3 min 10 W microwave irradiation (MWI). Red boxes highlight the indicative chromium carbonyl bands [21].

Ru-NP/$BMIm^+PF_6^-$ dispersions [105]. The low miscibility of substrates and products with the IL phase allows for easy separation by simple decantation of the hydrophobic phase [19]. The hydrogenation reaction of cyclohexene was run at 90 °C and 10 bar H_2 to 95% conversion where the reaction was intentionally stopped as thereafter the decrease in cyclohexene concentration lowered the reaction rate (Fig. 11) [21].

Silva, Dupont et al. have prepared cobalt nanoparticles with a size of around 7.7 nm by the decomposition of $Co_2(CO)_8$ in 1-alkyl-3-methylimidazolium Tf_2N^- ionic liquids at 150 °C. These Co-NPs were effective catalysts for the Fischer–Tropsch (FT) synthesis,

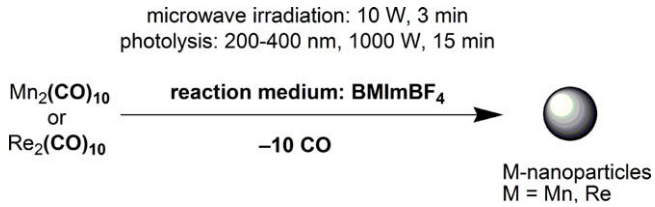

Scheme 8. Formation of Mn and Re nanoparticles by microwave, photolytic or thermal decomposition of the metal carbonyls $M_2(CO)_{10}$ under argon in the IL $BMIm^+BF_4^-$ [21].

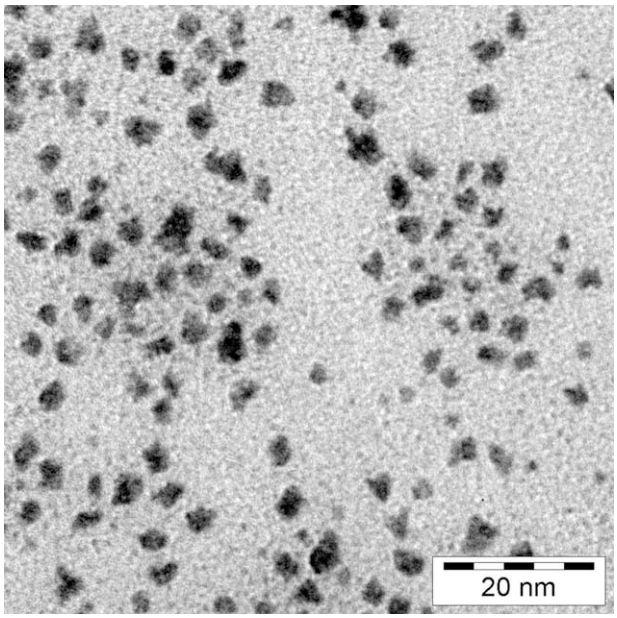

Fig. 6. TEM photograph of Re-NPs from $Re_2(CO)_{10}$ by MWI (Ø 2.4 (±0.9) nm, entry 5 in Table 4) [21].

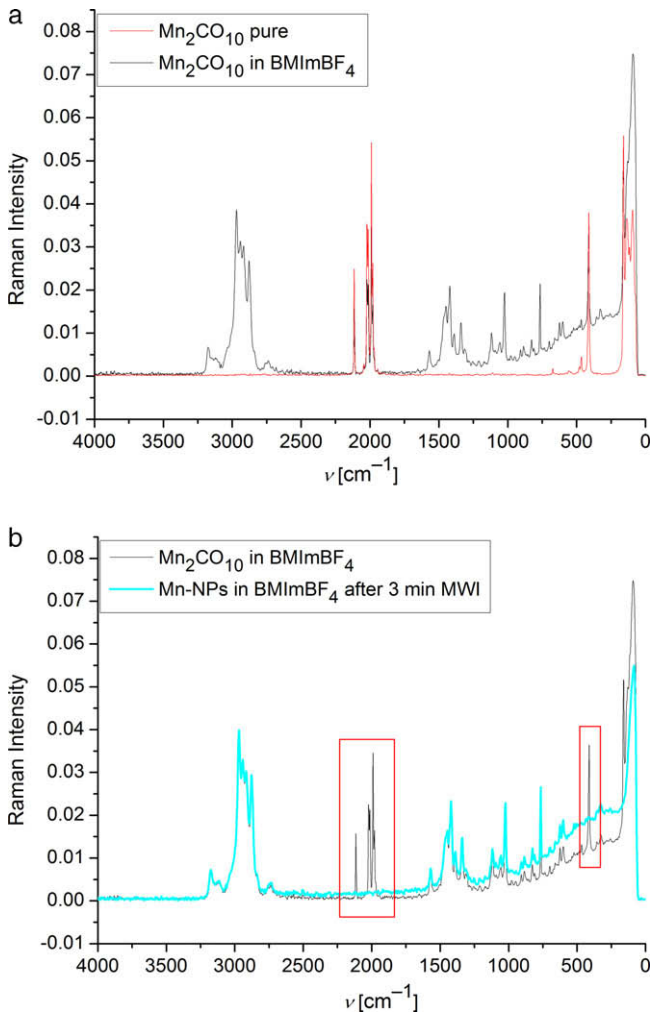

Fig. 7. Raman-FT spectra. Top: pure $Mn_2(CO)_{10}$ and $Mn_2(CO)_{10}$ in $BMIm^+BF_4^-$; bottom: $Mn_2(CO)_{10}$ in $BMIm^+BF_4^-$ before and after 3 min 10 W microwave irradiation (MWI). Red boxes highlight the indicative manganese carbonyl bands [21].

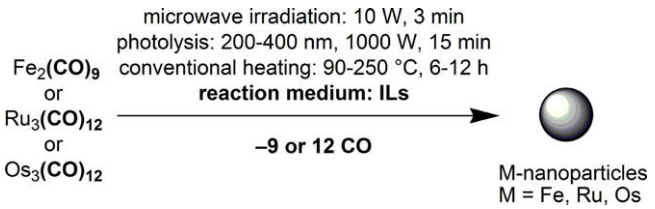

Scheme 9. Formation of Fe, Ru and Os nanoparticles by microwave, photolytic or thermal decomposition of metal carbonyls $M_x(CO)_y$ under argon in the IL $BMIm^+BF_4^-$ [9,21].

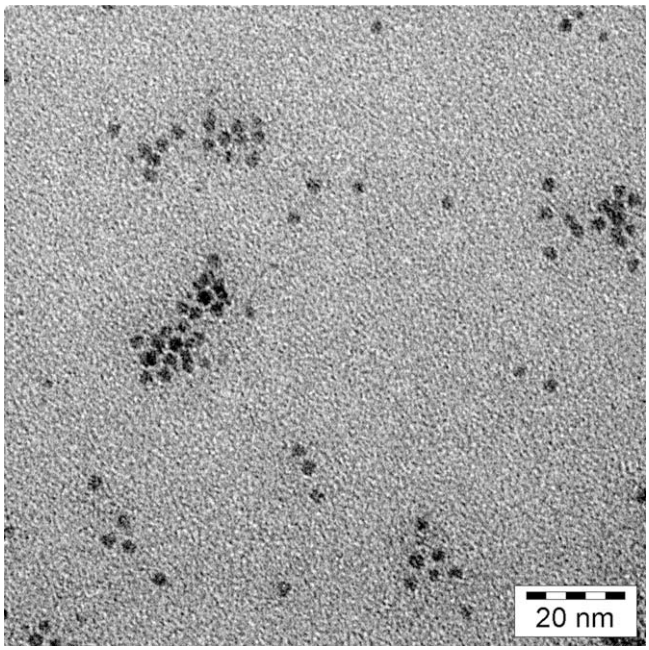

Fig. 8. TEM photograph of Ru-NPs from $Ru_3(CO)_{12}$ by photolytic decomposition (0.08 wt.% Ru in $BMIm^+BF_4$) (Ø 2.0 (±0.5) nm, entry 7 in Table 4) [9].

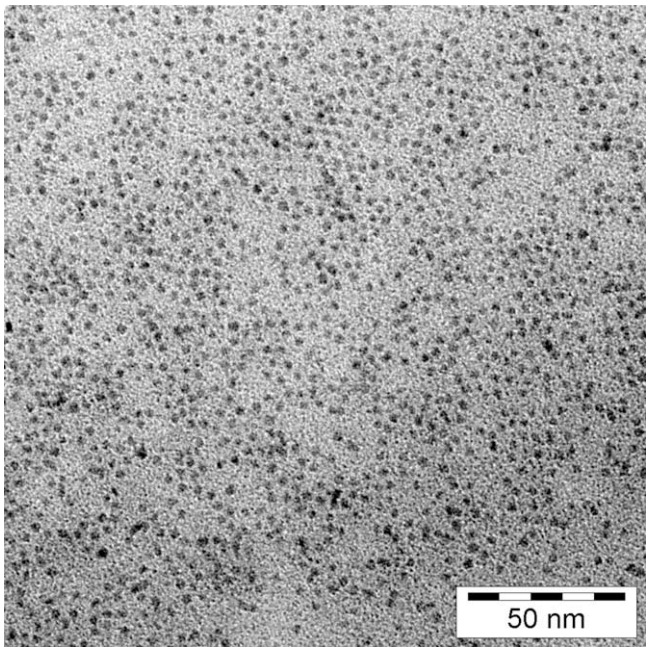

Fig. 9. TEM photograph of Os-NPs from $Os_3(CO)_{12}$ by conventional thermal decomposition (0.2 wt.% Os in $BMIm^+BF_4^-$) (Ø 2.5 (±0.4) nm, entry 8 in Table 4) [9].

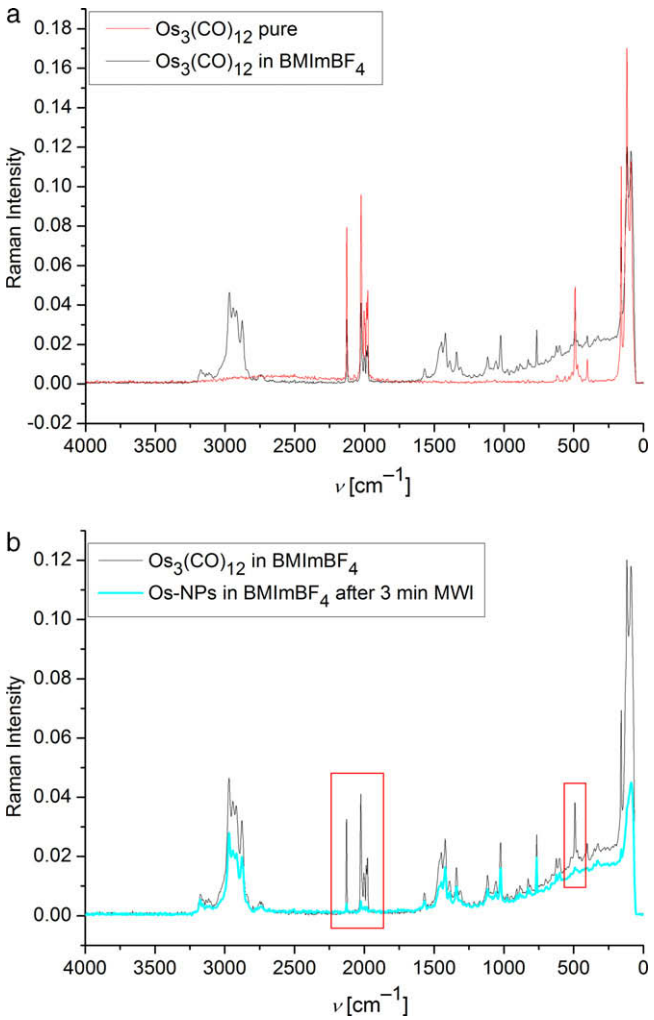

Fig. 10. Raman-FT spectra. Top: pure $Os_3(CO)_{12}$ and $Os_3(CO)_{12}$ in $BMIm^+BF_4^-$; bottom: $Os_3(CO)_{12}$ in $BMIm^+BF_4^-$ before and after 3 min 10 W microwave irradiation (MWI). Red boxes highlight the indicative osmium carbonyl bands [21].

yielding olefins, oxygenates, and paraffins (C_7–C_{30}) and could be reused at least three times if they were not exposed to air [155].

The decomposition of $Co_2(CO)_8$ dispersed in 1-*n*-decyl-3-methylimidazolium bis(trifluoromethylsulfonyl)amide ($DMIm^+Tf_2N^-$) at 150 °C over 1 h afforded a black solution containing Co-NPs with a cubic shape (53 ± 22 nm), together with Co-NPs of irregular shape [156].

Stable cobalt, rhodium and iridium nanoparticles were obtained reproducibly by thermal decomposition under argon from $Co_2(CO)_8$, $Rh_6(CO)_{16}$ and $Ir_4(CO)_{12}$ dissolved in the ionic liquids $BMIm^+BF_4^-$, $BMIm^+TfO^-$ and $BtMA^+Tf_2N^-$ (Scheme 10, Fig. 12, Table 4) [20]. Later an even more rapid and energy-saving decomposition could be achieved with a 10 W microwave irradiation for 3 min of 0.4 ml (0.48 g) of a $BMIm^+BF_4^-$ sample with a 0.5 wt.% $M_x(CO)_y$/IL-dispersion to yield the M-NP/IL-dispersion [21]. The very small and uniform nanoparticle size of about 1–3 nm for the Co-, Rh- or Ir-NPs in $BMIm^+BF_4^-$ (Table 4) increases with the molecular volume of the ionic liquid anion in $BMIm^+TfO^-$ and $BtMA^+Tf_2N^-$ (Fig. 13). Characterization of the nanoparticles was done by TEM, transmission electron diffraction (TED), X-ray powder diffraction (XRPD) and dynamic light scattering (DLS). The rhodium or iridium nanoparticle/IL systems function as highly effective and recyclable catalysts in the biphasic liquid-liquid hydrogenation of cyclohexene to cyclohexane with activities of up to 1900 mol cyclohexane × $(mol\,Ir)^{-1} \times h^{-1}$ and

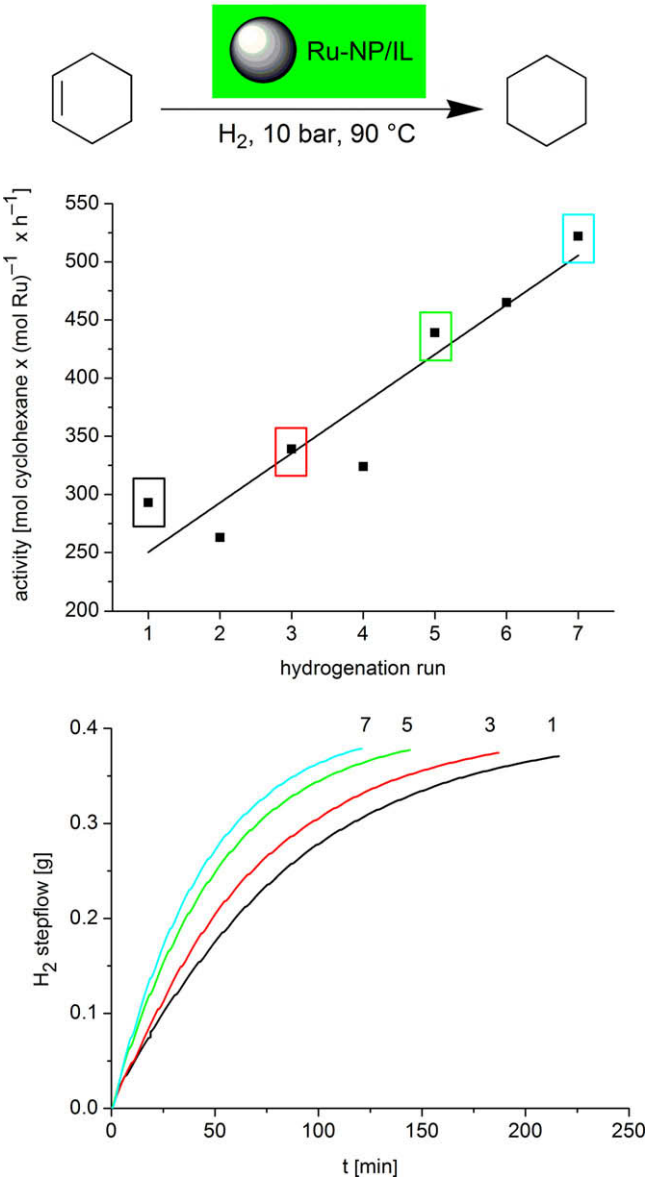

Fig. 11. Activity for seven runs of the hydrogenation of cyclohexene with the same Ru-NP/BMIm$^+$BF$_4^-$ catalyst at 90 °C, 10 bar H_2 pressure, run to 95% conversion and H_2 uptake over time for the 1st, 3rd, 5th and 7th hydrogenation run. An H_2 uptake of 0.38 g corresponds to 95% conversion (100% are 0.2 mol or 0.4 g H_2) [21].

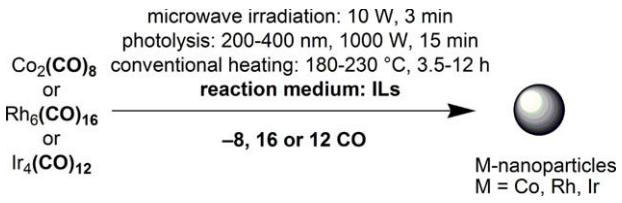

Scheme 10. Formation of Co, Rh and Ir nanoparticles by microwave, photolytic or thermal decomposition of metal carbonyls $M_x(CO)_y$ under argon in ionic liquids [20,21].

380 mol cyclohexane × (mol Rh)$^{-1}$ × h^{-1} for quantitative conversion at 4 bar H_2 pressure and 75 °C (Fig. 14).

Stable ruthenium or rhodium metal nanoparticles could be supported on chemically derived graphene (CDG) surfaces with small and uniform particle sizes (Ru 2.2 ± 0.4 nm and Rh 2.8 ± 0.5 nm) by decomposition of their metal carbonyl precursors $Ru_3(CO)_{12}$ and $Rh_6(CO)_{16}$, respectively, by rapid microwave irradiation in a suspension of CDG in BMIm$^+$BF$_4^-$ (Scheme 11, Fig. 15). The obtained hybrid nanomaterials Rh-NP/CDG and Ru-NP/CDG were – without further treatment – catalytically active in hydrogenation reactions yielding complete conversion of cyclohexene or benzene to cyclohexane under organic-solvent-free and mild conditions (50–75 °C, 4 bar H_2) with reproducible turnover frequencies of 1570 mol cyclohexane × (mol Ru)$^{-1}$ × h^{-1} and 310 mol benzene × (mol Rh)$^{-1}$ × h^{-1}. The catalytically active M-NP/CDG-nanocomposite material could be recycled and used for several runs without any loss of activity. (Scheme 11, Fig. 16) [157].

5. DLVO theory

This section gives a brief overview on the theory for the treatment of particle dispersions.

The classic theory for interaction of two particles in a dispersion is the DLVO (Derjaugin–Landau–Verwey–Overbeek) theory, developed by the research groups of Derjaugin and Landau in the USSR and the group of Vervey and Overbeek in the Netherlands nearly simultaneously in the 1940s. This basic and most commonly theory is considered as a combination of the repulsive Coulomb and the attraction van der Waals forces. Hence DLVO potential is the sum of an effective electrostatic term and a direct van der Waals term.

Some simplifications and assumptions are involved in this theory: the surfaces of the particles are flat. The charge density is homogeneous and remains homogenous, even when particles approach each other. Also there is no change of the concentration of the counter ions which cause the electric potential. The solvent itself has only an influence through its dielectric constant.

It is quite clear that the surface of a particle is not flat and the charge density changes when two particles approach each other. It is evident that the theory can only approximate the real-life interactions of two particles. DLVO theory works very well and is the best predictor of the stability of lyophobic colloids. This theory is fundamental for chemists working on and with colloids [158].

It should be pointed out that there are two main types of stabilizers for NPs: Electrostatic or "DLVO-type" stabilizers which are considered as point charge stabilizers and "classical" steric stabilizers. Small anions like halides seem to be the closest real-life electrostatic stabilizers.

Concerning nanoparticles and their interactions, the anion is the main focus because anions will bind to the unsaturated surface of the electrophilic NP [159]. Thus, the NPs with their anion layer assume a negative charge and turn into a large multi-negative anion. The repulsion between two such negatively charged NPs is the Coulomb part of the DLVO theory.

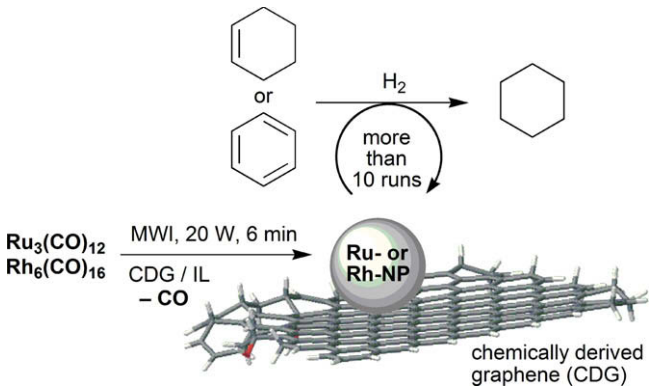

Scheme 11. The use of microwave irradiation for the easy synthesis of transition metal nanoparticles supported on chemically derived graphene (CDG) in ILs. The hybrid nanomaterials Ru-NP/CDG and Rh-NP/CDG were active hydrogenation catalysts [157].

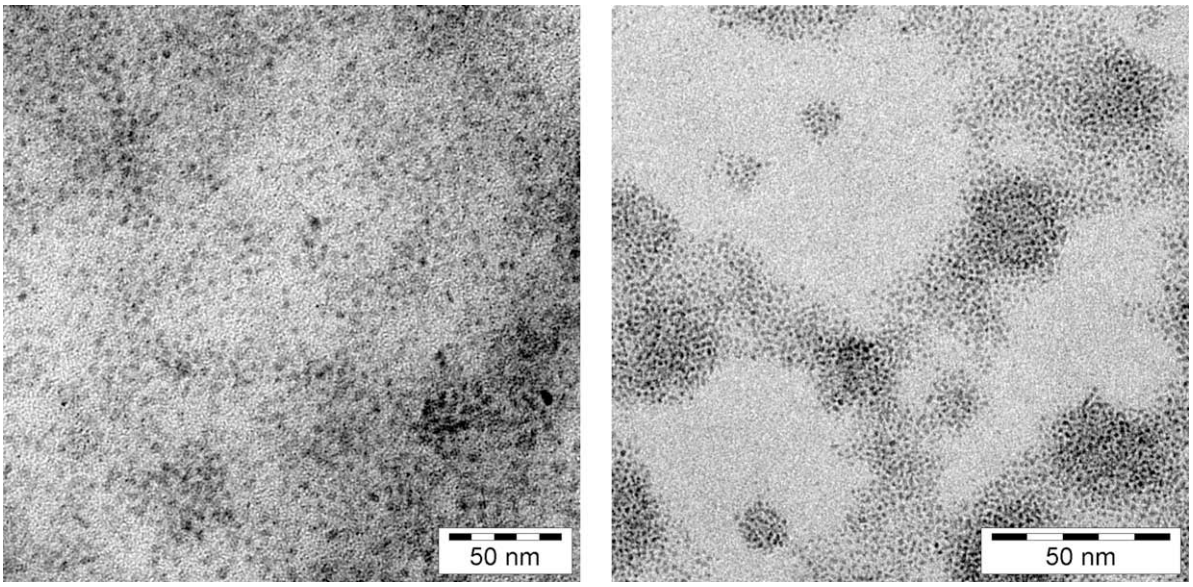

Fig. 12. TEM photographs. Left: Rh-NPs from $Rh_6(CO)_{16}$ (0.5 wt.% Rh in $BMIm^+BF_4^-$, Ø 3.5 (±0.8) nm, entry 10 in Table 4); right: Ir-NPs from $Ir_4(CO)_{12}$ (0.5 wt. % Ir in $BMIm^+BF_4^-$, 18 h, Ø 1.3 (±0.2) nm,, entry 11b in Table 4), both by conventional thermal decomposition [20].

The stability of colloids is a balance between Coulomb forces and van der Waals attraction. A measure of the stability of a colloid is the thickness of the Debye layer, which is the sum of the layers of counterions surrounding the particle. The thicker the Debye layer the more stable is the particle because the distance to the next particle is greater and the van der Waals attraction is reduced. Finke et al. studied the stability of colloids in different solvents and found that the higher the dielectric constant of the medium the better is the stabilization of the colloid [160].

The DLVO theory has its limits. It can only be applied to dilute systems ($<5 \times 10^{-2}$ mol/l). It does not work for higher concentrations. It cannot be applied to ions with multiple charge and sterically stabilized systems [161]. Nowadays the DLVO theory has been supplemented with "extra-DLVO" forces which include effects such as hydrogen bonding, the hydrophobicity and steric interactions.

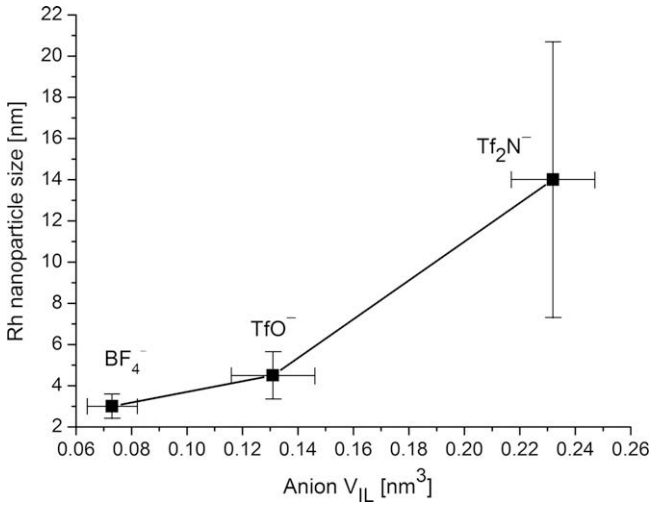

Fig. 13. Correlation between the molecular volume of the ionic liquid anion ($V_{IL\text{-anion}}$) and the observed Rh nanoparticle size with standard deviations as error bars (from TEM). IL anions range from BF_4^- (smallest) over trifluoromethylsulfonate (triflate, $CF_3SO_3^-$, TfO^-) to the largest bis(trifluoromethylsulfonyl)amide [$(CF_3SO_2)_2N^-$, Tf_2N^-] [20].

The van der Waals term is calculated as an integral of interatomic dispersion interactions over the volume of both particles (Eq. (2)) [162].

$$\frac{\mathrm{PMF}^{\mathrm{el}}_{\mathrm{DLVO}}(r)}{k_{\mathrm{b}}T} = L_{\mathrm{B}}Z_1Z_2\frac{\exp(\kappa a_1)\,\exp(\kappa a_2)}{(1+\kappa a_1)(1+\kappa a_2)}\,\frac{\exp(-\kappa r)}{r} \qquad (2)$$

where PMF is the potential of mean force, L_B the Bjerrum length ($L_B = (e^2/4\pi\varepsilon_r\varepsilon_0)k_bT$), k^{-1} the Debye length, $\kappa^2 = 4\pi L_B\sum_{i=1}^{2}\rho_i Z_i^2$, ρ_i

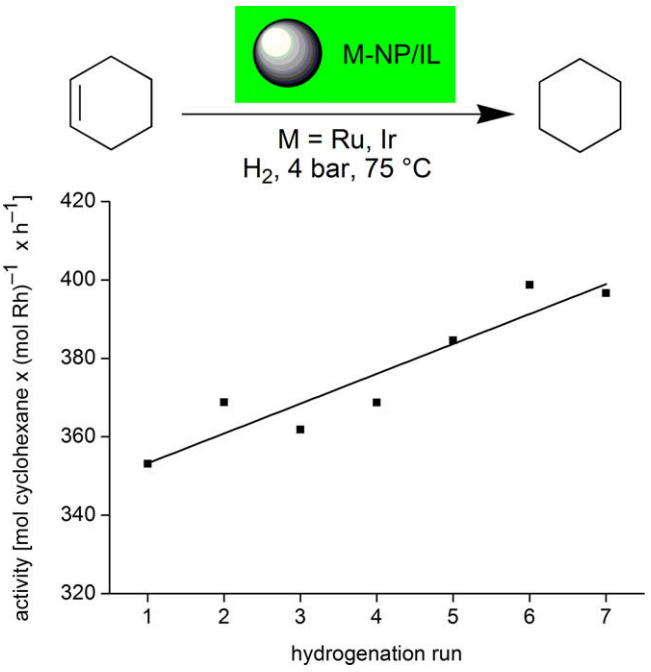

Fig. 14. Activity over seven catalytic runs for the hydrogenation of cyclohexene with the same Rh-NP/$BMIm^+BF_4^-$ catalyst at 75 °C, 4 bar H_2 pressure and 2.5 h reaction time. An activity of 350 mol product × (mol Rh)$^{-1}$ × h^{-1} corresponds to 88% and an activity of 400 to quantitative (100%) conversion. With the homologous Ir-NP/$BMIm^+BF_4^-$ catalyst even higher activities up to 1900 mol cyclohexane × (mol Ir)$^{-1}$ × h^{-1} could be obtained under the same conditions, also due a shorter reaction time of 1 h for near quantitative conversion [20].

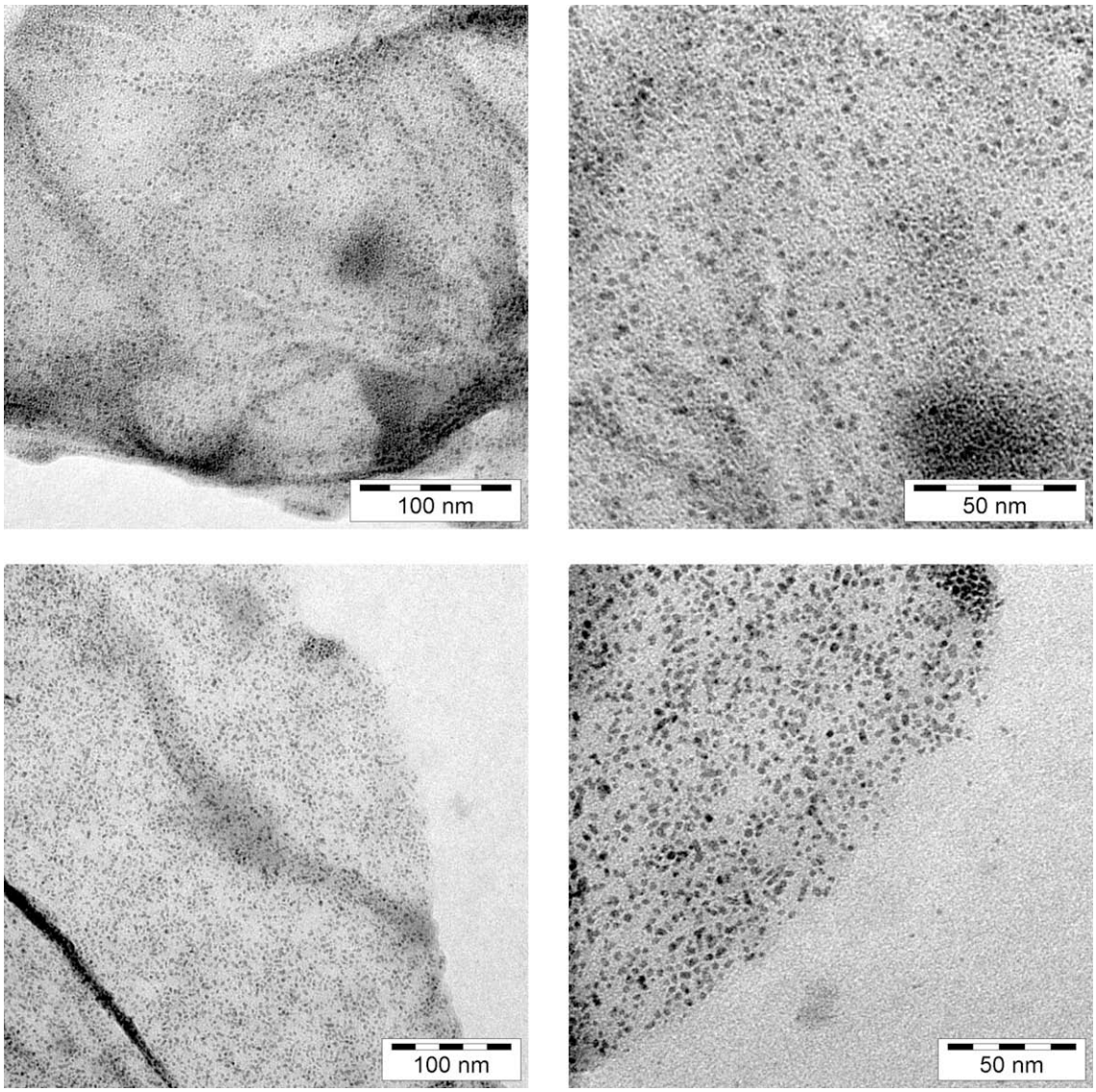

Fig. 15. TEM and TED pictures. Top row: Ru-NP supported on chemically derived graphene (CDG), bottom row: Rh-NP on CDG, from microwave irradiation of $Ru_3(CO)_{12}$ and $Rh_6(CO)_{16}$, respectively, in CDG/$BMIm^+BF_4^-$ [158].

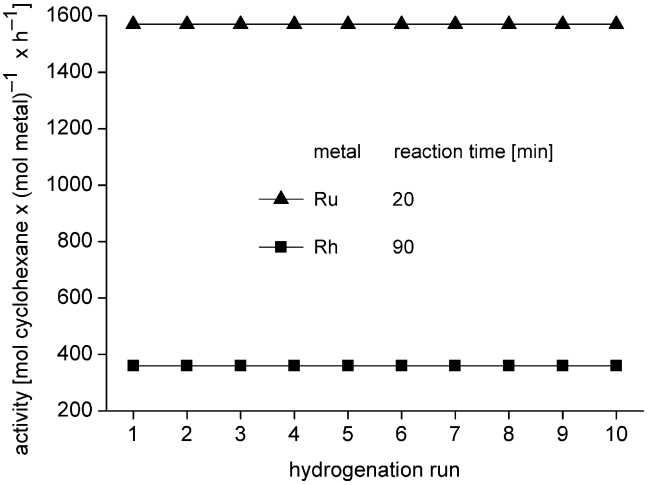

Fig. 16. Activities for the hydrogenation of cyclohexene to cyclohexane with the same M-NP/CDG catalyst in 10 consecutive runs [157].

the concentration of microion i, Z_i the charge of the colloids 1 and 2, a_i the radius of the colloids, and r is the distance between the colloids.

This term is neglected within the basic model, but it is important for large colloidal particles. To compute the effective electrostatic component, microions are described by point charges and two approximations are made, the Poisson–Boltzmann (PB) approximation (that is, a mean-field treatment of micro ions), and an expansion of the charge density to linear order in the electrostatic potential.

Despite its success, the DLVO theory fails to predict some experimental behaviors. The attraction between equally charged particles in the presence of multivalent counterions is the most surprising one [163]. Numerical simulations within the basic model have remarkably contributed to understand such failure. It has been proven that Poisson–Boltzmann theory cannot predict an attraction, while the PMF computed by simulations can be attractive. Therefore, the attraction can be explained by the correlations between microions, missed within the mean field PB treatment, but present in the simulations. The review by Dijkstra devoted to the simulations of charged colloids summarizes work on this issue [163].

6. Conclusions

In this review is shown that ionic liquids (ILs) are remarkable and excellent media for the synthesis and stabilization of metal nanoparticles (M-NPs) without the need of additional stabilizers, surfactants or capping ligands. ILs can be regarded as a supramolecular three-dimensional electrostatic and hydrogen-bonded network. The stabilization of metal nanoparticles in ILs can, thus, be attributed to "extra-DLVO" forces which include effects from the network properties of ILs such as hydrogen bonding, the hydrophobicity and steric interactions to prevent M-NPs agglomeration. Various chemical synthesis methods of metal nanoparticles in ILs allow for the design of a variety of M-NP shapes and sizes. The synthesis of M-NPs can proceed by chemical reduction, thermolysis, photochemical decomposition, electroreduction, microwave and sonochemical irradiation. A microwave induced thermal decomposition of metal carbonyls $M_x(CO)_y$ in ILs provides an especially rapid and energy-saving access to M-NPs because of the ILs significant absorption efficiency for microwave energy due to their high ionic charge, high polarity and high dielectric constant. Metal carbonyls $M_x(CO)_y$ present attractive synthons as they are readily commercially available and contain the metal atoms already in the zero-valent oxidation state needed for M-NPs. No extra reducing agent is necessary and the only side product CO is given off to the gas phase and removed from the dispersion, thereby largely avoiding contaminations of the M-NP/IL dispersion.

Acknowledgments

Our work is supported by the Deutsche Forschungsgemeinschaft through grant Ja466/17-1. We thank the company *IoLiTec* (Germany, www.iolitec.de) for donations of ionic liquids.

References

[1] A.H. Lu, E.L. Salabas, F. Schüth, Angew. Chem. Int. Ed. 46 (2007) 1222; A.H. Lu, E.L. Salabas, F. Schüth, Angew. Chem. 118 (2007) 1242.
[2] A. Gedanken, Ultrasonics Sonochem. 11 (2004) 47.
[3] C.N.R. Rao, S.R.C. Vivekchand, K. Biswas, A. Govindaraj, Dalton Trans. (2007) 3728.
[4] Y. Mastai, A. Gedanken, in: C.N.R. Rao, A. Müller, A.K. Cheetham (Eds.), Chemistry of Nanomaterials, vol. 1, Wiley-VCH, Weinheim, 2004, p. 113.
[5] J. Park, J. Joo, S.G. Kwon, Y. Jang, T. Hyeon, Angew. Chem. Int. Ed. 46 (2007) 4630; J. Park, J. Joo, S.G. Kwon, Y. Jang, T. Hyeon, Angew. Chem. 119 (2007) 4714.
[6] D. Astruc, F. Lu, J.R. Aranzaes, Angew. Chem. Int. Ed. 44 (2005) 7852; D. Astruc, F. Lu, J.R. Aranzaes, Angew. Chem. 117 (2005) 8062.
[7] C. Pan, K. Pelzer, K. Philippot, B. Chaudret, F. Dassenoy, P. Lecante, M.-J. Casanove, J. Am. Chem. Soc. 123 (2001) 7584.
[8] J.D. Aiken III, R.G. Finke, J. Am. Chem. Soc. 121 (1999) 8803.
[9] J. Krämer, E. Redel, R. Thomann, C. Janiak, Organometallics 27 (2008) 1976.
[10] K. Ueno, H. Tokuda, M. Watanabe, Phys. Chem. Chem. Phys. 12 (2010) 1649.
[11] J. Dupont, J.D. Scholten, Chem. Soc. Rev. 39 (2010) 1780.
[12] J. Dupont, J. Brazil. Chem. Soc. 15 (2004) 341.
[13] M.-A. Neouze, J. Mater. Chem. 20 (2010) 9593.
[14] C.S. Consorti, P.A.Z. Suarez, R.F. de Souza, R.A. Burrow, D.H. Farrar, A.J. Lough, W. Loh, L.H.M. da Silva, J. Dupont, J. Phys. Chem. B 109 (2005) 4341.
[15] J. Dupont, P.A.Z. Suarez, R.F. de Souza, R.A. Burrow, J.-P. Kintzinger, Chem. Eur. J. 6 (2000) 2377.
[16] R.A. Sheldon, Chem. Commun. (2008) 3352.
[17] P. Wasserscheid, T. Welton, Ionic Liquid in Synthesis, vol. 1, Wiley-VCH, Weinheim, 2007, pp. 325.
[18] P. Wasserscheid, W. Keim, Angew. Chem. Int. Ed. 39 (112) (2000) 3773; P. Wasserscheid, W. Keim, Angew. Chem. 112 (2000) 3926.
[19] C. van Doorslaer, Y. Schellekens, P. Mertens, K. Binnemanns, D. De Vos, Phys. Chem. Chem. Phys. 12 (2010) 1741.
[20] E. Redel, J. Krämer, R. Thomann, C. Janiak, J. Organomet. Chem. 694 (2009) 1069.
[21] C. Vollmer, E. Redel, K. Abu-Shandi, R. Thomann, H. Manyar, C. Hardacre, C. Janiak, Chem. Eur. J. 16 (2010) 3849.
[22] V. Parvulescu, C. Hardacre, Chem. Rev. 107 (2007) 2615.
[23] D. Astruc, Nanoparticles and Catalysis, Wiley-VCH, New York, 2007.
[24] J. Dupont, R.F. de Souza, P.A.Z. Suarez, Chem. Rev. 102 (2002) 3667.
[25] H. Weingärtner, Angew. Chem. Int. Ed. 47 (2008) 654; H. Weingärtner, Angew. Chem. 120 (2008) 664.
[26] D. Xiao, J.R. Rajian, A. Cady, S. Li, R.A. Bartsch, E.L. Quitevis, J. Phys. Chem. B 111 (2007) 4669.
[27] I. Krossing, J.M. Slattery, C. Daguenet, P.J. Dyson, A. Oleinikova, H. Weingärtner, J. Am. Chem. Soc. 128 (2006) 13427.
[28] K.R. Seddon, Chem. Soc. Rev. 37 (2008) 123.
[29] P. Bonhôte, A.-P. Dias, N. Papageorgiou, K.K. Kalyanasundaram, M. Grätzel, Inorg. Chem. 35 (1996) 1168.
[30] J.M. Pringle, J. Golding, K. Baranyai, C.M. Forsyth, B.B. Deacon, J.L. Scott, D.R. Mc Farelane, New J. Chem. 27 (2003) 1504.
[31] T.J. Gannon, G. Law, R.P. Watson, A.J. Carmichael, K.R. Seddon, Langmuir 15 (1999) 8429.
[32] J.N.A. Canongia Lopes, M.F.C. Gomes, A.A.H. Pádua, J. Phys. Chem. B 110 (2006) 16816.
[33] G. Law, R.P. Watson, A.J. Carmichael, K.R. Seddon, Phys. Chem. Chem. Phys. 3 (2001) 2879.
[34] J.N.A. Canongia Lopes, A.A.H. Pádua, J. Phys. Chem. B 110 (2006) 3330.
[35] D.G.E. Kerfoot, X. Nickel, E. Wildermuth, H. Stark, G. Friedrich, F.L. Ebenhöch, B. Kühborth, J. Silver, R. Rituper, in: Ullmann's Encyclopaedia of Industrial Chemistry, 5th ed., Wiley (online), 2008.
[36] T. Hyeon, Chem. Commun. (2003) 927.
[37] P.H. Hess, P.H. Parker Jr., J. Appl. Polym. Sci. 10 (1966) 1915.
[38] J.R. Thomas, J. Appl. Phys. 37 (1966) 2914.
[39] E. Papirer, P. Horny, H. Balard, R. Anthore, C. Petipas, A. Martinet, J. Colloid Interface Sci. 94 (1983) 207.
[40] E. Papirer, P. Horny, H. Balard, R. Anthore, C. Petipas, A. Martinet, J. Colloid Interface Sci. 94 (1983) 220.
[41] G.H. Lee, S.H. Huh, H.I. Jung, J. Mol. Struct. 400 (1998) 141.
[42] M. Giersig, M. Hilgendorff, J. Phys. D: Appl. Phys. 32 (1999) L111–L113.
[43] U. Wiedwald, M. Spasova, E.L. Salabas, M. Ulmeanu, M. Farle, Z. Frait, A. Fraile Rodriguez, D. Arvanitis, N.S. Sobal, M. Hilgendorff, M. Giersig, Phys. Rev. B 68 (2003) 064424.
[44] J. van Wonterghem, S. Mørup, S.W. Charles, S. Wells, J. Villadsen, Phys. Rev. Lett. 55 (1985) 410.
[45] J. van Wonterghem, S. Mørup, S.W. Charles, S. Wells, J. Colloid Interface Sci. 121 (1988) 558.
[46] C. Pathmamanoharan, N.L. Zuiverloon, A.P. Philipse, Progr. Colloid Polym. Sci. 115 (2000) 141.
[47] A. Goossens, L.J. de Jongh, K. Butter, A.P. Philipse, M.W.J. Crajé, A.M. van der Kraan, Hyperfine Interact. 141–142 (2002) 381.
[48] K. Butter, P.H.H. Bomans, P.M. Frederik, G.J. Vroege, A.P. Philipse, Nat. Mater. 2 (2003) 88.
[49] E. Bauer-Grosse, G. Le Caër, Phil. Mag. B 56 (1987) 485.
[50] S.H. Huh, S.J. Oh, Y.N. Kim, G.H. Lee, Rev. Sci. Instrum. 70 (1999) 4366.
[51] S. Sun, C.B. Murray, D. Weller, L. Folks, A. Moser, Science 287 (2000) 1989.
[52] M. Chen, D.E. Nikles, J. Appl. Phys. 91 (2002) 8477.
[53] M. Chen, D.E. Nikles, Nano Lett. 2 (2002) 211.
[54] V.F. Puntes, K.M. Krishnan, P. Alivisatos, Appl. Phys. Lett. 78 (2001) 2187.
[55] T. Hyeon, S.S. Lee, J. Park, Y. Chung, H.B. Na, J. Am. Chem. Soc. 123 (2001) 12798.
[56] S.-W. Kim, S.U. Son, S.S. Lee, T. Hyeon, Y.K. Chung, Chem. Commun. (2001) 2212.
[57] N.A.D. Burke, H.D.H. Stöver, F.P. Dawson, Chem. Mater. 14 (2002) 4752.
[58] M. Rutnakornpituk, M.S. Thompson, L.A. Harris, K.E. Farmer, A.R. Esker, J.S. Riffle, J. Connolly, T.G. St. Pierre, Polymer 43 (2002) 2337.
[59] F.S. Diana, S.-H. Lee, P.M. Petroff, E.J. Krämer, Nano Lett. 3 (2003) 891.
[60] H. Bönnemann, W. Brijoux, R. Brinkmann, N. Matoussevitch, H. Waldöfner, N. Palina, H. Modrow, Inorg. Chim. Acta 350 (2003) 617.
[61] H. Bönnemann, R.A. Brand, W. Brijoux, H.-W. Hofstadt, M. Frerichs, V. Kempter, W. Maus-Friedrichs, N. Matoussevitch, K.S. Nagabhushana, F. Voigts, V. Caps, Appl. Organomet. Chem. 19 (2005) 790.
[62] S. Behrens, H. Bönnemann, N. Matoussevitch, A. Gorschinski, E. Dinjus, W. Habicht, J. Bolle, S. Zinoveva, N. Palina, J. Hormes, H. Modrow, S. Bahr, V. Kempter, J. Phys.: Condens. Matter 18 (2006) S2543–S2561.
[63] N. Matoussevitch, A. Gorschinski, W. Habicht, J. Bolle, E. Dinjus, H. Bönnemann, S. Behrens, J. Magn. Magn. Mater. 311 (2007) 92.
[64] Y. Yin, R.M. Rioux, C.K. Erdonmez, S. Hughes, G.A. Somorjai, A.P. Alivisatos, Science 304 (2004) 711.
[65] M. Zubris, R.B. King, H. Garmestani, R. Tannenbaum, J. Mater. Chem. 15 (2005) 1277.
[66] B.D. Korth, P. Keng, I. Shim, S.E. Bowles, C. Tang, T. Kowalewski, K.W. Nebesny, J. Pyun, J. Am. Chem. Soc. 128 (2006) 6562.
[67] R.A. Mercuri, PCT Int. Appl. (2007), WO 2007136389, Chem. Abstr. 148 (2007) 37461.
[68] R.A. Mercuri, U.S. Pat. Appl. Publ. (2007), US 2007034050, Chem. Abstr. 146 (2007) 233646.
[69] J.S. Gergely, E.S. Marston, S. Subramoney, L. Zhang, U.S. Pat. Appl. Publ. (2007), US 2007085053, Chem. Abstr. 146 (2007) 433242.
[70] C. Gürler, M. Feyen, S. Behrens, N. Matoussevitch, A.M. Schmidt, Polymer 49 (2008) 2211.
[71] N. Doan, K. Kontturi, C. Johans, J. Colloid Interface Sci. 350 (2010) 126.
[72] L.E.M. Howard, H.L. Nguyen, S.R. Giblin, B.K. Tanner, I. Terry, A.K. Hughes, J.S.O. Evans, J. Am. Chem. Soc. 127 (2005) 10140.
[73] R.D. Rutledge, W.H. Morris III, M.S. Wellons, Z. Gai, J. Shen, J. Bentley, J.E. Wittig, C.M. Lukehart, J. Am. Chem. Soc. 128 (2006) 14210.
[74] I. Robinson, S. Zacchini, L.D. Tung, S. Maenosono, N.T.K. Thanh, Chem. Mater. 21 (2009) 3021.

[75] K.S. Suslick, M. Fang, T. Hyeon, J. Am. Chem. Soc. 118 (1996) 11960.
[76] S.-J. Park, S. Kim, S. Lee, Z.G. Khim, K. Char, T. Hyeon, J. Am. Chem. Soc. 122 (2000) 8581.
[77] K. Butter, A.P. Philipse, G.J. Vroege, J. Magn. Magn. Mater. 252 (2002) 1.
[78] O.A. Platonova, L.M. Bronstein, S.P. Solodovnikov, I.M. Yanovskaya, E.S. Obolonkova, P.M. Valetsky, E. Wenz, M. Antonietti, Colloid Polym. Sci. 275 (1997) 426.
[79] D.P. Dinega, M.G. Bawendi, Angew. Chem. Int. Ed. 38 (1999) 1788; D.P. Dinega, M.G. Bawendi, Angew. Chem. 111 (1999) 1906.
[80] J.-I. Park, J. Cheon, J. Am. Chem. Soc. 123 (2001) 5743.
[81] A. Hütten, D. Sudfeld, I. Ennen, G. Reiss, K. Wojczykowski, P. Jutzi, J. Magn. Magn. Mater. 293 (2005) 93.
[82] D. Sudfeld, I. Ennen, A. Hütten, U. Golla-Schindler, H. Jaksch, G. Reiss, D. Meißner, K. Wojczykowski, P. Jutzi, W. Saikaly, G. Thomas, J. Magn. Magn. Mater. 293 (2005) 151.
[83] A. Taubert, Z. Li, Dalton Trans. (2007) 723.
[84] E. Redel, R. Thomann, C. Janiak, Inorg. Chem. 47 (2008) 14.
[85] T. Gutel, J. Garcia-Anton, K. Pelzer, K. Philippot, C.C. Santini, Y. Chauvin, B. Chaudret, J.-M. Basset, J. Mater. Chem. 17 (2007) 3290.
[86] L.S. Ott, R.G. Finke, Inorg. Chem. 45 (2006) 8382.
[87] G.S. Fonseca, A.P. Umpierre, P.F.P. Fichtner, S.R. Teixeira, J. Dupont, Chem. Eur. J. 9 (2003) 3263.
[88] Z. Li, A. Friedrich, A. Taubert, J. Mater. Chem. 18 (2008) 1008.
[89] P. Migowski, D. Zanchet, G. Machado, M.A. Gelesky, S.R. Teixeira, J. Dupont, Phys. Chem. Chem. Phys. 12 (2010) 6826.
[90] P. Migowski, G. Machado, S.R. Teixeira, M.C.M. Alves, J. Morais, A. Traverse, J. Dupont, Phys. Chem. Chem. Phys. 9 (2007) 4814.
[91] M. Ruta, G. Laurenczy, P.J. Dyson, L. Kiwi-Minsker, J. Phys. Chem. C 112 (2008) 17814.
[92] R.R. Deshmukh, R. Rajagopal, K.V. Srinivasan, Chem. Commun. (2001) 1544.
[93] K. Anderson, S.C. Fernández, C. Hardacre, P.C. Marr, Inorg. Chem. Commun. 7 (2004) 73.
[94] J.M. Zhu, Y.H. Shen, A.J. Xie, L.G. Qiu, Q. Zhang, X.Y. Zhang, J. Phys. Chem. C 111 (2007) 7629.
[95] M.A. Firestone, M.L. Dietz, S. Seifert, S. Trasobares, D.J. Miller, N.J. Zaluzec, Small 1 (2005) 754.
[96] K. Peppler, M. Polleth, S. Meiss, M. Rohnke, J.Z. Janek, Phys. Chem. 220 (2006) 1507.
[97] A. Safavi, N. Maleki, F. Tajabadi, E. Farjami, Electrochem. Commun. 9 (2007) 1963.
[98] K. Kim, C. Lang, P.A. Kohl, J. Electrochem. Soc. 152 (2005) E9.
[99] E. Redel, R. Thomann, C. Janiak, Chem. Commun. 15 (2008) 1789.
[100] G. Schmid, Nanoparticles, 2nd ed., Wiley-VCH, Weinheim, 2010, pp. 214.
[101] M. Antonietti, D. Kuang, B. Smarly, Y. Zhou, Angew. Chem. Int. Ed. 43 (2004), pp. 4988; M. Antonietti, D. Kuang, B. Smarly, Y. Zhou, Angew. Chem. 116 (2004) 5096.
[102] F. Endres, M. Bukowski, R. Hempelmann, H. Natter, H. Angew, Chem. Int. Ed. 42 (2003) 3428; F. Endres, M. Bukowski, R. Hempelmann, H. Natter, H. Angew, Angew. Chem. 115 (2003) 3550.
[103] Y.J. Zhu, W.W. Wang, R.J. Qi, X.L. Hu, Angew. Chem. Int. Ed. 43 (2004) 1410; Y.J. Zhu, W.W. Wang, R.J. Qi, X.L. Hu, Angew. Chem. 116 (2004) 1434.
[104] E.T. Silveira, A.P. Umpierre, L.M. Rossi, G. Machado, J. Morais, G.V. Soares, I.J.R. Baumvol, S.R. Teixeira, R.F.P. Fichtner, J. Dupont, Chem. Eur. J. 10 (2004) 3734.
[105] J. Dupont, G.S. Fonseca, A.P. Umpierre, P.F.P. Fichtner, S.R. Teixeira, J. Am. Chem. Soc. 124 (2002) 4228.
[106] C.W. Scheeren, G. Machado, J. Dupont, P.F.P. Fichtner, S.R. Texeira, Inorg. Chem. 42 (2003) 4738.
[107] A.I. Bhatt, A. Mechler, L.L. Martin, A.M. Bond, J. Mater. Chem. 17 (2007) 2241.
[108] H. Itoh, K. Naka, Y. Chujo, J. Am. Chem. Soc. 126 (2004) 3026.
[109] H. Zhang, H. Cui, Langmuir 25 (2009) 2604.
[110] H.S. Schrekker, M.A. Gelesky, M.P. Stracke, C.M.L. Schrekker, G. Machado, S.R. Teixeira, J.C. Rubim, J. Dupont, J. Colloid Interface Sci. 316 (2007) 189.
[111] R.A. Alvarez-Puebla, E. Arceo, P.J.G. Goulet, J.J. Garrido, R.F. Aroca, J. Phys. Chem. B 109 (2005) 3787.
[112] E.J.W.J.T.G Verwey, Overbeek in Theory of the Stability of Lyophobic Colloids, Dover Publications Mineola, New York, 1999, pp. 1.
[113] E. Redel, J. Krämer, R. Thomann, C. Janiak, GIT Labor-Fachzeitschrift 2008, April, 400.
[114] A.N. Shipway, E. Katz, I. Willner, ChemPhysChem 1 (2000) 18.
[115] T. Cassagneau, J.H. Fendler, J. Phys. Chem. B 103 (1999) 1789.
[116] C.D. Keating, K.K. Kovaleski, M.J. Natan, J. Phys. Chem. B 102 (1998) 9404.
[117] M.N. Kobrak, H. Li, Phys. Chem. Chem. Phys. 12 (2010) 1922.
[118] L.S. Ott, R.G. Finke, Coord. Chem. Rev. 251 (2007) 1075.
[119] B.L. Bhargava, S. Balasubramanian, M.L. Klein, Chem. Commun. (2008) 3339.
[120] E. Redel, M. Walter, R. Thomann, C. Vollmer, L. Hussein, H. Scherer, M. Krüger, C. Janiak, Chem. Eur. J. 15 (2009) 10047.
[121] E. Redel, M. Walter, R. Thomann, L. Hussein, M. Krüger, C. Janiak, Chem. Commun. 46 (2010) 1159.
[122] R.G. Pearson, Chemical Hardness. Application from Molecules to Solids, Wiley-VCH, 1997, pp. 1.
[123] T.A. Baker, C.M. Friend, E. Kaxiras, J. Am. Chem. Soc. 130 (2008) 3720.
[124] K.-S. Kim, D. Demberelnyamba, H. Lee, Langmuir 20 (2004) 556.
[125] S. Gao, H. Zhang, X. Wang, W. Mai, C. Peng, L. Ge, Nanotechnology 16 (2005) 1234.
[126] R. Marcilla, D. Mecerreyes, I. Odriozola, J.A. Pomposo, J. Rodriguez, I. Zalakain, I. Mondragon, Nano 2 (2007) 169.
[127] M.A. Gelesky, A.P. Umpierre, G. Machado, R.R.B. Correia, W.C. Magno, J. Morais, G. Ebeling, J. Dupont, J. Am. Chem. Soc. 127 (2007) 4588.
[128] G.S. Fonseca, G. Machado, S.R. Teixeira, G.H. Fecher, J. Morais, M.C.M. Alves, J. Dupont, J. Colloid Interface Sci. 301 (2006) 193.
[129] C.W. Scheeren, J.B. Domingos, G. Machado, J. Dupont, J. Phys. Chem. C 112 (2008) 16463.
[130] J. Turkevich, P.C. Stevenson, J. Hillier, Discuss. Faraday Soc. 11 (1951) 55.
[131] H.R. Ryu, L. Sanchez, H.A. Keul, A. Raj, M.R. Bockstaller, Angew. Chem. Int. Ed. 47 (2008) 7639; H.R. Ryu, L. Sanchez, H.A. Keul, A. Raj, M.R. Bockstaller, Angew. Chem. 120 (2008) 7751.
[132] Y. Hatakeyama, S. Takahashi, K. Nishikawa, J. Phys. Chem. C 114 (2010) 11098.
[133] T. Kameyama, Y. Ohno, T. Kurimoto, K.-I. Okazaki, T. Uematsu, S. Kuwabata, T. Torimoto, Phys. Chem. Chem. Phys. 12 (2010) 1804.
[134] T. Suzuki, K.-I. Okazaki, S. Suzuki, T. Shibayama, S. Kuwabata, T. Torimoto, Chem. Mater. 22 (2010) 5209.
[135] K. Richter, A. Birkner, A.-V. Mudring, Angew. Chem. Int. Ed. 49 (2010) 2431; K. Richter, A. Birkner, A.-V. Mudring, Angew. Chem. 122 (2010) 2481.
[136] H. Wender, L.F. de Oliveira, P. Migowski, A.F. Feil, E. Lissner, M.H.G. Prechtl, S.R. Teixeira, J. Dupont, J. Phys. Chem. C 114 (2010) 11764.
[137] M.H.G. Prechtl, J.D. Scholten, J. Dupont, Molecules 15 (2010) 3441.
[138] V. Calo, A. Nacci, A. Monopoli, S. Laera, N. Coffi, J. Org. Chem. 68 (2003) 2929.
[139] L. Xu, W. Chen, J. Xiao, Organometallics 19 (2000) 1123.
[140] J.D. Scholten, G. Ebeling, J. Dupont, Dalton Trans. (2007) 5554.
[141] M. Harada, Y. Kimura, K. Saijo, T. Ogawa, S. Isoda, J. Colloid Interface Sci. 339 (2009) 373.
[142] A. Imanishi, M. Tamura, S. Kuwabata, Chem. Commun. (2009) 1775.
[143] P. Roy, R. Lynch, P. Schmuki, Electrochem. Commun. 11 (2009) 1567.
[144] C. Fu, Y. Kuang, Z. Huang, X. Wang, N. Du, J. Chen, H. Zhou, Chem. Phys. Lett. 499 (2010) 250.
[145] S.Z. El Abedin, F. Endres, Electrochim. Acta 54 (2009) 5673.
[146] L. Yu, H. Sun, J. He, D. Wang, X. Jin, X. Hu, G.Z. Chen, Electrochem. Commun. 9 (2007) 1374.
[147] D. Bogdal, Microwave-Assisted Organic Synthesis, Elsevier, New York, USA, 2006, pp. 47.
[148] A.L. Buchachenko, E.L. Frankevich, Chemical Generation and Reception of Radio- and Microwaves, Wiley-VCH, Weinheim, Germany, 1993, pp. 41.
[149] V.K. Ahluwulia, Alternative Energy Processes in Chemical Synthesis, Alpha Science International Ltd., Oxford, United Kingdom, 2008.
[150] J. Berlan, P. Giboreau, S. Lefeuvre, C. Marchand, Tedrahedron Lett. 32 (1991) 2363.
[151] F. Langa, P. de la Cruz, A. de la Hoz, A. Diaz-Ortiz, E. Diez-Barra, Contemp. Org. Synth. 4 (1997) 373.
[152] L. Perreux, A. Loupy, Tetrahedron 57 (2001) 9199.
[153] A. Stadler, C.O. Kappe, J. Chem. Soc. Perkin Trans. 2 (2000) 1363.
[154] A. Stadler, C.O. Kappe, Eur. J. Org. Chem. (2001) 919.
[155] D.O. Silva, J.D. Scholten, M.A. Gelesky, S.R. Teixeira, A.C.B. Dos Santos, E.F. Souza-Aguiar, J. Dupont, ChemSusChem 1 (2008) 291.
[156] M. Scariot, D.O. Silva, J.D. Scholten, G. Machado, S.R. Teixeira, M.A. Novak, G. Ebeling, J. Dupont, Angew. Chem. Int. Ed. 47 (2008) 9075; M. Scariot, D.O. Silva, J.D. Scholten, G. Machado, S.R. Teixeira, M.A. Novak, G. Ebeling, J. Dupont, Angew. Chem. 120 (2008) 9215.
[157] D. Marquardt, C. Vollmer, R. Thomann, P. Steurer, R. Mülhaupt, E. Redel, C. Janiak, Carbon 49 (2011) 1326.
[158] B.W. Ninham, Adv. Colloid Interface Sci. 83 (1999) 1.
[159] R.G. Finke, in: D.L. Feldheim, C.A. Foss Jr. (Eds.), Metal Nanoparticle: Synthesis, Characterization and Applications, Marcel Dekker, New York, 2002 (Chapter 2).
[160] L.S. Ott, R.G. Finke, Inorg. Chem. 45 (2006) 8283.
[161] M. Boström, D.R.W. Williams, B.W. Ninham, Phys. Rev. Lett. 87 (2001) 168103.
[162] J. Lyklema, Fundamentals of Interface and Colloid Science, Elsevier, Amsterdam, 2005.
[163] M. Dijkstra, Curr. Opin. Colloid Interface Sci. 6 (2001) 372.

CARBON 49 (2011) 1326–1332

available at www.sciencedirect.com

ScienceDirect

journal homepage: www.elsevier.com/locate/carbon

The use of microwave irradiation for the easy synthesis of graphene-supported transition metal nanoparticles in ionic liquids

Dorothea Marquardt [a], *Christian Vollmer* [a], *Ralf Thomann* [b], *Peter Steurer* [b], *Rolf Mülhaupt* [b,c], *Engelbert Redel* [a], *Christoph Janiak* [a,*]

[a] *Institut für Anorganische und Analytische Chemie, Universität Freiburg, Albertstr. 21, D-79104 Freiburg, Germany*
[b] *Freiburger Material Forschungszentrum (FMF) and Institut für Makromolekulare Chemie, Universität Freiburg, Stefan-Meier-Str. 21-31, 79104 Freiburg, Germany*
[c] *FRIAS, Freiburg Institute for Advanced Studies, Albertstr. 19, 79104 Freiburg, Germany*

ARTICLE INFO

Article history:
Received 16 July 2010
Accepted 29 September 2010
Available online 4 December 2010

ABSTRACT

Stable ruthenium or rhodium metal nanoparticles were supported on chemically derived graphene (CDG) surfaces with small and uniform particle sizes (Ru 2.2 ± 0.4 nm and Rh 2.8 ± 0.5 nm) by decomposition of their metal carbonyl precursors by rapid microwave irradiation in a suspension of CDG in the ionic liquid 1-butyl-3-methylimidazolium tetrafluoroborate. The graphene-supported hybrid nanoparticles were shown to be active and could be re-used at least 10 times as catalysts for the hydrogenation of cyclohexene and benzene under organic-solvent-free conditions with constant activities up to 1570 mol cyclohexane × (mol metal)$^{-1}$ × h^{-1} at 4 bar and 75 °C.

1. Introduction

Metal nanoparticles (M-NPs) are of high interest in catalysis [1]. M-NPs can be synthesized in ionic liquids (ILs) [2] by thermal decomposition of their metal carbonyls [3–5] in a rapid (min) and low-energy (10–20 W) procedure using microwave irradiation (MWI) [1,6]. ILs are an ideal media for microwave reactions with a significant absorption efficiency for microwave energy and also for the stabilization of M-NPs, both because of their high ionic charge, high polarity and high dielectric constant [1,7–9]. An efficient M-NP stabilization is also possible on solid surfaces [10,11] including graphenes [12–17].

During the last few years, chemically derived graphene (CDG) [16–20], also called thermally reduced graphite oxide [21–23] or simply graphene, has been rediscovered as an extremely versatile carbon material [14,17,24]. Because of the functional groups present in CDG (Fig. S1b in Supporting information), the sorption of ions and molecules is possible [14]. This and the high specific surface area of CDG of 400 m^2 g^{-1} up to 1500 m^2 g^{-1}, make them promising materials for catalytic applications [14]. Metal-nanoparticles on carbon materials are of recent interest [25–31]. Pt-, Ru- or Pd-NPs on exfoliated graphene sheets were produced from heating graphite oxide (GO) with the metal complexes $[Pt(NH_3)_4]Cl_2 \cdot H_2O$, $[Ru(NH_3)_6]Cl_2$ or $[Pd(NH_3)_4]Cl_2 \cdot H_2O$ under an N_2 atmosphere [32]. Graphene supported M-NPs are composite materials [33] that may find applications as chemical sensors [34], electrodes for fuel cells [35–37], catalysis [38–41] or hydrogen storage [42].

Here we show that Ru- and Rh-NPs can easily be deposited on CDG-surfaces by decomposition of their metal carbonyls $Ru_3(CO)_{12}$ and $Rh_6(CO)_{16}$, respectively, through low-energy and rapid microwave irradiation (20 W, 6 min) in suspensions

* *Corresponding author:*
E-mail address: janiak@uni-freiburg.de (C. Janiak).
0008-6223/$ - see front matter
doi:10.1016/j.carbon.2010.09.066

of CDG in $BMImBF_4$. The resulting M-NP/CDG composites are active hydrogenation catalysts.

2. Experimental

2.1. Materials and instrumentation

$Ru_3(CO)_{12}$ and $Rh_6(CO)_{16}$ were obtained from *ABCR*, benzene (p.A.) from Merck, cyclohexene (p.A., purity >99.5%) from *Acros Organics* and *Sigma–Aldrich* and used without further purification. CDG was prepared in a two step oxidation/thermal reduction process using natural graphite (type KFL 99.5 from Kropfmühl AG, Passau, Germany) as raw material. The graphite oxidation process of Hummers and Offeman [43] was employed (see Supporting information). The ionic liquid (IL) 1-butyl-3-methylimidazolium tetrafluoroborate, $BMImBF_4$ was received from *IoLiTec* (Denzlingen, Germany, www.iolitec.de) (H_2O content «100 ppm; Cl^- content «50 ppm). The IL was dried under high vacuum (10^{-3} mbar) for several days.

All synthesis experiments were done using Schlenk techniques or a glove box under argon since the metal carbonyls are hygroscopic and air sensitive. The microwave reactions were carried out in the laboratory microwave system *Discover* by *CEM*.

Transmission electron microscopy (TEM) photographs were taken at room temperature from a 200 μm carbon-coated copper grid on a *Zeiss LEO* 912 transmission electron microscope operating at an accelerating voltage of 120 kV. The particle size was determined by measuring manually at least 100 particles from different images using *iTEM* software tools for manual measurements by *OlympusSIS*. Completely automatic measurements, which can be easily performed for well separated particles, fail in the case of heavily clustered particles. For a better comparison of the samples also particles which would have allowed automatic detection were measured manually.

Metal analyses were performed by flame atomic absorption spectroscopy (AAS) on a *Vario 6* from *Analytik Jena*.

Gas chromatographic analyses were done on a *Perkin–Elmer 8500* with an *HS-6B* inlet (HS headspace), equipped with a *DB* 5 column (60 m × 0.32 mm, film thickness 25 μm, oven temperature 60 °C) for cyclohexene or a *PEG* column (25 m × 0.32 mm, film thickness 1.0 μm, oven temperature 40 °C) for benzene (both at an N_2 carrier flow of 120 L/min) and flame ionization detector (FID, 250 °C detector temperature). Probe injection occurred through the headspace sampler thermostated for 20 min to 50 °C. The benzene or cyclohexene to cyclohexane conversion was analyzed by putting a drop of the mixture into a GC sample vial with 1 ml of distilled water. The addition of water as a non-electrolyte can enlarge the activity coefficient of organic components, thereby increase their detection sensitivity through the increase in peak area. The FID does not detect the water [44] itself. The vial was closed with aluminum crimp caps (with butyl rubber septum), placed into the headspace sampler of the GC-headspace. After the thermostatization time a sample was automatically drawn from the gas phase in the vial. The product was analyzed by the GC retention time versus authentic samples of benzene or cyclohexene and cyclohexane. Hydrogenation conversion (%) was calculated from the obtained cyclohexane-to-benzene or -cyclohexene peak area, respectively, and compared to a calibration curve from different ratios of given benzene or cyclohexene/cyclohexane mixtures which had been measured under identical headspace conditions.

2.2. Synthesis of chemically derived graphene ("graphene")-supported transition metal-nanoparticles (M-NP/CDG)

In a typical experiment chemically derived graphene (CDG, 4.8 mg, 0.2 wt.% related to 2.4 mg IL) was dissolved/suspended in the dried and degassed (desoxygenated) ionic liquid $BMImBF_4$ (2.0 ml, 2.4 g, $\rho = 1.2$ g/mL) at room temperature with magnetic stirring for 20 h in a microwave-reaction vial. The solid metal carbonyl powders $M_x(CO)_y$ [50.6 mg $Ru_3(CO)_{12}$, 0.230 mmol Ru or 62.5 mg $Rh_6(CO)_{16}$, 0.235 mmol Rh, see Table S1a, Supporting information] were added to the CDG slurry in $BMImBF_4$ (1 wt.% metal, related to 2.4 g $BMImBF_4$) and suspended with magnetic stirring for 18 h under argon atmosphere. Then, the stirring bars were removed and the mixture was subjected to microwave irradiation (6 min, 20 W) under argon atmosphere.

For workup the slurry was degassed from CO *in vacuo*. Distilled water (6 ml) was added to remove the ionic liquid from the M-NP/CDG system. The black slurry was centrifuged (2 × 15 min, 2000 rpm, *Hettich Rotina 46*) and the supernatant liquid H_2O/IL phase decanted and discarded. The addition of H_2O, centrifugation and decantation was repeated three times. At last, the residue was again dispersed in water, filtered and dried under vacuum. The dry black-greyish residue formed flakes which could easily be removed from the filter to yield 25.0 mg (83%) Ru-NP/CDG and 15.7 mg (54%) Rh-NP/CDG.

The primary characterization of the M-NP/CDG composite was carried out by transmission electron microscopy (TEM).

The Ru or Rh metal content of the M-NP/CDG samples was determined with AAS by digestion of the sample (15 mg) in hot aqua regia [30 ml, HCl (37%)/HNO_3 (65%) 3:1]. After the aqua regia was boiled down, the residue was re-dissolved in HCl (30 ml, 37%) and boiled down again. The residue was resolved in conc. HCl (37%) and the solution was filtered to remove particles. Aqua regia was added to a total volume of 25 ml followed by AAS analysis. Ru and Rh contents of the M-NP/CDG samples were 17.4 and 17.0 wt.%, respectively.

2.3. Hydrogenation of cyclohexene

The hydrogenation reactions of cyclohexene with graphene-supported Ru and Rh-nanoparticles were carried out in stainless steel autoclaves. The autoclave was conditioned by evacuation and re-filling with argon. All autoclave loading was carried out under argon. Each autoclave was equipped with a glass inlay, to eliminate any catalytic influence of the stainless steel surface on the reaction process, into which the catalyst (Ru-NP/CDG 11 mg containing 17.4 wt.% Ru or 1.89×10^{-5} mol Ru; Rh-NP/CDG, 11 mg, containing 17.0 wt.% Rh or 1.82×10^{-5} mol Rh) and the cyclohexene substrate (1.0 ml, density 0.811 g/ml, $M = 82.14$ g/mol, 0.01 mol) were loaded. The autoclave was heated to 75 °C and pressurized to 4 bar of H_2 which was kept constant over the reaction time.

The reaction mixture was stirred for an optimized set time of 1.5 h or 20 min. After this time the reactor was depressurized, and the volatile organic components condensed under vacuum (15 min) into a clean cold trap (liquid nitrogen cooled). Decanting of the organic layer from solid M-NP/CDG was not feasible because the later formed a fine dispersion which did not settle even after a prolonged time. The M-NP/CDG catalyst is left behind in the autoclave and was re-used by adding fresh cyclohexene. Organic substrate workup and catalyst recycling was done 10 times for Ru or Rh. The cyclohexene to cyclohexane conversions were investigated by GC [Perkin–Elmer, DB 5 column (60 m × 0.32 mm)].

2.4. Hydrogenation of benzene

The hydrogenation reactions of benzene with graphene-supported Ru and Rh-nanoparticles were carried out in stainless steel autoclaves. The autoclave was conditioned by evacuation and re-filling with argon. All autoclave loading was carried out under argon. Each autoclave was equipped with a glass inlay, to eliminate any catalytic influence of the stainless steel surface on the reaction process, into which the catalyst (Rh-NP/CDG, 5 mg, containing 17.0 wt.% Rh or 8.26×10^{-6} mol Rh) and the benzene substrate (0.92 ml, 0.81 g, 10.36 mmol) were loaded. The autoclave was heated to the desired temperature (25, 50 or 75 °C) and pressurized to 4 bar of H_2 which was kept constant over the reaction time. The reaction mixture was stirred for a set time of 4 h. After this time the reactor was depressurized, and the volatile organic components condensed under vacuum (15 min) into a clean cold trap (liquid nitrogen cooled). Decanting of the organic layer from solid M-NP/CDG was not feasible because the later formed a fine dispersion which did not settle even after a prolonged time. The M-NP/CDG catalyst is left behind in the autoclave and was re-used by adding fresh benzene. The benzene to cyclohexane conversions were investigated by GC [Perkin–Elmer, PEG column (25 m × 0.32 mm)].

3. Results and discussion

The fluffy CDG powder (Fig. 1, synthesis according to Fig. 2) can be suspended in the IL 1-butyl-3-methylimidazolium tetrafluoroborate ($BMImBF_4$) to form a stable dispersion of single graphene sheets. Stable dispersions of graphene sheets were shown to be obtainable in ILs without the need of additional surfactants/stabilizers [45,46]. The subsequent TEM pictures with M-NPs show single graphene sheets (cf. Fig. 3) which

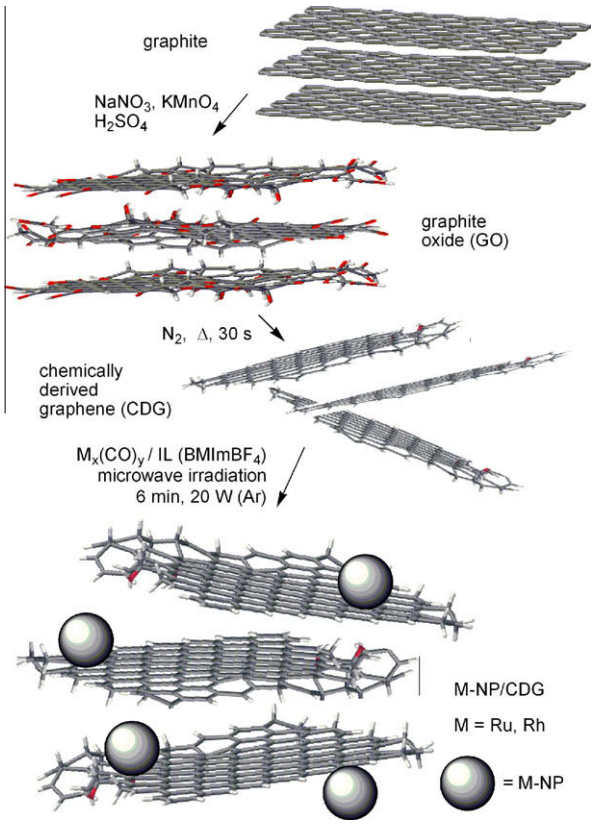

Fig. 2 – Synthesis from natural graphite over GO (Hummers and Offeman [42]) to CDG (thermal reduction process [22]) and M-NP/CDG. GO bearing epoxy, hydroxyl, carbonyl and carboxyl groups was heated up to 560 °C and CO, CO_2 and H_2O were eliminated under enormous expansion of the CDG volume. The graphene sheets with mainly hydroxyl, carbonyl groups [21,22,47] are exfoliated by the gas release and the specific surface area becomes 510 m^2/g in the CDG used here (Fig. 1); for further details see Supporting information.

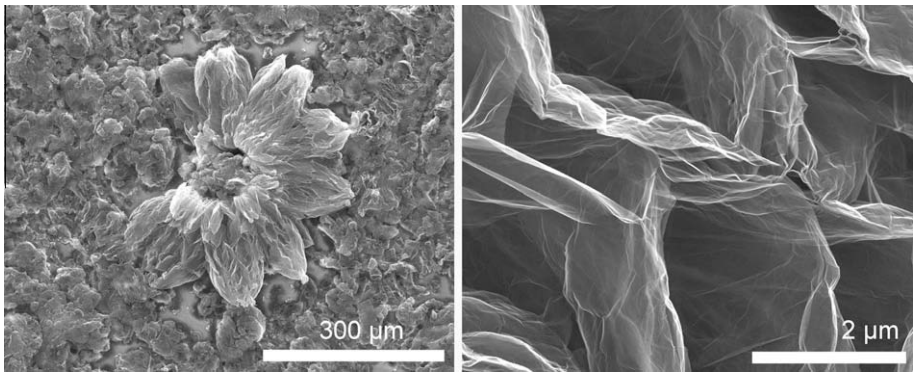

Fig. 1 – Scanning electron microscope (SEM) images of CDG from thermally reduced GO, showing the exfoliated sheets at the larger magnification at the right.

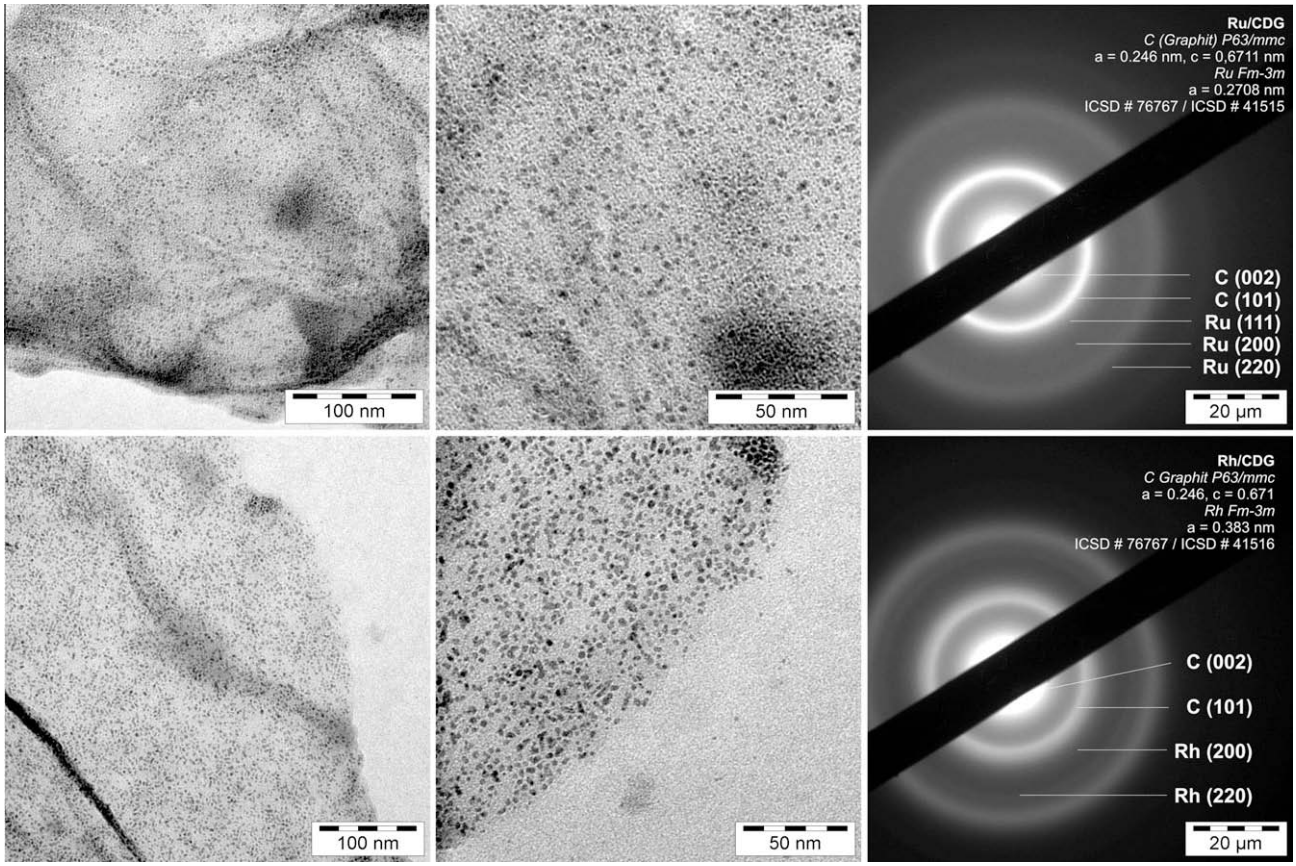

Fig. 3 – TEM and TED of Ru- (top row) and Rh-NP (bottom row) supported on CDG from MWI of $Ru_3(CO)_{12}$ and $Rh_6(CO)_{16}$ in CDG/$BMImBF_4$. The black bar in the TED is the beam stopper. The *d*-values match with the *d*-spacing of Rh metal and graphite. Additional TEM pictures of Ru-NP/CDG and Rh-NP/CDG in Figs. S2 and S3, Supporting information.

suggest that the CDG is dispersed into individual flakes in the IL.

The solid metal carbonyl powders $M_x(CO)_y$ (M = Ru, Rh) were added to the CDG slurry in $BMImBF_4$ and suspended under argon atmosphere. The mixture was subjected to microwave irradiation (6 min, 20 W) under argon atmosphere. The M-NP/CDG materials (M = Ru, Rh) can be separated from the IL and unsupported M-NP/IL by centrifugation of the slurry, washing with water and drying in air. Black-grayish flake-like solids of M-NP/CDG were obtained in good yield. Defined and small Ru- and Rh-NPs with narrow size distributions (2.2 ± 0.4 nm [standard deviation σ] for Ru, 2.8 ± 0.5 nm for Rh, see also Table S1b in Supporting information) can be seen on the almost transparent CDG surfaces in the TEM image of the Ru- and Rh-NP/CDG hybrid structures (Fig. 3).

In a proof-of-principle, the M-NP/CDG materials (M = Rh, Ru) are shown to be catalysts in hydrogenation reactions of cyclohexene and benzene to cyclohexane (Fig. 4). The benzene hydrogenation to cyclohexane is a multi-million ton (IFP – Institute Francais du Petrol) process with the subsequent oxidation to adipic acid and caprolactam as building blocks for Nylon 6.6 and Nylon 6 [48–53].

The M-NP/CDG catalyst (M = Ru, Rh) was suspended in the substrate cyclohexene or benzene without any additional solvent. The hydrogenation reaction times with Ru- and Rh-NP/CDG were optimized for near quantitative conversion. For

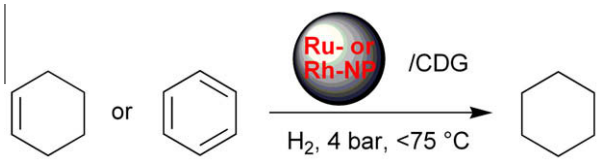

Fig. 4 – Hydrogenation of cyclohexene or benzene to cyloclohexane with Ru- or Rh-NP/CDG under organic-solvent-free conditions.

work-up after each catalytic run the organic phase was removed under reduced pressure and condensed in a cold trap for GC analysis. It was possible to re-use the remaining catalyst for 10 repeated runs each with quantitative conversion and a constant activity of 1570 mol product × (mol metal)$^{-1}$ × h^{-1} for Ru-NP/CDG and 360 mol product × (mol metal)$^{-1}$ × h^{-1} for Rh-NP/CDG (Fig. 5, Table S2b in Supporting information). The pressure-normalized cyclohexene hydrogenation activities of Ru-NP/CDG at 4 bar (390 mol product × (mol metal)$^{-1}$ × h^{-1} × bar^{-1}) at quantitative conversions are higher by about one order of magnitude than the activities of similar Ru-NP/IL systems at 10 bar H_2 pressure (30–53 mol product × (mol metal)$^{-1}$ × h^{-1} × bar^{-1}) [6]. With rhodium the normalized activities of 90 mol product × (mol metal)$^{-1}$ × h^{-1} × bar^{-1} were comparable to those of a Rh-attapulgite (Atta-IL-Rh) catalyst which

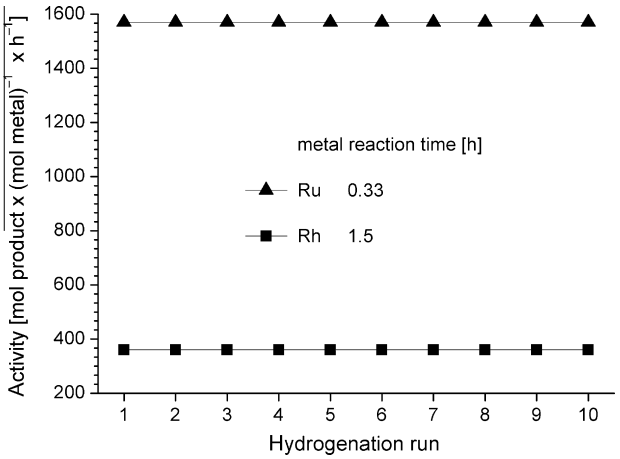

Fig. 5 – Activities for the hydrogenation of cyclohexene with the same M-NP/CDG catalyst in 10 consecutive runs (entry 1–10 for Rh and entry 11–20 for Ru in Table S2b, Supporting information). A lower reaction time of 15 min for M = Ru gave only 94.5% conversion (Table S2a).

was prepared by an ionic liquid-assisted immobilization of Rh from complexes, such as $Rh(PPh)^{3+}$, $Rh(COD)(PPh_3)^{2+}$, and $[Rh(COD)(PPh_3)_2]BF_4$ (COD 1,5-cyclooctadiene) on the natural mineral attapulgite. The pressure-normalized activities of Atta-IL-Rh at 30 bar reached ~90 mol product × (mol metal)$^{-1}$ × h^{-1} × bar^{-1} for >99% conversion in 5.5 h [54]. Rh-NPs immobilized on silica-coated magnetite nanoparticles gave high cyclohexene hydrogenation activities between 2500 and 6600 mol product × (mol metal)$^{-1}$ × h^{-1} × bar^{-1} (at 6 bar, 75 °C, >99% conversion) for up to 20 consecutive runs [55]. TEM/TED pictures of Rh-NP/CDG after five or ten consecutive catalytic runs do not show marked changes in Rh-NP size but somewhat higher crystallinity is apparent from TED (Fig. 6 and S7). The metal-NP size distributions of 2.4 ± 0.4 and 3.0 ± 1.0 nm after five runs for Ru and Rh, respectively and of 2.7 ± 0.7 and 2.8 ± 0.8 nm after 10 runs for Ru and Rh, respectively, (referring to Table S2b in Supporting information) were very similar to those of the starting samples (2.2 ± 0.4 nm for Ru, 2.8 ± 0.5 nm for Rh). While there seems to be a slight increase in the Ru-NP size with prolonged catalytic use, the average size of the Rh-NPs stays invariant within experimental error.

Table 1 – Hydrogenation of benzene with Rh-NP/CDG catalyst.[a]

Entry	Temp. (°C)	Conversion (%)	Activity (mol product × (mol Rh)$^{-1}$ × h^{-1})
1	25	72.8	228
2	50	98.8	310
3	75	94.8	297

[a] The reactions were carried out in steel autoclaves, equipped with glass inlays to eliminate any catalytic influence of the metal surface on the reaction. General conditions 4 bar H_2, time 4 h, benzene 0.81 g (0.92 ml, 10.36 mmol), Rh-NP/CDG 5 mg, 17.0 wt.%, 8.26×10^{-6} mol Rh, benzene/Rh ratio = 1255.

Benzene could be hydrogenated under similar mild conditions to cyclohexane with essentially complete conversion at a temperature of 50 °C, 4 h and 4 bar (Table 1) and a pressure-normalized activities of Rh-NP/CDG of ~78 mol product × (mol Rh)$^{-1}$ × h^{-1} × bar^{-1}. This is a much higher activity (TOF) than for other M-NP/IL systems [56–58] albeit lower than for Rh-NPs immobilized on silica-coated magnetite nanoparticles. The latter gave high benzene hydrogenation activities between 100 and 180 mol product × (mol Rh)$^{-1}$ × h^{-1} × bar^{-1} (at 6 bar, 75 °C, >99% conversion) for up to 20 consecutive runs.

4. Conclusions

We describe here a simple, rapid and low-energy strategy to deposit small 2–3 nm metal nanoparticles of Ru and Rh with uniform sizes on CDG surfaces, by decomposition of their metal carbonyls under MWI in the IL $BMImBF_4$. Microwave irradiation provides a very simple and reproducible way for the rapid (6 min) and energy-saving (20 W power) synthesis of defined and very small M-NPs from their binary metal carbonyl complexes in ILs. This method should be extendable to other metals with the microwave-induced binary metal carbonyl

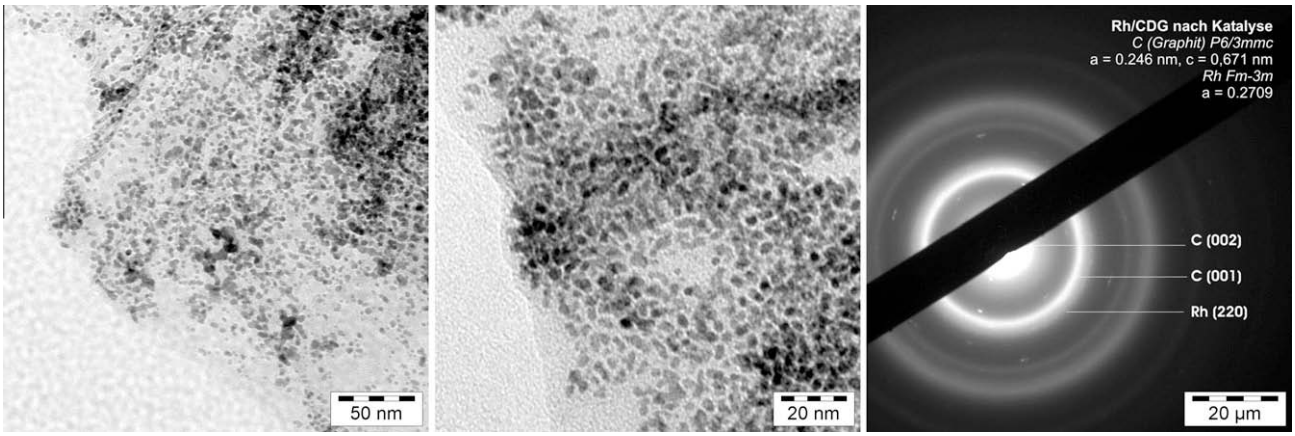

Fig. 6 – TEM and TED of Rh-NP/CDG after 10 consecutive catalytic hydrogenation runs of cyclohexene (after entry 10 of Table S2b, Supporting information).

$M_x(CO)_y$ decomposition and subsequent M-NP deposition on CDG. The obtained hybrid nanomaterials (Rh-NP/CDG and Ru-NP/CDG) were shown – without further treatment – to be catalytically active in hydrogenation reactions yielding complete conversion of cyclohexene or benzene to cyclohexane under organic-solvent-free and mild conditions (50–75 °C, 4 bar H_2) with reproducible activities of 1570 mol cyclohexane × (mol Ru)$^{-1}$ × h^{-1} and 310 mol benzene × (mol Rh)$^{-1}$ × h^{-1}. The catalytically active M-NP/CDG-nanocomposite material could be recycled and used for several runs without any loss of activity.

Acknowledgments

We thank the DFG for Grant Ja466/17-1 and *IoLiTec* (Denzlingen, Germany, www.iolitec.de) for a gift of $BMImBF_4$.

Appendix A. Supplementary data

Supplementary data associated with this article can be found, in the online version, at doi:10.1016/j.carbon.2010.09.066.

REFERENCES

[1] Dupont J, Scholten JD. On the structural and surface properties of transition metal nanoparticles in ionic liquids. Chem Soc Rev 2010;39:1780–804.
[2] Taubert A, Li Z. Inorganic materials from ionic liquids. Dalton Trans 2007:723–7.
[3] Krämer J, Redel E, Thomann R, Janiak C. Use of ionic liquids for the synthesis of iron, ruthenium and osmium nanoparticles from their metal carbonyl precursors. Organometallics 2008;27:1976–8.
[4] Redel E, Thomann R, Janiak C. Use of ionic liquids (ILs) for the IL-anion size-dependent formation of Cr, Mo and W nanoparticles from metal carbonyl $M(CO)_6$ precursors. Chem Commun 2008:1789–91.
[5] Redel E, Krämer J, Thomann R, Janiak C. Synthesis of Co, Rh and Ir nanoparticles from metal carbonyls in ionic liquids and their use as biphasic liquid–liquid hydrogenation nanocatalysts for cyclohexene. J Organomet Chem 2009;694:1069–75.
[6] Vollmer C, Redel E, Abu-Shandi K, Thomann R, Manyar H, Hardacre H, et al. Microwave irradiation for the facile synthesis of transition-metal nanoparticles (NPs) in ionic liquids (ILs) from metal carbonyl precursors and Ru-, Rh-, and Ir-NP/IL dispersions as biphasic liquid liquid hydrogenation nanocatalysts for cyclohexene. Chem Eur J 2010;16:3849–58.
[7] Dupont J. On the solid, liquid and solution structural organization of imidazolium ionic liquids. J Braz Chem Soc 2004;15:341–50.
[8] Consorti CS, Suarez PAZ, de Souza RF, Burrow RA, Farrar DH, Lough AJ, et al. Identification of 1,3-dialkylimidazolium salt supramolecular aggregates in solution. J Phys Chem B 2005;109:4341–9.
[9] Wasserscheid P, Keim W. Ionic liquids – new "solutions" for transition metal catalysis. Angew Chem Int Ed 2000;39:3772–89.
[10] Durán Pachón L, Rothenberg G. Transition-metal nanoparticles: synthesis, stability and the leaching issue. Appl Organomet Chem 2008;22:288–99.
[11] White RJ, Luque R, Budarin VL, Clark JH, Macquarrie DJ. Tuneable porous carbonaceous materials from renewable resources. Chem Soc Rev 2009;38:3401–18.
[12] Kong BS, Geng JX, Jung HT. Layer-by-layer assembly of graphene and gold nanoparticles by vacuum filtration and spontaneous reduction of gold ions. Chem Commun 2009;16:2174–6.
[13] Yang X, Zhang X, Ma Y, Huang Y, Wang Y, Chen Y. Superparamagnetic graphene oxide–Fe_3O_4 nanoparticles hybrid for controlled targeted drug carriers. J Mater Chem 2009;19:2710–4.
[14] Goncalves G, Marques PAAP, Granadeiro CM, Nogueira HIS, Singh MK, Grácio J. Surface modification of graphene nanosheets with gold nanoparticles: the role of oxygen moieties at graphene surface on gold nucleation and growth. Chem Mater 2009;21:4796–802.
[15] Rao CNR, Biswas K, Subrahmanyam KS, Govindaraj A. Graphene, the new nanocarbon. J Mater Chem 2009;19:2457–69.
[16] Scheuermann GM, Rumi L, Steurer P, Bannwarth W, Mülhaupt R. Palladium nanoparticles on graphite oxide and its functionalized graphene derivatives as highly active catalysts for the Suzuki-Miyaura coupling reaction. J Am Chem Soc 2009;131:8262–70.
[17] Rao CNR, Sood AK, Voggu R, Subrahmanyam KS. Some novel attributes of graphene. J Phys Chem Lett 2010;1:572–80.
[18] Stankovich S, Dikin DA, Dommett GHB, Kohlhaas KM, Zimney EJ, Stach EA, et al. Graphene-based composite materials. Nature 2006;442:282–6.
[19] Geim AK, Novoselov KS. The rise of graphene. Nat Mater 2007;6:183–91.
[20] Li D, Kaner RB. Materials science – graphene-based materials. Science 2008;320:1170–1.
[21] Steurer P, Wissert R, Thomann R, Mülhaupt R. Functionalized graphenes and thermoplastic nanocomposites based upon expanded graphite oxide. Macromol Rapid Commun 2009;30:316–27.
[22] McAllister MJ, Li JL, Adamson DH, Schniepp HC, Abdala AA, Liu J, et al. Single sheet functionalized graphene by oxidation and thermal expansion of graphite. Chem Mater 2007;19:4396–404.
[23] Schniepp HC, Li JL, McAllister MJ, Sai H, Herrera-Alonso M, Adamson DH. Functionalized single graphene sheets derived from splitting graphite oxide. J Phys Chem B 2006;110:8535–9.
[24] Boehm HP, Stumpp E. Citation errors concerning the first report on exfoliated graphite. Carbon 2007;45:1381–3.
[25] Li HB, Kang WJ, Xi BJ, Yan Y, Bi HY, Zuhu YC, et al. Thermal synthesis of Cu@carbon spherical core–shell structures from carbonaceous matrices containing embedded copper particles. Carbon 2010;48:464–9.
[26] Park H, Kim JS, Choi BG, Jo SM, Kim DY, Hong WH, et al. Sonochemical hybridization of carbon nanotubes with gold nanoparticles for the production of flexible transparent conducing films. Carbon 2010;48:1325–30.
[27] Ventura DN, Stone RA, Chen KS, Hariri HH, Riddle KA, Fellers TJ, et al. Assembly of cross-linked multi-walled carbon nanotube mats. Carbon 2010;48:987–94.
[28] Kudo S, Maki T, Miura K, Mae K. High porous carbon with Cu/ZnO nanoparticles made by the pyrolysis of carbon material as a catalyst for steam reforming of methanol and dimethyl ether. Carbon 2010;48:1186–95.
[29] Scholz K, Scholz J, McQuilla AJ, Wagner G, Klepel O. Partially embedded highly dispersed Pt nanoparticles in mesoporous carbon with enhanced leaching stability. Carbon 2010;48:1788–98.
[30] Kim YH, Kim YT, Kim H, Lee D. Catalytic oxidation kinetics of iron-containing carbon particles generated by spraying

ferrocene-mixed with diesel fuel into a hydrogen–air diffusion flame. Carbon 2010;48:2072–84.
[31] Tzitzios V, Georgakilas V, Oikonomou E, Karakassides M, Petridis D. Synthesis and characterization of carbon nanotube/metal nanoparticle composites well dispersed in organic media. Carbon 2006;44:848–53.
[32] Gotoh K, Kawabata K, Fujii E, Morishige K, Kinumoto T, Miyazaki Y, et al. The use of graphite oxide to produce mesoporous carbon supporting Pt, Ru or Pd nanoparticles. Carbon 2009;47:2120–4.
[33] Li J, Liu CY. Ag/graphene heterostructures: synthesis, characterization and optical properties. Eur J Inorg Chem 2010:1244–8.
[34] Bui MPN, Lee S, Han KN, Pham XH, Li CA, Choo J, et al. Electrochemical patterning of gold nanoparticles on transparent single-walled carbon nanotube films. Chem Commun 2009:5549–51.
[35] Li WZ, Waje M, Chen ZW, Larsen P, Yan YS. Platinum nanoparticles supported on stacked-cup carbon nanofibers as electrocatalysts for proton exchange membrane fuel cell. Carbon 2010;48:995–1003.
[36] Lee G, Shim JH, Kang H, Nam KM, Song H, Park JT. Monodisperse Pt and PtRu/C-60 hybrid nanoparticles for fuel cell anode catalysts. Chem Commun 2009:5036–8.
[37] Seger B, Kamat PV. Electrocatalytically active graphene–platinum nanocomposites. Role of 2-D carbon support in PEM fuel cells. J Phys Chem 2009;113:7990–5.
[38] Dong L, Gari RRS, Li Z, Craig MM, Hou S. Graphene-supported platinum and platinum–ruthenium nanoparticles with high electrocatalytic activity for methanol and ethanol oxidation. Carbon 2010;48:781–7.
[39] Karimi B, Kabiri Esfahani F. Gold nanoparticles supported on Cs_2CO_3 as recyclable catalyst system for selective aerobic oxidation of alcohols at room temperature. Chem Commun 2009:5555–7.
[40] Sun M, Zhang J, Zhang Q, Wang Y, Wan H. Polyoxometalate-supported Pd nanoparticles as efficient catalysts for the direct synthesis of hydrogen peroxide in the absence of acid or halide promoters. Chem Commun 2009:5174–6.
[41] Armelao L, Dell'Amico DB, Braglia R, Calderazzo F, Garbassi F, Marra G, et al. Loading silica with metals (palladium or platinum) under mild conditions by using well-defined molecular precursors. Dalton Trans 2009:5559–66.
[42] Lightcap IV, Kosel TH, Kamat PV. Anchoring semiconductor and metal nanoparticles on a two-dimensional catalyst mat. Storing and shuttling electrons with reduced graphene oxide. Nano Lett 2010;10:577–83.
[43] Hummers WS, Offeman RE. Preparation of graphitic oxide. J Am Chem Soc 1958;80:1339.
[44] Hachenberg H, Beringer K. Die headspace-gaschromatographie als analysen- und meßmethode. Braunschweig/Wiesbaden, Germany: Vieweg; 1996. p. 32–5.
[45] Zhang B, Ning W, Zhang J, Qiao X, Zhang J, He J, et al. Stable dispersions of reduced graphene oxide in ionic liquids. J Mater Chem 2010;20:5401–3.
[46] Zhou X, Wu T, Ding K, Hu B, Hou M, Han B. Dispersion of graphene sheets in ionic liquid [bmim][PF_6] stabilized by an ionic liquid polymer. Chem Commun 2010;46:386–8.
[47] Li Z, Zhang W, Luo Y, Yang J, Hou JG. How graphene is cut upon oxidation? J Am Chem Soc 2009;131:6320–1.
[48] Brunner H. Hydrogenation. In: Cornils B, Herrmann WA, editors. Applied homogeneous catalysis with organometallic compounds. Weinheim: Wiley-VCH; 2000. p. 216–7.
[49] Parshall GW, Ittel SD. Homogeneous catalysis. 2nd ed. New York: Wiley; 1992. p. 180–1.
[50] Clerici MG, Ricci M, Strukul G. Formation of C–O bonds by oxidation. In: Chiusoli GP, Maitlis PM, editors. Metal-catalysis in industrial organic processes. Cambridge: RSC Publishing; 2008. p. 28–9.
[51] Elias HG. Makromoleküle, vol. 3. Weinheim: Wiley-VCH; 2001. p. 368–454.
[52] Hodnett BK. Heterogeneous catalytic oxidations. Weinheim: Wiley-VCH; 2000. p. 240–63.
[53] Behr A. Angewandte homogene katalyse, vol. 516. Weinheim: Wiley-VCH; 2008. p. 524–5.
[54] Miao S, Liu Z, Zhang Z, Han B, Miao Z, Ding K, et al. Ionic liquid-assisted immobilization of Rh on attapulgite and its application in cyclohexene hydrogenation. J Phys Chem C 2007;111:2185–90.
[55] Jacinto MJ, Kiyohara PK, Masunaga SH, Jardim RF, Rossi LM. Recoverable rhodium nanoparticles: synthesis, characterization and catalytic performance in hydrogenation reactions. Appl Catal A: Gen 2008;338:52–7.
[56] Silveira ET, Umpierre AP, Rossi LM, Machado G, Morais J, Soares GV, et al. The partial hydrogenation of benzene to cyclohexene by nanoscale ruthenium catalysts in imidazolium ionic liquids. Chem Eur J 2004;10:3734–40.
[57] Fonseca GS, Umpierre AP, Fichtner PFP, Teixeira SR, Dupont J. The use of imidazolium ionic liquids for the formation and stabilization of Ir^0 and Rh^0 nanoparticles: efficient catalysts for the hydrogenation of arenes. Chem Eur J 2003;9:3263–9.
[58] Scheeren CW, Machado G, Dupont J, Fichtner PFP, Texeira SR. Nanoscale Pt(0) particles prepared in imidazolium room temperature ionic liquids: synthesis from an organometallic precursor, characterization, and catalytic properties in hydrogenation reactions. Inorg Chem 2003;42:4738–42.